ORNL-1605
Progress

HOMOGENEOUS REACTOR PROJECT

QUARTERLY PROGRESS REPORT

FOR PERIOD ENDING JULY 31, 1953

OAK RIDGE NATIONAL LABORATORY
OPERATED BY
CARBIDE AND CARBON CHEMICALS COMPANY
A DIVISION OF UNION CARBIDE AND CARBON CORPORATION
UCC
POST OFFICE BOX P
OAK RIDGE, TENNESSEE

[redacted]

ORNL-1605

This document consists of 186 pages.

Copy 8 of 211 copies. Series A.

Contract No. W-7405-eng-26

HOMOGENEOUS REACTOR PROJECT

QUARTERLY PROGRESS REPORT

For Period Ending July 31, 1953

Project Director - J. A. Swartout
Engineering - J. A. Lane
Chemistry - S. C. Lind, C. H. Secoy
Corrosion - E. G. Bohlmann
Chemical Technology - F. L. Culler, F. R. Bruce
Compiled by W. E. Thompson

DATE ISSUED

SEP 28 1953

OAK RIDGE NATIONAL LABORATORY
Operated by
CARBIDE AND CARBON CHEMICALS COMPANY
A Division of Union Carbide and Carbon Corporation
Post Office Box P
Oak Ridge, Tennessee

[redacted]

[redacted]

[redacted]

[redacted]

INTERNAL DISTRIBUTION

1. C. E. Center
2. Biology Library
3. Health Physics Library
4. Metallurgy Library
5-6. Reactor Experimental Engineering Library
7-8. Central Research Library
9-15. Laboratory Records Dept.
16. Laboratory Records, ORNL R.C.
17-18. ANP Report Office
19. R. E. Aven
20. S. E. Beall
21. W. B. Berggre
22. E. P. Blizard
23. E. G. Bohlmann
24. G. E. Boyd
25. W. M. Breazeale (C ultant)
26. R. C. Briant
27. R. B. Briggs
28. F. R. Bruce
29. A. D. Callihan
30. D. W. Cardwell
31. G. H. Cartledge
32. G. H. Clewett
33. T. E. Cole
34. D. D. Cowen
35. F. L. Culler
36. J. S. Culver
37. L. B. Emlet (Y-12)
38. J. L English
39. D. E. Ferguson
40. W. R. Gall
41. J. P. Gill
42. R. J. Goldstein
43. C. B. Graham
44. J. C. Griess
45. W. D. Harms
46. C. S. Harrill
47. P. N. Haubenreich
48. C. G. Heisig
49. A. Hollaender
50. A. S. Householder
51. W. B. Humes (K-25)
52. G. R. Jenkins (C&CCC, South Charleston)
53. G. H. Jenks
54. R. W. Johnson
55. C. P. Keim
56. M. T. Kelley
57. E. M. King
58. A. S. Kitzes
59. J. A. Lane
60. C. E. Larson
61. S. C. Lind
62. R. S. Livingston
63. R. N. Lyon
64. W. L. Marshall
65. H. F. McDuffie
66. J. R. McWherter
67. E. C. Miller
68. K. Z. Morgan
69. E. J. Murphy
70. L. R. Quarles
71. P. M. Reyling
72. W. L. Ross
73. J. P. Sanders
74. H. C. Savage
75. C. H. Secoy
76. C. L. Segaser
77. E. D. Shipley
78. A. H. Snell
79. Spiewak
80. D. Susano
81. J. Swartout
82. E. Taylor
83. W. E. ompson
84. M. Tobi
85. S. Visne
86. W. P. Walk
87. A. M. Weinbe

[redacted]

T. A. Welton
E. P. Wigner (Consultant)
C. E. Winters
F. C. VonderLage
F. C. Zapp
P. C. Zmola
G. C. Williams
J. C. Wilson

EXTERNAL DISTRIBUTION

96. AF Plant Representative, Burbank
97. F Plant Representative, Seattle
98. Plant Representative, Wood-Ridge
99. A Project Office, Fort Worth
100-110. Ar ne National Laboratory
111. Arm Forces Special Weapons Project (Sandia)
112-116. Atom Energy Commission, Washington
117. Batte Memorial Institute
118. Bechte orporation
119-121. Brookha National Laboratory
122. Bureau of hips
123-124. California esearch and Development Company
125-130. Carbide and arbon Chemicals Company (Y-12 Plant)
131. Chicago Pate Group
132. Chief of Nava Research
133. Commonwealth E on Company
134. Department of t Navy - Op-362
135. Detroit Edison C any
136-139. duPont Company, A sta
140. duPont Company, Wi ngton
141. Foster Wheeler Corpo tion
142-144. General Electric Comp y, (ANPP)
145-148. General Electric Compa Richland
149. Hanford Operations Offi
150-157. Idaho Operations Office copy to Phillips Petroleum Company)
158. Iowa State College
159-162. Knolls Atomic Power Labora y
163-164. Los Alamos Scientific Labor ry
165. Massachusetts Institute of T nology (Kaufmann)
166. Monsanto Chemical Company
167. Mound Laboratory
168. National Advisory Committee for onautics, Cleveland
169. National Advisory Committee for A nautics, Washington
170. Naval Research Laboratory
171-172. New York Operations Office
173-174. North American Aviation, Inc.
175. Nuclear Development Associates, Inc.

[redacted]

[redacted]

[redacted] Patent Branch, Washington
[redacted] Pioneer Service and Engineering Company
178. [redacted]owerplant Laboratory (WADC)
179. [redacted]tt and Whitney Aircraft Division (Fox Project)
180. Ra[redacted] Corporation
181. San [redacted]ncisco Operations Office
182. Savann[redacted] River Operations Office, Augusta
183. USAF Hea[redacted]arters
184. U. S. Nava[redacted]diological Defense Laboratory
185-186. University o[redacted]lifornia Radiation Laboratory, Berkeley
187-188. University of C[redacted]fornia Radiation Laboratory, Livermore
189. Vitro Corporation [redacted] America
190. Walter Kidde Nuclear [redacted]boratories, Inc.
191-196. Westinghouse Electric C[redacted]oration
197-211. Technical Information Ser[redacted], Oak Ridge

[redacted]

[redacted]

Reports previously issued in this series are as follows:

ORNL-527	Date Issued, December 28, 1949
ORNL-630	Period Ending February 28, 1950
ORNL-730	Feasibility Report - Date Issued, July 6, 1950
ORNL-826	Period Ending August 31, 1950
ORNL-925	Period Ending November 30, 1950
ORNL-990	Period Ending February 28, 1951
ORNL-1057	Period Ending May 15, 1951
ORNL-1121	Period Ending August 15, 1951
ORNL-1221	Period Ending November 15, 1951
ORNL-1280	Period Ending March 15, 1952
ORNL-1318	Period Ending July 1, 1952
ORNL-1424	Period Ending October 1, 1952
ORNL-1478	Period Ending January 1, 1953
ORNL-1554	Period Ending March 31, 1953

[redacted]

[redacted]

SUMMARY

PART I

HOMOGENEOUS REACTOR EXPERIMENT

The details of experimental operation of the HRE at power levels as high as 1500 kw are presented. An unexpected increase in core outlet temperature of 32°C was shown to result partly from concentration of the fuel by vapor and gas removal from the high-pressure system and partly from holdup of condensate in the low-pressure piping.

Failures of the main circulating pump and the high-pressure feed pump were experienced during this quarter. The replacement of these pumps is described.

Corrosion samples removed from the high-pressure fuel system indicated a corrosion rate of 1 mpy for a 1500-hr exposure period. This rate was in very good agreement with the rate indicated by the nickel content of the fuel solution if it is assumed that all the nickel came from the stainless steel of the high-pressure system.

An apparent shortage in fuel inventory was investigated by treating the piping and fuel storage tanks with dilute sulfuric acid followed by nitric acid. This treatment resulted in a recovery of 500 g of U^{235}, or at least one-half the apparent shortage. In order to get a more accurate fuel inventory, as well as for other reasons, the entire batch of fuel was removed for reprocessing.

The Experimental Physics Group has completed a series of calculations intended to predict the response of the HRE to reactivity changes already planned in the experimental program. It is estimated that stopping the main circulating pump with the reactor at 1000 kw will cause the fuel temperature to increase from 250 to 282°C. For such a "serious" operating error as pumping the fully concentrated fuel into the core during a startup, which might result in a continuous reactivity increase of 0.05%/sec, the resulting peak power is estimated to be only slightly greater than 1000 kw. Furthermore, it is estimated that a continuous reactivity increase of 5.7%/sec would be necessary for the power surge (2.0×10^5 kw) to result in a pressure sufficient to burst the 3/16-in.-thick stainless steel core vessel. There is no known mechanism by which a reactivity increase of such magnitude can be introduced either accidentally or experimentally.

PART II

BOILING REACTOR STUDIES

Plans have been completed for experiments on the kinetic behavior of boiling reactors to be performed on the Supo Reactor at Los Alamos during the first week in August. In the experiments, reactivity will be added to the reactor at known high rates and the power level will be recorded as a function of time. In some cases, the reactor will be boiling, and, in other cases, it will be below the boiling point before the reactivity is added.

Equipment has been completed for studying the stability of uranyl sulfate solution in stainless steel

[redacted]

[redacted]

at low oxygen pressures when boiling at 250°C.

Bubble nucleation studies have shown that supersaturation of a uranyl sulfate solution with hydrogen does not change the superheat required for nucleation of a bubble by fission within the solution. It has also been demonstrated that the nucleation by fission occurs within the bulk of the the liquid, not necessarily at the container walls.

Component parts are being assembled in the Teapot mockup. The first tests will involve the development and testing of a suitable fuel feed and dump system.

Power removal studies have been extended to 3 atm pressure. The changes resulting from increased pressure cannot be entirely explained on the basis of the model used in developing the theory reported previously. One reason for this is the increase in static pressure, and hence boiling point, with depth below the surface. This effect should be less pronounced at higher pressures.

A draft tube did not increase materially the density or circulation rate of a 6-ft-dia water system through which air was bubbled to simulate boiling.

PART III
GENERAL HOMOGENEOUS REACTOR STUDIES

Intermediate-Scale Homogeneous Reactor Design

Design data, a flow sheet, and preliminary designs for some of the equipment associated with a 50-megawatt two-region reactor for converting U^{235} into U^{233}, which would serve as a pilot plant for a power-breeder reactor, were reported previously.[1] The reactor consisted of a 4-ft-dia enriched core, containing a uranyl sulfate solution with 5 g of uranium per liter in D_2O, surrounded by a 2-ft-thick blanket containing thorium oxide in D_2O. Neutron balances were presented with estimates of the conversion ratios and the effect of blanket thickness upon the conversion ratio. Data were also given for the production of tritium from lithium alloys in the blanket.

The use of copper as an internal catalyst, estimates of the required concentration, and the effect of the copper on critical concentration and conversion ratio were discussed in ORNL-1554.[2] Use of the gas separator as an evaporator to effect concentration control was reported, and a concept was presented of the Cooling-Tower Reactor in which all the heat is removed from the reactor circulating stream by evaporation into a recirculating gas stream.

Work has continued on the flow sheets, conceptual design of the system, and components for the two-region reactor. A study of the general problems of production of economical power in aqueous homogeneous breeders has been started. The status of the conceptual design of the ISHR and some of its components and some of the nuclear data for the large breeder reactors are contained in this report.

---

(1) R. B. Briggs *et al.*, *HRP Quar. Prog. Rep. Jan. 1, 1953*, ORNL-1478, p. 23 *ff.*

(2) R. B. Briggs *et al.*, *HRP Quar. Prog. Rep. Mar. 31, 1953*, ORNL-1554, p. 31 *ff.*

[redacted]

[redacted]

Reactor Physics

Refinement of the calculations of neutron leakage from a breeder reactor of the ISHR type is in progress. Multigroup equations have been coded for the UNIVAC to enable a parameter optimization for blanket concentrations, poisoning, and processing conditions for two- and three-region reactors.

A system of dynamic equations that are similar to those used in calculating HRE kinetics has been developed for a simplified reactor model that simulates important features of the ISHR design. Among the factors to be computed are the influence of core wall thickness and the influence of size and length of the core outlet pipe on reactor safety and the effect of reactivity changes upon pressures in the core.

Engineering Development

A 4-ft pear-shaped core with flow distributing screens is being installed in the water-test facility. Tests will start in approximately one month. An alternate design, which uses vanes to distribute the flow, has been tested in an 18-in. plastic model. The 8-ft rotational-flow type of core was tested, and the theoretical predictions were confirmed. There were no stagnant regions, and the pressure drop across the core was much higher than that in the more recent straight-through types of cores.

A pipe-line gas separator which operates satisfactorily with a large vortex has been developed, and thus it will be possible to use the separator as a pressurizer. The installation of a full-scale separator in the water-test facility is under way, and tests should start in approximately one month.

Operation of the small-scale catalytic-recombiner facility has made possible the following conclusions. The reaction rate increases gradually above 300°C; increases slightly with pressure; varies with the Reynolds number, as predicted by the diffusion hypothesis; is controlled by the hydrogen or the oxygen diffusion rate, depending upon conditions; and is slightly lower with deuterium than with hydrogen.

A spark-ignited flame recombiner was operated at pressures of up to 70 psi. It operated very efficiently and without flashbacks.

The design and the cost estimate being prepared by the Allis-Chalmers Manufacturing Company for a 20,000-gpm canned-rotor pump are essentially complete. A final report is expected in approximately three months. A special "shaft seal" pump is being developed by the Worthington Corporation, and bearing tests will start about August 1.

Tentative specifications for the ISHR main circulating pump, gas blower, and heat exchanger are presented. It is expected that the 4000-gpm stainless steel loop will be completed during August. A mockup of the in-pile loop has operated satisfactorily; water was circulated at 250°C.

Controls and Instrumentation

Instrumentation for the 4000-gpm high-pressure high-temperature loop has been completed. Control and recording mechanisms for the experiments to be performed with the Los Alamos

[redacted]

[redacted]

Water Boiler have been completed. The control rod mechanism provides for the addition of reactivity at known, high rates.

Corrosion

Loop K, which has been operated at 250°C with uranyl sulfate containing 5 g of uranium per liter for approximately 7500 hr, was sectioned. The interior surfaces of the pipe were in excellent condition, with no visible evidence of pitting or corrosion even in regions of high turbulence, such as tees and orifices.

In contrast, loop I was operated approximately 2000 hr at 250°C with a solution which gives substantial localized attack, that is, uranyl sulfate containing 40 g of uranium per liter plus 25 mole % sulfuric acid. After this period, several leaks in the piping developed, so the loop was sectioned. Substantial localized attack was generally correlated with configuration.

The titanium loop was operated 750 hr at 250°C with uranyl sulfate solution containing 5 g of uranium per liter, but it is presently inoperable because of the use of the titanium impeller in a new HRE pump.

Nine, Westinghouse, Model 100A stators have been rebuilt with type 347 or type 321 stainless steel cans being used in place of the Inconel cans. A total of 24,000 operating hours has been accumulated on these pumps without a can failure even though these repaired pumps are usually used in operations involving the more corrosive solutions.

Preliminary data obtained on pin and coupon specimens in 0.02 *M* uranyl sulfate solutions at 275 and 300°C indicate that the corrosion rate of stainless steel at these temperatures is as low as that at 250°C.

Early studies of the effect of oxygen concentration gave inconclusive results when based on generalized corrosion rates as indicated by nickel analyses. Recent studies with pin and coupon specimens suggest that oxygen concentration may have a complex influence on the velocity variable.

Studies with the pin and coupon specimens have begun to establish the broad outlines of the relationship between the velocity variable and the other system variables, such as time, temperature, and concentration. While at the present time these relationships are qualitative at best, the fact that the experimental measurements are sufficiently reproducible to allow some sorting is quite encouraging. It is of even greater significance that the over-all picture which is developing indicates that there is no serious velocity effect with uranyl sulfate solutions containing 5 g of uranium per liter, even with the addition of 25 mole % sulfuric acid.

One run with oxygenated water and another run with hydrogenated water at 250°C have been carried out in the first multipass loop, M.

A simplified toroid rotator has operated with uranyl sulfate solution at 250°C for 65 hours.

A general picture of some of the details of operation and handling of the in-pile loop has been developed.

Static tests at 250°C on a number of stainless steel alloys are summarized, as are 95°C tests on various ceramic materials.

[redacted]

[redacted]

Metallurgy

The recently established procedural specifications for welding and the operator's qualification tests have been used in making welds in 1-in. and 1 1/4-in. type 347 and type 304L stainless steel plates in several combinations of base metal. Three stainless steel lime-coated welding rods - types 347, 308L, and Composition H (fully austenitic, columbium-stabilized) - were used following initial root passes made by the bare-wire heliarc method. The welds were satisfactory in x-ray and mechanical tests, and they will now be subjected to corrosion tests.

Assistance to the Dynamic Corrosion Group has included the evaluation of results of dynamic corrosion tests on a large number of previously welded pin-type specimens tested under various conditions of uranyl sulfate concentration, flow rate, temperature, and time. Although differences in corrosion behavior of different combinations of base metal and welding rod were noted, no consistent general superiority of any one combination was apparent. In the higher concentration solutions, 300 g of uranium per liter at 250°C or 40 g of uranium per liter plus 25 mole % excess sulfuric acid at 250°C, the welds in the austenitic stainless steel pins were much more seriously attacked than the base metal, except in the case of one set of pins in which the base metal contained a rather high percentage of ferrite.

Work has continued in the investigation of the relative corrosion behavior of stainless steels given various metallurgical treatments to modify the nature of the surface exposed to the corrosive environment. These include static and dynamic tests in water and in uranyl sulfate solutions. A general, but not entirely consistent, pattern has developed, which indicates a possibility that specimens exposed to the corrosive environment either in the as-machined condition or after treatment at elevated temperatures (1000 to 1150°F, and probably a still wider range) in hydrogen or helium atmospheres with a very limited moisture content are apparently less severely attacked from the standpoint of formation of surface corrosion products than specimens which are given a full anneal (1850°F) in an air atmosphere and then descaled by standard commercial methods. Efforts are now in progress to determine the cause of such behavior and, particularly, to examine the possibilities of, in the one case, accelerated corrosion as a result of chromium depletion in the outer surface of the metal directly beneath the scale formed in the high-temperature anneal and of, in the other case, a possible protective action of a thin, tenacious, diffusion-resistant barrier formed by selective oxidation in the moist hydrogen or helium.

In the investigation of titanium as a potential structural reactor material, equipment is being constructed for a study of the brittle behavior of titanium and the comparison of this behavior with that of other materials exhibiting a temperature-sensitive notch brittleness. Tests designed for the further investigation of the likelihood of increasing the brittleness of commercial purity titanium by the

[redacted]

[redacted]

introduction of hydrogen from aqueous solutions have included a large number of impact tests to compare cold-worked with cathodically treated cold-worked material. No significant differences were observed. Similar impact specimens are being subjected to vacuum annealing and dynamic corrosion testing under simulated reactor conditions.

Impact tests on specimens made from swaged arc-melted titanium sponge of exceptionally high purity, obtained from the Bureau of Mines at Boulder City, Nevada, do not indicate a ductile-to-brittle transition, even down to liquid-nitrogen temperatures. Similar low-temperature ductility was observed previously in arc-melted crystal-bar titanium. It is encouraging to note that low-temperature impact ductility can be obtained in arc-melted high-purity sponge, as well as in the far more expensive arc-melted crystal-bar material, whose behavior in this regard has been previously reported.

Assistance in the selection, procurement, and preparation of materials and specimens has been provided to the Solid State Division in its survey of the effects of radiation on notched-bar impact behavior of materials of interest to this project. A summary of information pertinent to the effects of radiation on a potential pressure vessel and other structural materials is included.

Work similar to that on titanium is in progress on zirconium and on zirconium alloys which have been received recently. This work includes a study of brittle behavior as influenced by simulated reactor conditions, suitability of zirconium for component construction, and a limited study of the mechanical behavior of two alloys whose crystal structures are of some interest.

Aqueous Solution and Radiation Chemistry

A method of acidifying uranyl sulfate solutions in closed systems under high pressure and at high temperature has been developed and demonstrated to be satisfactory. The method depends upon the addition of sulfur dioxide and oxygen to the solution. Experimental data indicate that there are no undesirable reactions in the solution and that the desired oxidation of sulfur dioxide takes place in less than 1 hr at 200°C.

A search for thorium compounds or complexes that meet the requirements of adequate solubility, radiation stability, and low neutron capture losses for a simple aqueous-solution breeder blanket has been carried out with the result that it seems unlikely that any aqueous-solution thorium blanket system using other than thorium nitrate can be found. Anion combinations of phosphate, sulfate and/or fluoride were studied, as well as other combinations, such as thorium sulfate–lithium sulfate, thorium sulfate–magnesium sulfate, thorium selenate–lithium selenate, and thorium selenate–magnesium selenate.

Further in-pile static bomb tests provided additional data on corrosion rates at various power densities. Interpretation of the results awaits completion of tests now planned.

Related Chemistry Research

A refinement in the calculated value of the neutron-capture cross section of Pa^{233} for thermal reactor

[redacted]

[redacted]

[redacted]

neutrons resulted in a considerably higher value of 150 ± 15 barns.

The buildup of U^{234}, U^{235}, and U^{236} in a U^{233} breeder reactor and the resulting effects on neutron economy and total uranium concentration have been calculated.

The studies of fundamental chemistry of corrosion and its inhibition indicate that tungsten, as well as technetium, shows good inhibitory behavior in the corrosion of SAE 1010 carbon steel under the relatively low-temperature conditions of the test.

Slurry Chemistry

Studies on the effect of ignition temperature on the abrasive properties of slurries prepared from calcined thorium oxalate are encouraging in that a thoria slurry produced by calcination at 500°C and four days of hydrolysis in water at 250°C was much less abrasive than a slurry of the Ames oxide that was sieved through a 325-mesh screen but not hydrolyzed at 250°C. The effect of ignition temperature on the x-ray diffraction pattern and particle size of the residual thoria from oxalate decompositions is also being investigated.

A thorium oxide slurry produced from freshly precipitated and undried thorium hydroxide by hydrolysis in water at 250°C for 64 hr has proved to be nonabrasive to stainless steel. However, the high settled volume of the slurry indicates that the thorium content of a usable slurry prepared in this way may approximate 500 g/liter.

Oxides prepared by calcination exhibit low settled volumes (1500 to 2000 g of thorium per liter) upon hydrolysis in water at 250°C. Slurries prepared by the hydrolysis at 250°C in water of either the hydroxide or the carbonate show low bulk densities or high settled volumes (300 to 500 g of thorium per liter).

Autoclaving thorium oxide at 250°C in water with uranium in the form of either UO_2CO_3, UO_2SO_4, or UO_2F_2 and at low uranium-to-thorium ratios resulted in the production of a refractory mixed oxide of the uranium with thoria. The addition of NaF or LiF to a slurry of the mixed oxide and hydrolysis in water at 250°C under CO_2 pressure was efficacious in leaching the uranium from the mixed oxide.

A radiation experiment in which thorium oxide pellets were irradiated for three weeks in the LITR at room temperature and at a thermal-neutron flux of 5×10^{12} n/cm^2·sec resulted in some breakage which may have been due to inferior preparation of some of the pellets. If the pellets are to be given serious consideration for use in a blanket, further studies on the preparation of and the radiation damage to the pellets are indicated.

Physical Studies of Slurries

Preliminary evidence now indicates that the lower abrasiveness of thorium oxide made by calcining at lower temperatures is due to the presence of undecomposed thorium oxalate.

Three materials have been found which appear to withstand the abrasive action of thorium oxide slurries: hard chrome plate on stainless steel, Stellite, and oxidized zirconium.

The thermal conductivity of thorium oxide slurries has been computed by using new data on the conductivity of the solid.

[redacted]

[redacted]

Thorium hydroxide sols have been found to decompose at 250°C. Several additives were tried in unsuccessful attempts to stabilize the sols at the high temperature.

Combined thorium-uranium oxide particles have been produced and found to be inseparable in water at 250°C.

Hard chrome plating of the pump cans in a Richardson-Frithsen pump minimized abrasion in the upper can by thorium oxide slurries at 150°C, but the lower can was severely perforated by abrasion. This may have been caused by chrome flakes and corrosion products from the water rotor.

A second loop for uranium slurries is now in operation at 250°C after several modifications of the pressurizer connection. Preliminary results indicate little, if any, plating out of solids in the system.

The addition of $Ni(NO_3)_2$ to a uranium oxide slurry to stabilize the rod (alpha) form of $UO_3 \cdot H_2O$ at 250°C proved to be ineffective.

Uranyl carbonate was found to decompose at 250°C in spite of high CO_2 pressures (600 to 800 psi).

Based on a run lasting about 100 hr, uranyl phosphate slurry appears to offer no corrosion, stability, or abrasion problems.

Magnesium diuranate slurries were found to plate out in the pressurizer.

It was found that PbO will not prevent U_3O_8 from being oxidized at 250°C.

The solubility of CO_2 in water has been measured.

Chemical Processing

As now envisioned, fuel processing of a two-region, aqueous, homogeneous, breeder reactor would consist of the removal of rare earths and insoluble fission products from the fuel solution by an inorganic adsorbent. A more complete cleanup of the fuel solution would be accomplished by periodically sending a portion of the fuel through the blanket-processing plant. The blanket-processing plant would use the Thorex process to isolate uranium and thorium for return to the reactor. This combination of processes will give an economically feasible method of keeping the neutron losses low and the fuel solution chemically clean.

Of the adsorbents tried at both the Vitro Corporation and ORNL, calcium fluoride still appears to be the most promising. The solubility of calcium sulfate, which is formed by the reaction of rare earth sulfates with calcium fluoride, in fuel solution was found to be only 0.13 mg/ml at 250°C. Since this solubility is appreciably greater at lower temperatures, an adsorption process using calcium fluoride must be operated near 250°C to avoid precipitation of calcium sulfate inside the reactor. The testing of this adsorption process on a continuous basis at 250°C has not yet been successfully carried out because of uranium precipitation. This precipitation of uranium apparently is not due to the presence of calcium fluoride, but rather to hydrolysis and reduction in the stainless steel equipment.

[redacted]

[redacted]

A material suitable for packing a calcium fluoride adsorption column has been prepared by fusion of reagent-grade calcium fluoride in an inert atmosphere and by a cold, hydrostatic-pressing procedure.

Based on an optimized scheme of blanket processing by Thorex and fuel processing by both calcium fluoride adsorption and in the blanket-processing plant, the total cost of processing a two-region U^{233} breeder reactor is estimated to be 1.3 mills per kilowatt-hour for 3% poisons in the core. For 5% poisons, the cost will be less than 1 mill per kilowatt-hour. The estimated cost of processing a one-region reactor is about 30% less on the same basis.

[redacted]

[redacted]

CONTENTS

[redacted]

Part I

HOMOGENEOUS REACTOR EXPERIMENT

HRP QUARTERLY PROGRESS REPORT

STATUS OF THE HRE

S. E. Beall, Section Chief

S. Visner, Experimental Physics Group Leader

J. J. Hairston J. W. Hill, Jr. T. H. Thomas
Operations Group Leaders

D. I. Eissenberg S. I. Kaplan
V. K. Paré P. M. Wood
Reactor Engineers

T. E. Haynes J. A. Watts W. B. Krick
A. L. Johnson G. H. Johnstone J. D. Jones
Technicians

OPERATION AT HIGH POWER

As reported, a second run was made at high power at the close of the previous quarter. The power and temperature behavior of the reactor on March 18, 1953 have since been analyzed, and the data are shown in Fig. 1. During the 11-hr period of operation, the reactor was controlled solely by power demand without the need of any conventional mechanism for reactivity control. From the standpoint of nuclear stability and control, the behavior of the reactor appeared to be satisfactory. The only short-term variability in power level – and this was no more than 2% in amplitude – appeared to be attributable to the operation of the let-down system which discharges a mixture of gas and fuel solution from the reactor core to the dump tanks.

From 4:30 to 5:15 PM, the reactor power was well in excess of the design figure of 1000 kw. In fact, a power level of 1500 kw was reached, and thus the operability of this type of reactor at an average power density of 30 kw/liter was demonstrated. The limitation which became apparent at this power level was an excessive increase in pressure in the low-pressure off-gas system because of pressure drop across a flow-measuring orifice and the burner nozzle in the flame recombiner. The pressure in the first gas condenser, where a minute leak is present, must be maintained below atmospheric to prevent the escape of radioactive gases to the cooling water. Another possible limitation is the temperature of the flame recombiner, which had reached 630°C at the time the power was decreased.

The temperature behavior of the reactor is of special interest since it is a measure of the reactivity changes. As was expected and demonstrated during the first power run, the temperature rise of the fuel solution from core inlet to outlet is proportional to the power level, that is, roughly 32°C for 1000 kw. For rapid changes in power level, requiring no more than 1 min, the core outlet temperature remains fairly constant and the inlet temperature changes in an appropriate manner. If the reactivity associated with gas in the core is as small as is anticipated, 0.5% at 1000 kw, the conclusion is that the effective nuclear temperature in the core is very nearly equal to the outlet temperature.

There is, in addition, a longer term variation of both inlet and outlet temperatures with power level, which is only apparent after a time

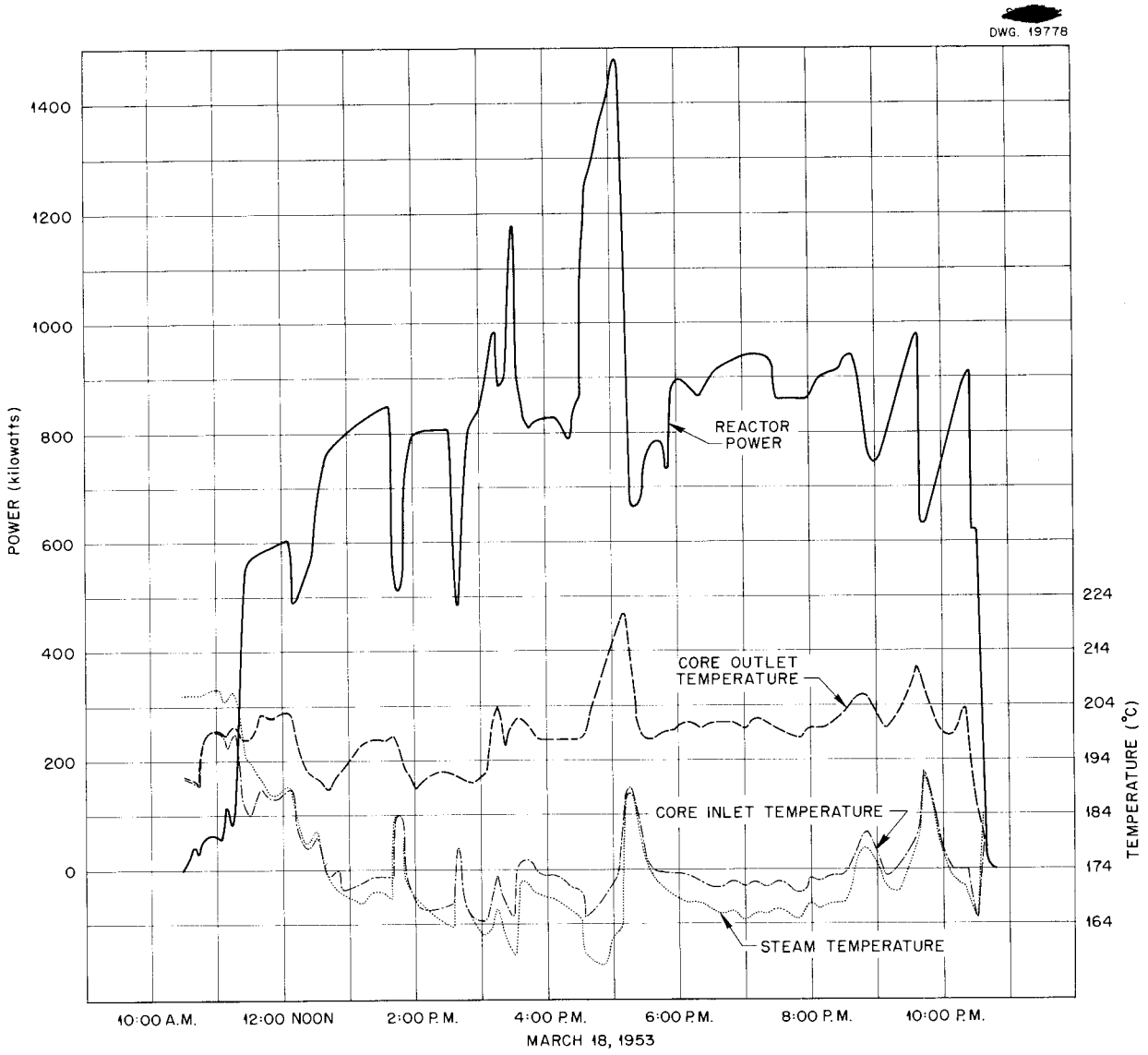

Second Power Run on H. R. E., March 18, 1953.

Fig. 1. Second Power Run on HRE, March 18, 1953.

lag of several minutes. For sufficiently large power increases, both temperatures increase and reflect an increase in reactivity, which is solely attributable to the power level. The change in core outlet temperature of 20°C associated with the power increase from 800 to 1500 kw corresponds to 2% in k_{eff}. Except for a temporary increase of 2 kg between 3:00 and 3:20 PM, the condensate holdup in the weigh tanks remained constant between 12:00 noon and 10:20 PM. None of the other reactivity controls were used during this period. As is explained in more detail in the next section, the bulk of the increase in reactivity results

from a fuel concentrating effect in the core that is due primarily to the dissociation of water and the removal of the wet gas. There is, in addition, a variation of condensate holdup in the lines in the off-gas system with variation in pressure drop, this effect being also in the direction of increasing the fuel concentration with increasing power.

Concentration Effect in Core Due to Gas Removal. As a result of the dissociation of the water in the fuel solution in the core and the removal of the decomposition gases, the concentration of fuel in the core becomes higher than that in the dump tanks. Solution is continually transferred from the dump tanks to the high-pressure system at a rate of about 1 gpm by means of a pulsafeeder pump. Sufficient solution is let down along with gas to maintain a constant level in the pressurizer stem above the core vessel. If f is the rate at which solution enters the high-pressure system, g is the rate at which gas and vapor leave, and γ is the ratio of solution mass in the high-pressure and low-pressure systems, it can be easily shown that the fractional increase in concentration of the high-pressure system at equilibrium, Δ^0, is given by

$$(1) \qquad \Delta^0 = \frac{g}{f(1+\gamma) - g} .$$

The time dependence of the fractional increase in concentration of the core, Δ, is

$$(2) \qquad \Delta = \Delta^0 \, e^{-t/\tau} .$$

Letting M_H and M_L be, respectively, the mass of solution in the high-pressure and low-pressure systems, the time constant is

$$(3) \qquad \tau = \left(\frac{M_H + M_L}{M_H M_L} f - \frac{g}{M_H} \right)^{-1} .$$

As an example, the concentration increase will now be calculated for the HRE operating at 1500 kw, 1000-psi pressure, and 220°C core outlet temperature:

$$g = 0.23 \text{ kg/min of gas} + 0.21 \text{ kg/min of steam} = 0.44 \text{ kg/min} ,$$

$$f = 3.0 \text{ kg/min} ,$$

$$M_H = 60.5 \text{ kg} ,$$

$$M_L = 28.0 \text{ kg} ,$$

$$\gamma = 60.5/28.0 = 2.16 .$$

The fractional increase in core concentration at equilibrium is then 0.049, and the time constant is 6.7 minutes. This increase in core concentration corresponds to an increase in k_{eff} by 1.6%, which requires a rise in temperature of 16°C. As noted earlier, there is also an additional concentration effect from the increased holdup of condensate in the off-gas system. At 1500 kw, the known holdup is about 1 kg, which corresponds to about 1% in concentration, or a 30°C temperature rise. Thus, the total temperature rise accounted for is 19°C, or two-thirds of the observed 32°C rise in core outlet temperature. The remainder of the rise may be due to other effects associated with reactor power or to the uncertainty in the values used for the pulsafeeder flow and solution mass in the low-pressure system. Further tests are planned for studying the effect.

Following the 1500-kw run, reactor operation was suspended because of an electrical failure of the fuel-circulating pump. In spite of a 50-r/hr radiation field at the pump, it was possible to remove and replace the unit by using extended (15 ft long) tool handles and temporary shielding of adjacent reactor components. The work consisted primarily of uncoupling and reassembling four 2500-psi ring-gasket flanges on 1 1/2-in. schedule-80 pipe lines, and it required about 350 man-hours.

At the time of the 1500-kw power run, there was an indication that several hundred grams of U^{235} was not available to the reactor core because of precipitation, leakage, or holdup in other parts of the system. After the new fuel circulating pump was installed, this apparent reduction in inventory was investigated. The entire reactor piping system was treated with 0.1 *M* H_2SO_4 in an attempt to dissolve any uranium precipitated as UO_3. However, only 15 g of uranium was recovered, and therefore the sulfuric acid treatment was followed by a 5% nitric acid wash to dissolve any precipitate present as U_3O_8 or UO_4. Although only an additional 30 g of uranium was recovered from the reactor system, approximately 350 g more appeared in the waste storage tank when the acid wash was received, which indicated that a precipitate or holdup had been present there. After recharging the original fuel into the reactor, the inventroy indicated a gain of approximately 100 g; thus the total recovery was nearly 500 grams.

In the process of transferring the nitric acid wash to the waste storage tank, several liters of the dilute acid leaked past a valve into the fuel storage vessel and thus contaminated the fuel solution with sufficient acid to cause concern from the standpoint of corrosion. It was decided to remove the fuel for chemical reprocessing and to resume operation with a new, clean charge of fuel.

Removal of the highly radioactive fuel was accomplished by first evaporating it to a concentration of about 150 g/l to reduce the volume and then filling 10-liter, evacuated, ever-safe containers that were shielded by 4 in. of lead. The activity at the surface of the cans was 600 r/hr and at the surface of the shield, 0.5 r/hr. The total time consumed by these operations was seven days.

In making preparations for a resumption of reactor operation, it was learned that the recently installed circulating pump had ceased to operate because of an electrical short circuit, and it was necessary to obtain and install a replacement. Since this pump had operated only 100 hr with mildly radioactive solutions, it was possible to cut it apart for examination.

The failure had resulted from one wire of the stator winding contacting the metal sleeve between the stator and the rotor. The pump was one which had failed previously and had been repaired at the Y-12 shops by rewinding the stator. The repair technique has been improved since that early repair, and it is not expected that more recently overhauled pumps will fail in the same manner.

Soon after the new circulating pump was put into operation, trouble was experienced with the pulsafeeder fuel-feed pump. The symptoms were recognized as indicating a bad suction check valve, and it was necessary to remove the pulsafeeder assembly, which is located at the lowest point in the fuel cell, approximately 25 ft below the top of the shield. The radiation level at the pump assembly was greater than 20 r/hr, and at the top of the shield where removal was accomplished with long-handled tools, the level was approximately 100 mr/hr. Disassembly of the pump showed that one of the two Stellite balls in the suction check was actually mild steel, which had corroded from 1 in. in diameter to approximately 1/4 in. in diameter. This size was sufficiently small to allow the ball to drop through its seat and jam the second ball check located immediately below. Of course, when this happened, the suction check valve ceased to function. The only explanation for the presence of the steel instead of Stellite is that at some point in the fabrication of the

check valve assembly a steel ball was erroneously substituted. Four weeks have been spent to date on the very difficult job of installing the new pulsafeeder assembly.

During the past quarter it has been possible to examine the over-all corrosion picture of the HRE in some detail. Furthermore, while the system was shut down for removal of the circulating pump, corrosion test specimens which had been exposed since January 1952 were removed and examined. Corrosion rates were estimated from the weight losses of the type 347 stainless steel specimens and also on the basis of the total nickel dissolved from the stainless steel of the high-pressure circulating system. Exposure time was based on the hours of operation at above 150°C, without correction for the possibly higher rate of attack during power operation. For the period from January 1952 to April 1953, the coupon weight loss indicated a corrosion rate of 1.0 mpy, and the nickel pickup of the fuel solution also showed a rate of 1.0 mpy. For the period from July 1952 to April 1953, test-specimen weight loss gave a corrosion rate of 2.8 mpy, while nickel pickup indicated 1.6 mpy. No pitting was observed on the coupons. The agreement and the low levels of these rates are very encouraging.

Future Program. One of the major uncertainties in the development of homogeneous reactors is the effect of radiation on corrosion. With the HRE as the only available large-scale facility for investigating this phase of the corrosion picture, emphasis has been centered on using the HRE to obtain more information on the effect of radiation damage. As a result, the program for the HRE has been revised to include a full-scale corrosion experiment as the next order of business. In order to establish a good corrosion baseline, plans now call for operating the reactor with a 40 g/l natural uranium solution at 200°C for two weeks, or until consistent corrosion data are obtained.

The natural uranium run will also allow a complete material balance to be repeated to provide additional information that there is no undetected leakage of solution from the reactor system at the present time. Following the natural uranium experiment, enriched fuel will be charged into the system, and a run will be made under conditions the same as those for the natural uranium run. The corrosion rate with enriched uranium at zero reactor power should be no different from that determined with the natural uranium. After verification of this, the power will be raised to 1000 kw and held there until the corrosion rate can be accurately established. Upon completion of the high-power run, the reactor power will be decreased again to a low level, and operation will be continued to see whether the previously determined low-power corrosion rate can be repeated. Although the total surface area which is likely to suffer radiation damage is only 7% of the total area undergoing corrosion, statistical analysis indicates that a two- to threefold increase in the corrosion rate of the core as a result of radiation effects should be detectable.

After the corrosion data are obtained, a series of experiments will be performed[1] to determine the reactivity changes associated with power level as a result of mixing in the core, gas residence, and concentration of the fuel solution in the core because of water dissociation. If it is not feasible (because of the radioactivity of large samples) to follow reactivity changes by fuel sampling during high-power operation,

[1] S. Visner, *Experimental Program for HRE at High Power. Part I. Core Mixing, Gas Coefficient of Reactivity, and Concentration Effect in Core*, ORNL CF-53-5-45 (May 7, 1953).

the core outlet temperature, in conjunction with the known temperature coefficient, will be used as a measure of reactivity. The three effects listed earlier will be reflected in a deviation of the core outlet temperature, T, from the temperature at "zero" power critical, T_c, which is then identical to the inlet and outlet temperatures. Since the temperature rise in the core, ΔT, is proportional to the power level, it can be postulated that

$$T = T_c + \Delta T\left(E - \frac{g}{p_{ex}} + b_1 + \frac{b_2}{p_{ex}}\right) ,$$

where

$p_{ex} \equiv$ the excess pressure,
$g \equiv$ gas coefficient of reactivity in terms of equivalent temperature change,
$b_1 \equiv$ core concentration coefficient, which is pertinent to the mass rate of gas removal,
$b_2 \equiv$ core concentration coefficient, which is pertinent to the volume rate of gas removal,
$E \equiv$ core mixing parameter.

The variables to be investigated are the power, excess pressure, fuel mass, and pulsafeeder pumping rate. For sufficiently rapid changes in power level and pressure, the response of the reactor will be independent of the concentration effect.

Another group of experiments (see below) is planned for the purpose of checking the kinetic response of the reactor to reactivity changes which are externally induced. The objective is to demonstrate further the self-regulatory feature of the reactor from the point of view of safety and control. The findings should be particularly applicable in facilitating the startup and operation of large-scale homogeneous reactors.

It is also planned to study the feasibility of the copper ion as a homogeneous catalyst in a circulating system.

EXPERIMENTAL PHYSICS PLANNING

S. Visner V. Paré

Estimated Effect of Stopping the Fuel Circulating Pump. A calculation has been made of the power and temperature behavior in the event the fuel circulating pump should stop while the HRE is operating at 1000 kw and an outlet temperature of 250°C.[2] As a result of the decrease in cooling, from lack of circulation, the core temperature will rise and the power will decay. A reasonably good estimate is obtained by noting that the heat production from the fission products is approximately equal to the cooling by conduction to the reflector and by convection flow to the heat exchanger. The asymptotic temperature rise in the core, S_m, is then obtained rigorously from the usual kinetic equations for the HRE that are based on the constant pressure model:

$$(4) \qquad S_m = \left[2\alpha\epsilon P_0\left(\delta + \frac{\beta}{\bar{\lambda}}\right)\right]^{1/2} ,$$

where $\beta/\bar{\lambda} = \sum_i (\beta_i/\lambda_i)$, α is the magnitude of the temperature coefficient of reactivity, ϵ is the heat capacity of the core, P is the reactor power, δ is the prompt-neutron generation time, and S is the deviation in core temperature from the initial value. The initial power, P_0, is 1000 kw.

The value of S_m is 25.5°C for the HRE at the given operating conditions. An additional 6.3°C should be added to account for the initial temperature rise which compensates the reactivity increase resulting from collapse of the vortex and recovery of delayed-neutron emitters when the pump stops. The total temperature increase is then 31.8°C and the final temperature is 282°C, which should not be excessive.

[2] S. Visner, *HRE Power and Temperature after Stopping Pump*, ORNL CF-53-5-208 (May 28, 1953).

The kinetic equations can be simplified by equating the reactor power to the product of the prompt multiplication and the delayed neutron source, and replacing all the delayed-neutron groups by a single group of mean life $\bar{\lambda}$. Analytic solutions are then obtainable for the time dependence of the power and temperature:

$$(5)\quad (S_m - S)^{1+(\beta/\alpha S_m)} (S_m + S)^{1-(\beta/\alpha S_m)} = S_m^2 e^{-\bar{\lambda}t},$$

$$(6)\quad P = \frac{1}{\beta + \alpha S}\left(\beta P_0 - \frac{\bar{\lambda}\alpha S^2}{2\epsilon}\right).$$

The reactor fission power and temperature are shown in Fig. 2 for the 30 sec following the stopping of the pump. The power remains at 1000 kw for the first second because the reactivity increase which results from stopping the pump roughly compensates for the decrease in power demand by the heat exchanger during this time.

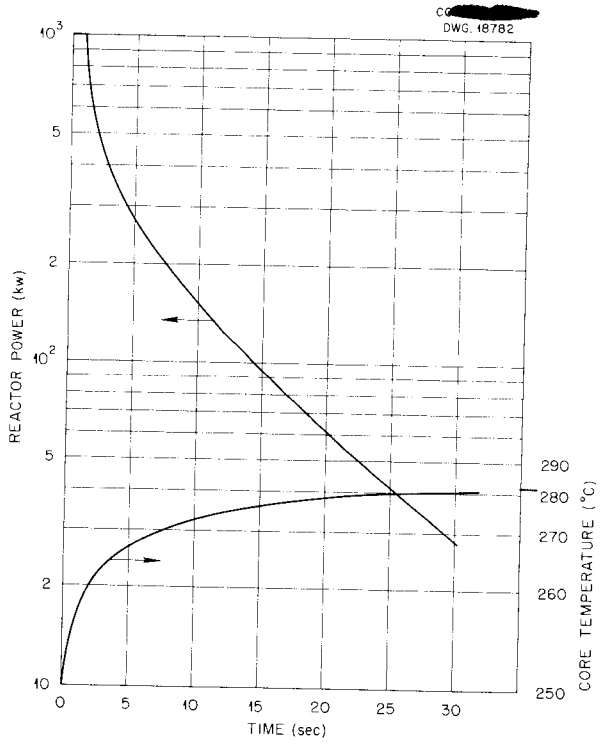

Response of H. R. E. to Stopping of Fuel Circulating Pump.

Fig. 2. Response of HRE to Stopping of Fuel-Circulating Pump.

Estimated Response of HRE to Reactivity Increases at Low Initial Power. In connection with proposed experiments on reactor kinetics, calculations[3] of an approximate nature have been made to predict the power response to reactivity changes which can be realistically attained in the HRE. These calculations are intended to supplement earlier calculations that were primarily concerned with sudden increases in reactivity at design operating power. Step increases in reactivity are not readily available, but continuous increases that are large both in magnitude and rate are possible. At high power, nothing startling is expected to result, since continuous increases in reactivity are easily absorbed by the reactor through an increase in power level by a factor of 2 or 3.

At very low initial power, the situation is less favorable from a safety standpoint, because the power must rise by as many as five or six factors of 10 before it begins to compensate for even a moderate rate of increase of reactivity. In this time, considerable reactivity can be introduced. Therefore, to provide stringent tests of the safety of the reactor, much of the proposed experimental program on the HRE kinetics consists of experiments involving low initial power. The approximate calculations presented here were made to predict the results of these experiments, with most attention being given to the peak power. The HRE simulator cannot be used for these problems because the maximum range of power variation which it can compute accurately is only two decades.

---

[3] V. K. Paré, *Estimated Response of HRE to Reactivity Increases at Low Initial Power*, ORNL CF-53-6-147 (June 18, 1953).

Zero power extraction is assumed throughout, the reactor being held initially at 200°C by external heating. Any cooling during the experiment is considered as a continuous reactivity increase, and the expansion of the core liquid is assumed to take place at constant pressure. The reactivity effect of decomposition gases in the core is not considered. Two types of experiments are distinguished: (1) The operator introduces a predetermined amount of reactivity and stops the increase *before* the power rises to a level at which appreciable heating occurs. (2) The externally imposed reactivity increase is linear in time (a "ramp") and *continues* through the maximum power phase of the power transient.

In case 1, after the operator has stopped adding reactivity, the power quickly approaches an exponential rise on the stable period that is appropriate to the total reactivity introduced. The subsequent behavior is essentially independent of the initial power and of the manner in which the reactivity is added, and the problem can therefore be analyzed as though a reactivity step had occurred at low power. Case 2 is more complicated in that heating compensates for some of the reactivity as it is introduced; so the reactivity actually achieved depends on the "ramp rate," $d\delta/dt$, and on the initial power. The maximum reactivity occurs when the rate of production of negative reactivity by heating is equal to the ramp rate.

Case 1 can be calculated by the method used above to obtain the temperature rise after stopping the fuel circulating pump; this method is applicable when there is no cooling or other external addition of reactivity while the power is varying. The procedure is to replace the initial reactivity by an equivalent decrease in temperature, S_0, and to replace the delayed-neutron groups by one equivalent group. Two approximations for the power that are dependent on whether the reactor is below or above prompt critical can then be obtained:

$$P = \frac{\lambda[(\alpha S_0)^2 - (\alpha S)^2]}{2\alpha\epsilon(\alpha S + \beta)}, \qquad |\alpha S_0| < \beta ; \tag{7a}$$

$$P_{max} = \frac{\lambda}{\alpha\epsilon}\left\{\beta - [\beta^2 - (\alpha S_0)^2]^{1/2}\right\}, \qquad |\alpha S_0| < \beta ; \tag{7b}$$

$$P = \frac{2(\alpha S_0 + \beta)^2}{\alpha\epsilon\delta} \frac{e^{[(\alpha S_0+\beta)/\delta]t}}{\left\{1 + e^{[(\alpha S_0+\beta)/\delta]t}\right\}^2}, \qquad |\alpha S_0| > \beta ; \tag{8a}$$

$$P_{max} = \frac{(\alpha S_0 + \beta)^2}{2\alpha\epsilon\delta}, \qquad |\alpha S_0| > \beta . \tag{8b}$$

Equations 8*a* and 8*b* follow easily from Stein's earlier results[4] with $t = 0$ at prompt critical. The time behavior of the temperature in Eq. 7 is obtained from Eq. 5 with S_m replaced by S_0 and with $t = 0$ at delayed critical. Figure 3 is a plot of P_{max} obtained from Eqs. 7*b* and 8*b* vs. the reciprocal

[4] *Homogeneous Reactor Experiment Feasibility Report*, ORNL-730, p. 64-78 (Aug. 15, 1950).

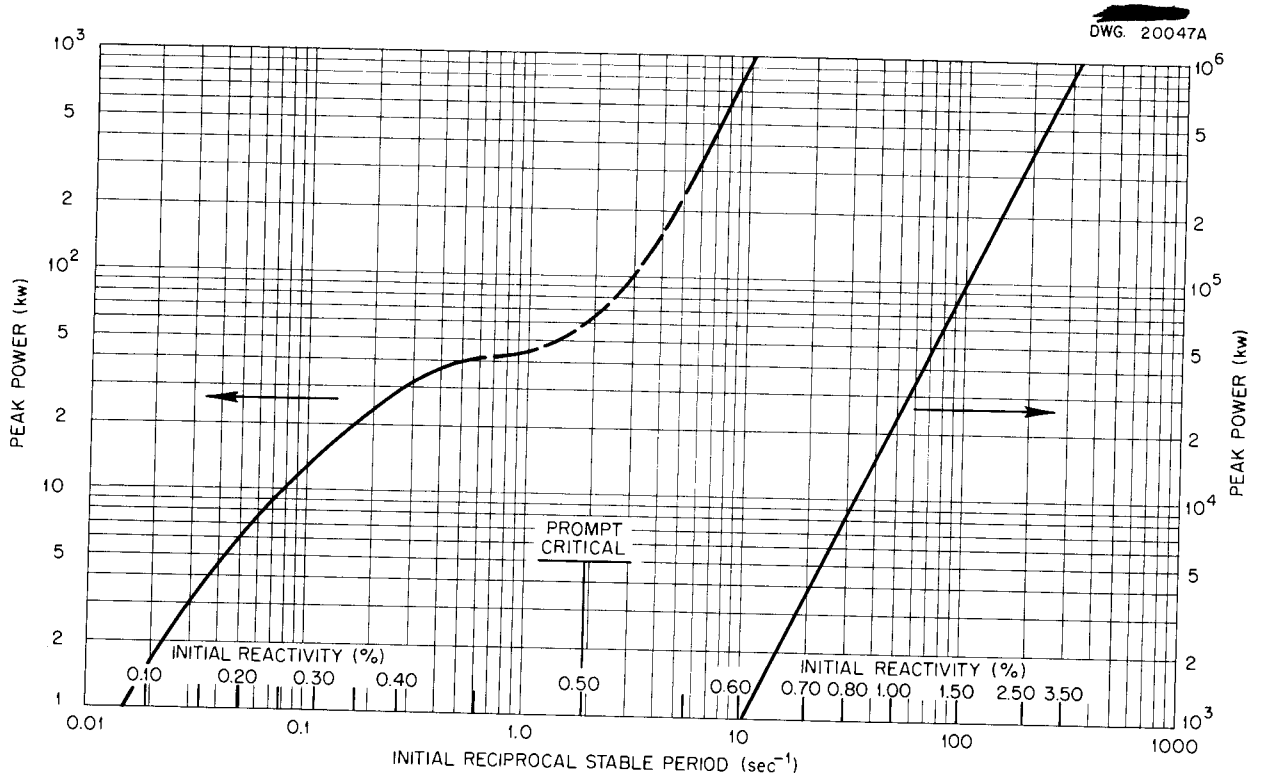

Fig. 3. Calculated Peak Power vs. Initial Reciprocal Stable Period for a Reactivity Step at Low Power in HRE at 200°C Without Power Extraction.

stable period calculated from the initial reactivity on the basis of one group of delayed neutrons.

In case 2, it is necessary to calculate the variation of the power while the reactivity is changing. No solution is available that does not, in general, require numerical integration, but a step toward such a solution can be taken by finding the response, without temperature coefficient, to a ramp, or linear increase in reactivity. Neglecting the temperature coefficient is valid as long as the power is appreciably below that required to compensate for the ramp.

An approximate solution obtained by Hurwitz[5] can be readily applied to this situation, since the second time derivative of the prompt multiplication factor can be neglected for reactivity changes that are not too rapid:

$$\frac{P}{P_0} = \eta\, e^{z/a} \quad , \tag{9}$$

where η is essentially the prompt multiplication factor, a is the ramp rate, and z/a is the time integral of the reciprocal stable period. Curves of P/P_0 vs. reactivity up to prompt critical are shown in Fig. 4 for various ramp rates.

For each curve, the power, P_e, required to compensate for the ramp by heating is indicated. It would be expected that these curves would be reasonably accurate as long as the reactor power was a decade or more below P_e. For cases in which P_e is reached below prompt critical, no

(5) H. Hurwitz, Jr., *On the Derivation and Integration of the Pile-Kinetic Equations*, AECD-2438 (Jan. 4, 1949).

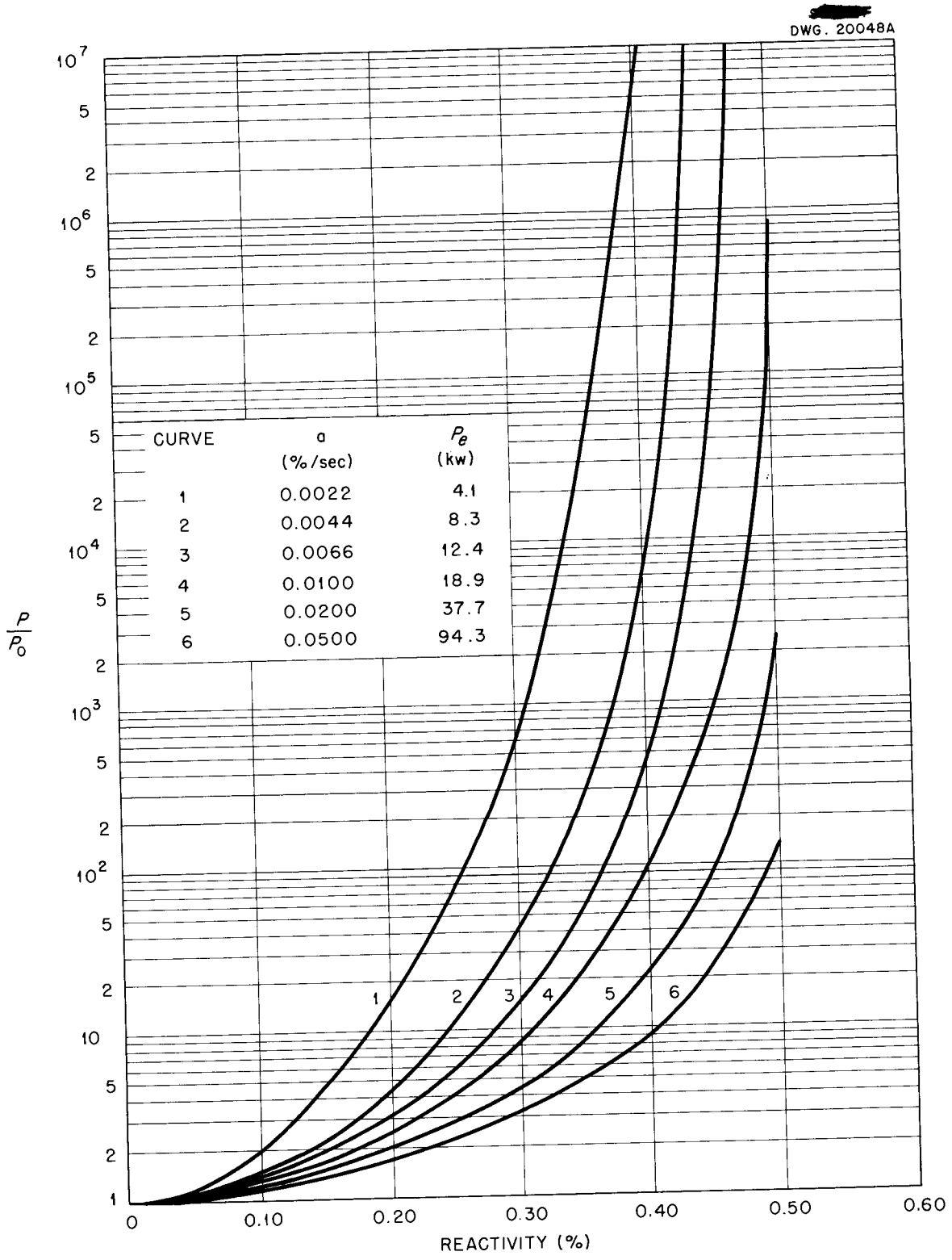

Fig. 4. Calculated P/P_0 vs. Reactivity for Ramps in HRE. No temperature coefficient; one delayed-neutron group.

method of calculating the maximum power has yet been found, but an upper limit for the power excursion can be found by assuming that the maximum reactivity achieved is that which corresponds to P_e on the curves of Fig. 4. Actually, the effect of the temperature coefficient of reactivity will be to steepen the curves; so P_e will be reached at a lower reactivity than that shown. The reactivity read from Fig. 4 is substituted into Eq. 7b to get P_{max} for a step increase of that amount at low initial power, and then P_e is added to take care of the additional reactivity introduced by the ramp after P_e is reached. The results are plotted in Fig. 5 as the portions of the curves below a = 0.015%/sec.

In the more dangerous cases in which the reactor goes prompt critical at a power P_{pc} that is well below P_e, a much better estimate is available. The power at prompt critical is taken as the initial power for a calculation that neglects delayed neutrons, uses the same ramp rate, and includes the temperature coefficient. Stein's solution for P_{max} for this case is[5]

$$(10)\quad P_{max} - P_{pc} = \frac{a}{\alpha\epsilon} \ln\frac{P_{max}}{P_{pc}} = P_e \ln\frac{P_{max}}{P_{pc}} .$$

Usually, $P_{pc} << P_{max}$, so it can be neglected on the left side of the equation. P_{pc} is given by Eq. 9 as

$$\eta_{pc} P_0 e^{z_{pc}/a} ,$$

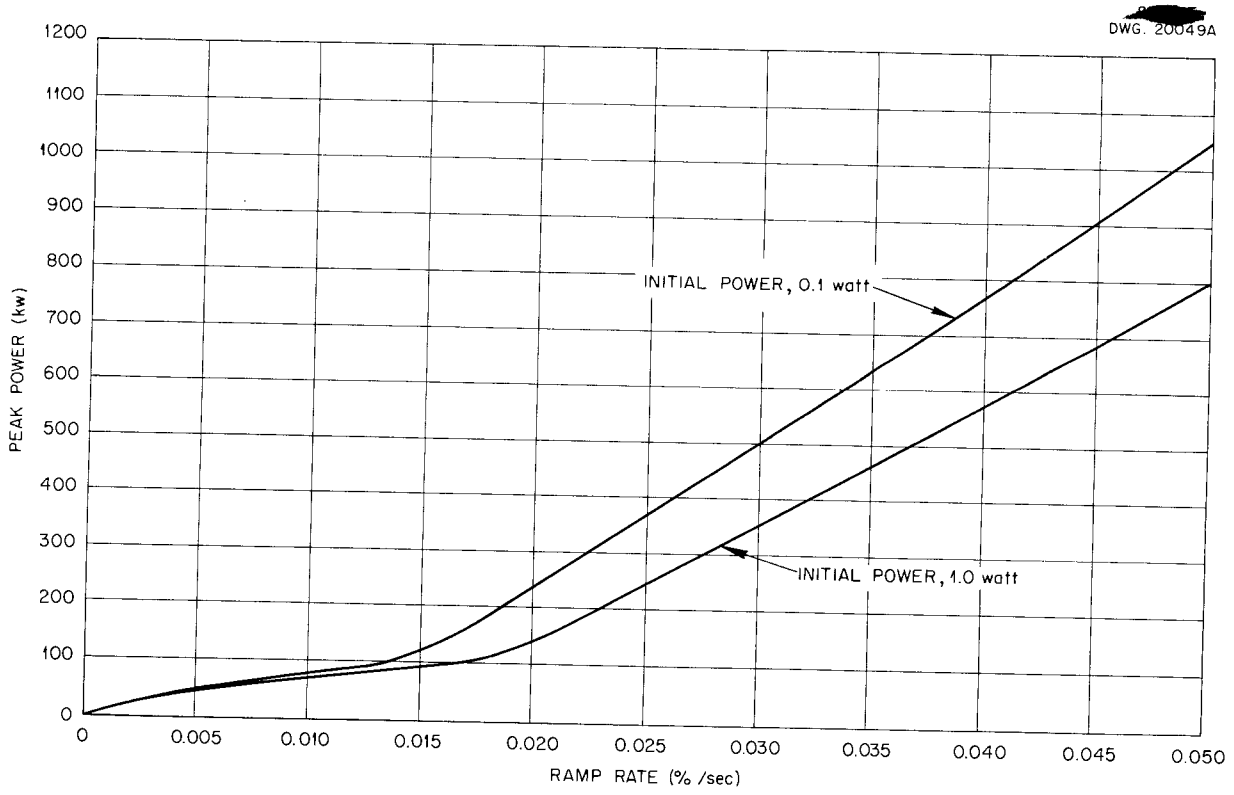

Fig. 5. Calculated Peak Power vs. Ramp Rate for HRE at 200°C Without Power Extraction.

and, if this is substituted into Eq. 10, the result is

$$(11) \qquad a = \frac{\alpha\epsilon P_{max} + z_{pc}}{\ln \frac{P_{max}}{\eta_{pc} P_0}} .$$

The function a is plotted as the upper portion of the curves in Fig. 5; it is almost linear because of the slow variation of $\ln P_{max}$. Curves are given for $P_0 = 0.1$ and 1.0 watt to show the effect of varying the initial power.

It is expected that the results obtained in these estimates may come within a factor of 2 of the exact solutions to the equations. They are useful in planning experiments and in considering new reactor designs, since they lend themselves to quantitative evaluation and make clear the effect of varying parameters. After kinetic experiments have been performed on the HRE, more accurate calculations may be made by numerical methods to determine how closely the equations describe the reactor behavior.

Calculated Core Pressures for Power Excursions. In a consideration of the nuclear safety of the HRE, probably the most important factor is the peak pressure that may develop in the core during a power excursion. The increase in core pressure arises from the expansion of the liquid upon heating, which, in the process of decreasing the reactivity, forces fuel out of the core and up through the relief pipe into the pressurizer. Sufficient pressure must be developed in the core to overcome the inertia and frictional drag of the fuel solution in the pipe. In the course of the planned experiments, it will be possible to observe the power variations but not the pressure, and, although considerable uncertainty may be allowed in predicting the power response, it is necessary that the pressure be calculated as accurately as possible. Fortunately, the pressure can be related to the observed power in a simple manner. Earlier calculations[6,7] of core pressures are pertinent to the old pressurizer stem design, which was subsequently changed to improve the damping characteristics for hydraulic oscillations. The damping coefficient was re-evaluated by Aven and Trammell.[8]

Short formulas have been obtained by Stein and Welton by simply assuming that the pressure developed does not affect the fuel density. It follows, since the rate of flow of fuel to the pressurizer is proportional to the excess power, that the peak pressure resulting from friction occurs at the peak power and that the peak pressure resulting from inertia occurs when the time derivative of the power is a maximum. For the case of the old pressurizer design, Sangren[7] compared short-formula calculations of peak pressures with the numerical solutions of the complete system of kinetic equations, and the former were shown to be consistently low by a factor of about 2. This discrepancy arises because the short formulas do not take into account the fact that the fuel solution is compressible and that therefore the Helmholtz resonator, consisting of the core and relief pipe, is shocked into oscillation.

In the present calculations, the peak pressures are obtained with the short formulas, and, in addition, an improved estimate of the inertial pressure is obtained from the peak power by an iterative type of solution of the equation for $\overline{\rho}$, the deviation of the density from its equilibrium value,

$$(12) \qquad \ddot{\overline{\rho}} + K_1\dot{\overline{\rho}} + K_2\dot{\overline{\rho}}|\dot{\overline{\rho}}| + \omega_H^2\overline{\rho} + \omega_H^2 bS = 0 ,$$

---

(6) *HRE Quar. Prog. Rep. Feb. 28, 1950*, ORNL-630.

(7) W. C. Sangren, *Kinetic Calculations for Homogeneous Reactors*, ORNL-1205 (Apr. 1, 1952).

(8) R. E. Aven and G. T. Trammell, *HRP Quar. Prog. Rep. Nov. 15, 1951*, ORNL-1221, p. 79.

where K_1 and K_2 are constants associated with the frictional pressure drops and have the values 3.032 sec^{-1} and 0.1881 ft^3/lb, respectively, ω_H is the resonant frequency of the Helmoltz resonator with the value of 226 sec^{-1}, and b is $(\partial\bar{\rho}/\partial S)_p$. The $\ddot{\bar{\rho}}$ and $\dot{\bar{\rho}}$ are derivatives of $\bar{\rho}$ with respect to time. The relief pipe has been idealized by dividing it into ten sections of appropriate length, hydraulic radius, and cross-sectional area, with the main fuel circulating flow of 110 gpm through the lower eight sections. Account has also been taken of the pressure changes at enlargements and contractions in cross section, the net pressure drops at these points being approximately three times greater than the frictional drop within the pipe sections.

The short formulas for the peak pressure resulting from inertia, p_I, and that resulting from friction, p_F, obtained by dropping the first three terms in Eq. 12, are given by

$$p_I = C_H \dot{P}_{max} \tag{13}$$

and

$$p_F = C_H \left[K_1 (P_{ex})_{max} + b\epsilon K_2 (P_{ex})^2_{max}\right] , \tag{14}$$

where C_H has the value of 3.71×10^{-3} lb·sec/ft²·kw.

For the case of a prompt-supercritical reactivity step at low initial power with no subsequent cooling or further addition of reactivity, the time behavior of the power is given by Eq. 8*a*. The maximum value of the time derivative of the power is obtained by equating P to zero, which gives

$$\dot{P}_{max} = 0.544 \left(\frac{\alpha\epsilon}{\delta}\right)^{1/2} P^{3/2}_{max} . \tag{15}$$

Sangren found that this formulation is approximately applicable in the more general case in which heat extraction and reactivity changes are present.

An improved estimate of p_I can be obtained by solving Eq. 12 after linearizing it. For the HRE conditions, however, additional simplification with negligible error results from neglecting the term in $\dot{\bar{\rho}}$. The temperature, S, is obtained by approximating the power given in Eq. 8*a* by a cosine function, $P = P_{max} \cos^2 \omega t$, with $\omega = 0.89(\delta - \beta)/\delta$. The net result is a correction factor to the short formula for p_I. The correction factor depends on ω/ω_H and has a maximum value of 1.8, which is in agreement with the previous observations.[7]

In Fig. 6, p_I and p_F are plotted as functions of the peak power obtained from the short formulas 13 and 14, the power being the total power for p_I and the excess power for p_F. The p_I obtained from the iterative calculations is also shown. The present values of p_F are smaller by a factor of 7 or 8 than the short-formula values presented in ORNL-630[6] and ORNL-1205[7] for the old pressurizer design. The short-formula values for p_I are only about 30% below those given in ORNL-1205 because the relief pipe cross-sectional area used there (0.037 ft²) is more appropriate to the new design than to the old (0.0123 ft²). As can be seen from the curves, the inertial pressure dominates in the present design.

A peak pressure of 2000 psi, the bursting pressure of the core vessel, is associated with a peak power of 5.3×10^5 kw, which requires a step increase in reactivity of 3.0% or to a rate of increase of 14%/sec at an initial power of 0.1 watt. If a safety factor of 4 is allowed for taking into account the uncertainties in structural strength and in the calculations of peak pressure, the peak pressure increase should be limited to 500 psi. This would be attained with a peak power of 2.0×10^5 kw, which would correspond to a reactivity step of 2.0% or a ramp of 5.7%/sec at an initial power of 0.1

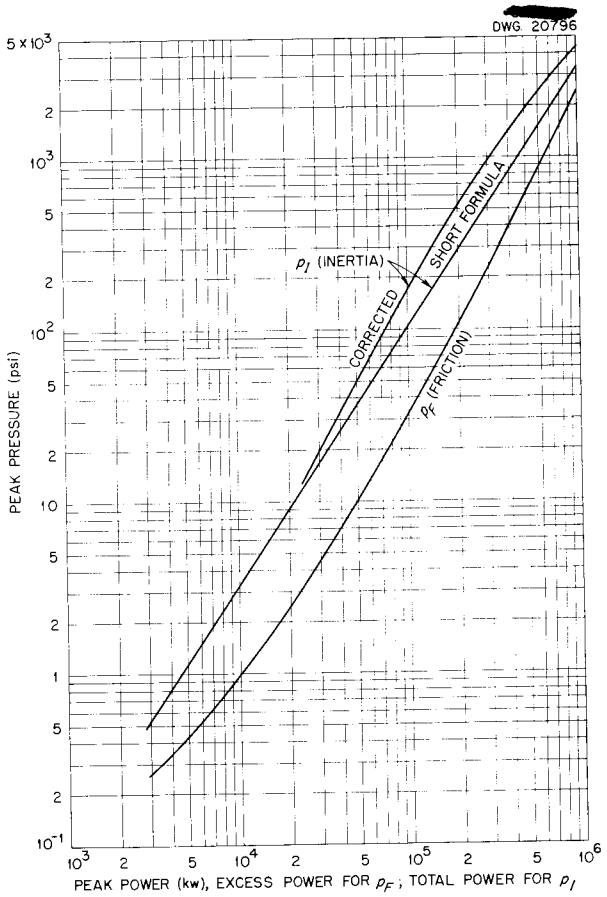

Fig. 6. Peak Pressure from Inertia of Relief Pipe Fluid (p_I) vs. Peak Power and Peak Pressure from Friction in Relief Pipe (p_F) vs. Peak Excess Power Calculated for HRE from Short Formulas.

watt. There is no known mechanism by which reactivities of such magnitudes can be introduced either by accident or by experiment.

HRE OFF-GAS PUMP

P. N. Stevens

Several changes were necessary in the basic design of the mercury piston off-gas pump before the desired performance was achieved. The major problems encountered were unreliable check valve operation and air leakage into the oil system. These difficulties, along with many other minor problems, were successfully resolved only after a great deal of developmental effort and extensive testing. Reliability of the many components has yet to be demonstrated, and further testing will be necessary before installation in the reactor can be recommended.

Part II

BOILING REACTOR RESEARCH

BOILING REACTOR RESEARCH

R. N. Lyon, Section Chief

PROPOSED REACTOR STABILITY EXPERIMENT ON THE LOS ALAMOS WATER BOILER

P. R. Kasten

There are two outstanding questions concerning the time behavior of aqueous homogeneous reactors: (1) how fast do decomposition gases form as such within the reactor and (2) if boiling of the fuel solution occurs, how fast is nuclear power transferred from liquid to vapor? To answer these questions, an experiment on the Los Alamos Water Boiler (Supo model) is planned for the first week in August, which, it is hoped, will provide the experimental data needed to evaluate the gas delay and steam delay functions. Essentially, the experiment will consist of adding reactivity to the reactor at a known rate to obtain pertinent data on the neutron flux and the reactivity addition as a function of time. By performing the experiment with the reactor under nonboiling and boiling conditions, a gas delay function and a steam delay function can be obtained.

Experimental Apparatus and Procedure. The Instrument Group has developed a control rod mechanism that can position a poison rod within the reactor core glory hole and can pull the poison out rapidly. With the given initial operating conditions, the poison rod will be drawn from the reactor core by means of the energy in the mechanism springs, and the rod position and the reactor power will be recorded as a function of time. Various sizes of poison rods will be used, and runs will be made under both nonboiling and boiling conditions. Details of the instrumentation for this experiment are given in the chapter on "Instrumentation and Controls."

SOLUTION STABILITY STUDIES

C. G. Lawson

Equipment has been fabricated for measuring the oxygen required for stability of uranyl sulfate solutions boiling at 250°C. Preliminary tests have indicated several small leaks, most of which have now been sealed.

BUBBLE NUCLEATION

R. J. Goldstein

Experiments to determine the nucleating characteristics of fission fragments in superheated and hydrogen supersaturated solutions of uranyl sulfate were continued during this quarter. For the supersaturations obtained, no appreciable difference in the nucleating superheat from that in relatively gas-free water[1] was obtained.

The original procedure used to obtain supersaturation with hydrogen,[1] that is, bubbling hydrogen gas through a sample at one pressure and then lowering the gas pressure over the sample, was found to be unsatisfactory. Virtually no superheat could be maintained in such samples, even in the absence of radiation, probably because small bubbles of gas remained in the liquid and acted as nucleating points. To eliminate these bubbles and to simulate more closely the gas formation in a reactor, gamma or x irradiation was used. With the assistance of J. A. Ghormley of the Radiation Chemistry Group, samples of uranyl sulfate were irradiated by the Radiation Chemistry's 1000-curie Co^{60} gamma source and by their 2-Mev Van de Graaff x-ray generator. With the rate of hydrogen formation and the rate of diffusion out of the sample known, the degree of supersaturation

(1) J. A. Ghormley, *Chem. Quar. Prog. Rep. Dec. 31, 1952*, ORNL-1482, p. 35.

could be obtained from values of the Henry's law coefficients.[2]

Small silica ampoules, used previously by Ghormley[1] in fission nucleation experiments, and some new ones of slightly different design were used. Small amounts of KBr were added to the uranyl sulfate solution to inhibit the back reaction[3] and to allow the buildup of hydrogen gas. These ampoules, with different pressures in them, were irradiated for various times at room temperature by the Co^{60} gamma rays or the Van de Graaff x rays. The ampoules were then heated in a constant-temperature bath, and the superheat required to nucleate macroscopic bubbles in the presence of neutrons (and the resultant fission recoils) was observed.

The pressure on the sample varied from that equivalent to a normal boiling point of 90°C up to that equivalent to a boiling point of 160°C. The irradiations were for various periods of up to several days in the Co^{60} source and up to 200 min with the Van de Graaff generator. At no time was the difference between the nucleating superheat in a relatively gas-free sample and in the same sample supersaturated with hydrogen more than a few tenths of a degree.

The maximum supersaturation, approximately 10 atm, was obtained by using the Van de Graaff generator and an ampoule in which the pressure was approximately 1 atmosphere. With gas in the liquid, the fission recoil nucleating temperature was 129.8°C, and when the liquid was relatively gas free (after boiling followed by repeated freezing and melting of the sample), it was 130.3°C.

It was also demonstrated that nucleation of bubbles takes place away from the walls of a vessel or away from solid particles. Previously, it was believed that although fission fragments were shown to nucleate vapor bubbles,[4] the actual nucleation might occur only around a fission recoil near the wall.

The neutron flux with the polonium-beryllium source present in the constant-temperature bath was measured at the ampoule by using gold foils. From this value and the concentration and heated volume of the sample, the average time between fissions in the sample was calculated and found to be approximately equal to the average time of irradiation required for nucleation in the superheated solution. Since the number of fission recoils which strike the wall is much smaller than the total number of fissions during the same period in the 0.7- to 1-mm-dia capillary, it is concluded that a fission recoil does not have to strike the wall to cause nucleation in superheated aqueous solutions.

TEAPOT MOCKUP

J. R. McWherter R. L. Cauble

A structural steel frame work has been fabricated and installed for mounting the Teapot mockup during its tests in Building 9204-1. The low-pressure (150 psi) core has been pressure tested, and a dump tank has been obtained from salvage.

A length of 18-in.-OD schedule-80 type 347 stainless steel pipe has been ordered for a high-pressure core vessel.

It is planned to test the feed systems which are listed below in the order of increasing complexity to determine which system is the most foolproof and, at the same time, provides maximum safety.

---

(2) J. M. Smith and D. L. Katz, *Physical Behavior of the H_2-O_2-H_2O System under Pressure*, ORNL-1069, p. 15 (Sept. 24, 1951).

(3) C. J. Hochanadel, *J. Phys. Chem.* **56**, 587 (1952).

(4) J. A. Ghormley, C. J. Hochanadel, and A. C. Stewart, *Chem. Quar. Prog. Rep. Sept. 30, 1952*, ORNL-1432, p. 45.

1. *"Kipp Generator" Feed.* Air pressure will be used to force water from the dump tank into the core. A series of interlocking valves that control the differential pressure between the core tank and the dump tank will be used to control feeding and dumping.

2. *Pressure Feed.* Compressed gas will force fuel solution from a weigh tank into the core.

3. *Pulsafeeder Feed Pump.* Fuel solution will be pumped into the core from a small weigh tank.

The flame recombiner discussed in the previous quarterly report has been built, and it gave unusually satisfactory performance in a variety of tests. Further details are given in the chapter on "Engineering Development."

POWER REMOVAL FROM BOILING REACTORS

R. V. Bailey H. A. MacColl
W. S. Brown M. Richardson
P. C. Zmola

The objective in power removal from a boiling reactor is to devise a core arrangement which will permit operation at the highest power density possible for a given mean fluid density. For convenience, the removal of vapor from the core can be considered as consisting of two steps. First, the vapor generated in the interior of the reactor must be moved to the surface of the core, and second, after having reached a surface, the vapor must be removed from the entraining liquid.

If the investigation is restricted to systems in which no external work is supplied for pumping the fuel solution, the two mechanisms by which vapor generated in the core is transported to a surface are natural vapor bubble rise and natural circulation of the liquid-vapor mixture. The energy-transport capacity of these mechanisms has been discussed in previous reports, and further work is reported here.

In regard to the problem of separating the vapor from the entraining liquid, most attention has been devoted to studying separation from systems having a free liquid surface. Where the problem of vapor separation from the liquid is severe in commercial practice, it is common to employ a centrifugal-force field to effect the separation. It is essential to know under what conditions, if any, it is necessary or desirable to utilize such devices in a boiling reactor system.

Natural Vapor Rise Systems. In the experimental work, described in the previous quarterly report,[5] dilute acid solutions were boiled by electrical-resistance heating in the 6-in. by 6-in. by 4-ft high apparatus. The experiments have been continued and power densities of up to 4.4 kw/liter for initial liquid levels of greater than 15 in. have been investigated. The results of the experiments were essentially the same as those reported previously.

In order to obtain information on the influence of pressure in a natural vapor rise system, a second volume-boiling apparatus was constructed for operation at pressures of up to 3 atmospheres. The apparatus consisted of two lengths of 4-in.-dia glass pipe with an over-all length of about 8.5 feet. The upper section of the apparatus housed a reflux condenser and the lower portion, which served as the test section, contained the solution and electrodes. Each of the two electrodes was made by welding a flat strip of stainless steel across the chord of a longitudinal strip cut from a length of stainless steel pipe. The curved portion of the electrode conformed roughly with the inside diameter of the glass pipe, and the flat sections formed the test region, which was 1.25 by 4 in. in cross section and

(5) W. S. Brown, H. A. MacColl, M. Richardson, and P. C. Zmola, *HRP Quar. Prog. Rep. Mar. 31, 1953*, ORNL-1554, p. 22.

4 ft high. The density measurement equipment was the same as that used for the 6- by 6-in. atmospheric pressure apparatus.

Vertical density distributions at 1, 2, and 3 atm were obtained for power densities of up to 13 kw/liter. Representative results are shown in Fig. 7. Mean density decrease ranged up to 80% for the high power density runs. The pressure effect observed was considerably less than the $(h_{fg}/v_{fg})^{2/3}$ variation predicted by the analytical model. However, examination of the data indicated that the influence of pressure on power removal in this pressure range (1 to 3 atm) might be somewhat less than that at higher pressures because of a competing effect, namely, that hydrostatic pressure causes a difference in saturation temperature of 3 to 6°F between the top and the bottom of the test region at atmospheric pressure which results in flashing of the liquid rising into a lower pressure region because of agitation of the boiling action. Since energy transport by this mechanism falls off rapidly with increasing pressure, there would be a tendency to mask a pressure effect resulting from an increase of vapor density. At present an attempt is being made to separate these two effects. If this is possible, it appears that high-pressure power-removal capability may be predicted more realistically.

Natural Circulation Systems. Expressions for the power-removal capability were developed and presented previously for three idealized cases:[6]

For Case I, it was postulated that the fluid flows downward in an annular region close to the containing walls and then up the center of the vessel and that the vapor forms in such a way that (1) the velocity of the fluid entering the annular downcomer equals the velocity of the fluid leaving the riser, (2) the average density in the descending annular region minus the average density in the rising section is equal to half the reduction in density as the fluid circulates around the system, and (3) the average density of the fluid is half the sum of the densities of the entering and leaving fluids.

For Case II, it was postulated that (1) the fluid flows downward in an annular region close to the walls of the containing vessel to the bottom of the reactor core, (2) the cross-sectional area of the riser, A_2, is equal to that of the downcomer, A_1, and (3) the rate of vapor formation is uniform throughout the reactor core.

For Case III, it was postulated that (1) the fluid flows downward in an annular region along the walls of the containing vessel to the bottom of the reactor core, reverses, and flows upward in the center to the top of the reactor core, (2) the cross-sectional area of the riser, A_2, is equal to that of the downcomer, A_1, and (3) the rate of vapor formation at any point is proportional to $J_0(2.405\ r)\ \sin \pi z$.

Briefly, the expressions for the power removal in the three cases have the form

$$(1)\quad \frac{P v_{fg}}{h_{fg}} \left(\frac{KZ}{2g}\right)^{1/2} = F\left(1 - \frac{\overline{\rho}}{\rho_f},\ \eta\right),$$

where

P = power density,
v_{fg} = specific volume change in evaporation,
h_{fg} = latent heat,
K = loss coefficient, equal to the number of velocity heads lost in each circulation pass,
Z = core height,
g = gravitational constant,
$\overline{\rho}$ = average density of the boiling fuel solution,

(6) R. V. Bailey, E. N. Lawson, H. A. MacColl, and P. C. Zmola, *HRP Quar. Prog. Rep. Oct. 1, 1952*, ORNL-1424, p. 16-19.

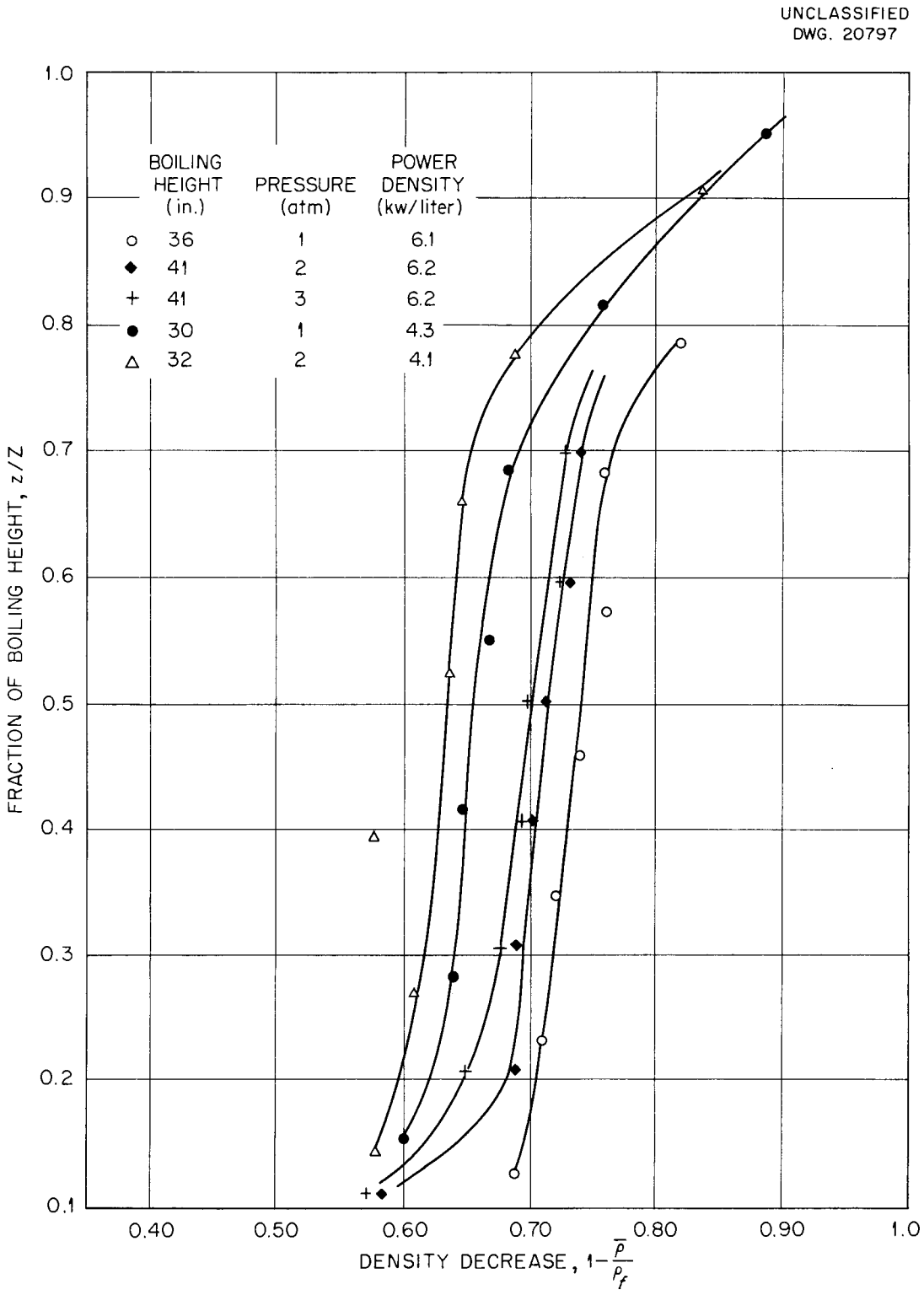

Fig. 7. Vertical Density Distribution in 4-in. Glass Volume-Boiling Apparatus at Various Pressures.

ρ_f = density of the nonboiling fuel solution,

η = fraction of vapor arriving at top of reactor core that is entrained and recirculated.

Any consistent set of dimensions may be used. Performance charts for the three models have been calculated and are shown in Figs. 8, 9, and 10.

To study the vapor transport in a natural circulation system, a convection loop apparatus was constructed of 4-in.-dia glass pipe. The test section, which was the riser, was the one used in the natural vapor rise apparatus described above. The condenser was mounted above the downcomer. In operation, liquid entered the bottom of the test section and the liquid-vapor mixture left at the top. The area for vapor disengagement was large compared with the cross-sectional area of the test section, and therefore very little vapor entrainment occurred in the downcomer. The density-measuring equipment was that used for the natural vapor rise apparatus. Temperatures were measured at a number of points in the circuit.

Fluid density distribution data were obtained over a range of power densities

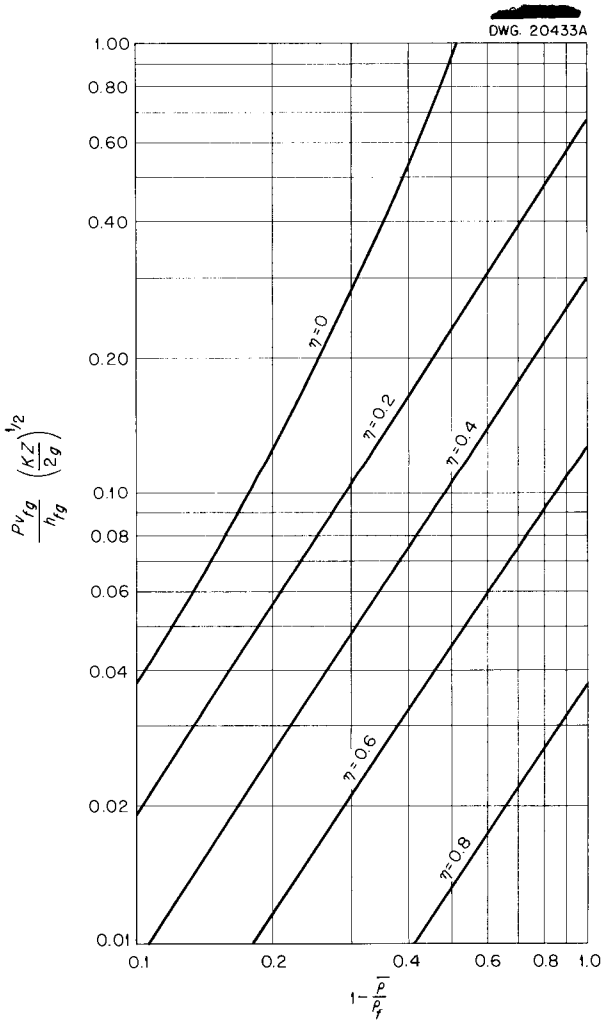

Fig. 8. Performance Chart for Natural Circulation System, Case I.

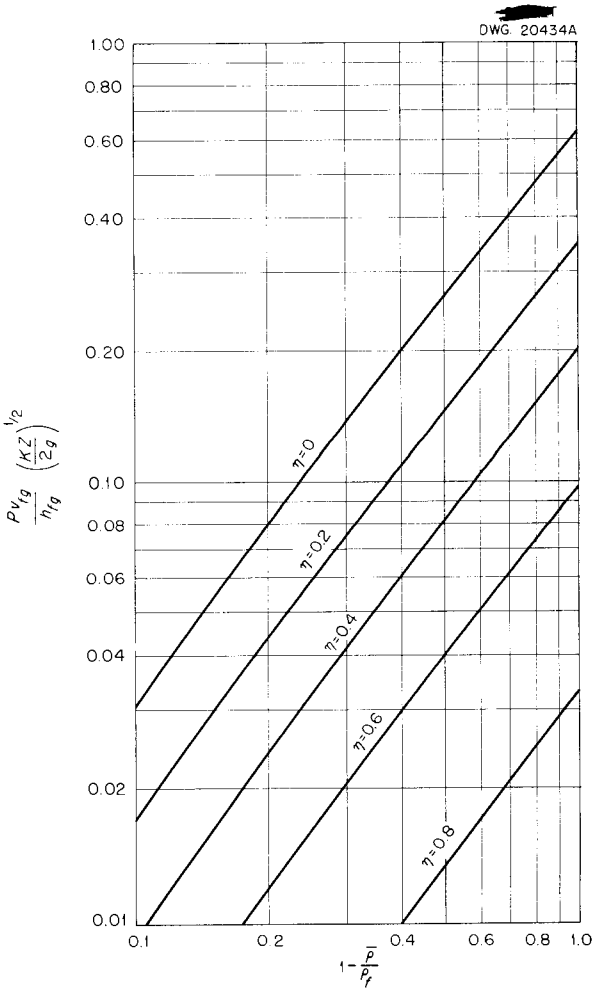

Fig. 9. Performance Chart for Natural Circulation System, Case II.

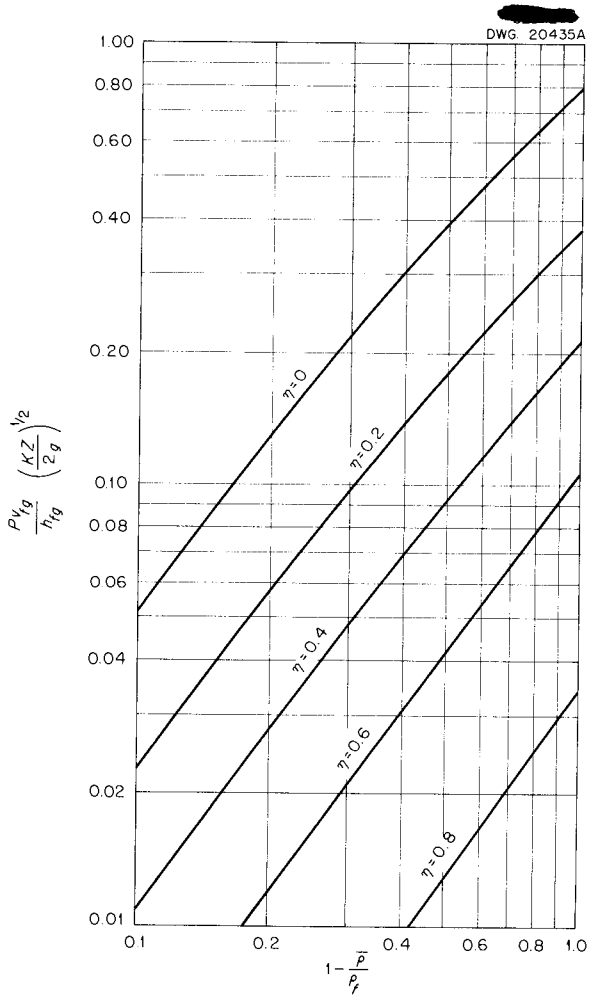

Fig. 10. Performance Chart for Natural Circulation System, Case III.

at atmospheric pressure. One run was made at a system pressure of 2 atm absolute. The mean density decreases for a number of power densities at atmospheric pressure are shown in Table 1. Examination of the measured fluid density distributions indicates that the effect of hydrostatic pressure and the resulting contribution of flashing to the vapor generation are even more pronounced in the circulating system than in the vapor rise system. This might be expected, since the liquid moves through the test section at appreciable velocities (rough

TABLE 1. MEASURED MEAN DENSITY DECREASE vs. POWER DENSITY FROM ATMOSPHERIC PRESSURE RUNS

POWER DENSITY (kw/liter)	MEAN FLUID DENSITY DECREASE, $1-\frac{\bar{\rho}}{\rho_f}$
3.6	0.25
8.7	0.36
8.7	0.41
13.2	0.47
14.4	0.53

estimates set the liquid inlet velocity to the test section at 1 to 3 fps).

Vapor Separation and Circulation in Large Systems. In order to obtain a qualitative check of the realism of postulates made in the analysis of large circulating systems and to get a rough indication of the vapor disengagement for a large system with a free surface, some preliminary experiments were performed by bubbling air through water in a cylindrical tank 12 ft high and 69 in. in diameter fitted with a canvas air diffuser at the bottom of the tank. The fractional height increase of the liquid level was measured as a function of the air flow rate up to the maximum obtainable rate of 400 scfm and for three initial water levels. The tank was then fitted with a sheet metal draft tube which was 50 in. in diameter and 70 in. high. The draft tube was supported from the top of the tank with the lower end 10 in. above the canvas. The increase of the free surface height was then measured as a function of the air flow rate for an initial water level of 84 inches. The results of these experiments are shown in Fig. 11.

In addition, local velocities in the downcomer region near the periphery of the tank were measured at various points with and without the draft tube in place. Average velocities, which were about the same with or without

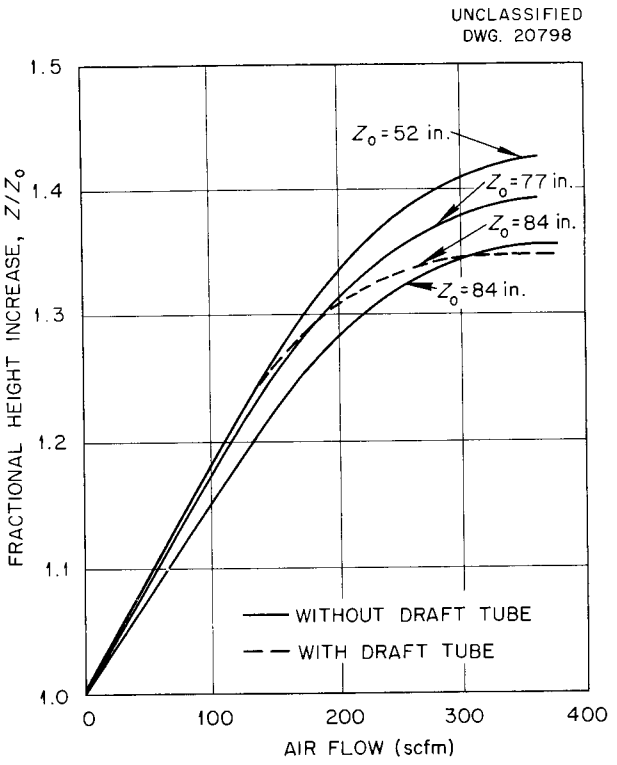

Fig. 11. Experimental Results Obtained with the Large Air-Water System.

the draft tube, ranged from about 1 to 3 fps in the downcomer region for air flow rates of approximately 100 to 350 scfm.

By noting that the term Pv_{fg}/h_{fg} in Eq. 1 corresponds to the air flow rate per unit fluid volume in the tank, it is possible to analyze this system by employing a model in which all the vapor is generated at the bottom of the core. The measured air flow rates, the height increase, and the downcomer velocities were used in the calculation, and values of $K \approx 7$ and $\eta \approx 0.6$ were obtained for this system. It is interesting to note that, within the limitations of the experiment, the insertion of a draft tube had little effect on the circulation pattern, the circulation velocity, and the density decrease within the tank.

Possible Core Arrangements for Boiling Homogeneous Reactors. The theoretical and experimental work on power removal from boiling systems as reported in this and previous quarterly reports has covered particular features, problems, or arrangements of a number of systems. The general objective of this work has been to evaluate the power-removal capabilities of various possible core arrangements, since the choice of a reactor core arrangement depends upon a large number of factors, only one of which is power removal. Schematic drawings of various core arrangements which have one or more attractive features in particular applications are shown in Fig. 12. Figure 12*a* shows the natural vapor rise system, and Fig. 12*b* shows the simplest natural circulation system; both systems have free surfaces. The present indication is that each of these systems has about the same power-removal capability and that circulation will take place in the large size units with or without a draft tube. It appears that if advantage is to be taken of circulation, a fixed-volume system with steam separation devices, such as those shown in Figs. 12*c* or *d*, must be employed. Satisfactory operation of these systems depends largely upon the flow properties of the steam separators. In Figs. 12*e* and *f*, the problem of vapor separation is removed by replacing it with another problem, namely, that of determining the performance of the system when the vapor is not separated but is condensed *in situ*. Thus far, little effort has been devoted to such systems.

DWG. 20799

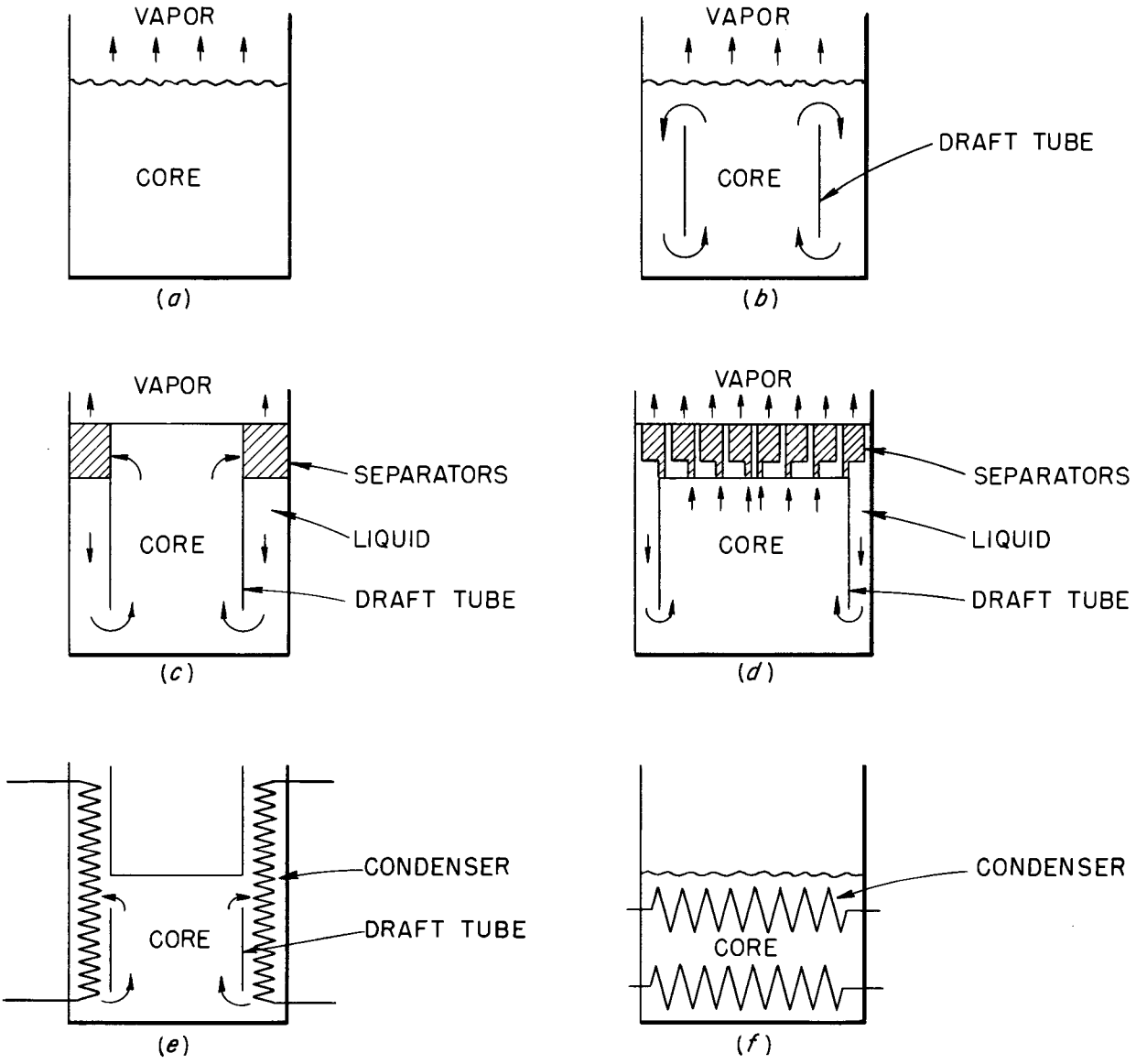

Fig. 12. Possible Core Arrangements for Boiling Homogeneous Reactors.

a. Natural Vapor Rise System.
b. Natural Circulation System.
c. Natural Circulation System with Large Vapor Separators.
d. Natural Circulation System with Small Vapor Separators.
e. Natural Circulation System with Internal Condensation in Downcomer.
f. Natural Circulation System with Internal Condensation in Core.

Part III

GENERAL HOMOGENEOUS REACTOR STUDIES

INTERMEDIATE-SCALE HOMOGENEOUS REACTOR DESIGN

R. B. Briggs, Section Chief

C. L. Segaser, F. C. Zapp, R. H. Chapman, D. K. Taylor, P. N. Haubenreich, R. E. Aven, W. Terry, J. P. Sanders

FLOW SHEET FOR ISHR FUEL SYSTEM

The most recent flow sheet for the ISHR fuel system is shown in Fig. 13. It is similar in many respects to the flow sheet shown in ORNL-1478,[1] but differs in the following ways.

1. The arrangement of the main heat exchanger and the gas separator has been changed, and the heat exchanger has been elevated to a position that permits fission heat produced after shutdown to be removed from the main circulating system by thermal convection. This eliminates the necessity of dumping the fuel solution if the main circulating pump is stopped and reduces the volume needed for storage of liquid in the high-pressure system.

2. The high-pressure evaporation system has been eliminated. When the reactor is operated at normal power, D_2O is condensed in the recombiner system at a rate of 9 gpm. When the reactor is operated at zero power, steam can be introduced into the main heat exchanger, and D_2O can be evaporated into the recirculated gas stream and condensed in the gas condenser at a rate of 1 to 2 gpm. Some dilution can be effected by transferring D_2O from a high-pressure storage tank to the fuel-circulating system.

3. The condensate and recirculating feed pumps have been eliminated. The pressures in the system are such that the condensate required for the main pump bearings can flow directly from the condensate storage tank to the pump and fuel in the high-pressure storage tank can flow directly into the suction of the main fuel-circulating pump. The recirculating feed pump was also intended for circulating solution when the main pump was shut off, but it will not be required with the thermal convection loop.

4. The recombiner, the entrainment separator, and the high-pressure fuel storage facility have been incorporated into a single vessel.

5. The pulsafeeder pumps originally intended only for adding fuel have been relocated so that they can be used for charging the high-pressure system and for returning valve leakage.

As presently conceived, the ISHR will run as a high-pressure recirculating loop in which only small changes in temperature will be required during normal operation. In the event of electrical failures, auxiliary power will be available for instrument operation. Cooling by thermal convection in the high-pressure recirculating system will make dumping of the fuel unnecessary. The operating power can be controlled by the rate of removal of steam from the main heat exchanger. Fuel will be dumped to the low-pressure system for long shutdown periods.

EQUIPMENT LAYOUTS

Figure 14 shows the present conception of the layout of equipment for the high-pressure and low-pressure fuel systems. This layout is similar in many respects to the one-region reactor layout presented in ORNL-1424.[2] The changes which have been made are

[1] R. B. Briggs *et al.*, *HRP Quar. Prog. Rep. Jan. 1, 1953*, ORNL-1478, Fig. 9, p. 26.

[2] R. B. Briggs *et al.*, *HRP Quar. Prog. Rep. Oct. 1, 1952*, ORNL-1424, Fig. 15, p. 45.

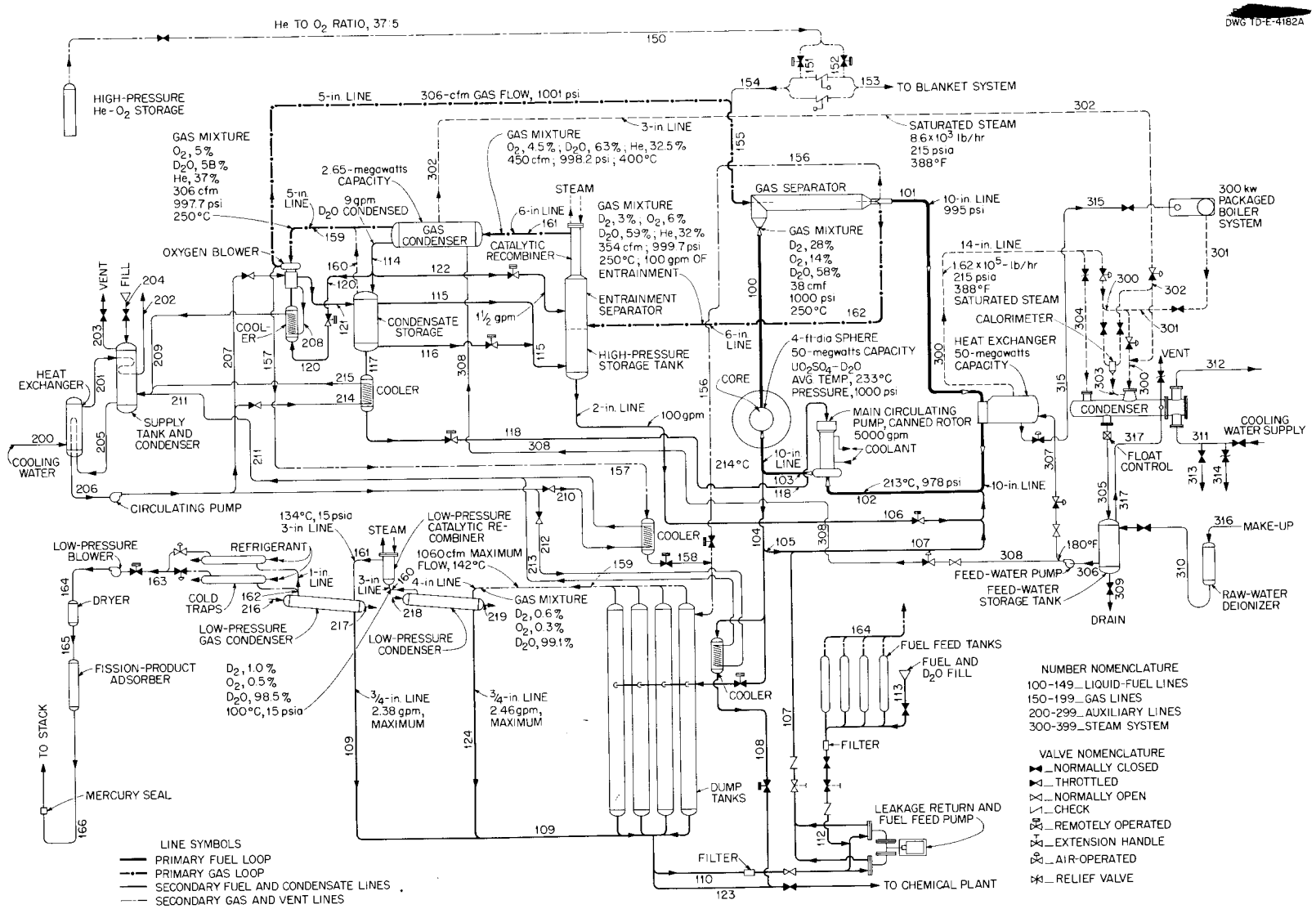

Fig. 13. Flow Sheet of the ISHR Fuel and Steam Systems.

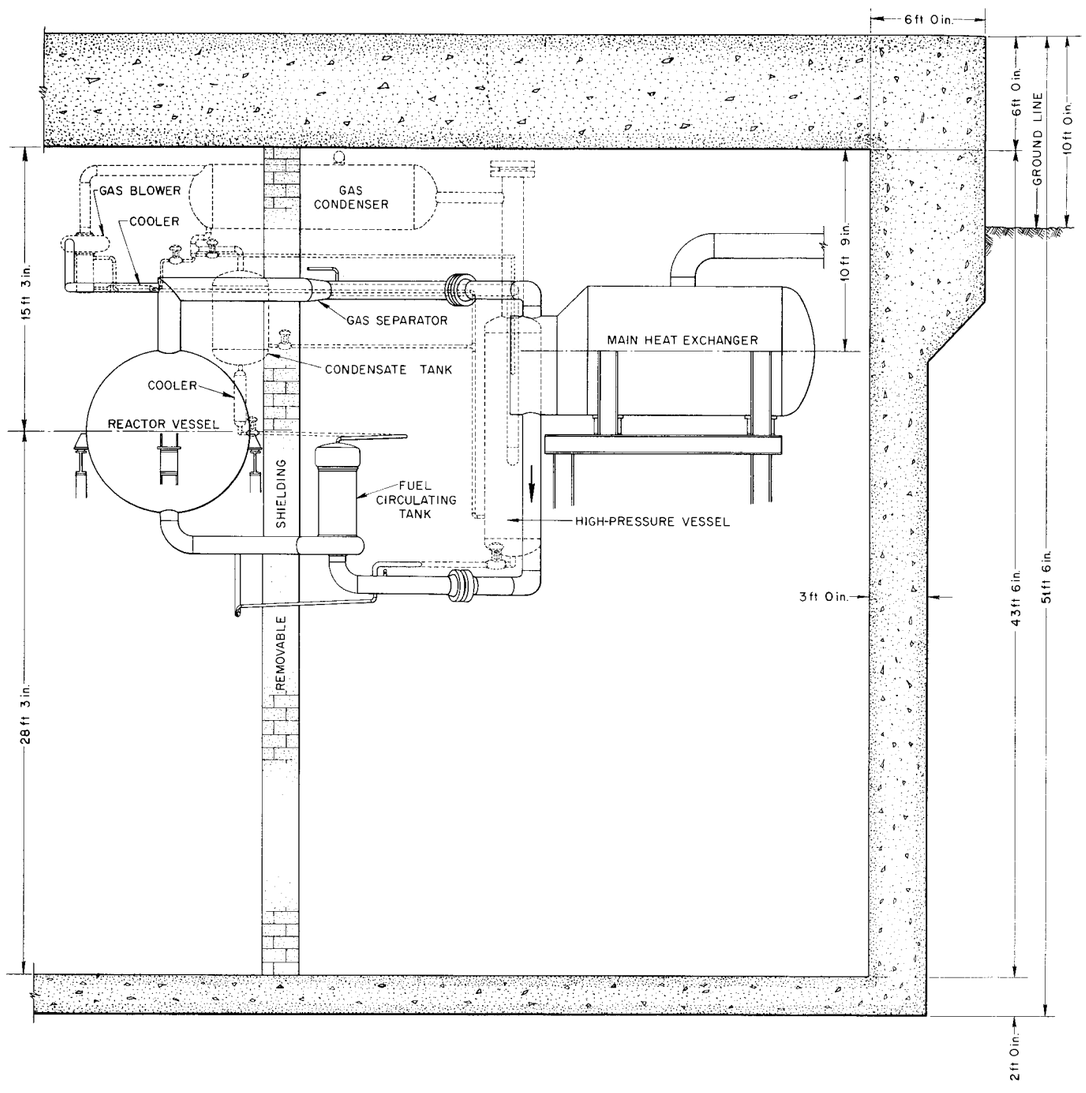

SECTION A-A

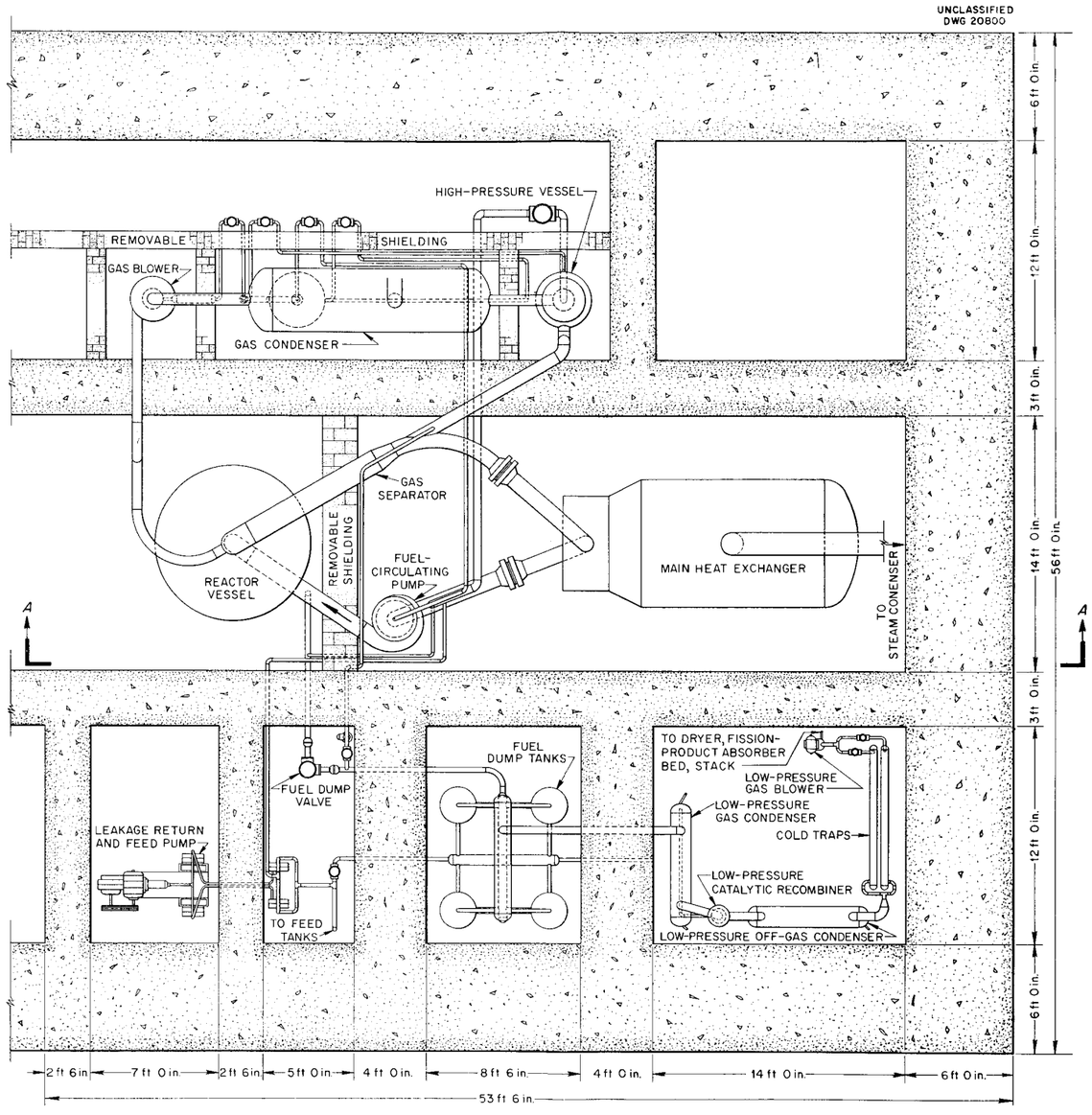

SECTIONAL PLAN

Fig. 14. Proposed ISHR Layout.

those required to permit natural convection cooling of the high-pressure recirculating system. It is intended that those pieces of equipment which require frequent maintenance be isolated from the remainder of the system with temporary shielding. The cells are to be designed so that they will retain all the fuel solution and fission product gases in the event of a serious break in the fuel piping.

REACTOR VESSEL

Three possible reactor vessel arrangements for two-region converters were presented in ORNL-1424.[3] Essentially the same arrangement as that shown by Fig. 20 in ORNL-1424 was reproduced in ORNL-1478[4] as a proposed vessel design for the ISHR, except that the control rod was removed.

Figure 15 is a modification of the design described in ORNL-1478. Cooled fuel solution from the heat exchanger enters the bottom of a 4-ft-ID spherical core where it is heated to 482°F by fission energy. The heated solution leaves the core through a 12-in. top outlet pipe and is returned to the heat exchanger for cooling. The breeding material is introduced to and removed from the 2-ft annulus around the core tank by means of a ring header arrangement, as shown. The arrangements of screens in the core tank and the small-diameter holes through the pressure shell from the breeder material inlet and outlet headers are intended to provide efficient flow of fluids through the vessel.

Calculations indicate that an effective pipe-line expansion joint of the type shown by Fig. 10 in ORNL-1478[4] must be of the order of 11 ft long to absorb a differential expansion of approximately 0.500 in. for a maximum fiber tensile stress of 10,000 psi in the pipe. Eleven feet of 12-in. schedule-20 pipe will add 256 liters of fuel solution holdup to the system. A bellows type of expansion joint of the type shown in Fig. 15 permits close coupling of the core and equipment in the circulating system. A sleeve, similar to that inserted in a turbine type of bellows expansion joint, has been provided to reduce turbulence in the bellows sections.

The core tank in a converter reactor can be fabricated of stainless steel at the expense of some loss of neutrons. Two-region breeders will probably require zirconium core tanks. A mechanical connection must be made between the core and the piping, because zirconium cannot be welded to stainless steel with the existing techniques. The joint design shown in Fig. 15 is being investigated because it requires less material than a conventional flanged joint for the same allowable pressure differential between the core and the blanket. This type of joint has proved effective for closures of large diameter in high-pressure heat exchanger heads. Welded connections could be used with a stainless steel core tank.

STRESS ANALYSIS OF REACTOR VESSEL

A preliminary stress analysis has been made for a 4-ft-dia spherical core tank of 1/8-in.-thick type 347 stainless steel. The thin wall imposes important limitations upon the allowable pressure difference between the core and the blanket. Rules of the 1952 ASME Unfired Pressure Vessel Code would permit the core tank to be operated continuously if the internal pressure were not more than 104 psi greater or 38 psi less than the external pressure. Failure of the tank by elastic buckling could be expected if the blanket pressure exceeded the core pressure by 100 to 150 psi. Yielding of the pressure vessel could be expected if the core pressure were 200 to 250 psi greater than the blanket pressure.

---

[3] *Ibid.*, Figs. 20, 21, and 22, p. 54-56.

[4] R. B. Briggs *et al.*, *HRP Quar. Prog. Rep. Jan. 1, 1953*, ORNL-1478, Fig. 10, p. 28.

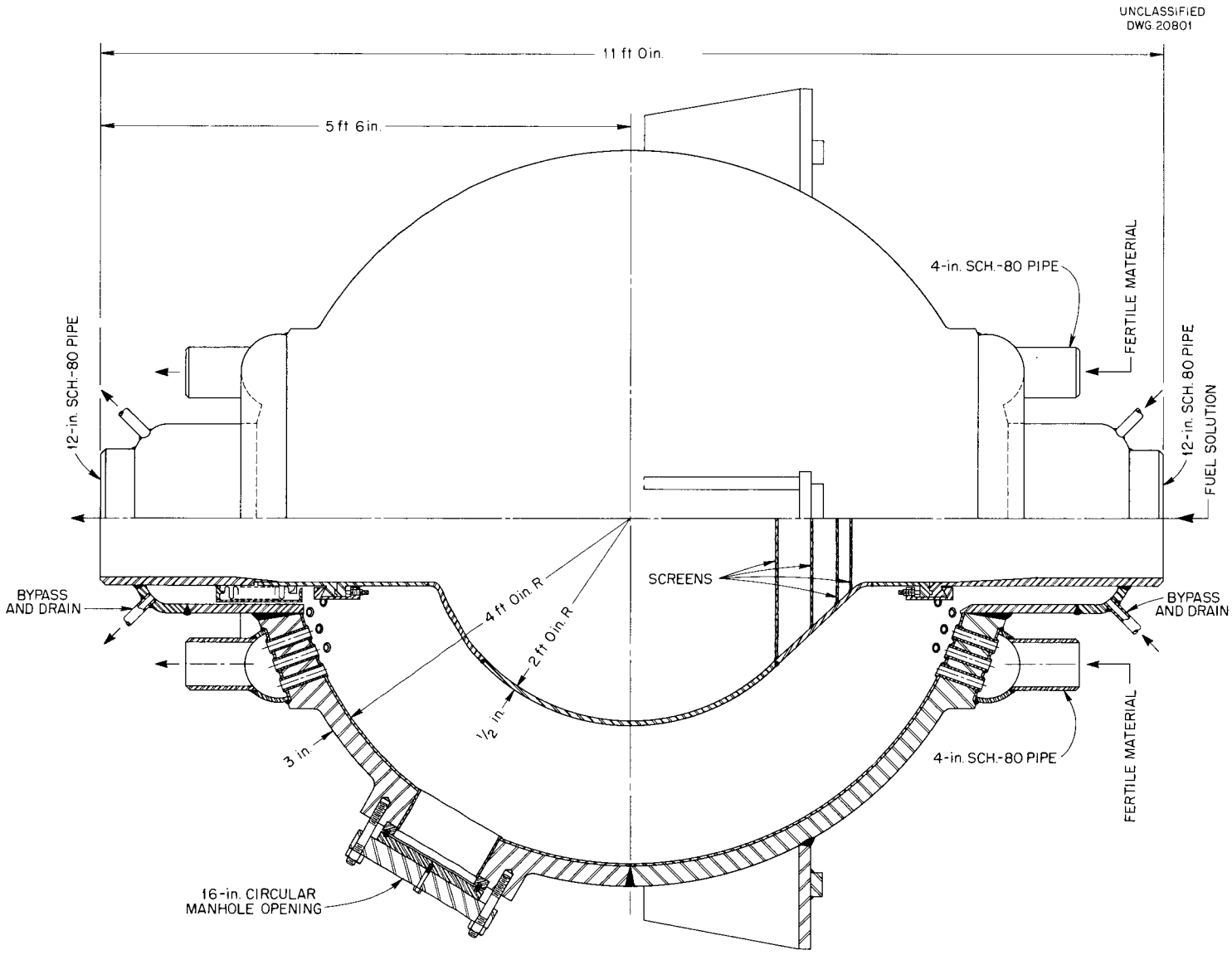

Fig. 15. Two-Region 50-Megawatt Reactor.

It is assumed that the reactor pressure vessel will be fabricated of carbon steel, which has a lower thermal coefficient of expansion than that of the stainless steel core tank and piping. Estimates indicate that a differential expansion of 0.2 to 0.4 in. between core and piping and pressure vessel must be taken up in bending of the core tank or in an expansion device. Excessive bending stresses could be expected in the core tank surrounding the pipe inlet and outlet connections if there were no provision for expansion. Calculations indicate that a total thrust load of 2000 lb may be applied to the core tank in operating the expansion device without exceeding a stress of 10,000 psi.

Thermal stresses in the core tank wall were found to be negligible. The effects of radiation damage have not been evaluated.

Some preliminary estimates have been made for a 1/2-in.-thick 4-ft-dia zirconium core tank. The greater thickness is permitted because of the lower neutron cross section. Calculations show that the vessel could be expected to yield with an excess internal or external pressure of 500 to 600 psi. Differential expansion problems would be less difficult because the thermal coefficients of expansion of zirconium and of carbon steel are about the same. If care were exercised in keeping the temperature of the pressure vessel within 50°F of the core tank temperature, an expansion device probably would not be required.

HEAT EXCHANGER

A steam generating heat exchanger now proposed for the ISHR is shown in Fig. 16. This design, prepared by the Development Section of the Reactor Experimental Engineering Division with some design assistance, differs from that shown in ORNL-1478[5] in the following features.

1. The steam drum space and the vaporizer shell are combined to provide a more compact unit which may be better fitted to a system in which the exchanger is to be located in the top of the pipe loop to achieve convective cooling.

2. A removable cover plate for the channel barrel is proposed for ease in access to the tube bundle for inspection and repair. A filler block is inserted in the channel to minimize holdup.

3. The inlet and outlet connections have been relocated from the end of the exchanger head to the top and bottom of the heat exchanger to provide better drainage of the exchanger. It is believed that, in general, this arrangement may result in a better system.

4. A composite-plate construction of stainless steel bonded to low-cost carbon steel is proposed instead of an all stainless steel tube sheet.

General specifications for the heat exchanger are presented in the following:

TUBE FLUID SIDE	
Heat transfer	50,000 kw 47,400 Btu/sec
Circulation rate	5000 gpm
Inlet temperature	482°F
Outlet temperature	418°F
Over-all heat transfer coefficient	750 Btu/hr·°F·ft^2
Heat transfer area	4300 ft^2
Velocity through tubes	13 fps
Number of 3/8-in.-OD 18-BWG tubes	2050 (U-bend)
Average tube length	21.2 ft
Holdup in tubes	18.4 ft^3
Average pressure drop	17.0 psi
Material	Type 347 stainless steel

[5] *Ibid.*, Fig. 11, p. 29.

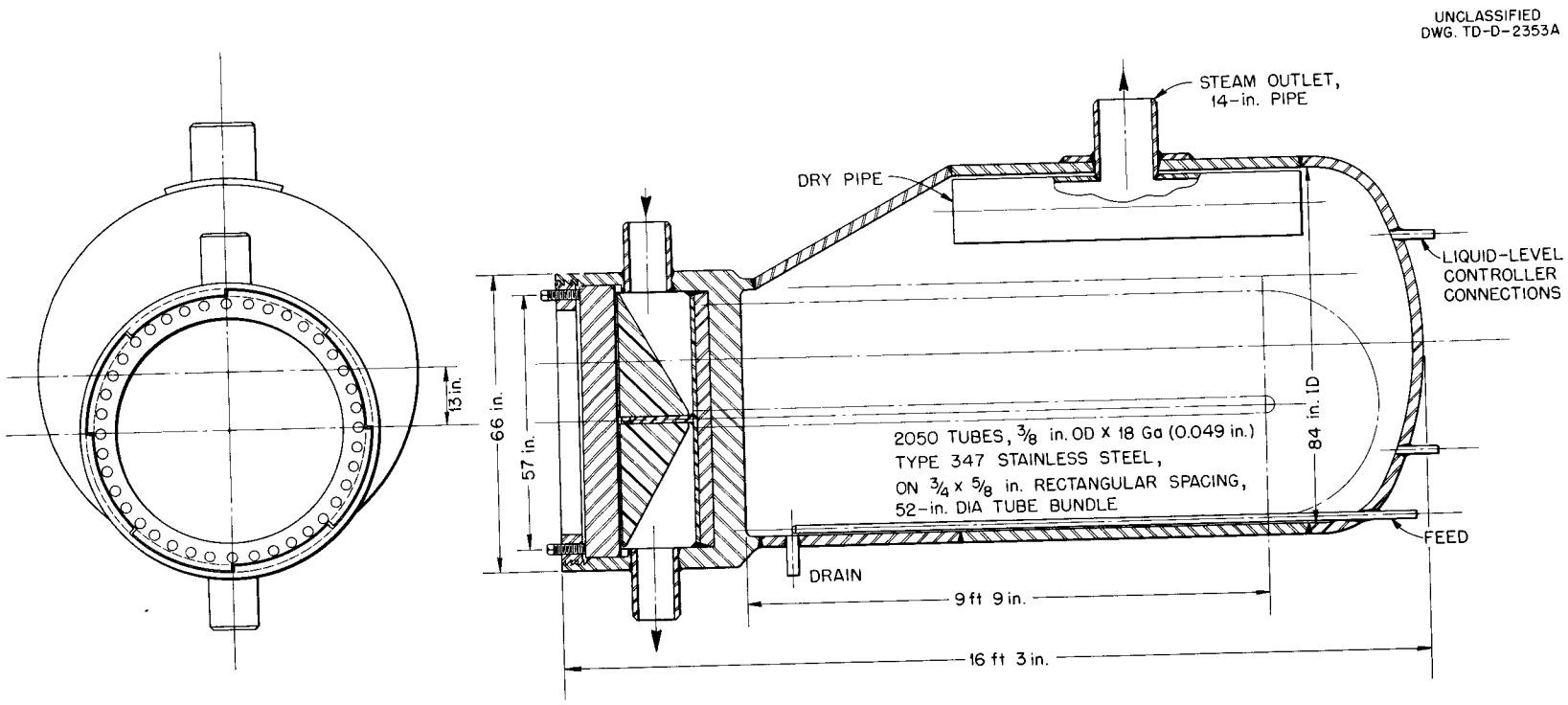

Fig. 16. ISHR 50-Megawatt Heat Exchanger.

SHELL FLUID SIDE	
Steam flow	1.62×10^5 lb/hr
Working pressure	200 psig
Design pressure	600 psig
Feed-water inlet temperature	180°F
Steam conditions	388°F saturated
Material	Carbon steel
PROPERTIES OF TUBE FLUID	
Density	56 lb/ft^3
Viscosity	0.29 lb/hr·ft
Specific heat	1.15 Btu/lb·°F
Thermal conductivity	$\sim$0.35 Btu/hr·ft^2 (°F/ft)

GAS SEPARATOR

In changing the arrangement of equipment to provide a thermal convection loop, the gas separator was moved from a vertical to a horizontal position. With this change in position, it has become possible to decrease the distance between the reactor core and the void in the separator into which liquid from the core will expand if power surges occur. This decrease in distance should reduce the magnitude of the pressure rise which accompanies a rapid power rise.

A drawing of the centrifugal gas separator is shown in Fig. 17. The operating principles and methods of calculation of performance were reported in ORNL-1478.[6] Vanes are provided in the inlet to cause the fluid to rotate and in the exit to recover some of the kinetic energy of rotation. About 4 ft of active length is calculated to be necessary for essentially complete removal of 3 lb-moles/min of entrained D_2, O_2, and D_2O vapor. This gas is diluted to 3 mole % D_2 by a diluent gas containing O_2 and He saturated with D_2O at 250°C.

The liquid pressure drop through the separator is estimated to be 5 psi. The calculated gas pressure drop is 0.3 psi.

HIGH-PRESSURE STORAGE TANK

A mixture of gas and entrained fuel solution is piped from the gas separator to the high-pressure storage tank, shown in Fig. 18, where the entrained liquid is separated from the gas and returned to the fuel circulating system. The tank also serves as a reservoir for some excess fuel solution. The gas flow through the tank will be about 350 cfm. It is expected that the liquid entrained in the gas will amount to 7 to 13 cfm.

The bulk of the liquid will be removed by a 1-ft-thick section of baffles. Following the baffles will be a 1-ft-thick section of packed, coarse-wire grids washed with 1 to 2 gpm of D_2O. The final cleanup section will be a 2-ft-thick section of fine wire packing. Wire packings designated by the Otto H. York Company of East Orange, New Jersey as Nos. 804 and 805 are suggested for the coarse and fine sections, at the present time. The superficial velocity through the bed will be near 1.2 fps; the pressure drop is estimated as 0.5 psi; and essentially complete removal of fuel-containing particles is expected.

CATALYTIC RECOMBINER

The catalytic recombiner proposed for the ISHR is a fixed bed of pellets installed in a pipe in the top of the high-pressure storage tank. The pellets are 0.3% platinized alumina, 1/8-in. right cylinders. Excellent recombination has been achieved with the catalyst in tests at space velocities as high as 2×10^6 scfh of gas per cubic foot of bed volume.

A bed, 3 1/2 ft long and 2 1/2 in. thick, in the form of a cylindrical annulus with an inside diameter of 7 in. has been specified for the ISHR. At the normal operating power of 50 megawatts, D_2 is combined with

(6) *Ibid.*, p. 31.

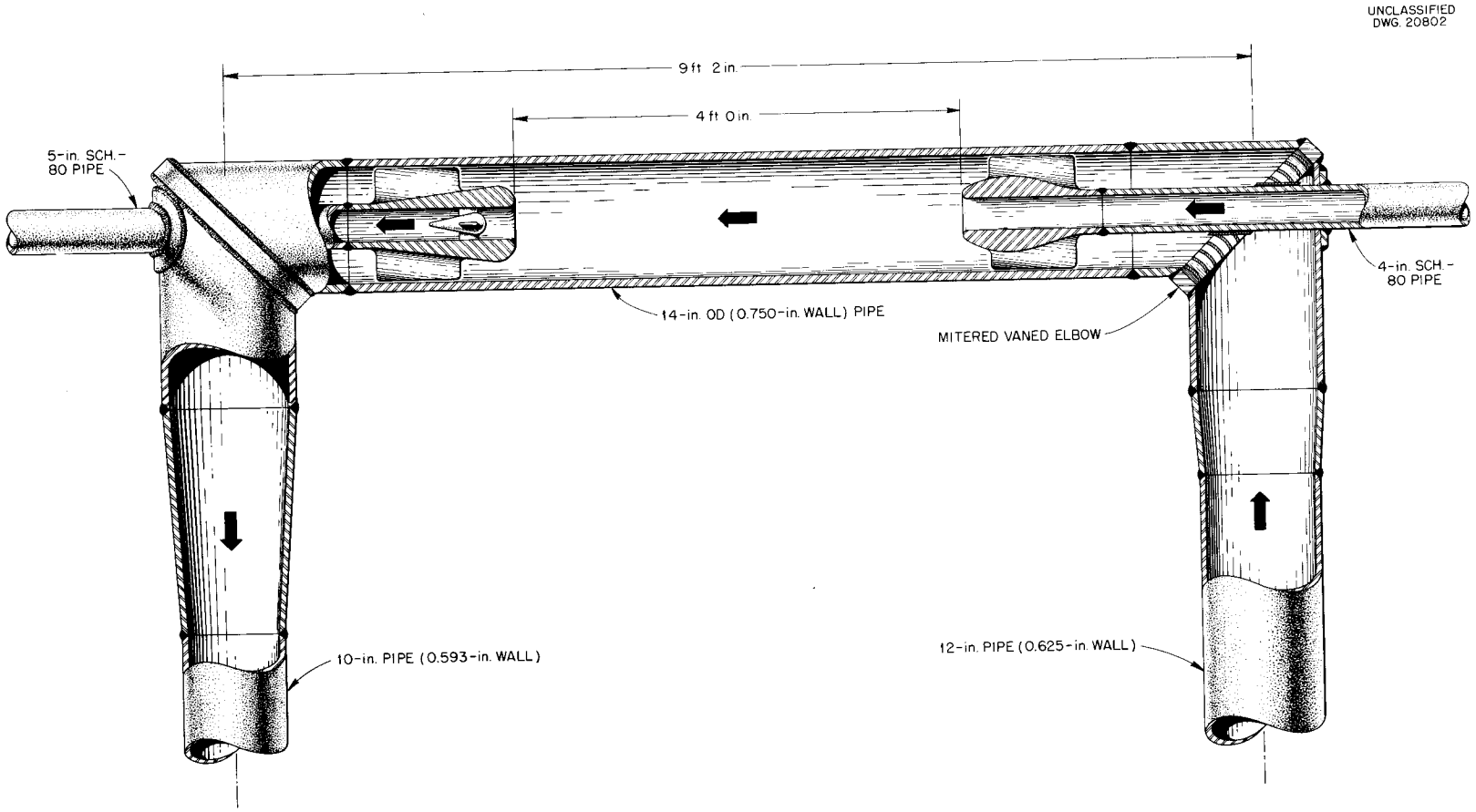

Fig. 17. ISHR Gas Separator.

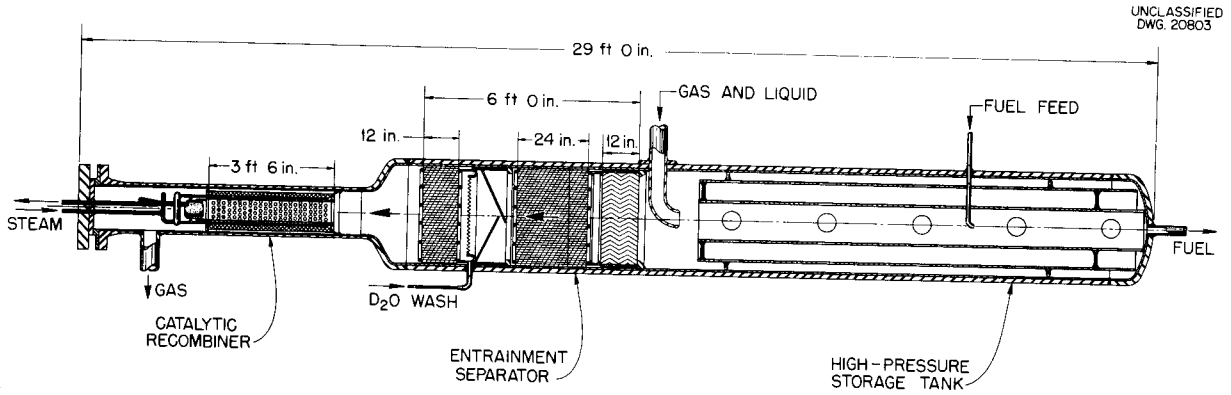

Fig. 18. ISHR High-Pressure Vessel.

O_2 at a rate of 1.03 lb-moles/min. D_2 in the gas passing into the catalyst is diluted to 3 mole % by O_2, He, and D_2O vapor. The total flow rate is 354 cfm at 250°C and 1000-psi pressure.

The design of the recombiner was based on the following equations. The equation used to predict the fraction of D_2 reacted in terms of partial pressure of D_2 vs. length into the bed[7] is

$$\ln \frac{P_{d0}}{P_d} = \frac{AP_t k_g a_v x}{Q} ,$$

where

P = pressure,
A = cross-sectional area available to flow,
k_g = mass transfer coefficient of gas film,
a_v = average surface area per cubic foot of pellets,
x = thickness of bed,
Q = flow rate of gas mixture through recombiner;

subscript d refers to D_2 component, 0 refers to initial conditions, and t refers to total pressure. This equation holds for reaction rates less than 1.2 ft^3 H_2 (STP)/min·in.^{3}.

The equation used to predict the pressure drop across the recombiner[8] is

$$\frac{dP}{dL} = \frac{2.36\,\mu^{0.15}\,\rho^{0.85}\,V_0^{1.85}\,A_f}{D_p^{1.15}} ,$$

where

μ = viscosity,
ρ = density,
V_0 = velocity,
D_p = diameter of pellet,
A_f = wall factor (assumed unity in this case).

The heat of reaction is assumed to be concentrated on the surface of the pellets. This heat is transferred from the pellets to the gas stream mainly by convection. The temperature, τ, of the gas stream is defined as a function of the radius, r, of the bed by

$$\tau = 265.6 + 130.4 \left[1 - e^{-47.25(r^{1.41} - r_i^{1.41})}\right] ,$$

where r_i is the inside radius of the section of bed. The rate of heat transfer, q_{out}, to the gas stream from the pellets is given by

$$q_{out} = h_p A (t - \tau) ,$$

where

h_p = heat transfer coefficient between the pellets and the gas stream,
A = area of heat transfer,
t = temperature of the pellet surface.

(7) I. Spiewak and R. E. Aven, *Design of ISHR Catalytic Recombiner*, ORNL CF-53-6-162 (June 26, 1953).

(8) J. H. Perry (ed.), *Chemical Engineers' Handbook*, 3d ed., p. 393, McGraw-Hill, New York, 1950.

By making a heat balance between the heat input to the pellets from the chemical recombination reaction of D_2 and O_2 and the heat output, that is, heat carried away by the gas stream, it is possible to predict the temperature of the gas stream and of the pellet surface as functions of the radius of the bed. Figure 19 gives this temperature distribution. The pressure drop across the recombiner is estimated to be 0.09 psi.[7]

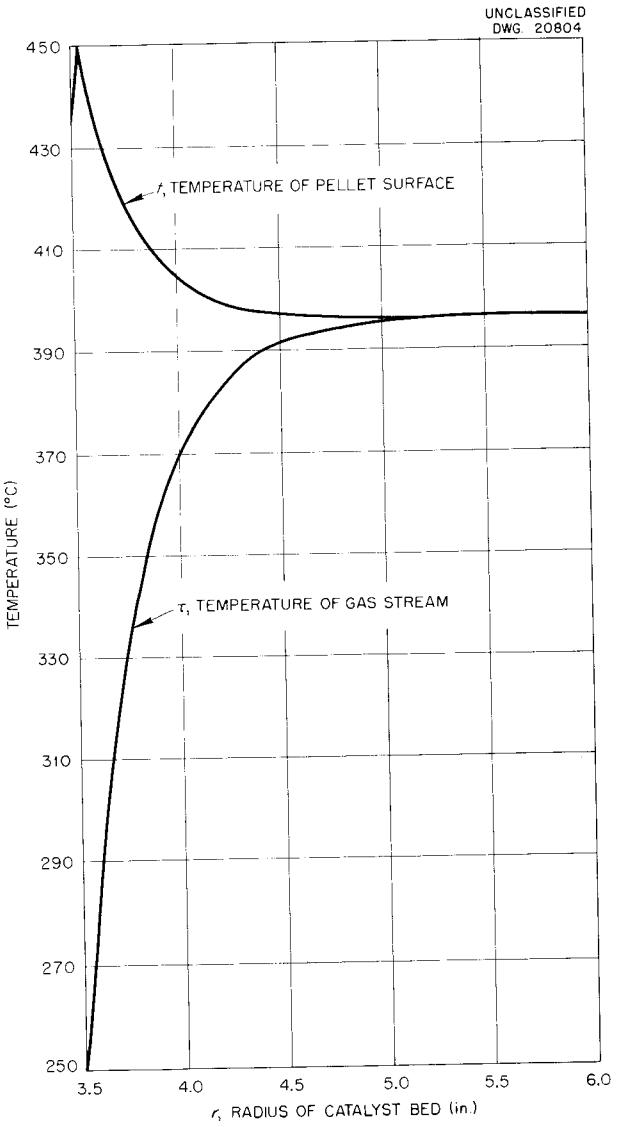

Fig. 19. Temperature Distribution in Gas Stream and Pellets in Catalyst Bed.

The catalytic reaction will not occur if the pellets are wet. Since this condition may occur at startup or during periods of low power, heating elements are embedded in the catalyst. The heating elements consist of ten U-tubes through which steam is passed at 700 psi and 262°C. Only those pellets immediately surrounding the steam tubes will be heated sufficiently to be dry. However, the catalytic reaction will occur on those pellets and the heat of the reaction will quickly dry the pellets of the surrounding bed.

CONDENSER

It is necessary to cool the gas mixture leaving the recombiner and to remove a fraction of the water vapor so that the remaining gas mixture may be recycled to the gas separator. The gas condenser, Fig. 20, is designed to cool the gas mixture from 396 to 250°C and to condense 3.27 lb-moles/min of D_2O, which is equivalent to 8.95 gpm of D_2O. Since approximately 2.65 megawatts of heat is removed in performing this operation, it is economical to recover the energy. Thus the condenser has been designed with the gas mixture flowing inside the tubes and with water boiling at 200°C as coolant on the shell side. The steam produced can then be added to that generated in the main heat exchanger and readily used in the turbines.

The present design has 84, 1-in.-dia 13-BWG tubes 10 ft 2 in. long to provide 210 ft^2 of surface. The cross-sectional area available to flow in the tubes is about 0.3 ft^2, which gives initial gas velocities of 25 fps into the tube and exit velocities of 17 1/2 fps. The gas leaving the condenser is at 250°C, and it is saturated with D_2O vapor.

Attached to the gas outlet will be a combination condensate separator and receiver, which will be nothing more than a device to change the direction

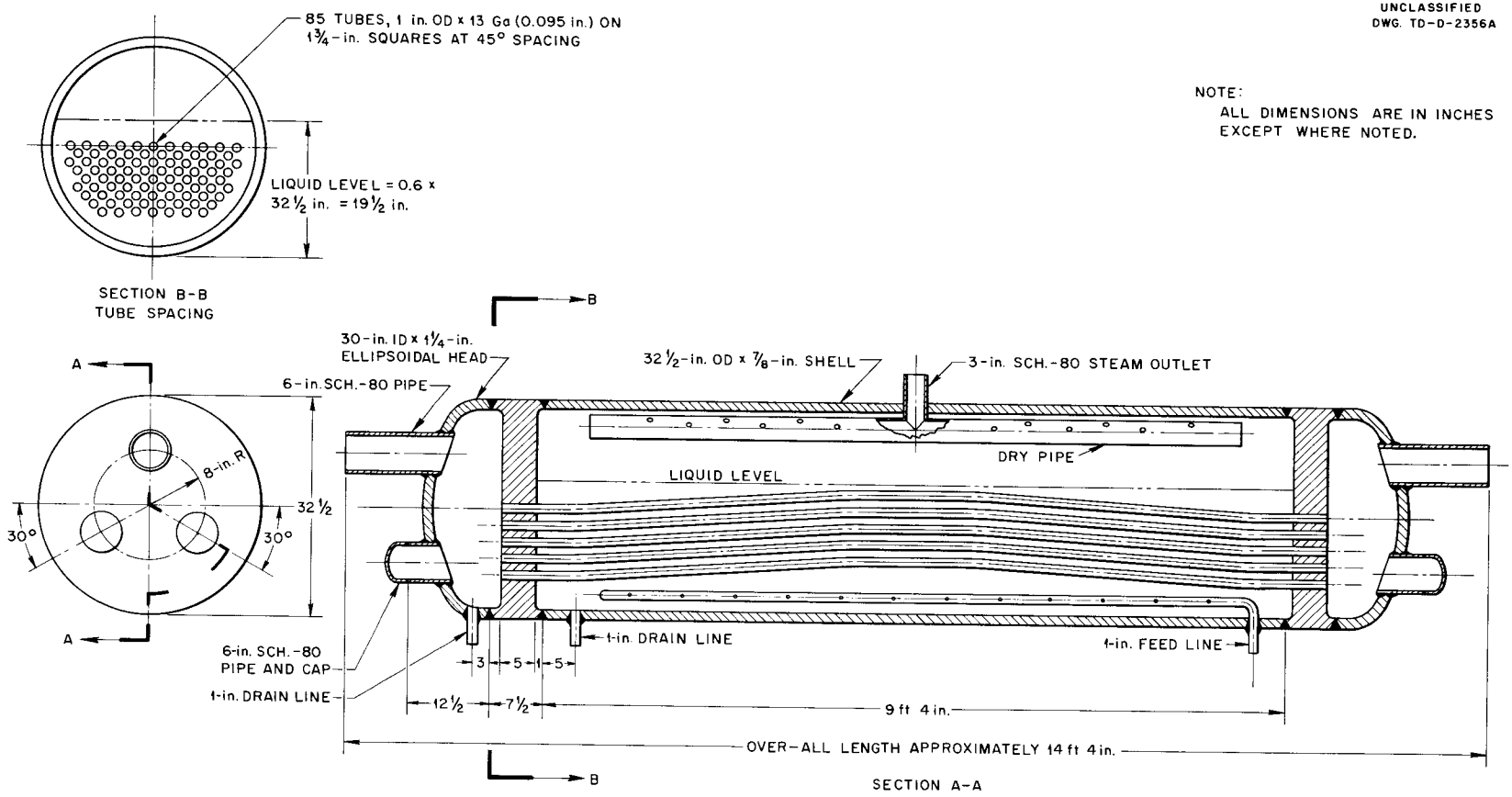

Fig. 20. ISHR Gas Condenser.

and velocity of gas flow suddenly so as to separate the condensate and collect it.

The pressure drop across the condenser is estimated to be about 0.38 psi.

NUCLEAR CALCULATIONS FOR TWO-REGION BREEDER REACTORS

Two-group calculations have been made for a two-region U^{233} breeder reactor with a 6-ft-dia core containing uranyl sulfate solution and a blanket containing thorium oxide as pellets or slurry. Breeding gain and critical concentration were found both for startup conditions and for the conditions existing after uranium has built up in the blanket.

The method of calculation is the same as that used for the ISHR. In this method, the conventional two-group two-region equations are modified to take into account the absorption of slow neutrons in the core tank. Absorption of fast neutrons in the thorium is calculated by using a resonance absorption cross section.[9]

The slurry blanket is assumed to be 2 ft thick and to have a thorium concentration of 1000 g/liter. The thorium oxide pellet blanket is 1 ft thick and has 4220 g of thorium per liter. Uncertainties in the age in the pellet blanket may require that the blanket be almost 2 ft thick to obtain the conversion reported here. Characteristics common to all the arrangements include the following:

Core power	320 megawatts
Temperature (core and blanket)	250°C
Moderator (core and blanket)	D_2O
Core tank	1/2-in. zirconium
Voids in core	3%
Fission-product poisons in core	3%

The thermal absorption cross sections at 250°C used in the calculations are given in the following:

ISOTOPE	σ_a (barns)
Th^{232}	7
Pa^{233}	100
U^{233}	143
U^{234}	60
U^{235}	478
U^{236}	6

$$\eta\ (U^{233}) = 2.30$$

$$\eta\ (U^{235}) = 2.09$$

It is possible that the thorium cross section should be as low as 5.2 barns at 250°C. Calculations are in progress to show the effect of this change in reducing the breeding gain reported in Tables 2 and 3.

In the startup calculations, it is assumed that the core uranium is all U^{233} and that there is no uranium in the blanket. Because of the high flux, fission products will build up rapidly,

TABLE 2. INITIAL CONDITIONS FOR TWO-REGION BREEDER REACTORS

Blanket type	Slurry	Pellet
Critical U^{233} concentration, g/l	1.31	1.45
Breeding gain	0.19	0.20
Neutron Balance		
Core U^{233}	1.000	1.000
Fission products	0.030	0.030
Sulfur	0.001	0.001
D_2O	0.028	0.025
Core tank	0.038	0.018
Blanket		
Th^{232}	1.196	1.209
D_2O	0.002	0.000
Fast leakage	0.004	0.019
Slow leakage	0.004	0.002

(9) S. Visner, *Nuclear Calculations for Homogeneous Reactors Producing U^{233}*, ORNL CF-51-10-110.

TABLE 3. OPERATING CONDITIONS FOR TWO-REGION BREEDERS

Blanket type	Slurry	Slurry	Pellet	Pellet
U^{233} in blanket, kg per ton of thorium	3	5	3	5
Critical U^{233} concentration, g/l	1.33	1.29	1.47	1.44
Breeding gain	0.17	0.18	0.20	0.21
Blanket power, megawatts	61	106	50	90
Processing rate, kg of thorium per day	95	63	112	71
Neutron Balance				
Core				
U^{233}	1.000	1.000	1.000	1.000
U^{234}	0.124	0.138	0.112	0.120
U^{235}	0.124	0.139	0.112	0.121
U^{236}	0.019	0.022	0.018	0.019
Fission products	0.030	0.030	0.030	0.030
Sulfur	0.003	0.003	0.003	0.003
D_2O	0.028	0.028	0.025	0.025
Core tank	0.043	0.043	0.024	0.023
Blanket				
Th^{232}	1.406	1.579	1.381	1.500
Pa^{233}	0.022	0.026	0.011	0.013
U^{233}	0.212	0.373	0.172	0.281
U^{234}	0.001	0.003	0.001	0.001
Fission products	0.009	0.023	0.005	0.012
D_2O	0.002	0.002	0.000	0.000
Fast leakage	0.019	0.032	0.037	0.052
Slow leakage	0.007	0.010	0.002	0.002

and therefore a poison equivalent to 3% of the U^{233} cross section is assumed. The results of the calculations are given in Table 2.

In the cases involving uranium in the blanket, the chemical processing rate necessary to maintain the desired U^{233} concentration is determined first. Concentrations of fission products and the higher isotopes of uranium in the blanket can then be calculated. The ratios of the uranium isotopes in the core are found by taking into account the isotopic ratios in the feed from the blanket. The results of these calculations are given in Table 3.

NUCLEAR CALCULATIONS FOR ONE-REGION BREEDER REACTORS

Calculations have also been made for breeder reactors in which the uranium and thorium are mixed together in a single core, 10, 15, or 20 ft in diameter. Critical concentration, breeding gain, and chemical processing rates have been calculated with thorium concentration, fission-product poisoning, and reactor power as parameters.

The method used is a simple two-group bare-reactor treatment that takes into account the buildup of Pa^{233} and of the higher uranium isotopes. The critical concentration and breeding gain have also been calculated at startup (with the reactor free of poisons). The results of these calculations are listed in Table 4. The constants used are the same as those used for the two-region reactors, except that $\sigma_a(Th^{232})$ is taken to be 5.2 barns at 250°C.

During the initial period of operation there will be no chemical processing and the fission products and protactinium will build up rapidly. Thus the critical concentration and the breeding gain after a short time will be quite different than at startup. An indication of the speed with which the Pa^{233} and the fission products build up is given in Table 5. It is assumed that the reactor will be started with pure U^{233} and Th^{232} and will be operated continuously at 1000 megawatts, with no chemical processing.

Because of the rapid buildup of poisons in the reactor, startup conditions are not a good measure of the performance after normal operation begins. Table 6 gives the breeding gain and critical concentration for various amounts of fission-product poisons. The equilibrium amount of Pa^{233}, as determined by the flux and processing rate, is also taken into account.

The fraction of the reactor volume which must be processed per day depends only on the flux and the desired poison fraction. The amount of thorium processed depends on the system volume and the concentration. Table 7 gives the processing rates and the U^{233} production rates for the conditions given for Table 6. The U^{233} production rate is the net rate at which it is being produced in the reactor and does not take into account losses in chemical processing. Negative production rates mean that U^{233} must be added to the reactor from some other source.

TABLE 4. CRITICAL CONCENTRATION AND BREEDING GAIN FOR CLEAN ONE-REGION BREEDER REACTORS

CORE DIAMETER (ft)	THORIUM CONCENTRATION (g/l)	CRITICAL U^{233} CONCENTRATION (g/l)	BREEDING GAIN
10	250	4.42	0.01
	300	5.49	0.03
	350	6.67	0.05
	400	7.98	0.06
	100	1.38	0.04
	150	2.08	0.10
	200	2.86	0.13
	300	4.66	0.17
	400	6.83	0.18
20	100	1.26	0.13
	150	1.93	0.17
	200	2.67	0.20
	300	4.39	0.22
	400	6.47	0.23

TABLE 5. CHANGE IN CONDITIONS DURING INITIAL PERIOD OF OPERATION OF A ONE-REGION BREEDER REACTOR*

TIME AFTER STARTUP (sec)	$\frac{\Sigma_a(Pa^{233})}{\Sigma_a(U^{233})}$	$\frac{\Sigma_a(\text{fission products})}{\Sigma_a(Pa^{233})}$	BREEDING GAIN	U^{233} CONCENTRATION (g/l)
0	0	0	0.13	2.86
10^6	0.011	0.013	0.10	2.94
3×10^6	0.024	0.026	0.06	3.02
6×10^6	0.033	0.043	0.03	3.12
10^7	0.036	0.065	0.00	3.21

*Core diameter, 15 ft; thorium concentration, 200 g/l; power, 1000 megawatts.

TABLE 6. CRITICAL CONCENTRATION AND BREEDING GAIN FOR REACTORS WITH FISSION PRODUCTS AND Pa^{233}

CORE DIAMETER (ft)	POWER (megawatts)	THORIUM CONCENTRATION (g/l)	WITH 3% POISONS		WITH 5% POISONS		WITH 7% POISONS		WITH 9% POISONS	
			Breeding Gain	U^{233} Concentration (g/l)	Breeding Gain	U^{233} Concentration (g/l)	Breeding Gain	U^{233} Concentration (g/l)	Breeding Gain	U^{233} Concentration (g/l)
10		300	-0.020	5.84	-0.041	6.04	-0.059	6.23	-0.076	6.42
		350	0.000	7.11	-0.021	7.35	-0.040	7.59	-0.057	7.85
		400	0.014	8.52	-0.006	8.83	-0.024	9.14	-0.042	9.46
15	1000	100	-0.030	1.46	-0.065	1.51	-0.090	1.55	-0.111	1.59
		150	0.031	2.20	0.001	2.27	-0.022	2.33	-0.042	2.39
		200	0.068	3.03	0.041	3.12	0.019	3.20	-0.001	3.28
		300	0.108	4.94	0.084	5.09	0.064	5.23	0.045	5.38
		400	0.131	7.25	0.108	7.50	0.090	7.72	0.071	7.97
15	1500	100	-0.033	1.47	-0.070	1.51	-0.097	1.56	-0.120	1.60
		150	0.028	2.21	-0.005	2.28	-0.030	2.34	-0.050	2.40
		200	0.064	3.03	0.035	3.13	0.012	3.21	-0.008	3.30
		300	0.104	4.95	0.079	5.10	0.058	5.25	0.040	5.40
		400	0.127	7.27	0.105	7.51	0.085	7.75	0.067	8.00
20	2000	100	0.051	1.33	0.015	1.37	-0.013	1.41	-0.036	1.44
		150	0.099	2.04	0.067	2.10	0.042	2.15	0.021	2.21
		200	0.126	2.83	0.098	2.91	0.076	2.98	0.055	3.06
		300	0.159	4.65	0.134	4.78	0.114	4.92	0.095	5.05
		400	0.176	6.86	0.154	7.07	0.135	7.28	0.116	7.50

TABLE 7. THORIUM PROCESSING RATE AND U^{233} PRODUCTION RATE

CORE DIAMETER (ft)	POWER (megawatts)	THORIUM CONCENTRATION (g/l)	WITH 3% POISONS		WITH 5% POISONS		WITH 7% POISONS		WITH 9% POISONS	
			Thorium Processing (kg/day)	U^{233} Production (g/day)	Thorium Processing (kg/day)	U^{233} Production (g/day)	Thorium Processing (kg/day)	U^{233} Production (g/day)	Thorium Processing (kg/day)	U^{233} Production (g/day)
10	500	300	181	-12	94	-26	62	-37	46	-47
		350	174	0	91	-13	60	-25	44	-35
		400	165	9	86	-4	57	-15	42	-26
15	1000	100	482	-37	252	-81	167	-112	124	-138
		150	479	38	251	1	167	-27	124	-52
		200	466	84	244	51	162	24	120	-1
		300	429	134	224	104	149	80	110	56
		400	389	163	203	134	134	112	99	88
15	1500	100	722	-61	376	-130	250	-181	185	-223
		150	719	52	375	-9	249	-56	184	-93
		200	697	119	364	65	242	23	179	-15
		300	641	194	335	147	222	108	164	75
		400	581	236	303	196	201	158	148	125
20	2000	100	1060	127	555	37	369	-32	273	-89
		150	1037	246	542	166	361	104	268	52
		200	997	313	522	243	348	189	258	137
		300	910	395	476	333	316	283	234	236
		400	823	437	430	382	285	335	210	288

REACTOR PHYSICS

M. C. Edlund
L. Cooper
P. R. Kasten
M. Tobias

REACTOR STATICS CALCULATIONS

Attention has been given to the problem of calculating resonance capture in breeder reactors. Two-group methods in which a resonance capture cross section is used were compared with two- and three-group methods in which a resonance escape probability was a more realistic model of the physical situation and produced more conservative estimates of breeding gains. The leakage, estimated by three-group calculations, in a reactor with 6-ft-dia core and a 1-ft THO_2-pellet blanket containing 4000 g of thorium per liter was five times as large as that estimated by the two-group calculations used previously. It is believed that use of a blanket about 2 ft thick will render leakage losses negligible. (The blanket design problem is now being considered in detail.) It was also observed that the breeding gains in the reactors studied were relatively insensitive to changes of ±20% in the reactor constants. In general, a change which would tend to decrease one type of loss was largely compensated by increases in other losses. For instance, decreasing the age in the blanket by using BeO in place of part of the D_2O to decrease leakage is compensated by increased core-tank absorption. (Details of the three-group method may be found in ORNL CF-53-6-158.)[1]

Since it is desirable to perform rapidly a parameter study involving various dimensions, blanket concentrations, poisoning, and processing conditions for two- and three-region reactors, the multigroup equations (three groups and three regions) have been coded for the UNIVAC. Statics calculations for two-region breeder reactors are now being performed on automatic computers.

The question of the effect of inlet and outlet piping upon the breeding ratio has been given some consideration. Preliminary estimates give an additional neutron loss on the order of 0.0003 neutrons per U^{233} atom burned for a 6-ft core with a 2-ft blanket and 2-ft inlet and outlet pipes. Although the holes seem large, only about 2% of the reactor surface is involved.

Calculation of protactinium losses is currently under way for multi-region pellet blankets in which the pellets are not mixed. If there is no mixing of the pellets, the protactinium losses in a single-region blanket are prohibitively high for blanket processing periods greater than a few days. For example, in the reactor with a 6-ft-dia core, which was discussed in the chapter on "Intermediate-Scale Homogeneous Reactor Design," a protactinium loss of about 0.12 neutron is obtained for blanket processing periods of greater than 50 days if there is no mixing of the pellets. If the blanket processing period is reduced to ten days, the protactinium losses are reduced to about 0.03 neutron. However, for the ten-day processing period, the blanket processing cost per unit mass of fuel produced increases by a factor of 5. By introducing two or more blanket regions, the regions closer to the core can be processed more rapidly to reduce protactinium losses without a marked increase in the blanket processing costs per unit mass of fuel produced.

[1] M. Tobias and M. C. Edlund, *The Influence of the Method of Calculating Resonance Capture on the Fast Leakage in Breeders*, ORNL CF-53-6-158 (June 16, 1953).

KINETICS OF ISHR

A system of dynamic equations similar to those used for previous HRE kinetic calculations has been developed for a model which simulates some features of the ISHR design. The model chosen for the physical system is given schematically in Fig. 21.

The essential difference between the system shown in Fig. 21 and that investigated in previous HRE kinetic calculations[2] is the location of the pressurizer in a fluid flow line. With this arrangement, pressure surges will influence the operation of the pump, which, in turn, will affect reactor operation. More attention will be given to conditions of reactor startup and low-power operation than has been given in previous calculations, and both instantaneous and linear increases of reactivity will be considered, along with gas effects.

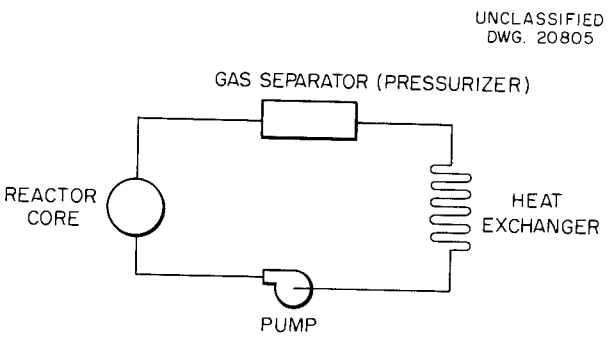

Fig. 21. Schematic Diagram of Reactor System.

Among the design features to be examined with respect to their influence upon reactor safety are the thickness of the reactor core shell and the size and length of the pipe leaving the reactor core. On the basis of previous calculations,[2] the primary variable to investigate will be the core pressure fluctuations.

(2) W. C. Sangren, *Kinetic Calculations for Homogeneous Reactors*, ORNL-1205 (Apr. 1, 1952).

ENGINEERING DEVELOPMENT

C. B. Graham, Section Chief

CORE AND GAS SEPARATOR DEVELOPMENT

J. M. Baker
Royce Goodman
J. A. Hafford
L. B. Lesem
I. Spiewak
R. H. Wilson

ISHR Core Flow Models. The best flow arrangement for a high-power-density core appears to be slug flow, with an equal temperature rise in each stream line. In addition to orderly heat removal, this type of core has other important advantages: low pressure drop, good gas removal, and a low turbulence level.

One excellent method of obtaining slug flow is the use of screens in the entrance diffuser to the core. This arrangement has been investigated in an 18-in. plastic model,[1] and a full-scale 48-in. model will be ready for operation with water during the next quarter.

Another scheme for producing slug flow through a spherical core is shown in Fig. 22. Stationary vanes in the southern hemisphere inlet give the liquid a rotational velocity component which allows the liquid to expand into the sphere without separation. Preliminary experiments on an 18-in. scale indicate that there is very little lateral mixing in the core. The axial velocity profile may be adjusted to conform to the power removal requirements by proper design of the turning vanes.

In this system, most of the gas is centrifuged into a central void, from which removal should be feasible. The major problem remaining to be solved is that of minimizing the precession of the void, which might lead to nuclear instability or difficulty in removing the gas.

The major advantage of the vaned core over the one with screens lies in the elimination of parasitic neutron capture by the screens.

ISHR Core Fabrication and Mechanical Testing. If stainless steel is used as the structural material for the ISHR core tank, it will be desirable to minimize the wall thickness of the vessel in order to conserve neutrons. At the same time, the core tank must be strong enough to withstand the variations in differential pressure and in thermal stress which are likely to occur during the life of the reactor. The core thicknesses being considered are between 1/16 and 1/4 inch.

Since a mathematical stress analysis of the core tank cannot accurately include all the complicated geometrical configurations (such as pipe connections, out-of-roundness, etc.), it is believed necessary to demonstrate experimentally that the core will withstand loads that simulate operational loads. These tests should allow the selection of a core tank of minimum thickness, establish the tolerance requirements in metal thickness and out-of-roundness, and suggest refinements in the geometrical shape of the inlet and the outlet.

As a first step, a number of spherical segments are being spun at the Y-12 shop. These represent the part of the core above 45 deg north latitude. Several of these segments will have outlet pipes welded to them, with various fillet radii between pipe and spherical surfaces. Spherical wall thickness will be varied. These segments will receive a compressive loading to simulate the differential expansion between the stainless steel core tank and the carbon steel pressure vessel of the ISHR. These tests should indicate the geometrical limits

(1) J. A. Hafford, L. B. Lesem, I. Spiewak, and R. H. Wilson, *HRP Quar. Prog. Rep. Jan. 1, 1953*, ORNL-1478, p. 45-46.

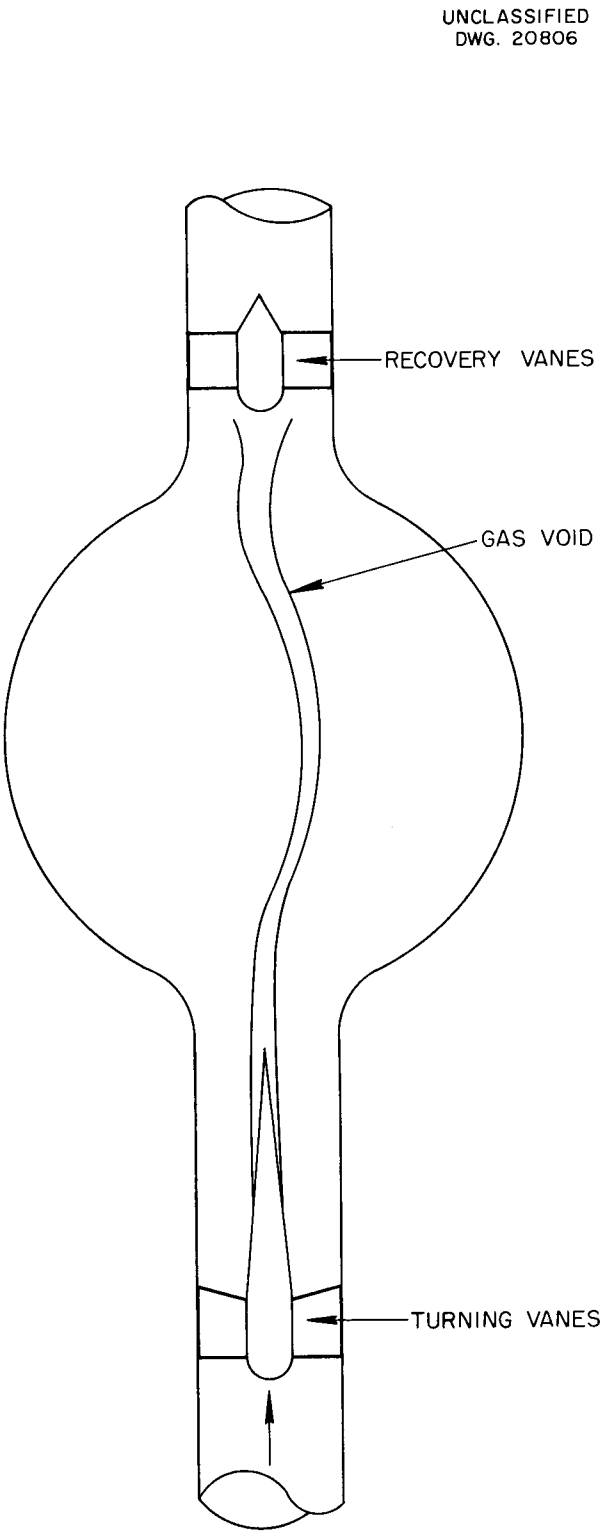

Fig. 22. Straight-through Core with Turning Vanes.

for which an expansion joint other than the sphere itself is required to keep thermal stresses below those allowable.

At the same time, compressive ring loadings will be applied to pure spherical segments and segments with a large hole at the center to check stress calculations made by the Design Section.

Following these tests and an intensive study of present manufacturing techniques, a full-scale core will be designed and tested under internal and external pressure combined with compressive loading.

Eight-Foot Rotational-Flow Model. The 8-ft rotational-flow model containing two 24-in. inlets and two 30-in. outlets was described in ORNL-1280.[2] The sphere was operated at flow rates ranging from 13,000 to 50,000 gpm, and measurements were made of static pressure drop and tangential velocity distribution.

The results of these tests were reported in ORNL CF-53-7-29.[3] The over-all pressure drop was found to conform very closely to the correlations which were developed on small spheres; it amounted to 15.6 inlet velocity heads or about 23 psi at 40,000 gpm (corresponding to 50 kw/liter). This is considered to be excessive for most reactor applications other than experimental reactors.

The tangential velocity distribution in the region outside the outlet pipe was found to vary with the -0.87 power of the radius, and thus there is nearly a free vortex. Visual observations disclosed that there were no stagnant regions but that gas removal was quite inferior to that obtained in the HRE.

---

[2] C. B. Graham *et al.*, *HRP Quar. Prog. Rep. Mar. 15, 1952*, ORNL-1280, p. 151.

[3] L. B. Lesem, R. H. Wilson, and I. Spiewak, *Hydrodynamic Studies in an Eight-Foot Sphere Utilizing Rotating Flow*, ORNL CF-53-7-29 (July 20, 1953).

Because of the high pressure drop, no further work is planned at this time with this type of core.

Pipe-Line Gas Separator. The use of straight-through flow in the ISHR core necessitates the development of an external gas separator. At the same time, it is desired to provide a "pressurizer" or surge chamber which will keep the high-pressure circulating system at 1000 psi. These objectives can best be met in a pipe-line separator, in which the liquid is given a rotational component and gas is centrifuged into a large central void which is maintained at 1000 psi by gas pressure in the void.

Developmental work on vanes and volutes to provide the spin and to recover the rotational energy has been described in previous quarterly reports.[1,4,5] During this quarter, a gas take-off has been developed which permits a large void to operate at separating efficiencies that cannot be differentiated experimentally from 100%. This take-off is shown in Fig. 23. The void size varies between the outside diameter of the frog and the inside diameter of the take-off pipe and depends on gas flow rate and the amount of liquid entrainment. In the event of a blower failure, a surge chamber will still be available, since the void size cannot become smaller than the outside diameter of the frog.

In order to predict the pressure drop in the take-off line, which will contain a mixture of gas and entrained liquid, a literature survey of two-phase pressure drop was made. The results of the survey are applied to the ISHR conditions in ORNL CF-53-5-112.[6]

A full-scale model of the ISHR gas separator is being constructed that will operate at low pressure. It is expected that the final design refinements can be worked out during testing. The most important information required is the precise velocity distribution leading to the recovery vanes, since an efficient design must be tailored to the actual velocity distribution. Information will also be obtained on the pressure drop in the gas outlet pipe, particularly across changes in cross section and elbows.

Vaned-Miter Elbows. The entrances to both the ISHR core and the gas separator follow 90-deg elbows. Since the velocity distribution in the inlets appears to influence the stability of the flow pattern through these devices, it is believed that the elbows should be built so that the downstream velocity distribution is approximately the same as that in a straight pipe.

Vaned-miter elbows properly designed will produce the desired results with a minimum of pressure drop and turbulence. An elbow has been built for testing in conjunction with the 48-in. ISHR core model. The design of this elbow was based on information obtained at the University of Minnesota.[7] A

(4) C. B. Graham *et al.*, *HRP Quar. Prog. Rep. Oct. 1, 1952*, ORNL-1424, p. 62.

(5) J. A. Hafford, L. B. Lesem, I. Spiewak, and R. H. Wilson, *HRP Quar. Prog. Rep. Mar. 31, 1953*, ORNL-1554, p. 36-38.

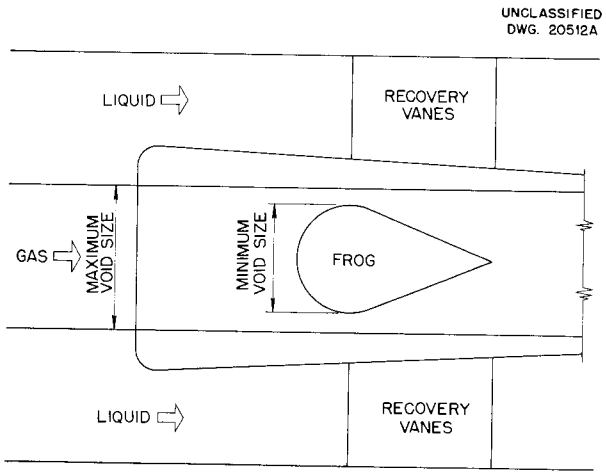

Fig. 23. Gas Take-off Arrangement for Maintenance of a Large Void.

(6) J. A. Hafford, *Two-Phase Flow*, ORNL CF-53-5-112 (May 18, 1953).

(7) L. G. Straub and E. Silberman, *Fluid Flow Diversion by Guide Vanes in Miter Bends*, Project Report No. 8, University of Minnesota (April 1949).

schematic diagram of the elbow is shown in Fig. 24. It contains 13 thin vanes, with the leading and trailing edges parallel to the flow direction and a circular arc between the edges.

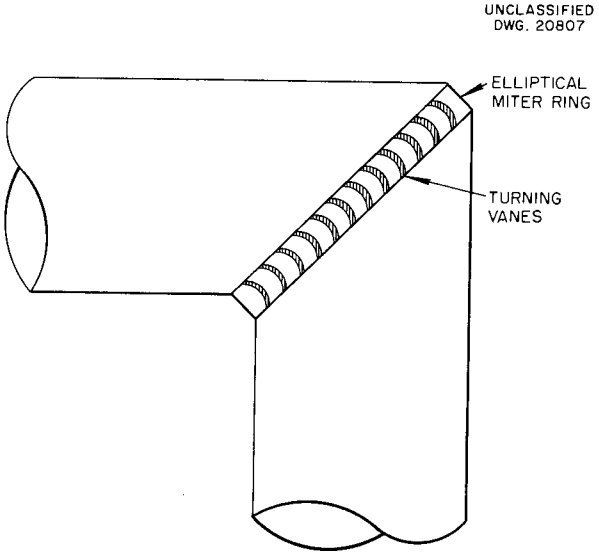

Fig. 24. Vaned-Miter 90-deg Elbow.

RECOMBINER DEVELOPMENT

J. A. Ransohoff R. H. Wilson
I. Spiewak Royce Goodman

Catalytic Recombiner. A small catalytic recombiner containing 1.39 $in.^3$ of platinized alumina catalyst has been operated over a wide range of temperature, pressure, flow rate, and gas composition. A detailed presentation of this investigation is reported in ORNL-1583.[8]

It was concluded that diffusion of hydrogen and oxygen to the catalyst was the major factor in determining the kinetics of the reaction, although the influence of other factors was apparent. The effect of the variables being considered may be summarized as follows:

1. *Temperature, Experimental Range 230 to 550°C.* The reaction rate increased slowly as temperature was increased between the limits 300 to 500°C in conformity with the diffusion mechanism. Below 300°C, rates began to decrease more sharply and indicated that chemical effects were becoming important.

2. *Pressure, Experimental Range 25 to 110 psia.* As pressure was increased, the reaction rate increased but remained well below that predicted by diffusion. Since diffusion theory predicts rates that are independent of pressure, it is believed that at the test pressures the surface adsorption was influencing the kinetics.

3. *Flow Rate, Experimental Range 600,000 to 1,750,000 scfh per ft^3 of Bed.* The reaction rate varied with Reynolds number over the entire range in a manner that was consistent with the diffusion hypothesis.

4. *Gas Composition, Experimental Range 2 to 8% H_2, O_2-to-H_2 Ratio Greater than 0.5, Diluent-Gas-Dry Steam.* As the O_2-to-H_2 ratio increased, the bed became more efficient because oxygen does not diffuse so rapidly as hydrogen. When the ratio reached about 1.0, a further increase in oxygen did not change the reaction rate because hydrogen diffusion controlled throughout the bed.

Several runs were made with D_2 substituted for H_2. No quantitative conclusions could be made because of the occurrence of the side reaction that exchanged D for H in steam in the presence of a platinum catalyst. However, the oxygen-rich runs in which the side reaction was minimized seemed to indicate that diffusion was controlling the kinetics. The rates were below those for hydrogen by an amount that corresponds to the difference in diffusivities.

Flame Recombiner. It is known that H_2-O_2-steam mixtures containing less than 25% $2H_2 + O_2$ will arrest the

(8) J. A. Ransohoff and I. Spiewak, *Development of Hydrogen-Oxygen Recombiners*, ORNL-1583 (to be issued).

explosion of a combustible mixture of the gases elsewhere in the system. This suggests an explosion-proof type of flame recombiner that would be useful for boiling reactors or other applications in which there is a high ratio of steam to combustible gas. The initial mixture is fed into a vertical column containing alternate cooling coils and spark plugs. As the gas travels up, it will become combustible when enough steam has condensed on the cooling coils. Above this position, which varies with the flow rate and gas composition, the gas will burn.

Figure 25 shows such a device, which is an experimental flame recombiner 4 in. in diameter and 48 in. long. The unit was operated at pressures of up to 70 psia and stoichiometric gas flow rates of up to 9.6 scfm. The efficiency of recombination was above 99% in all runs and could be brought to 100% by blanking off the top of the unit. The maximum temperature observed was 350°C. There were no explosions during the tests. This investigation is described in detail in ORNL-1583.[8]

LARGE COMPONENT DEVELOPMENT

Allis-Chalmers Pump Development (W. L. Ross). A description of the Allis-Chalmers, 20,000-gpm, canned-rotor, totally enclosed pump was given previously.[9] Allis-Chalmers has completed preliminary design, engineering studies, and final design of the pump. The final design includes detail drawings and manufacturing specifications. Allis-Chalmers will make an estimate of manufacturing costs and submit a final report on this design.

Worthington Corporation Pump Development (W. L. Ross). The 20,000-gpm centrifugal pump proposed by Worthington Corporation has been described.[9,10] Worthington has completed preliminary design and engineering studies of the pump which indicate the need for a testing program to prove the feasibility of the design, fabrication, and operation of the main pump bearing. Equipment to expedite the test program has been designed and fabrication is expected to be complete by August 1, 1953. The testing program will proceed as soon as the equipment is completed.

Main Circulating Pump for ISHR Fuel System (W. L. Ross). Preliminary specifications have been developed for the ISHR main circulating pump. Briefly, a canned-rotor type, 5000-gpm, 100-ft head, 1000-psi working pressure, stainless steel pump will be adequate for a 50-megawatt (heat) reactor power level. Special provisions will be made to replace all pump parts, including the stator, through a single flanged opening on the top of the pump-motor housing without disturbing the mainstream piping.

Gas Circulator for an ISHR Recombiner System (W. L. Ross). Some changes have been effected in the recombiner system of the ISHR since the previous report.[11] It is proposed that some of the oxygen be replaced with helium in the gas-vapor mixture so that a minimum of approximately 50 psia of oxygen pressure will always be present in the void of the gas separator. This change will allow the hydrogen partial pressure to be increased to 3% of the total pressure and yet permit a nonexplosive gas-vapor mixture to be maintained. The requirements of the recombiner system are based on the allowable fraction of hydrogen in the mixture, and therefore the requirements of the gas circulator and the other components of the system are effected by this change.

(9) C. B. Graham *et al.*, *HRP Quar. Prog. Rep. July 1, 1952*, ORNL-1318, p. 112.

(10) C. B. Graham *et al.*, *HRP Quar. Prog. Rep. Oct. 1, 1952*, ORNL-1424, p. 65.

(11) W. L. Ross, *HRP Quar. Prog. Rep. Mar. 31, 1953*, ORNL-1554, p. 40.

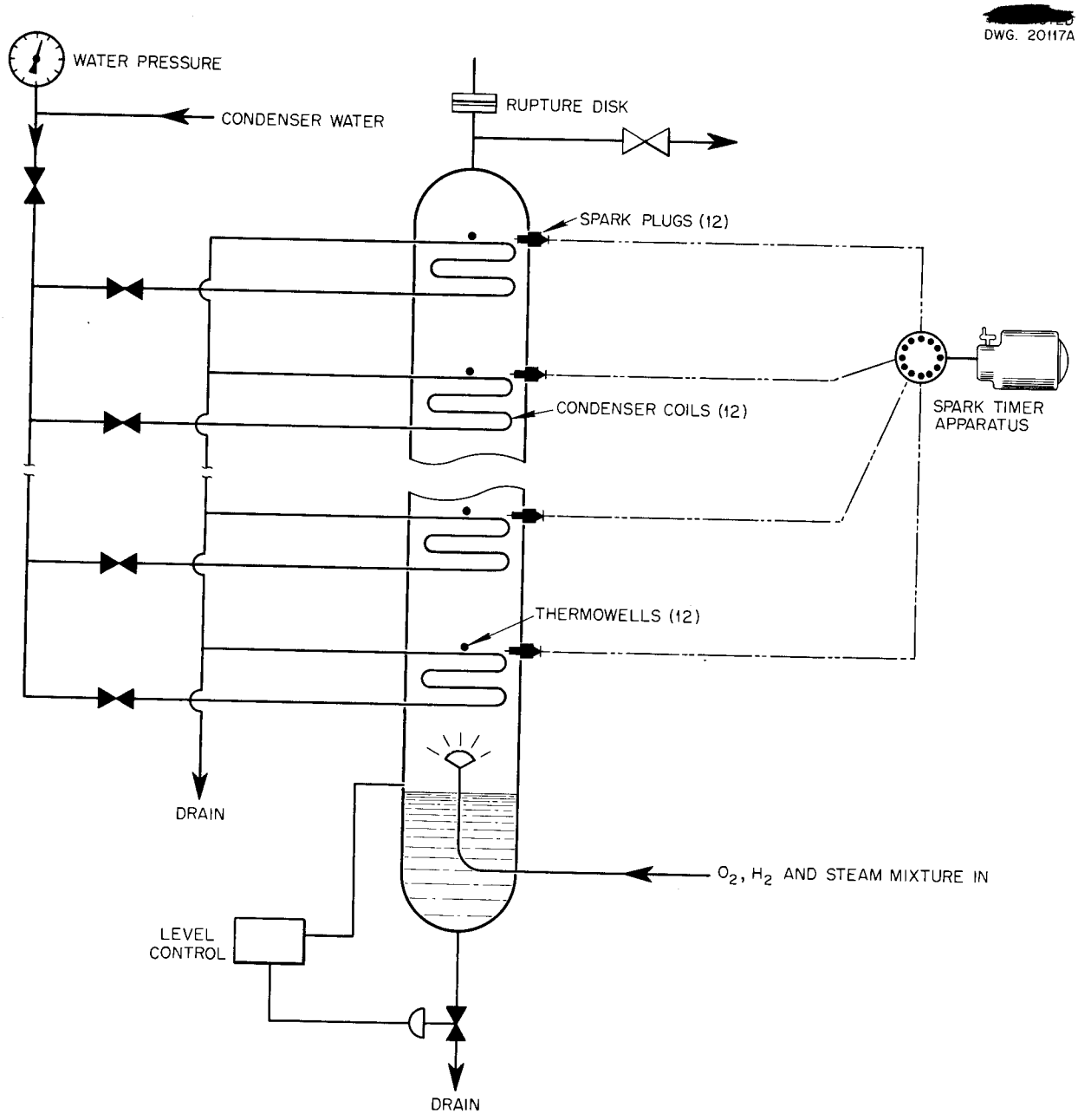

Fig. 25. Experimental Flame Recombiner.

Recent calculations[12] indicate that approximately 34.3 lb-moles/min of gas mixture must be withdrawn from the gas separator and that approximately 30.5 lb-moles/min will be fed to the gas separator. The 3.8 lb-moles/min difference is condensed from the mixture in the gas condenser. The calculations of pressure drop are for a system made up of a gas separator, an entrainment separator, a packed-bed type of catalytic recombiner, a gas condenser which cools and condenses a portion

[12] R. E. Aven, *Pressure Drop in High Pressure Gas System for ISHR*, ORNL CF-53-6-203 (June 23, 1953).

of the flow, and the associated, connecting pipe. The total pressure drop for the required gas flows through the system is approximately 3.0 psi.

The service requirements of the gas circulator needed to provide sufficient gas-vapor flow under the present ISHR design conditions are approximately as follows:

Capacity	500 lb/min (320 cfm)
Developed head	280 ft (3.0 psi)
Suction pressure	990 psia
Gas temperature	480°F
Gas density	1.55 lb/ft^3
Fluid horsepower	4.3 (theoretical)
Gas mixture	Steam, oxygen, helium, with radioactive contamination
Leakage	No atmospheric leakage permissible
Maintenance	All parts subject to failure must be replaceable by remote means

The use of a semistandard canned-rotor-pump motor to drive the gas circulator has been discussed with two manufacturers, and it appears that this approach to the problem will provide a suitable unit for the ISHR system. The unit will be mounted vertically, with the impeller in the gas mixture. Below the impeller, the motor and bearings will be flooded with condensate (D_2O) from the gas condenser. Hence, it will be possible to use for the gas circulator a motor drive which already has been developed and has demonstrated reliability in other service.

ISHR Heat Exchanger (L. F. Goode, W. L. Ross). The preliminary design of the heat exchanger, shown in Fig. 16, evolved from the recent 50-megawatt heat exchanger studies based on more liberal heat transfer coefficients than were considered previously. Preliminary specifications have been developed and proposals to do design evaluation, development, final design, and fabrication will be requested from prospective manufacturers in the near future. The contract will include developmental work on welded tube joints, feed-water treatment, and other necessary items, as well as complete design and fabrication of the exchanger.

Test Loop for 4000-gpm Pump (J. S. Culver). Progress on the construction of the loop[13] for testing the 4000-gpm pump is illustrated in Fig. 26. Practically all work on small piping is complete and all instruments are installed except those that will be connected to the large pipe loop. Test welds are now being made on the large pipe to standardize welding techniques and inspection before welding of the loop is started. Because of delays in the shipment of some major parts, completion of the loop will be delayed until about September 1.

Pulsafeeder Pump Tests (P. N. Stevens). Studies of the elastic behavior of pulsafeeder pump diaphragms[14] have continued with a new approach dictated by the practical limitations of such a pump. To obtain the full displacement of a diaphragm pump, it is necessary to completely fill the cavity between the contoured flanges. This implies sufficient suction head to stretch the diaphragm until it contacts the contoured flange over its entire area. The manufacturer of the pump used in the HRE stated that only 4 in. of H_2O pressure was required to completely fill the head, but measurements show that a pressure of 10 in. Hg is required to fully deflect the diaphragm. Measurements of volume displaced vs. pressure required are shown in Fig. 27. The diaphragms tested were made of type 347 stainless steel; one was 0.019 in. thick, that is, identical to the HRE pump diaphragm, and another was twice as thick, or 0.038 in. thick. The tests showed that the 0.038-in.-thick diaphragm required little more pressure than the 0.019-in.-thick diaphragm to

[13] J. R. McWherter *et al.*, *HRP Quar. Prog. Rep. Nov. 15, 1951*, ORNL-1221, p. 18.

[14] P. N. Stevens and C. D. Zerby, *HRP Quar. Prog. Rep. Mar. 31, 1953*, ORNL-1554, p. 41.

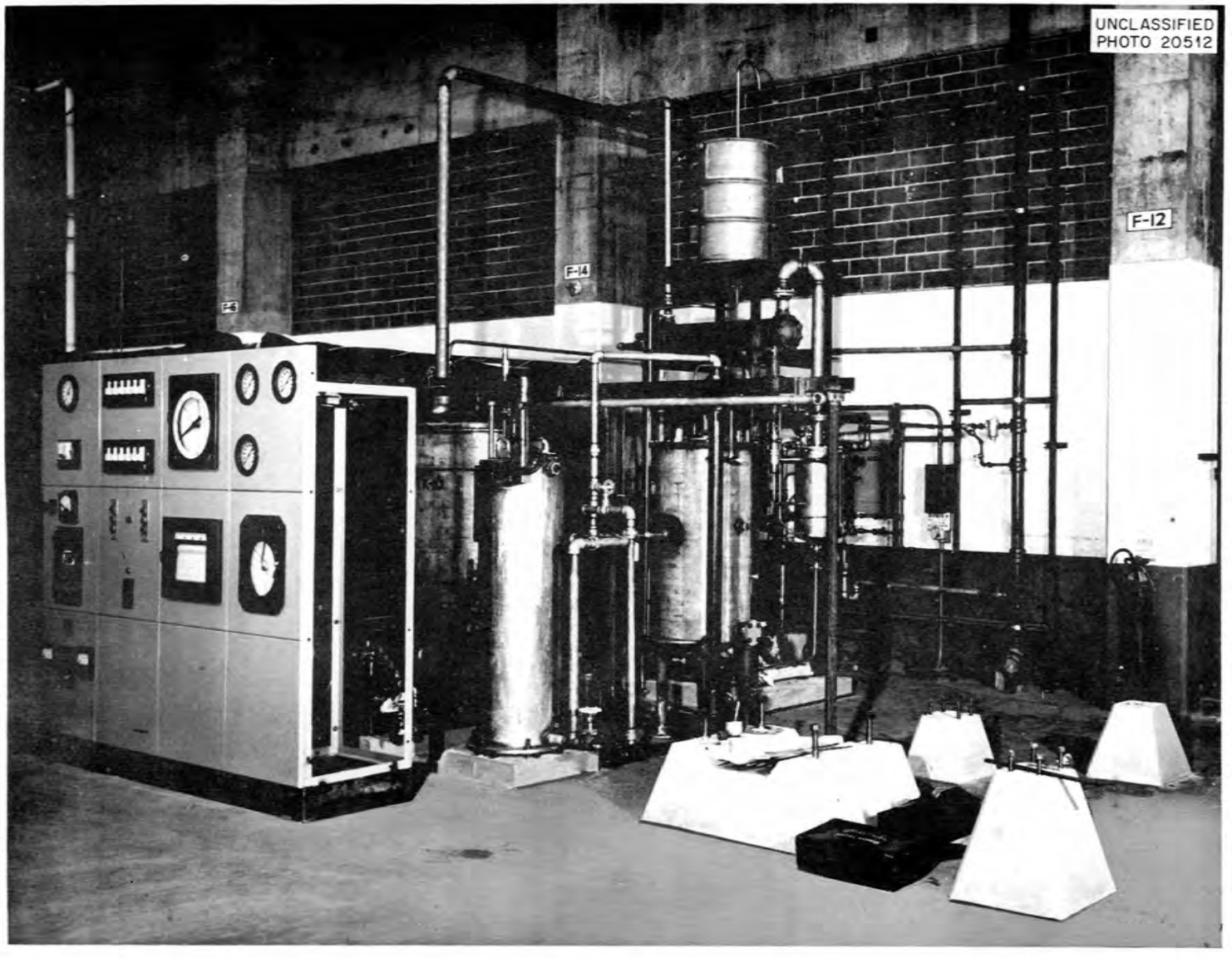

Fig. 26. Components Installed for the 4000-gpm Pump Loop as of August 1, 1953.

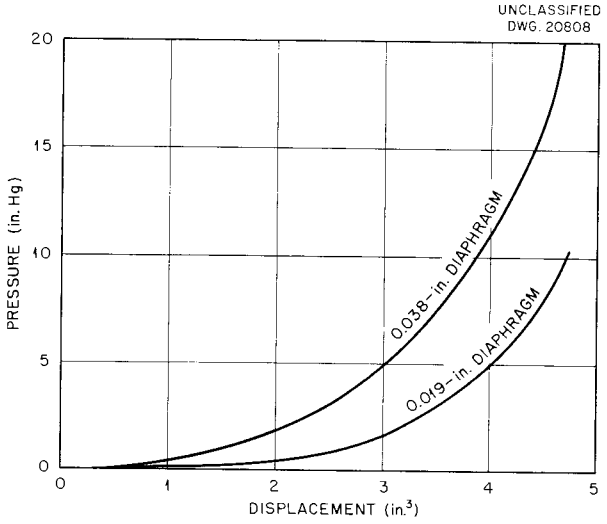

Fig. 27. Pulsafeeder Diaphragm Test.

obtain most of the available displacement.

Previous tests indicated that the stress in the diaphragm rises rapidly in the extreme positions and thus that the contour in the flanges was not ideal. Since the diaphragm tends to assume the free deflection curve if unrestrained, it would appear that the center portion of the contour is too deep and gives rise to a high diaphragm stress and a high suction pressure requirement for a very small increase in pumping capacity. Since the maximum available suction pressure in the pulsafeeder is limited to 10 in. Hg, it is doubtful whether this final small volume has ever been obtained in practice.

Tests are continuing with strain gages to determine diaphragm stress at reduced deflections and with thicker diaphragms in an effort to develop a more rugged pump with longer fatigue life.

Stellite Piston Pump Test (J. M. Baker). The present phase of testing of the Stellite piston pump is now completed. In addition to tests previously reported,[15] the Stellite 3 piston and cylinder were operated in excess of 500,000 strokes at 63 to 65°C in uranyl sulfate solution containing 40 g of uranium per liter. The temperature of the test was considered to be as high as would be normally encountered in the suction stream from a reactor dump tank that would supply a feed pump of this type. The temperature was maintained by means of a heat lamp trained on the cylinder.

Examination of the piston showed only some scoring in one particular area. The original finish on the piston was 8 to 10 μin., whereas the roughened spot showed 15 to 19 μin. Analysis of the solution showed 25 ppm cobalt and 125 ppm tungsten. Since the rest of the piston and the cylinder wall retained a mirror finish, it is believed that there was no appreciable general corrosion and that the cobalt and the tungsten found were from the scored area.

Leakage past the piston in this pump is directed back into the suction stream; however, there is a limit to the amount of leakage that can be tolerated in a useful pump. To determine the expected leakage, the pistons and cylinders were assembled with blank heads and the system was pressurized with a small piston pump. The leakage was measured at various pressures up to a maximum of 1000 psi. The results of this test are shown in Fig. 28.

The tests made to date indicate that the combination of a Stellite 3 piston in a cylinder of the same material will run without excessive corrosion or erosion at temperatures up to 65°C with water or with uranyl sulfate solution containing 40 g of uranium per liter.

Future development of this pump will depend on the requirements of the reactor program. No driving mechanism has been built for this pump, as yet, because the mechanism will have to be suited to the conditions of temperature, pressure, and radiation present.

(15) C. B. Graham *et al.*, *HRP Quar. Prog. Rep. Jan. 1, 1953*, ORNL-1478, p. 45-60.

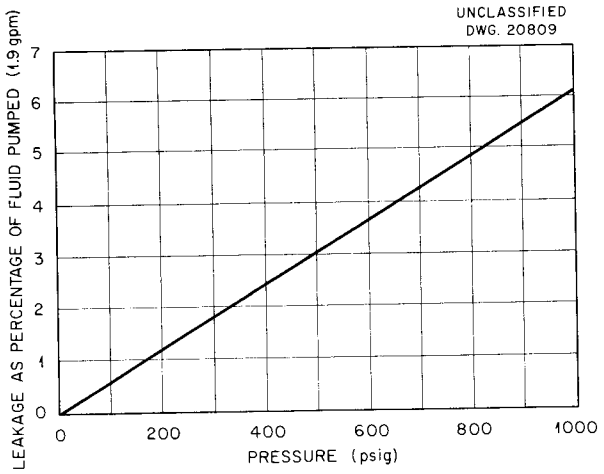

Fig. 28. Leakage-vs.-Pressure Test of Stellite Piston Pump.

ORNL Small Pump (C. D. Zerby, T. H. Mauney, C. B. Graham). Since the ORNL small pump has been described in a previous report,[16] only a very general review of the pump is included here. The pump is of the centrifugal type, but it has the following added features: (1) it is totally enclosed and has no packing, and thus it is leak free; (2) it can be operated at relatively high temperatures and pressures. The pump is designed for operation at 250°C and 1000-psi pressure. The capacity of the pump is in the range of 0 to 15 gpm, with a head of 40 ft at approximately 5 gpm. All parts that come in contact with the fluid being pumped are made of type 347 stainless steel, except for bearings, which are Graphitar, and a portion of the rotor, which is chrome plated. The back of the pump is cooled to reduce any corrosive tendency of the chrome plate and to prevent any deterioration of the bearings that might be caused by the elevated temperature.

Two small pumps were fabricated and subjected to test during this quarter. Both pumps have been operated satisfactorily at pressures of up to 1300 psi and at circulating-fluid temperatures of up to 250°C.. One pump has now operated 250 hr at various temperatures with approximately 100 starts and stops. The other pump has operated approximately 50 hr with approximately 25 starts and stops.

One of the original rotors was machined from a solid rod of type 410 stainless steel. This rotor has been discarded because of its low efficiency, and a standard-motor rotor canned in type 347 stainless steel and otherwise the same as the other rotor is being used in its place.

Two different discharge outlets from the volute have been designed and are presently in operation. One consists of a normal tangential outlet; the other has an axial outlet. The axial outlet was designed primarily for use in the in-pile loop, which is described in the chapter on "Corrosion." At 5 gpm, the head with the tangential outlet is 40.2 ft, and with the axial outlet, it is 39.7 feet. In general, the head from the pump with the axial outlet drops linearly from 39.7 ft at 5 gpm to 31.2 ft at 16 gpm. The head with the radial discharge will stay substantially above that for the axial discharge, but it has only been measured to 10 gpm, where it is 39.4 feet. Both of these discharge outlets have proved satisfactory for passing a considerable amount of gas in the circulating fluid without creating a gas-binding condition. In fact, once the back of the pump is full of fluid, it is possible to start the pump and the pumping action without bleeding the gas from the volute.

The pump is driven by a stator from a standard, single-phase, 110-volt, 1/2-hp motor. The stator has been altered to slip over the pump housing and to accommodate water-cooling tubes that are laid into the iron laminations to cool the windings. Both pump stators are satisfactorily cooled by this method. The maximum temperature in the stator is at the end windings, where the temperature increases to

(16) *Ibid.*, p. 58.

approximately 100 °C under operating conditions.

There was no difficulty in keeping the back end of the pump cool where the bearings and rotor are located. Sufficient cooling is provided by the pump cooling jacket to keep the temperature well below 120 °C in the back of the pump while pumping fluid at 250 °C.

All other features of the pump, including the bearings, have operated without indication of unusual wear or unsatisfactory operation. Tests will continue on the pumps in an effort to extend the operating time at temperature and pressure, and one pump will be started in a loop circulating uranyl sulfate at 250 °C.

CONTROLS AND INSTRUMENTATION

J. N. Baird
A. M. Billings
D. G. Davis
C. G. Heisig
J. L. Redford
D. S. Toomb
W. P. Walker

VALVE TEST LOOP

The valve test loop (Fig. 29) has operated for a total of 150 hr, and several valve designs are being tested in water at 150°C and 1000-psi pressure. Performance of each valve will be reported upon completion of its test. The valves being tested are:

1. three Fulton-Sylphon 1/2-in. type 347 stainless steel bellows-sealed valves with the following trim sets:
   a. seat, type 347 stainless steel with Stellite 6 inlay; plug, Stellite 6;
   b. seat, titanium 75A; plug, titanium 75A, with a gold gasket;
   c. seat, titanium 150A; plug, titanium 150A, nitrided;
2. a diaphragm-sealed poppet-plug type of sampling valve with a crystal-bar-titanium seat and a nitrided crystal-bar-titanium conical poppet;
3. a corrosion loop type of sampling valve with a valve body and an integral seat of titanium 75A and a plug of titanium RC-70.

Considerable trouble has been experienced with leakage past the plunger of the 65-gph Milton-Roy pump used for circulation in the loop. The type 316 stainless steel plunger has now been polished to a 10-μin. finish, and, if a suitable seal can be made of Chevron-type Teflon packing rings, the loop will be run with fuel circulating through the valves.

IN-PILE LOOP

Instrumentation has been provided for the high-temperature test loop and the component test facility for the in-pile loop. The control cabinet for this loop is shown in Fig. 30. Instrument selection and assistance in the design are proceeding for the in-pile mockup loop, as required.

LOOP FOR 4000-gpm PUMP

August 1 has been set as the date for completion of the instrumentation of the 4000-gpm pump loop.

The control panel board is designed to utilize the ORNL standard 24- by 26-in. replaceable steel panels, which permit changes in instrumentation requirements to be met easily by the addition of 24-in. sections or by the filling of unused spaces by blank panels.

An electrical probe to detect seal water in the 4000-gpm Bryon-Jackson pump bearing chamber will be used as an interlock in the pump starting circuit. Two types of high-pressure probes are presently being evaluated. The first is designed around a modified Conax thermocouple gland (Fig. 31), it utilizes porcelain as the insulating material and talc as the sealant. The second probe is a standard Fielden Instrument Division, Robertshaw-Fulton Controls Company, type 703, high-pressure electrode (Fig. 32); it utilizes a Teflon compression seal and a Synthane insulator. All metal parts of both probes are stainless steel.

BOILING REACTOR PROGRAM

Control and recording mechanisms have been furnished for the proposed reactor stability experiment on the Los Alamos water boiler. The control cabinet, the neutron chamber, and the

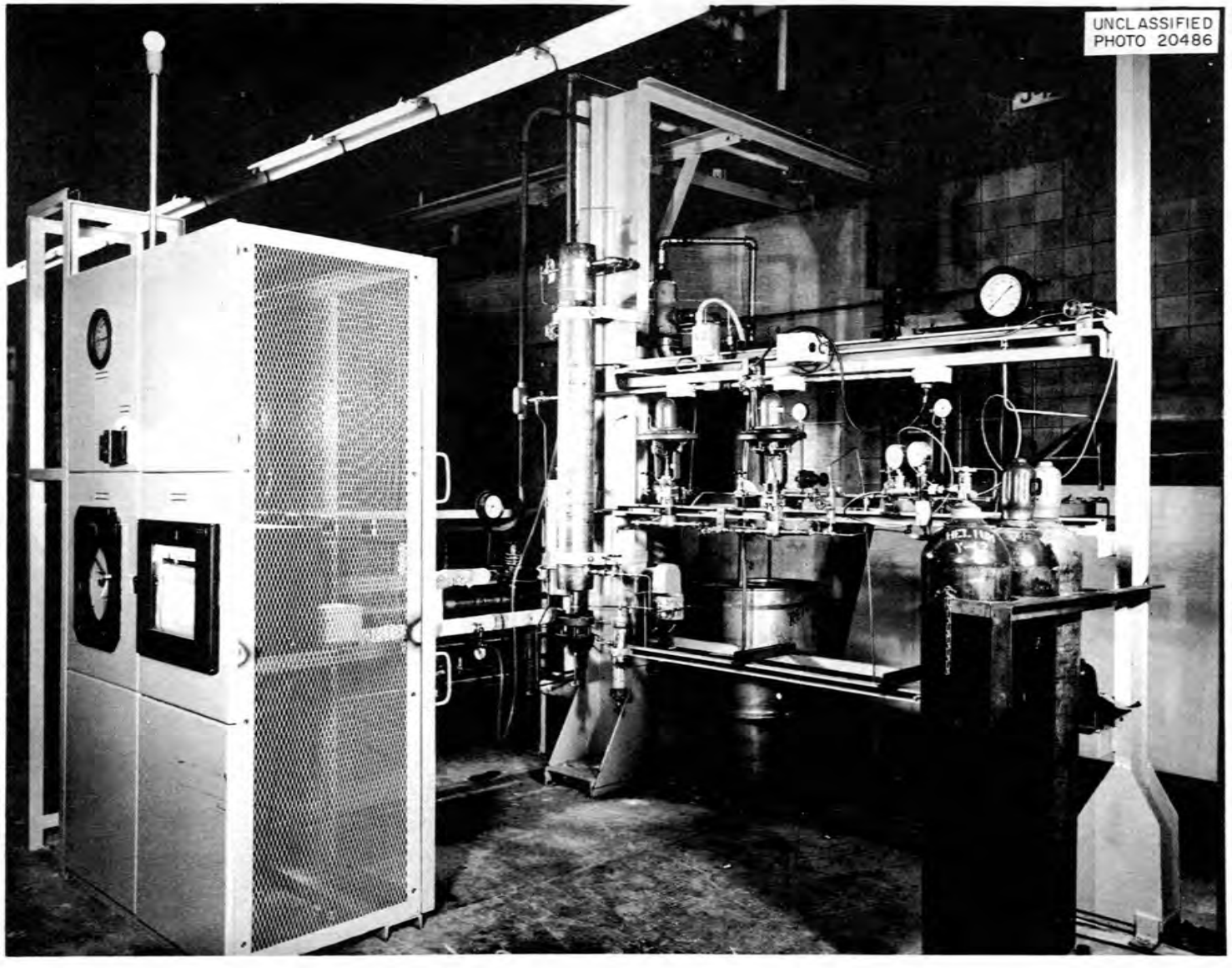

Fig. 29. Valve Test Loop.

OFFICIAL USE ONLY
PHOTO 20485

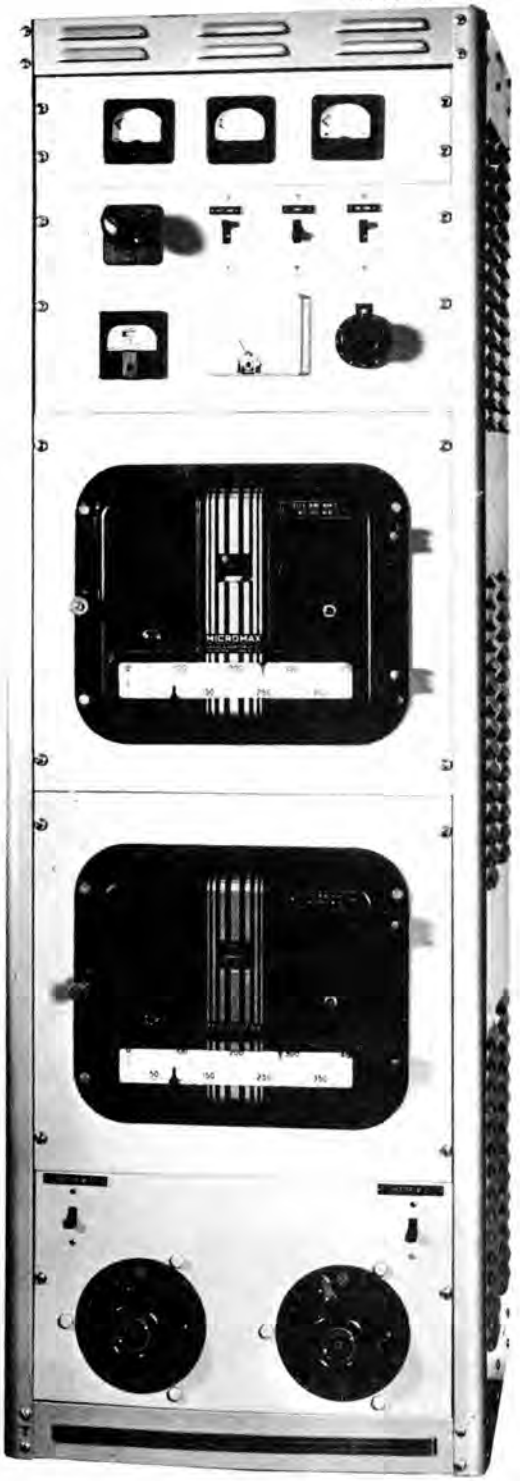

Fig. 30. In-Pile Loop Control Cabinet.

UNCLASSIFIED
DWG. 20810

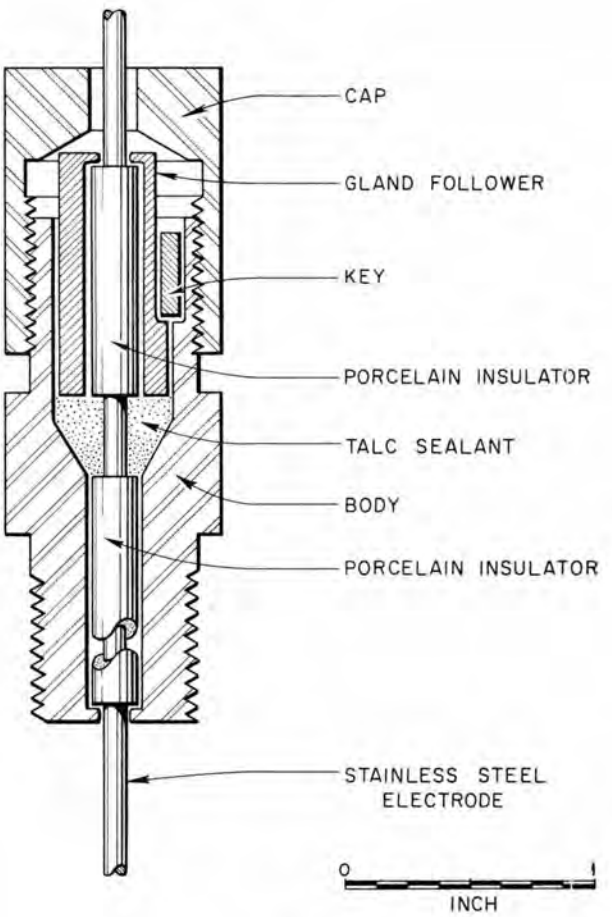

Fig. 31. Modified Conax Company Gland Probe.

KAPL rod-drive mechanism are shown in Fig. 33. With the use of an ORNL, 3-in., PCP, ionization chamber to measure the neutron flux, a high-speed potentiometer to indicate rod position, and a two-pen Brush recorder, simultaneous records will be presented of reactor power and reactivity addition by the removal of the absorption rod. Since the response of the recording system is approximately 100 cps, accurate representation of transients is expected. Analysis of these records is expected to yield the gas and steam

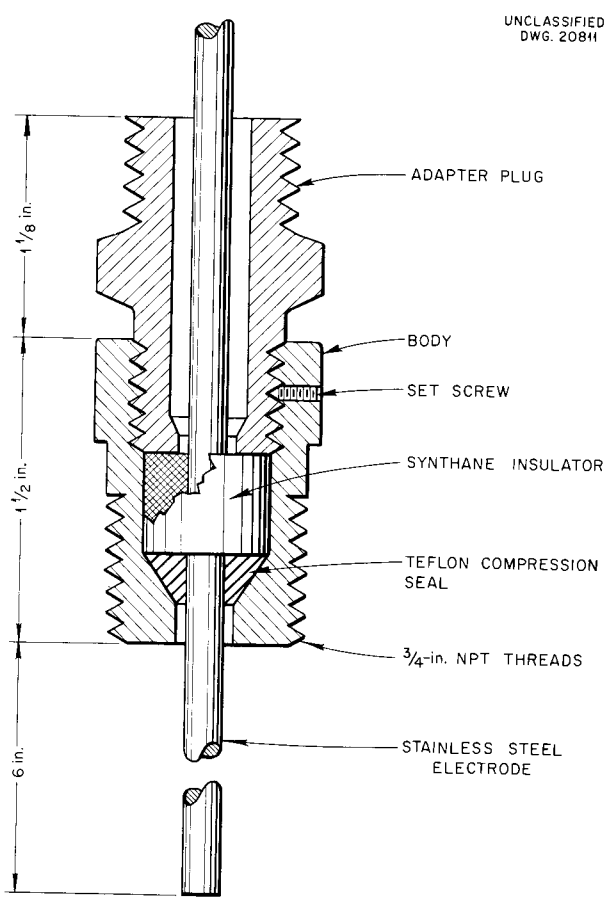

Fig. 32. Fielden Company Probe.

formation delay functions (cf., section on "Proposed Reactor Stability Experiment on the Los Alamos Water Boiler" in the chapter on "Boiling Reactor Research").

Recent activation of the Teapot mockup to investigate proposed boiling reactor feed systems has required assistance in the design and control of the rig. Instrumentation requirements for the control and evaluation of the mockup are expected to be met with the equipment already procured for the former mockup design.

INTERMEDIATE-SCALE HOMOGENEOUS REACTOR PROGRAM

Assistance in the design of the flow sheet for optimum control and desired performance of the instrumentation for the ISHR is being supplied as required. Preliminary valve requirements have been outlined, and a program for the development and procurement of these valves is under way. In addition, requirement sheet forms, which will be issued for all instrumentation, are being drawn up and will be circulated in the near future. Detailed requirements will then be prepared, subject to changes in the flow sheet, to initiate the required developmental programs.

[redacted]

PHOTO 20487

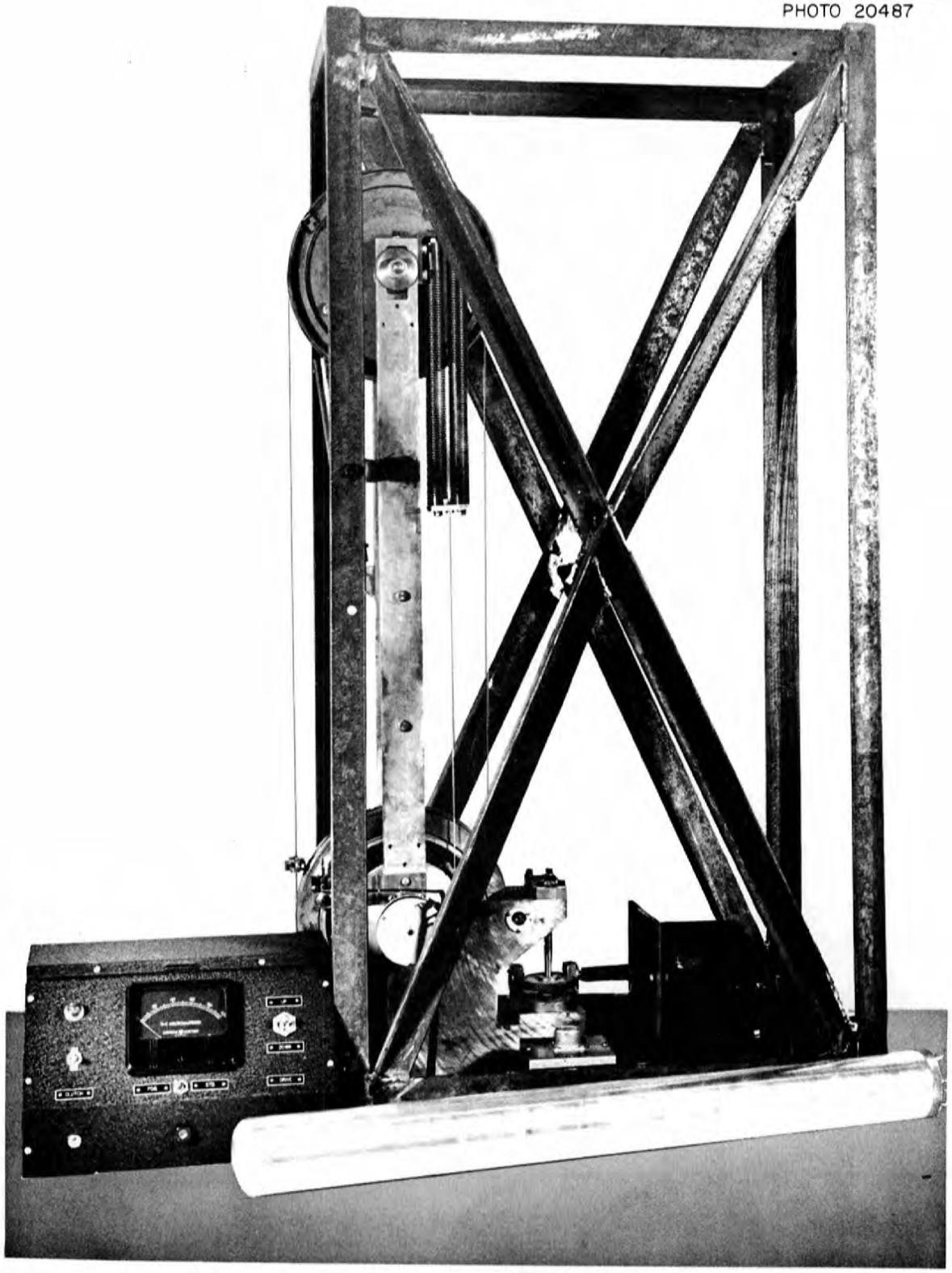

Fig. 33. Equipment for Los Alamos Experiment.

CORROSION

E. G. Bohlmann, Section Chief

PUMP LOOP OPERATION AND MAINTENANCE

H. C. Savage R. A. Lorenz
F. J. Walter

Eleven dynamic corrosion test loops are now in operation. Loop M,[1] which provides eight specimen holders,[2] was tested and put into operation during this quarter. Flow rates of up to about 80 fps past the pin-type corrosion specimen can be obtained. The remaining loops have been, or are being, reworked to increase the corrosion specimen capacity and to increase the flow rate past the specimens. In five of the dynamic corrosion test loops, it is now possible to expose sample specimens simultaneously to both high (~80 fps) and low (10 to 20 fps or below) flow.

Two runs have now been completed on loop M. Each run was for 1000 hr with distilled water at 250°C and 1000-psig pressure. In the first run, oxygen was used to maintain excess pressure, and as a result the water used as the circulating liquid was oxygen saturated. The second run was identical, except that hydrogen gas was substituted for the oxygen. Corrosion results of these two runs are given in the section on "Loop Test Results."

During this quarter, a large number of relatively short-term (50 to 400 hr) runs have been made in the dynamic test loops to evaluate the effects of time, flow rate, uranyl sulfate concentration, and excess acid (where required for solution stability) on the corrosion of various metals and alloys. Loop B is operating on a long-term basis with uranyl sulfate containing 5 g of uranium per liter and 25 mole % excess sulfuric acid at 250°C and 1000-psi pressure with oxygen concentrations ranging from 500 to 2000 ppm. This system has now been operating continuously for more than 3500 hr with a generalized corrosion rate of 0.04 to 0.08 mpy, as indicated by nickel analyses. The run will be continued to about 5000 hr before examination of the loop parts and corrosion specimens. The same loop and pump had been operated under these same conditions in two previous runs for periods totaling 1825 hours.

During this quarter, loop K was dismantled and cut open for an examination of the interior of the pipe similar to that made on loop F.[3] Loop K had been in operation for about 7500 hr with uranyl sulfate solution containing 5 g of uranium per liter at 250°C with an oxygen concentration of 1000 to 1500 ppm. The velocity of the solution in the 1 1/2-in. pipe was about 18 fps. The operating time accumulated on loop K corresponds to about ten and one-half months of continuous operation. The interior surfaces of the pipe were in excellent condition, and there were no visible evidences of pitting or corrosion even at areas of high turbulence, such as tees (Fig. 34) and orifices. The pipe was coated with a very thin, tightly adhering film.

Loop I was also dismantled and sectioned for inspection during this quarter. This loop was made of 1-in. schedule-40 type 347 stainless steel pipe and contained a number of pipe bends, welded joints, tees, and elbows for evaluation of corrosion damage.

---

[1] H. C. Savage, R. A. Lorenz, and D. Schwartz, *HRP Quar. Prog. Rep. Mar. 31, 1953*, ORNL-1554, p. 48.

[2] H. C. Savage *et al.*, *HRP Quar. Prog. Rep. Mar. 15, 1952*, ORNL-1280, p. 41.

[3] H. C. Savage, R. A. Lorenz, and D. Schwartz, *HRP Quar. Prog. Rep. Mar. 31, 1953*, ORNL-1554, p. 43.

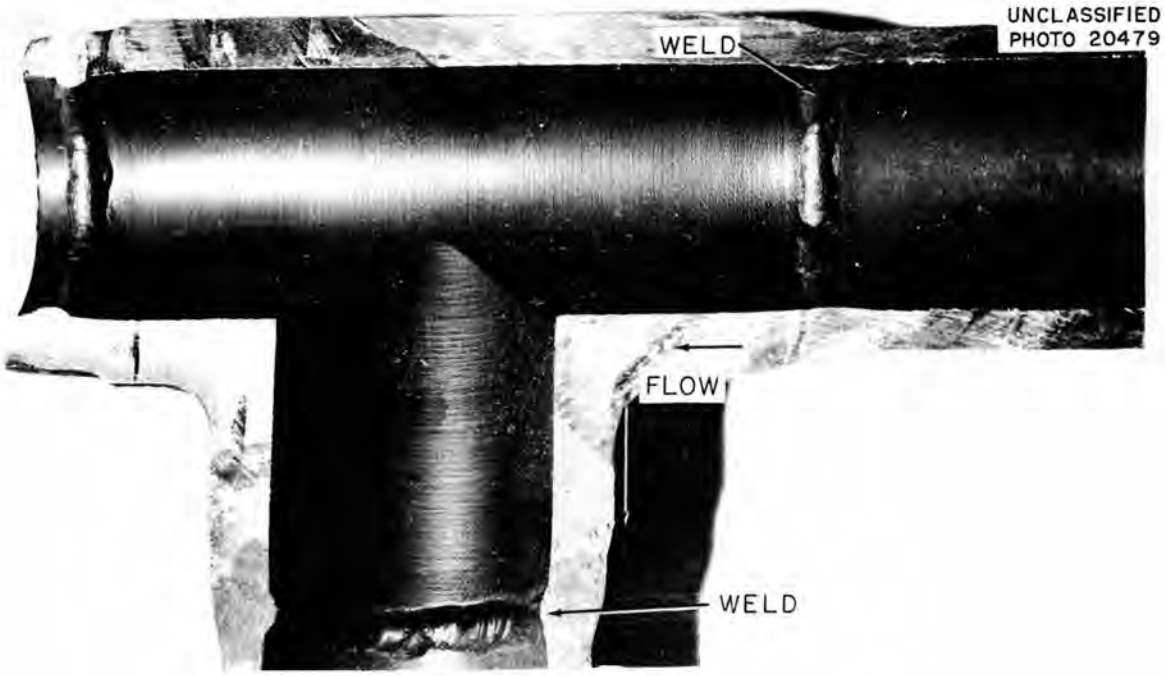

Fig. 34. Forged Tee, Loop K.

Severe corrosion at tees and other regions of sharp change of flow direction resulted in several leaks after about 2000 hr of operation at 250°C with 0.17 *M* UO_2SO_4 containing 25 mole % excess sulfuric acid. The flow rate in the loop was maintained at about 20 fps.

Figures 35 through 40 show typical corrosion and erosion damage in various sections of the loop. It can be seen that even with a highly corrosive solution relatively little damage occurs in welds of straight pipe (Fig. 37) and smooth bend sections (Fig. 39). This has been true in all observations made during the dynamic corrosion test program. Loop I was designed and tested to illustrate the relative degree of attack in a large number of such fabricated sections with various degrees of turbulence.

Loops K and I have been replaced with new loops of 1 1/2-in. type 347 stainless steel; they are duplicates of loop M.

Loop F was operated during this quarter in an effort to evaluate the effect of excess gas on corrosion and/or erosion. After several runs, no appreciable difference was found between samples exposed to solution containing "excess gas" and those exposed to saturated solution. However, analyses for contained gas in solution samples taken from a number of points throughout the loop were so erratic that no definite conclusion could be made as to the amount of contained gas or gas bubbles in the solution passing corrosion samples. Therefore, it did not seem feasible to continue the use of loop F for evaluation of the effect of gas on corrosion. A summary of the corrosion test results obtained in loop F is given in the section "Loop Test Results." Loop F has now been converted for use in evaluating the out-of-pile corrosion rate of the in-pile corrosion test units.

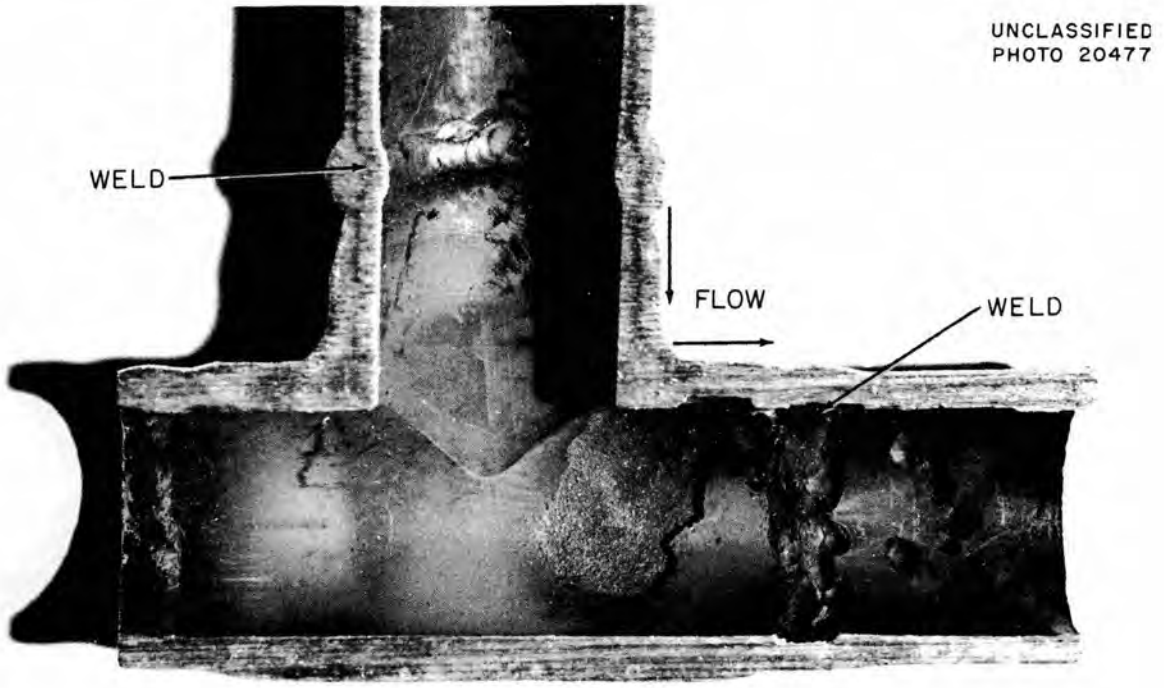

Fig. 35. Forged Tee, Loop I.

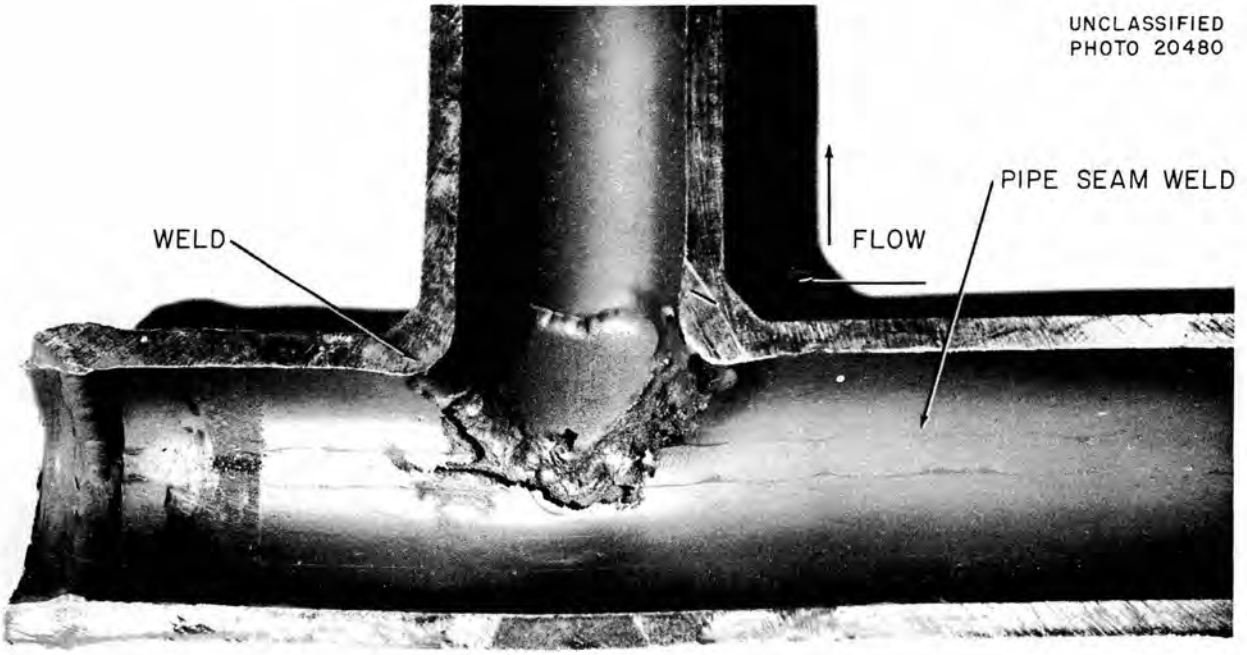

Fig. 36. Saddle Weld, Loop I.

UNCLASSIFIED
PHOTO 20476

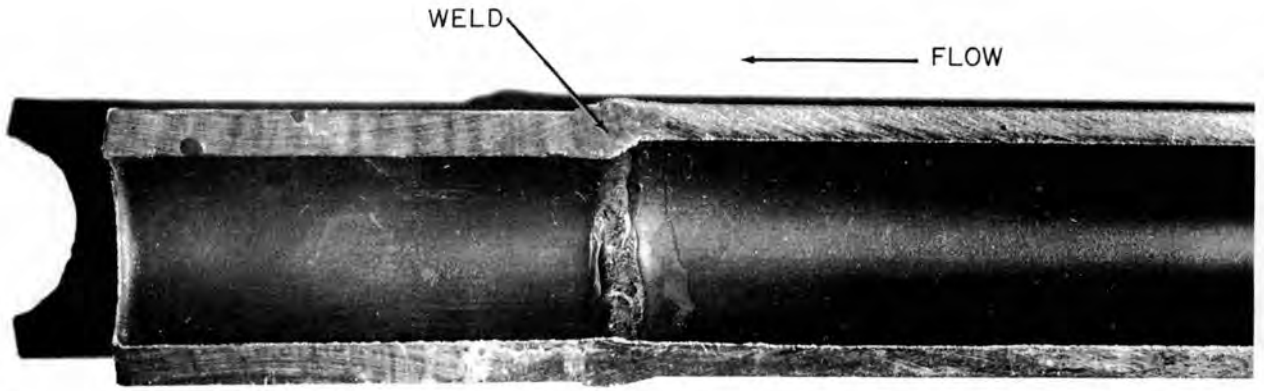

Fig. 37. Straight Section, Loop I.

UNCLASSIFIED
PHOTO 20482

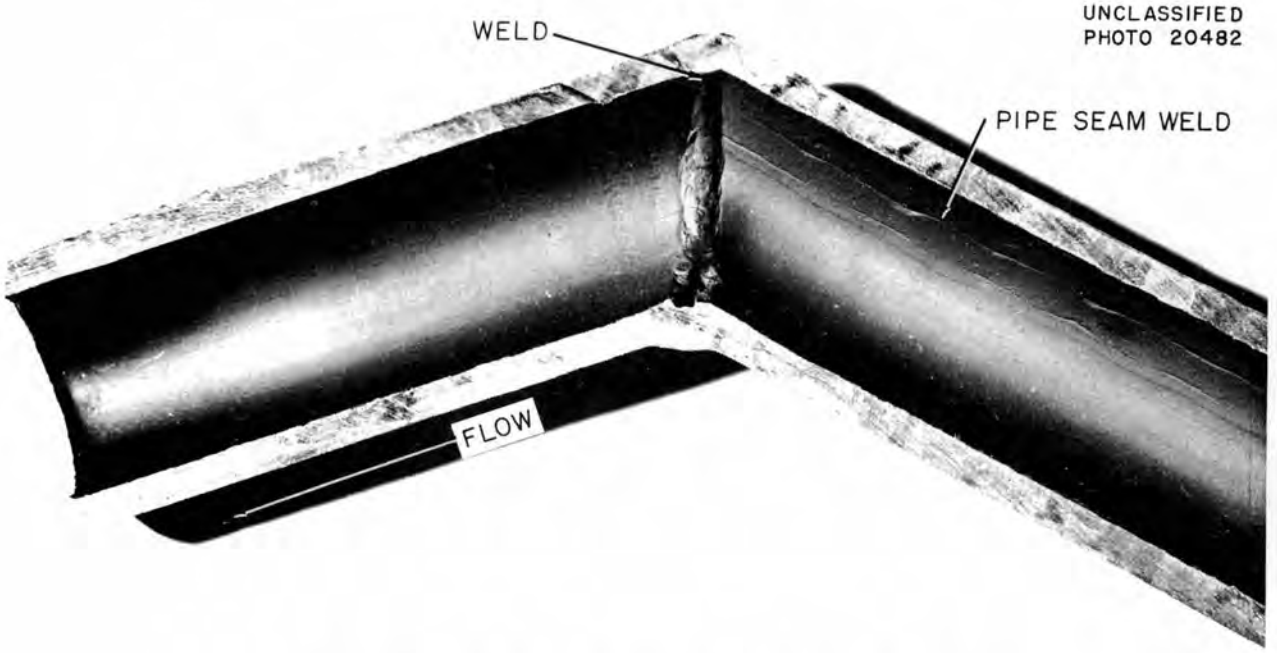

Fig. 38. Forty-Five-Degree Butt Weld, Loop I.

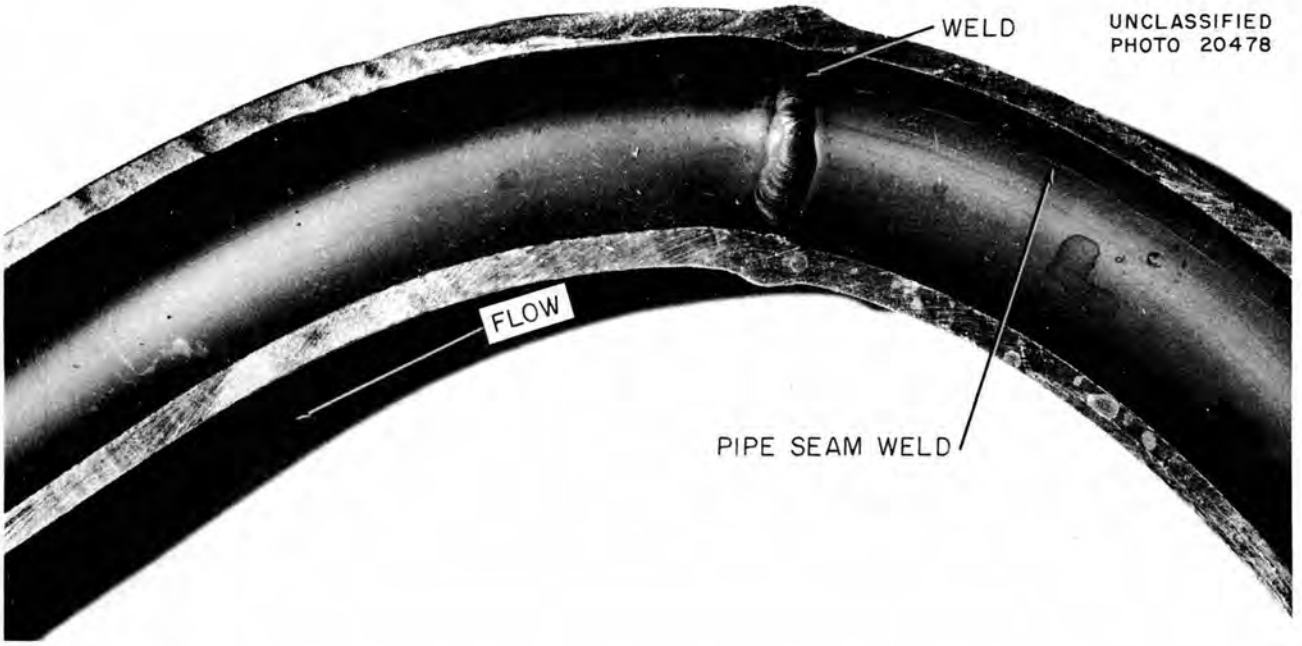

Fig. 39. Ninety-Degree Bend and Weld, Loop I.

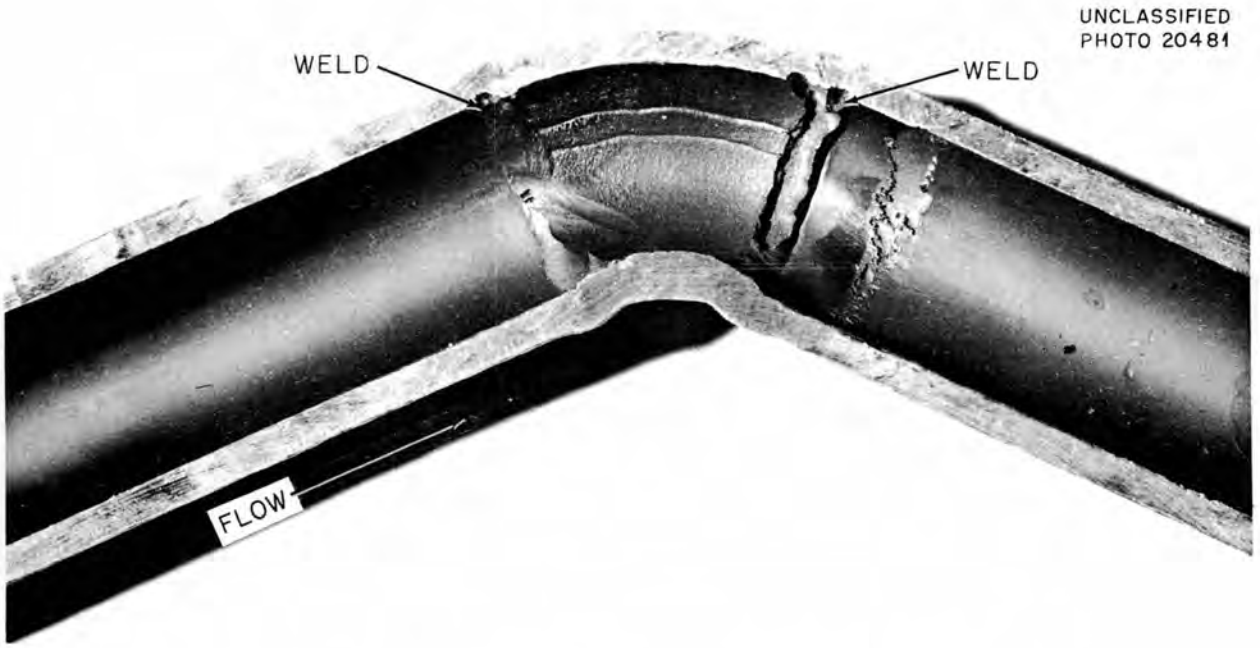

Fig. 40. Forty-Five-Degree Ell, Loop I.

Loop D, designed for operation with a relatively small volume (~4 liters), has been enclosed in a shield with an exhaust duct. This was done to allow use of solutions containing fission products in corrosion and decontamination studies. Any vapor from leakage or from a sudden loss of solution would be contained and exhausted through a roof fan.

Titanium Loop. Loop G, an all-titanium loop that was described[4] previously, was put in operation during this quarter. Three uranyl sulfate runs were made: the first two runs were made with uranyl sulfate solution containing 5 g of uranium per liter at 250°C and 1000-psi pressure; the third run was made with uranyl sulfate solution containing 5 g of uranium per liter and 25 mole % sulfuric acid at 250°C and 1000-psi pressure. The total operating time was 750 hours. No mechanical difficulties were encountered during these runs, and thus, in this limited test, the feasibility of fabricating and welding a titanium system was demonstrated. No hydrogen has been used in this system, to date, and additional runs with mechanical and corrosion test specimens under various operating conditions are still required before definite conclusions can be drawn. Further operation of the titanium loop has been delayed because the titanium impeller was removed and installed in the Westinghouse model 100A pump now in the HRE. Solution stability and corrosion results obtained on the two runs are given in the section on "Loop Test Results."

HRE Mockup. The HRE mockup in Building 9204-1 at Y-12 was operated about 800 hr during this quarter. Before these runs were made, a bypass sample holder was installed to allow the use of the round-pin and flat-plate types of corrosion test specimens. Three runs were made in which the generalized corrosion rate was followed by periodic analysis of the circulating solution for dissolved nickel. Corrosion rates on the round-pin and flat-plate types of corrosion specimens were compared with those found in similar runs in the standard dynamic corrosion test loops. The conditions were those under which it is planned to operate the HRE during a test of the effect of radiation on corrosion. Operating conditions for the three runs are given in Table 8, and the corrosion results are given in the section on "Loop Test Results."

TABLE 8. CONDITIONS OF OPERATION OF HRE MOCKUP

UO_2SO_4 concentration: 40 g of uranium per liter
Pressure: 950 psig
Oxygen concentration: 200 ppm

RUN NO.	OPERATING TIME (hr)	OPERATING TEMPERATURE (°C)
M-10	400	200
M-11	200	250
M-12	200	200

After run M-10, it was found that the remote pulsafeeder head had a leak through the stainless steel diaphragm; however, since the intermediate oil-to-water diaphragm was still intact, runs M-11 and M-12 were made as planned. No leakage through the oil-to-water diaphragm was observed.

Prior to any additional runs, the remote pulsafeeder head will be repaired. When the repairs have been made, it is planned to operate the mockup to evaluate the effect of oxygen concentration on solution stability and corrosion rate. The oxygen addition system, consisting of a capillary-tube DP-cell metering system, is quite accurate and reliable, and therefore oxygen concentration in the circulating solution can be controlled and maintained over a wide range (50 to 1000 ppm) to within about ±10%.

[4] *Ibid.*, p. 47.

Westinghouse Model 100A Pumps. There are now 18 Westinghouse model 100A pumps in service in the dynamic corrosion test program, slurry program, and the HRE. Nineteen pumps are on hand to meet these requirements. To date, it has been possible to repair and return to service all pumps which failed, except the two pumps used in the HRE. These two pumps are too contaminated to work on, and because all flanges had been seal welded, they were extensively damaged in disassembly for inspection. At some later date, it may be possible to salvage and repair one of these pumps.

Three pump failures occurred during this quarter. Two were electrical failures, and in both cases the cooling oil circulating through the stator windings had become contaminated with water. Although contamination of the oil with water does not always cause an electrical failure, if corrected in time, the water probably was a contributing factor in these two failures.

One pump failed because of a leak through the Inconel diaphragm that separates the rotor chamber and the stator windings.[5] In this particular pump, uranyl sulfate solution containing 5 g of uranium per liter and from 25 to 100 mole % excess sulfuric acid had been used as the circulating solution. In making pump repairs involving the stator, all Inconel diaphragms that have failed are replaced with stainless steel (type 347 or type 321) diaphragms. The cumulative operating time for the nine pumps now containing stainless steel diaphragms has been about 24,000 hr while circulating uranyl sulfate solutions with and without added sulfuric acid and with various concentrations of uranium. To date, no failure of a stainless steel diaphragm has occurred.

One of the pumps that failed was in the HRE. This pump was seal welded by the heliarc method at all flanges prior to installation in the HRE. Electrical failure of the stator windings occurred after about 60 hr of operation. The electrical failure was coincidental with the discovery that the pump cooling oil had become contaminated with water because of a leak in the oil-to-water heat exchanger. The pump has now been replaced with a pump containing a type 321 stainless steel diaphragm and a titanium impeller for increased corrosion resistance. Information is to be obtained on the effect of radioactive solutions on titanium.

Heat Exchanger Tests. Tests with the heat exchanger test assembly[6] have been completed. A final report is now being written.

LOOP TEST RESULTS

J. C. Griess R. E. Wacker

The major objective in the operation of the dynamic test loops during this quarter has been to achieve a better understanding of the corrosive action of uranyl sulfate solutions (and to a lesser extent, uranyl fluoride solutions) on stainless steel. Short-term tests have yielded information on such variables as concentrations of uranium and oxygen, time, temperature, and velocity. From such data, standards have been obtained which, in the future, will permit an evaluation of the effect of foreign substances such as fission products, copper sulfate, and inhibitors on the corrosion of stainless steel by uranyl sulfate solutions.

Preliminary data obtained in dilute uranyl sulfate solutions at 300°C have indicated that the corrosion of stainless steel is as low at 300°C as it is at 250°C. Further testing, some of which is now in progress, will be needed to verify this observation.

[5] H. C. Savage *et al.*, *HRP Quar. Prog. Rep. Mar. 15, 1952*, ORNL-1280, Fig. 13.

[6] H. C. Savage, R. A. Lorenz, and D. Schwartz, *HRP Quar. Prog. Rep. Jan. 1, 1953*, ORNL-1478, p. 62-63.

In addition to stainless steel, zirconium and titanium have been exposed under a number of different conditions. The titanium loop was completed and operated, and an increase in the number of tests involving both titanium and zirconium is planned for the next quarter.

Two runs have been completed in which various alloys have been exposed to water at 250°C. In one case, the water contained dissolved hydrogen and in the other, dissolved oxygen. The results of all the tests completed during this quarter are given in the following sections.

General Corrosion Rates. All the data obtained previously from pin-type corrosion specimens have been listed in previous quarterly reports,[7,8] and the data collected this quarter are presented in Table 9. All previous data were reported in mils of penetration per year, and therefore the data in Table 9 are presented on the same basis. As was previously pointed out, the reporting of corrosion damage as a constant-rate process is misleading because the corrosion rate, in most cases, varies with the duration of the test. This is particularly true in regions of low flow. Hence, when using or comparing the data in Table 9, the duration of the exposure should be carefully considered. All rates are calculated on the basis of the amount of metal oxidized, as determined by weight loss of the pin-type corrosion specimens after removal of the oxide scale.

A number of specially prepared specimens, such as those containing welds or those that received various heat and surface treatments, have also been tested; these are not shown in Table 9. They are being examined by the Metallurgy Group (cf., chapter on "Metallurgy"), and a report will be issued after the investigation has been completed.

Effect of Oxygen Concentration. The data obtained from the loops during the past two years have given indications that the oxygen content of the uranyl sulfate solution has an effect on the corrosion rate of the system. Unfortunately, most of the systems did not contain corrosion specimens, and hence it was impossible to determine reliably the extent of corrosion, particularly under different flow conditions.

Therefore a series of three runs, C-25, C-27, and C-28, was made in which all conditions were kept constant except the oxygen concentration. In each run, the solution used was 1.26 *M* UO_2SO_4, the operating temperature was 250°C, the operating time was 100 hr, and both pin and coupon corrosion specimens were included. The oxygen concentrations and oxygen partial pressures used are shown in Table 10, along with the nickel and chromium concentrations of the solutions at the ends of the runs. From the nickel concentration, the generalized corrosion rate of the entire system was calculated. The corrosion rates of of the pin-type specimens are shown in Table 9, runs C-25, C-27, and C-28; the coupon data are given in Fig. 41. The data obtained from run C-26 were similar to those obtained for run C-27. However, mechanical difficulties prevented the completion of a 100-hr operating period for run C-26, and therefore an additional run was considered necessary.

---

(7) J. C. Griess and R. E. Wacker, *HRP Quar. Prog. Rep. Mar. 31, 1953*, ORNL-1554, p. 49.

(8) J. C. Griess, J. M. Ruth, and R. E. Wacker, *HRP Quar. Prog. Rep. Jan. 1, 1953*, ORNL-1478, p. 63.

TABLE 9. SUMMARY OF CORROSION RESULTS WITH PIN-TYPE SPECIMENS

RUN NO.	TEST CONDITIONS						PIN MATERIAL	NO. OF PINS	CORROSION RATE (mpy)		
	Solution	Uranium Concentration (g/l)	Temperature (°C)	Time (hr)	Additions	Flow Rate (fps ± 10%)			Minimum	Average	Maximum
A-41	UO_2SO_4	15	250	12	200 psi O_2 0.015 *M* H_2SO_4	13	Type 347 stainless steel	4	72	77	81
							Type 309 SCb stainless steel	3	57	59	61
							Type 304 stainless steel	2	89	90	91
							Type 304 ELC stainless steel	2	79	84	88
							Type 321 stainless steel	3	88	94	98
						77	Type 347 stainless steel	4	78	82	91
							Type 309 SCb stainless steel	3	65	66	67
							Type 304 stainless steel	2	110	110	110
							Type 304 ELC stainless steel	2	81	85	88
							Type 321 stainless steel	3	89	95	100
A-42	UO_2SO_4	15	250	50	200 psi O_2 0.015 *M* H_2SO_4	13	Type 347 stainless steel	2	46	47	48
							Type 309 SCb stainless steel	3	50	52	56
							Type 304 stainless steel	2	40	42	43
							Type 304 ELC stainless steel	3	36	40	44
							Type 321 stainless steel	3	43	44	47
						77	Type 347 stainless steel	3	110	110	110
							Type 309 SCb stainless steel	3	83	98	110
							Type 304 stainless steel	2	140	140	140
							Type 304 ELC stainless steel	3	96	120	140
							Type 321 stainless steel	3	110	130	150
A-43	UO_2SO_4	15	250	100	200 psi O_2 0.015 *M* H_2SO_4	13	Type 347 stainless steel	2	22	24	26
							Type 309 SCb stainless steel	3	28	29	29
							Type 304 stainless steel	2	9.4	14	18
							Type 304 ELC stainless steel	3	12	18	21
							Type 321 stainless steel	3	20	22	22
						77	Type 347 stainless steel	3	120	130	130
							Type 309 SCb stainless steel	3	120	130	130
							Type 304 stainless steel	2	150	160	160
							Type 304 ELC stainless steel	3	100	120	130
							Type 321 stainless steel	3	140	170	190
A-44	UO_2SO_4	15	250	200	200 psi O_2 0.015 *M* H_2SO_4	13	Type 347 stainless steel	2	12	13	14
							Type 309 SCb stainless steel	3	14	16	17
							Type 304 stainless steel	2	8.9	10	11
							Type 304 ELC stainless steel	3	10	11	12
							Type 321 stainless steel	3	11	12	14

TABLE 9. (continued)

RUN NO.	TEST CONDITIONS						PIN MATERIAL	NO. OF PINS	CORROSION RATE (mpy)		
	Solution	Uranium Concentration (g/l)	Temperature (°c)	Time (hr)	Additions	Flow Rate (fps ± 10%)			Minimum	Average	Maximum
						77	Type 347 stainless steel	3	110	120	130
							Type 309 SCb stainless steel	3	110	110	110
							Type 304 stainless steel	2	130	130	140
							Type 304 ELC stainless steel	3	110	130	170
							Type 321 stainless steel	3	100	110	110
A-45	UO_2SO_4	15	250	403	200 psi O_2 0.015 *M* H_2SO_4	13	Type 347 stainless steel	2	8.4	9.2	10
							Type 309 SCb stainless steel	3	7.8	9.0	11
							Type 304 stainless steel	2	5.9	6.8	7.7
							Type 304 ELC stainless steel	3	1.9	5.0	6.6
							Type 321 stainless steel	3	8.2	8.5	8.9
						77	Type 347 stainless steel	3	110	120	120
							Type 309 SCb stainless steel	3	100	110	110
							Type 304 stainless steel	2	120	130	130
							Type 304 ELC stainless steel	3	110	110	110
							Type 321 stainless steel	3	120	160	180
A-46	UO_2SO_4	40	250	400	200 psi O_2	13	Type 347 stainless steel	3	3.4	11	16
							Type 309 SCb stainless steel	3	15	15	16
							Type 304 stainless steel	2	10	11	11
							Type 304 ELC stainless steel	2	3.9	10	16
							Type 321 stainless steel	3	11	15	17
						77	Type 347 stainless steel	4	190	200	210
							Type 309 SCb stainless steel	3	230	230	240
							Type 304 stainless steel	2	220	220	220
							Type 304 ELC stainless steel	2	280	290	300
							Type 321 stainless steel	3	190	210	240
A-47	UO_2SO_4	40	250	200	200 psi O_2	13	Type 347 stainless steel	3	12	24	30
							Type 309 SCb stainless steel	3	21	24	27
							Type 304 stainless steel	2	19	19	19
							Type 304 ELC stainless steel	2	28	30	32
							Type 321 stainless steel	3	27	27	28
						77	Type 347 stainless steel	4	170	220	260
							Type 309 SCb stainless steel	3	230	250	280
							Type 304 stainless steel	2	230	230	230
							Type 304 ELC stainless steel	2	190	230	270
							Type 321 stainless steel	3	170	240	280

TABLE 9. (continued)

RUN NO.	TEST CONDITIONS						PIN MATERIAL	NO. OF PINS	CORROSION RATE (mpy)		
	Solution	Uranium Concentration (g/l)	Temperature (°C)	Time (hr)	Additions	Flow Rate (fps ± 10%)			Minimum	Average	Maximum
A-48	UO_2SO_4	40	250	100	200 psi O_2	13	Type 347 stainless steel	3	47	50	52
							Type 309 SCb stainless steel	3	48	54	65
							Type 304 stainless steel	2	38	39	39
							Type 304 ELC stainless steel	2	50	51	51
							Type 321 stainless steel	3	48	64	76
						77	Type 347 stainless steel	4	160	170	170
							Type 309 SCb stainless steel	3	170	180	190
							Type 304 stainless steel	2	200	200	200
							Type 304 ELC stainless steel	2	150	200	250
							Type 321 stainless steel	3	140	170	240
A-49	UO_2SO_4	40	250	50	200 psi O_2	13	Type 347 stainless steel	3	47	68	80
							Type 309 SCb stainless steel	3	62	80	95
							Type 304 stainless steel	2	23	50	86
							Type 304 ELC stainless steel	2	83	90	96
							Type 321 stainless steel	3	53	60	72
						77	Type 347 stainless steel	4	98	100	120
							Type 309 SCb stainless steel	3	100	120	120
							Type 304 stainless steel	2	170	220	260
							Type 304 ELC stainless steel	2	140	170	200
							Type 321 stainless steel	3	110	190	230
C-22	UO_2SO_4	300	275	100	75 psi O_2	16 to 20	Type 347 stainless steel	7	110	210	330
					75 psi He		Type 309 SCb stainless steel	5	100	320	430
							Type 304 stainless steel	6	140	260	390
							Type 304 ELC stainless steel	6	110	190	260
							Type 321 stainless steel	6	94	140	300
							Type 316 stainless steel	4	260	400	540
							Type 316 ELC stainless steel	4	200	220	240
							Stellite 25	2	2500	2600	2700
C-23	UO_2SO_4	300	125	101	200 psi O_2	16 to 20	Type 347 stainless steel	8	0	0.34	1.2
							Type 309 SCb stainless steel	6	0	0.42	1.0
							Type 304 stainless steel	6	0.34	0.76	1.5
							Type 304 ELC stainless steel	6	0	0.56	1.7
							Type 321 stainless steel	6	0.17	0.56	1.2
							Type 316 stainless steel	4	0	0.47	0.84
							Type 316 ELC stainless steel	4	0.17	0.51	0.84
							Stellite 25	2	0.84	1.0	1.2

TABLE 9. (continued)

RUN NO.	TEST CONDITIONS						PIN MATERIAL	NO. OF RUNS	CORROSION RATE (mpy)		
	Solution	Uranium Concentration (g/l)	Temperature (°C)	Time (hr)	Additions	Flow Rate (fps ± 10%)			Minimum	Average	Maximum
C-24	UO_2SO_4	300	300	12	75 psi O_2 75 psi He[a]	16 to 20	Type 347 stainless steel	8	510	660	800
							Type 309 SCb stainless steel	6	440	620	810
							Type 304 stainless steel	6	490	590	750
							Type 304 ELC stainless steel	6	510	630	740
							Type 321 stainless steel	6	740	810	860
							Type 316 stainless steel	4	860	900	950
							Type 316 ELC stainless steel	4	750	840	950
							Stellite 25	2	4500	4900	5300
C-25	UO_2SO_4	300	250	100	150 psi O_2	8	Type 347 stainless steel	4	110	120	120
							Type 309 SCb stainless steel	1		130	
							Type 304 ELC stainless steel	4	130	170	200
							Type 321 stainless steel	4	110	160	190
C-26	UO_2SO_4	300	250	65	75 psi O_2 75 psi He	8	Type 347 stainless steel	4	75	84	95
							Type 309 SCb stainless steel	2	67	80	93
							Type 304 ELC stainless steel	4	81	97	130
							Type 321 stainless steel	4	77	110	150
C-27	UO_2SO_4	300	250	99	75 psi O_2 75 psi He	8	Type 347 stainless steel	4	69	74	81
							Type 309 SCb stainless steel	2	70	81	91
							Type 304 ELC stainless steel	4	67	73	82
							Type 321 stainless steel	4	59	72	82
C-28	UO_2SO_4	300	250	101	300 psi O_2	8	Type 347 stainless steel	4	110	110	110
							Type 309 SCb stainless steel	1		130	
							Type 304 ELC stainless steel	4	120	130	140
							Type 321 stainless steel	4	100	140	160
D-1	UO_2SO_4	300	250	101	200 psi O_2 50 ppm Tc[b]	6	Type 347 stainless steel	3	15	19	22
							Type 309 SCb stainless steel	2	7.6	10	13
							Type 304 stainless steel	2	22	23	23
							Type 304 ELC stainless steel	3	12	12	12
							Type 321 stainless steel	3	40	40	40
D-2	UO_2SO_4	300	250	100	200 psi O_2[b]	6	Type 347 stainless steel	3	180	200	220
							Type 309 SCb stainless steel	2	190	220	240
							Type 304 stainless steel	2	150	170	180
							Type 304 ELC stainless steel	4	130	160	180
							Type 321 stainless steel	3	180	190	200
D-4	UO_2SO_4	40	250	232	200 psi O_2[b]	17	Type 347 stainless steel	5	20	24	34
							Type 304 ELC stainless steel	5	22	25	32
							Type 321 stainless steel	4	17	32	51

TABLE 9. (continued)

RUN NO.	TEST CONDITIONS						PIN MATERIAL	NO. OF PINS	CORROSION RATE (mpy)		
	Solution	Uranium Concentration (g/l)	Temperature (°C)	Time (hr)	Additions	Flow Rate (fps ± 10%)			Minimum	Average	Maximum
E-9	UO_2SO_4	15	250	992	200 psi O_2	11 to 13	Type 347 stainless steel	6	2.1	2.7	4.1
					0.016 *M*		Type 347 stainless steel[c]	2	2.1	2.2	2.2
					H_2SO_4		Type 347 stainless steel[d]	1		1.9	
							Type 309 SCb stainless steel	4	2.2	2.5	2.8
							Type 304 stainless steel	3	2.6	2.7	2.9
							Type 304 stainless steel[e]	2	1.4	1.8	2.2
							Type 304 ELC stainless steel	4	2.0	2.2	2.4
							Type 321 stainless steel	3	3.1	3.1	3.1
							Zirconium, crystal bar	2	0	0	0
							Zirconium-2.5% tin	2	0	0	0
F-20	UO_2SO_4	300	250	117	250 psi O_2[f]	13	Type 347 stainless steel	2	36	38	39
							Type 304 stainless steel	2	64	71	87
							Type 304 ELC stainless steel	2	40	80	120
							Type 321 stainless steel	2	50	56	62
						5	Type 347 stainless steel	2	33	36	39
							Type 304 stainless steel	2	29	35	41
							Type 304 ELC stainless steel	2	28	32	35
							Type 321 stainless steel	2	35	39	43
F-21	UO_2SO_4	300	250	98	200 psi O_2[g]	9	Type 347 stainless steel	2	220	280	330
							Type 304 stainless steel	2	240	270	290
							Type 304 ELC stainless steel	1		240	
							Type 321 stainless steel	2	210	240	270
						8	Type 347 stainless steel	2	130	150	160
							Type 304 stainless steel	2	150	160	170
							Type 304 ELC stainless steel	1		170	
							Type 321 stainless steel	2	190	260	320
H-14	UO_2SO_4	40	250	113	200 psi O_2	13	Type 347 stainless steel	4	24	33	47
							Type 304 ELC stainless steel	2	27	31	35
							Experimental alloy[h]	2	24	25	26
							Stellite 25	2	200	210	210
H-15[i]	1.0 *M* HCl		85	4	200 psi He	15	Type 304 ELC stainless steel	1		6300	
	1.4 *M* H_2SO_4				Alkyl		Type 304 stainless steel	1		10000	
	0.2 *M* H_2O_2				pyridines		Type 321 stainless steel	1		5500	
							Stellite 1	1		3700	
							Stellite 3	1		2100	
							Stellite 6	1		2500	
							Stellite 25	1		870	
							Stellite 98M2	1		1300	
							Low-carbon Inconel	1		3000	
							Inconel X	1		2400	
							Titanium, RC-70	1		55	
							Zirconium, crystal bar	1		17	
							Zirconium-2.5% tin	1		0	

TABLE 9. (continued)

RUN NO.	TEST CONDITIONS						PIN MATERIAL	NO. OF PINS	CORROSION RATE (mpy)		
	Solution	Uranium Concentration (g/l)	Temperature (°C)	Time (hr)	Additions	Flow Rate (fps ± 10%)			Minimum	Average	Maximum
H-16	UO_2SO_4	25	250	200	200 psi O_2	15	Type 347 stainless steel	4	2.6	2.8	3.0
							Type 304 ELC stainless steel	4	2.0	2.3	2.6
							Type 321 stainless steel	4	1.4	2.8	3.4
							Zirconium, crystal bar	1		0	
							Zirconium-2.5% tin	1		0	
						77	Type 347 stainless steel	4	120	180	260
							Type 304 ELC stainless steel	4	110	120	140
							Type 321 stainless steel	4	130	140	150
							Zirconium, crystal bar	1		0	
							Zirconium-2.5% tin	1		4	
H-17	UO_2SO_4	25	250	100	200 psi O_2	15	Type 347 stainless steel	4	20	22	26
							Type 304 ELC stainless steel	4	3.6	10	18
							Type 321 stainless steel	4	21	23	26
							Zirconium, crystal bar	1		0	
							Zirconium-2.5% tin	1		0	
						77	Type 347 stainless steel	3	160	190	230
							Type 304 ELC stainless steel	4	160	170	180
							Type 321 stainless steel	4	140	160	200
							Zirconium, crystal bar	1		0	
							Zirconium-2.5% tin	1		0	
H-18	UO_2SO_4	25	250	399	200 psi O_2	15	Type 347 stainless steel	4	4.6	5.1	6.1
							Type 304 ELC stainless steel	4	3.2	3.7	4.6
							Type 321 stainless steel	4	4.8	5.8	6.4
							Zirconium, crystal bar	1		0	
							Zirconium-2.5% tin	1		0	
						77	Type 347 stainless steel	3	160	160	170
							Type 304 ELC stainless steel	3	150	170	200
							Type 321 stainless steel	4	160	210	270
							Zirconium, crystal bar	1		0	
							Zirconium-2.5% tin	1		0	
H-19	UO_2SO_4	25	250	200	200 psi O_2	15	Type 347 stainless steel	4	6.2	8.5	11
							Type 304 ELC stainless steel	4	2.2	6.2	9.0
							Type 321 stainless steel	4	2.1	4.2	9.1
							Zirconium, crystal bar	1		0	
							Zirconium-2.5% tin	1		0	

TABLE 9. (continued)

RUN NO.	TEST CONDITIONS						PIN MATERIAL	NO. OF PINS	CORROSION RATE (mpy)		
	Solution	Uranium Concentration (g/l)	Temperature (°C)	Time (hr)	Additions	Flow Rate (fps ± 10%)			Minimum	Average	Maximum
						77	Type 347 stainless steel	3	190	200	200
							Type 304 ELC stainless steel	3	170	180	190
							Type 321 stainless steel	3	150	150	160
							Zirconium, crystal bar	1		0	
							Zirconium-2.5% tin	1		0	
H-20	UO_2SO_4	25	250	50	200 psi O_2	15	Type 347 stainless steel	4	39	43	47
							Type 304 ELC stainless steel	4	28	34	46
							Type 321 stainless steel	4	11	37	50
							Zirconium, crystal bar	1		0	
							Zirconium-2.5% tin	1		0	
						77	Type 347 stainless steel	3	120	140	160
							Type 304 ELC stainless steel	4	130	140	150
							Type 321 stainless steel	4	110	130	160
							Zirconium, crystal bar	1		0	
							Zirconium-2.5% tin	1		0	
I-4	UO_2SO_4	40	250	499	200 psi O_2	14	Type 347 stainless steel	5	4.4	6.7	8.8
					0.1 *M* $CuSO_4$		Type 309 SCb stainless steel	1		8.3	
					0.005 *M* H_2SO_4[j]		Type 304 stainless steel	2	4.6	5.6	6.5
							Type 304 ELC stainless steel	2	4.5	5.0	5.5
							Type 316 stainless steel	1		16	
							Type 316 ELC stainless steel	1		16	
J-22	UO_2F_2	15	250	1017	200 psi O_2	11	Type 347 stainless steel	4	0.15	0.20	0.23
					0.018 *M* HF		Type 309 SCb stainless steel	2	0.25	0.30	0.35
							Type 304 stainless steel	2	0.20	0.22	0.23
							Type 304 stainless steel[k]	2	0.22	0.22	0.22
							Type 304 ELC stainless steel	2	0.20	0.20	0.20
							Type 310 stainless steel	2	0.40	0.41	0.42
							Type 310S stainless steel[k]	2	0.32	0.39	0.45
							Type 321 stainless steel	2	0.20	0.21	0.22
							Type 316 stainless steel	2	0.25	0.29	0.33
							Type 430 stainless steel	2	0.08	0.23	0.37
							Titanium, RC-70	3	0.07	0.12	0.20
							Titanium, Ti-100A	1		0.10	
							Titanium, Ti-150A	1		0.12	

TABLE 9. (continued)

RUN NO.	TEST CONDITIONS						PIN MATERIAL	NO. OF PINS	CORROSION RATE (mpy)		
	Solution	Uranium Concentration (g/l)	Temperature (°C)	Time (hr)	Additions	Flow Rate (fps ± 10%)			Minimum	Average	Maximum
J-23	UO_2F_2	40	250	1000	200 psi O_2	10	Type 347 stainless steel	5	1.0	1.4	2.3
							Type 309 SCb stainless steel	2	1.9	2.5	3.1
							Type 304 stainless steel	2	0.24	0.52	0.80
							Type 304 stainless steel[k]	2	0.78	0.94	1.1
							Type 304 ELC stainless steel	2	0.87	2.6	4.4
							Type 310 stainless steel	2	2.7	3.7	4.6
							Type 310S stainless steel[k]	2	4.2	4.5	4.8
							Type 321 stainless steel	2	0.78	0.89	1.0
							Type 316 stainless steel	2	0.37	0.62	0.89
							Type 430 stainless steel	1		0.70	
							Titanium, RC-70	3	0.07	0.12	0.20
							Titanium, Ti-100A	1		0.10	
							Titanium, Ti-150A	1		0.12	
E-10	UO_2SO_4	5	250	100	200 psi O_2	10 to 13	Type 347 stainless steel	4	2.6	3.1	3.6
					0.005 *M* H_2SO_4		Type 304 ELC stainless steel	4	1.9	2.3	2.7
							Type 321 stainless steel	4	1.7	2.4	2.9
						77	Type 347 stainless steel	2	30	32	34
							Type 304 ELC stainless steel	2	3.9	6.2	8.5
							Type 321 stainless steel	2	28	30	31
J-24	UO_2SO_4	5	275	100	150 psi O_2	17	Type 347 stainless steel	3	2.8	3.0	3.3
					0.005 *M* H_2SO_4		Type 309 SCb stainless steel	2	3.0	3.2	3.3
							Type 304 ELC stainless steel	3	2.0	2.6	3.2
							Type 321 stainless steel	2	2.5	3.0	3.5
							Type 316 stainless steel	2	2.3	2.8	3.3
							Zirconium, crystal bar	1		0.7	
							Zirconium-2.5% tin	1		0	
						77	Type 347 stainless steel	3	5.3	5.5	5.8
							Type 309 SCb stainless steel	2	4.8	4.8	4.8
							Type 304 ELC stainless steel	3	4.3	4.9	5.3
							Type 321 stainless steel	2	5.7	5.8	5.8
							Type 316 stainless steel	2	5.8	6.1	6.3
							Zirconium, crystal bar	1		0.2	
							Zirconium-2.5% tin	1		0.2	
J-26	UO_2SO_4	5	295	100	100 psi O_2	17	Type 347 stainless steel	2	2.9	3.1	3.2
					0.005 *M* H_2SO_4		Type 309 SCb stainless steel	2	2.7	3.1	3.4
							Type 304 ELC stainless steel	2	2.5	3.1	3.6
							Type 321 stainless steel	2	2.9	3.9	4.8
							Type 316 stainless steel	2	3.3	3.5	3.7
							Zirconium, crystal bar	1		0	
							Zirconium-2.5% tin	1		0	

TABLE 9. (continued)

RUN NO.	TEST CONDITIONS						PIN MATERIAL	NO. OF PINS	CORROSION RATE (mpy)		
	Solution	Uranium Concentration (g/l)	Temperature (°C)	Time (hr)	Additions	Flow Rate (fps ± 10%)			Minimum	Average	Maximum
						77	Type 347 stainless steel	2	5.6	5.7	5.8
							Type 309 SCb stainless steel	2	5.4	5.6	5.8
							Type 304 ELC stainless steel	2	5.1	5.2	5.3
							Type 321 stainless steel	2	2.6	5.1	7.5
							Type 316 stainless steel	2	7.0	7.3	7.6
							Zirconium, crystal bar	1		0	
							Zirconium-2.5% tin	1		0	
L-14[l]	UO_2SO_4	40	250	100	200 psi O_2 0.07 *M* HNO_3	10	Type 347 stainless steel	6	9.7	11	12
L-15[m]	UO_2SO_4	5	250	684	200 psi O_2 0.005 *M* H_2SO_4	22 to 27	Type 322W stainless steel[n]	1		0.8	
							Type 17-4PH stainless steel[n]	1		0.7	
							Type 416 stainless steel[n]	1		26	
							Inconel X	1		170	
M-1	Water	0	250	1000	200 psi O_2	31	Zirconium, crystal bar	4	0	0	0
							Zirconium-2.5% tin	4	0	0	0
							Zirconium-5% tin	1		0	
							Zirconium-5% titanium	1		0	
							Zirconium-10% titanium	1		0	
							Zirconium-20% titanium	1		0	
							Zirconium-30% titanium	1		0	
							Titanium, RC-70	4	0	0	0
							Titanium, Ti-75A	4	0	0	0
							Titanium, Ti-100A	2	0	0	0
							Titanium, Ti-150A	2	0	0	0
							Experimental alloy[o]	1		0.03	
							Experimental alloy[h]	1		0.03	
							Misco A[p]	2	0.41	0.52	0.63
							Misco B[p]	2	0.15	0.25	0.34
							Misco C[p]	2	0.07	0.11	0.14
							Miscro 4[p]	2	0	0.05	0.09
							Inconel X	2	2.2	2.6	3.0
							Low-carbon Inconel	2	0.58	2.2	3.8
							Incoloy	2	0	0.05	0.10
							Chromium-plated type 347 stainless steel	2	[q]		
							Type 347 stainless steel	4	0.02	0.04	0.05
							Type 347 stainless steel[c]	2	0.02	0.03	0.03
							Type 347 stainless steel[d]	2	0	0.01	0.02
							Type 309 SCb stainless steel	2	0.02	0.02	0.02
							Type 304 stainless steel	2	0.02	0.04	0.05
							Type 304 stainless steel[e]	1		0.02	

TABLE 9. (continued)

RUN NO.	TEST CONDITIONS						PIN MATERIAL	NO. OF PINS	CORROSION RATE (mpy)		
	Solution	Uranium Concentration (g/l)	Temperature (°C)	Time (hr)	Additions	Flow Rate (fps ± 10%)			Minimum	Average	Maximum
M-1 (cont'd)	Water	0	250	1000	200 psi O_2	31	Type 304 ELC stainless steel	14	0.02	0.05	0.07
							Type 304 ELC stainless steel[r]	2	0	0.10	0.19
							Type 321 stainless steel	2	0.02	0.03	0.03
							Type 316 stainless steel	2	0	0.02	0.03
							Type 316 stainless steel[s]	1		0	
							Type 322W stainless steel	1		0.05	
							Type 322W stainless steel[n]	1		0.08	
							Type 322W stainless steel[t]	1		1.9	
							Type 416 stainless steel[n]	1		0.61	
							Type 416 stainless steel	1		0.07	
							Type 440C stainless steel[n]	1		0.48	
							Type 440C stainless steel	1		0.19	
							Type 410 stainless steel[n]	1		0.66	
							Type 430 stainless steel	1		0.02	
							Type 446 stainless steel	1		0.03	
							Type 17-4PH stainless steel[n]	2	0.46	0.48	0.49
							Type 17-4PH stainless steel	1		0.02	
							Stellite 1	1		140	
							Stellite 3	1		94	
							Stellite 6	1		170	
							Stellite 25	1		53	
							Stellite 98M2	1		51	
M-2	Water	0	250	1001	200 psi H_2	31	Zirconium, crystal bar	4	0	0	0
							Zirconium-2.5% tin	4	0	0	0
							Zirconium-5% tin	1		0	
							Zirconium-5% titanium	1		0	
							Zirconium-10% titanium	1		0	
							Zirconium-20% titanium	1		0	
							Zirconium-30% titanium	1		0	
							Titanium, RC-70	4	0	0	0
							Titanium, Ti-75A	4	0	0	0
							Titanium, Ti-100A	2	0	0	0
							Titanium, Ti-150A	1		0	
							Experimental alloy[h]	1		0	
							Experimental alloy[o]	1		0.07	
							Misco A[p]	2	0	0.01	0.02
							Misco B[p]	2	0	0.01	0.02
							Misco C[p]	2	0.02	0.06	0.10
							Miscro 4[p]	2	0.44	0.53	0.61
							Inconel X	2	0	0	0
							Low-carbon Inconel	2	0	0	0

TABLE 9. (continued)

RUN NO.	TEST CONDITIONS						PIN MATERIAL	NO. OF PINS	CORROSION RATE (mpy)		
	Solution	Uranium Concentration (g/l)	Temperature (°C)	Time (hr)	Additions	Flow Rate (fps ± 10%)			Minimum	Average	Maximum
M-2 (cont'd)	Water	0	250	1001	200 psi H_2	31	Incoloy	2	0.02	0.03	0.03
							Chromium-plated type 347 stainless steel	4	0	0	0
							Type 347 stainless steel	4	0.03	0.05	0.09
							Type 347 stainless steel[c]	2	0.02	0.04	0.05
							Type 347 stainless steel[d]	2	0.09	0.10	0.10
							Type 309 SCb stainless steel	2	0.03	0.03	0.03
							Type 304 stainless steel	2	0.07	0.10	0.12
							Type 304 stainless steel[e]	1		0.07	
							Type 304 ELC stainless steel	14	0.03	0.10	0.17
							Type 321 stainless steel	2	0.02	0.02	0.02
							Type 316 stainless steel	2	0.07	0.08	0.09
							Type 316 stainless steel[s]	1		0.02	
							Type 322W stainless steel	1		0.22	
							Type 322W stainless steel[n]	1		0.27	
							Type 322W stainless steel[t]	1		1.6	
							Type 416 stainless steel[n]	1		0.39	
							Type 416 stainless steel	1		0.70	
							Type 440C stainless steel[n]	1		1.0	
							Type 440C stainless steel	1		0.73	
							Type 410 stainless steel[n]	1		0.87	
							Type 446 stainless steel	1		0.02	
							Type 17-4PH stainless steel[n]	2	0.26	0.30	0.34
							Type 17-4PH stainless steel	1		0.12	
							Carpenter-20	1		0.12	
							Stellite 1	1		0.20	
							Stellite 3	1		0.07	
							Stellite 6	1		0.14	
							Stellite 25	1		0.03	
							Stellite 98M2	1		0.02	
Mockup-10	UO_2SO_4	40	200	396	~25 psi O_2 (200 ppm O_2)	16	Type 347 stainless steel	6	13	17	20
							Type 304 ELC stainless steel	3	16	19	21
							Stellite 1	1		120	
							Stellite 6	1		110	
							Stellite 98M2	1		530	
Mockup-11	UO_2SO_4	40	250	200	~25 psi O_2 (200 ppm O_2)	16	Type 347 stainless steel	6	26	35	48
							Type 304 ELC stainless steel	3	4.8	12	23
							Stellite 1	1		290	
							Stellite 6	1		500	
							Stellite 98M2	1		210	

TABLE 9. (continued)

RUN NO.	TEST CONDITIONS						PIN MATERIAL	NO. OF PINS	CORROSION RATE (mpy)		
	Solution	Uranium Concentration (g/l)	Temperature (°C)	Time (hr)	Additions	Flow Rate (fps ± 10%)			Minimum	Average	Maximum
Mockup-12	UO_2SO_4	4	200	199	~25 psi O_2 (200 ppm O_2)	16	Type 347 stainless steel	6	11	17	20
							Type 304 ELC stainless steel	3	11	14	16
							Stellite 1	1		73	
							Stellite 6	1		140	
							Stellite 98M2	1		34	

(a) Solution separated into two liquid phases.

(b) Solution dissolved copper from the rotor of the pump and caused the pH of the solution to increase during the run.

(c) Cast type 347 stainless steel.

(d) Centrifugally cast type 347 stainless steel.

(e) Cast type 304 stainless steel.

(f) Specimens tested at 13 fps were exposed to a stream whicb was supposed to contain only dissolved oxygen; those tested at 5 fps were exposed to a stream which contained gas bubbles.

(g) Specimens tested at 9 fps were exposed to a stream which contained oxygen gas bubbles; those tested at 8 fps were exposed to a stream which was supposed to contain only dissolved oxygen.

(h) An experimental, low-nickel, ferritic stainless steel in the "as received" condition (not fully annealed).

(i) This run made to remove scale from the loop.

(j) During this run the pH of the solution decreased slightly because about 20% of the copper precipitated as a basic copper sulfate.

(k) This alloy contained a small amount of misch metal in addition to the standard alloying elements.

(l) This run was made at a time when the solution in the HRE was contaminated with nitric acid. The concentration of nitric acid was about the same as in the HRE.

(m) This run contained a number of other alloys which had been given various metallurgical treatments. These specimens are being examined by the Metallurgy Group of the HRP.

(n) These steels had been hardened by appropriate heat treatments.

(o) An experimental, low-nickel, ferritic stainless steel in the fully annealed condition.

(p) These alloys were obtained from the Michigan Steel Casting Company and had the following compositions:

	COMPOSITION (%)			
	Ni	Cr	C	Si
Misco A	37.9	19.2	0.26	1.57
Misco B	13.3	25.4	0.36	1.45
Misco C	10.0	28.7	0.22	1.73
Miscro 4	0.15	13.1	0.07	1.41

(q) Chromium plate completely removed from both pins.

(r) Cast type 304 ELC stainless steel.

(s) Cast type 316 stainless steel.

(t) Malcomized type 322W stainless steel.

TABLE 10. EFFECT OF OXYGEN PRESSURE ON THE CORROSION RATE OF STAINLESS STEEL IN 1.26 *M* URANYL SULFATE AT 250°C

RUN NO.	OXYGEN PRESSURE (psi)	SOLUTION OXYGEN CONCENTRATION* (ppm)	SOLUTION NICKEL CONCENTRATION (ppm)	SOLUTION CHROMIUM CONCENTRATION (ppm)	CORROSION RATE OF SYSTEM (mpy)
C-27	75**	340	940.	170	28
C-25	150	720	1530	340	47
C-28	300	1800	1340	630	40

*These concentrations were obtained by chemical analyses after the solution reached 250°C.
**Contained 75 psi helium in addition to the oxygen.

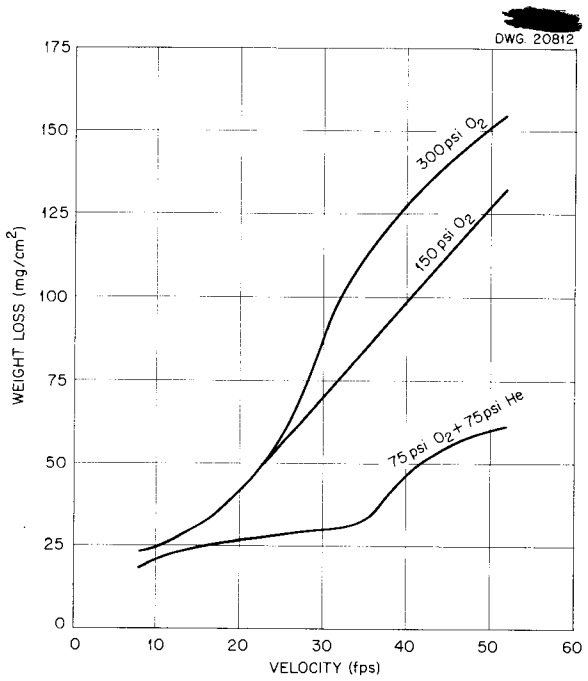

Fig. 41. Effect of Oxygen Pressure on Corrosion of Type 347 Stainless Steel as a Function of Velocity.

It is interesting to note that in runs C-25 and C-27, the total pressure of added gases was the same, that is, 150 psi. However, the corrosion damage to both the pins and coupons in run C-25 was almost a factor of 2 higher than in run C-27. Hence, it appeared that the increase in corrosion damage in run C-25 over that in run C-27 was due to the difference in oxygen and not to the difference in total dissolved gas. (At 250°C under the same conditions, the solubilities of helium and oxygen are nearly equal.) The coupon data indicate that at low velocities the oxygen concentration is not so significant as it is at high velocities. This complex influence of oxygen concentration may explain why previous studies of the effect of oxygen concentration on the generalized corrosion of the system, as indicated by nickel analyses, gave inconclusive results.

The amount of chromium in solution at the end of a run was proportional to the oxygen concentration in solution. Also, increasing the oxygen pressure from 75 to 150 psi appeared to cause a larger change in corrosion damage than did increasing the oxygen pressure from 150 to 300 psi. These data are very similar to results obtained in static systems.[9]

Effect of Time, Velocity, and Uranium Concentration. Previously,[7] data were presented on the effect of velocity and time on the corrosion rate of several stainless steels in 0.17 *M* UO_2SO_4 at 250°C. At that time, it was shown that pins in a stream flowing at the bulk rate of approximately 15 fps corroded rather rapidly during the first 50 to 100 hr and then corrosion

[9] J. C. Griess and D. J. Sasmor, *HRP Quar. Prog. Rep. July 1, 1952*, ORNL-1318, p. 22.

practically ceased. At velocities reported to be about 100 fps, the corrosion rate was constant and high. For no apparent reason, the coupon data were not self-consistent. Since the previous report was written, it has been determined that the velocity through the channel of the in-line pin holder was 77 fps, not 100 fps, as previously reported.

To determine the reproducibility of the data obtained in 0.17 *M* UO_2SO_4 and to determine the effect of various uranium concentrations on the corrosion rate of several stainless steels, a series of runs for various periods was made with each of the following solutions: 0.17 *M* UO_2SO_4 (40 g of uranium per liter); 0.105 *M* UO_2SO_4 (25 g of uranium per liter); and 0.06 *M* UO_2SO_4 (15 g of uranium per liter) plus 25 mole % H_2SO_4 (0.015 *M*). In each run, one pin holder was placed in the main line where the solution flowed past the pins at the rate of 77 fps. In addition, each run contained one pin holder and one tapered coupon holder mounted in a bypass line. The flow past the pins in the bypass line was 13 to 15 fps. All runs were made at 250°C with an oxygen partial pressure of 200 psi.

Figures 42, 43, and 44 show plots of weight loss per square centimeter vs. time for the pin data obtained with 0.17 *M* UO_2SO_4, 0.105 *M* UO_2SO_4, and 0.06 *M* UO_2SO_4 plus added sulfuric acid. Since there appeared to be no large differences in the austenitic stainless steels examined, the data from each run were plotted as a unit. Each data point represents the average of the data for 12 to 14 pins, and the vertical line through the point shows the maximum spread of the weight losses included in that particular average. The corrosion rates of the individual alloys are given in Table 9 for the following runs: runs A-41 through A-45 and run E-9 for 0.06 *M* UO_2SO_4 (Fig. 44), runs A-46 through

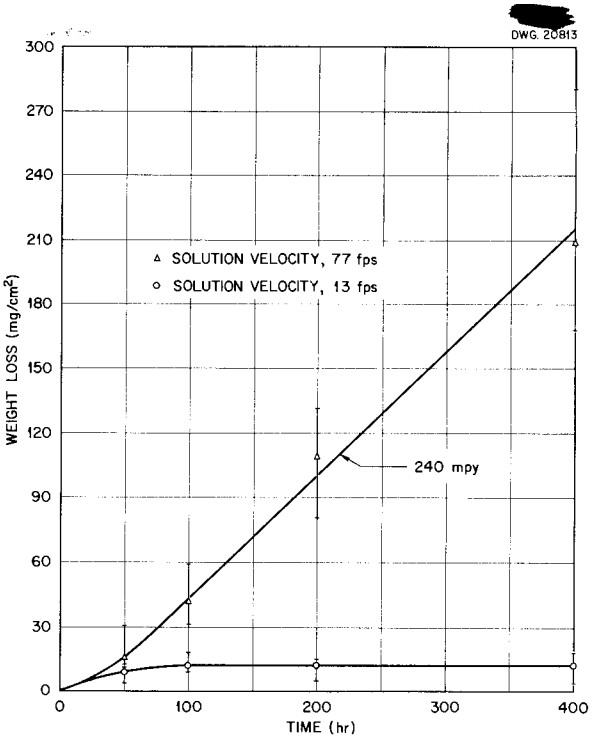

Fig. 42. Corrosion Rate of Stainless Steel Pins in 0.17 *M* UO_2SO_4 at 250°C.

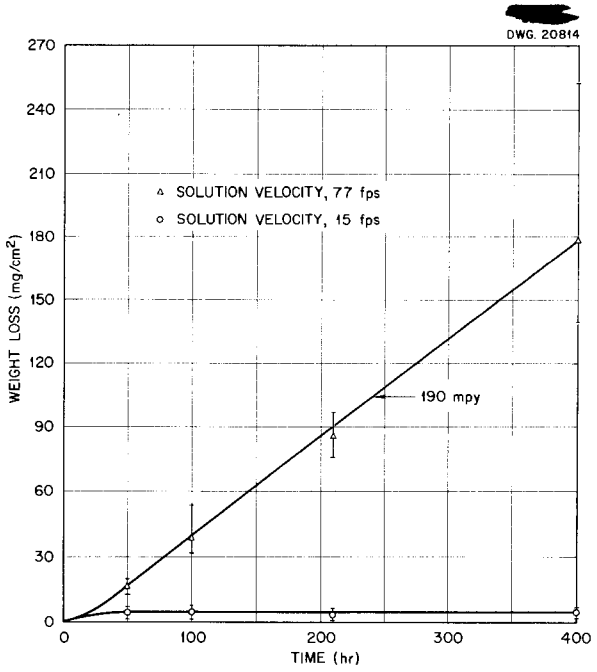

Fig. 43. Corrosion Rate of Stainless Steel Pins in 0.105 *M* UO_2SO_4 at 250°C.

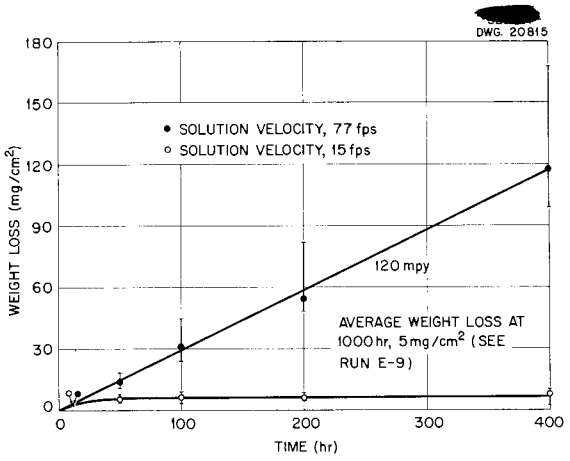

Fig. 44. Corrosion Rate of Stainless Steel Pins in 0.06 *M* UO_2SO_4 and 0.015 *M* H_2SO_4 at 250°C.

A-49 for 0.17 *M* UO_2SO_4 (Fig. 42), runs H-16 through H-20 for 0.105 *M* UO_2SO_4 (Fig. 43). Note that all series gave data of a similar type, that is, a constant, high corrosion rate at the high velocity and, at the low velocity, a high initial rate followed by apparent cessation of corrosion.

Figure 45 shows the coupon data for the 0.17 *M* UO_2SO_4 series, Fig. 46 shows those for 0.105 *M* UO_2SO_4, and Fig. 47 shows those for 0.06 *M* UO_2SO_4 with added sulfuric acid. For the 0.17 *M* UO_2SO_4 series, type 347 stainless steel coupons were used. In the other two series, type 304 ELC stainless steel coupons were exposed. In each series, the data were self-consistent; the coupons exposed in low-velocity streams exhibited behavior similar to the pins in low-velocity streams, and the coupons exposed in high-velocity streams showed corrosion rates nearly equal to those of the pins exposed in high-velocity streams.

Only a limited amount of data is available at present on the effect of velocity on the corrosion of stainless steel in 0.02 *M* UO_2SO_4 containing 0.005 *M* H_2SO_4; short-term tests

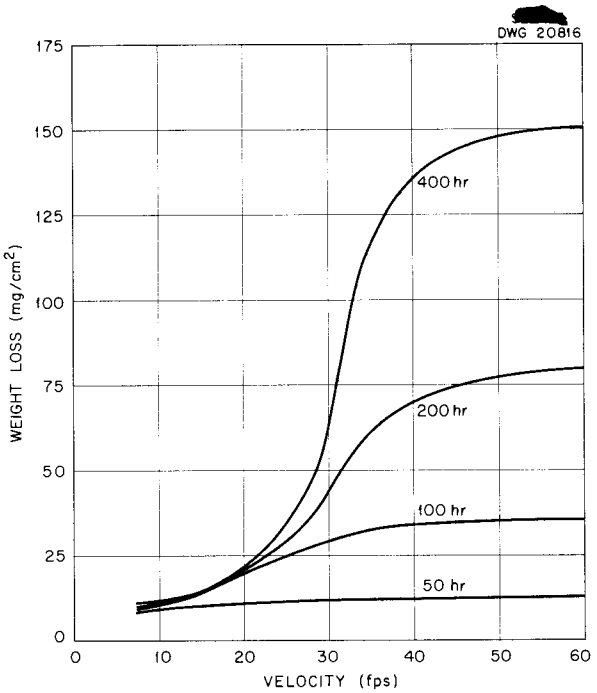

Fig. 45. Effect of Time and Velocity on Corrosion Damage to Type 347 Stainless Steel in 0.17 *M* UO_2SO_4 at 250°C.

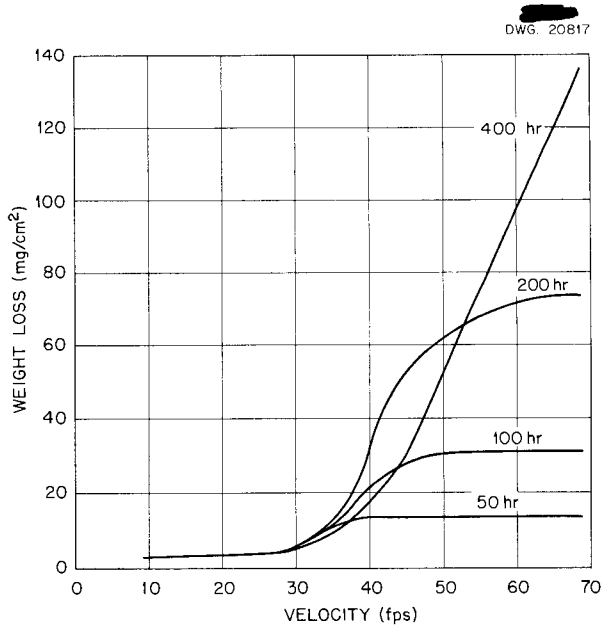

Fig. 46. Effect of Time and Velocity on Corrosion Damage to Type 304 ELC Stainless Steel in 0.105 *M* UO_2SO_4 at 250°C.

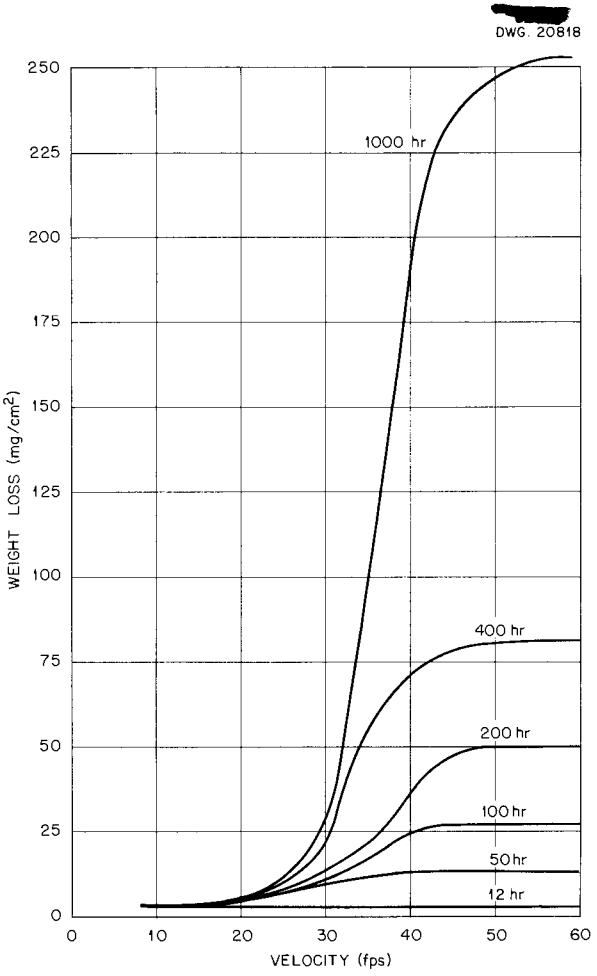

Fig. 47. Effect of Time and Velocity on Corrosion Damage to Type 304 ELC Stainless Steel in 0.06 *M* UO_2SO_4 and 0.015 *M* H_2SO_4 at 250°C.

(<1000 hr) indicated no serious velocity effect. Figure 48 shows some of the data that have been collected, and long-term experiments are now in progress which should give more definitive results. Note in Fig. 48 that the ordinate scale is greatly expanded in comparison with that of Figs. 45, 46, and 47, and that in the 100-hr run, type 304 ELC stainless steel coupons were exposed, whereas type 347 stainless steel was used in the 1000-hr run. From Fig. 48, it is evident that even at the high velocity the corrosion rate is low.

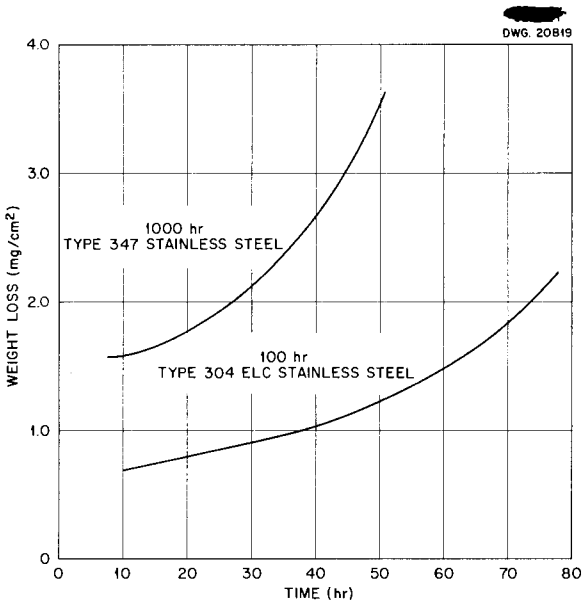

Fig. 48. Effect of Time and Velocity on Corrosion Damage to Stainless Steel in 0.02 *M* UO_2SO_4 Containing 0.005 *M* H_2SO_4 at 250°C. Note different ordinate scale.

Effect of Temperature. In the previous quarterly report,[7] mention was made of a series of runs that had been made at various temperatures with 1.26 *M* UO_2SO_4 (300 g of uranium per liter). At that time, the temperature range investigated was 150 to 250°C, and, since that time, three additional temperatures have been examined, namely, 125, 275, and 300°C. As in the previous cases, all runs were of 100-hr duration, except the one at 300°C in which the solution separated into two liquid phases when the run had been in operation for only 12 hours. In all these runs, the oxygen partial pressure of the system was such that the oxygen concentration of the solution was 300 to 500 ppm.

The corrosion rates of the various austenitic stainless steels did not appear to differ greatly, and hence only an average rate is reported in Table 11 for all the steel pins. Runs C-22 through C-24 in Table 9 show the

types and numbers of pins included in the average. Table 11 also gives the corrosion rate of the entire system, as calculated from nickel analyses of the solutions. At least a large part of the difference between the corrosion rates of the loop and the average corrosion rate of the specimens was caused by the loop having been used previously; there was a heavy oxide scale on the loop surfaces, in contrast to the specimen surfaces which were newly machined.

TABLE 11. CORROSION RATE OF STAINLESS STEEL EXPOSED IN 1.25 *M* URANYL SULFATE FOR 100 HOURS

RUN NO.	TEMPERATURE (°C)	CORROSION RATE (mpy)	
		Pins (avg.)	Total System
C-23	125	0.51	0.30
C-17	150	4.9	1.0
C-18	175	24	5.7
C-19	200	94	8.2
C-20	225	130	14
C-21	250	260	19
C-22	275	250	25
C-24*	300	830	40

*The duration of run C-24 was only 12 hr because the solution separated into two liquid phases.

Tapered coupons were included in each run, but a velocity effect was apparent only in the runs at 275 and 300°C. Even the effect observed at 275°C was not so severe as was expected. At all temperatures up to and including 250°C, the weight losses of the individual coupons were independent of the velocity up to the maximum velocity studied, about 50 fps; the corrosion rates on the coupons checked rather closely with the rates observed for the pins at that temperature.

In this series of runs, some mechanical difficulties were encountered with the coupon holders. In nearly all cases there was excessive leakage along the sides of the holders, and this may have been at least partially responsible for the lack of a velocity effect. Another factor that may have been responsible for the absence of the velocity effect was the low oxygen concentration of the solution (cf., section above on "Effect of Oxygen Concentration").

Recently, one short run was made at 275°C (J-24) and another was made at 290 to 295°C (J-26); both of these runs were made with 0.02 *M* UO_2SO_4 and 0.005 *M* H_2SO_4. In Table 9, the corrosion rates of the pin-type specimens are given, and it can be seen by comparison with run E-10 that the corrosion rate was as favorable at 275 and at 295°C as it was at 250°C. In each of these runs, a tapered coupon holder containing ten type 304 ELC stainless steel coupons was included. The corrosion rates of the coupons for these runs varied from 2.5 mpy at 10 fps to only 4.6 mpy at 85 fps. Since these were short runs, it is probable that with increased exposure time the corrosion rates would show a marked decrease.

HRE Mockup Operation. The HRE mockup has been operated for approximately 800 hr, and during that time three separate runs were made. Before starting the runs, a bypass line was installed to permit exposure of corrosion specimens to the solution (cf., section above on "HRE Mockup").

The conditions of operation were similar to those proposed for the corrosion testing procedure to be used in the HRE. All runs were made with 0.17 *M* UO_2SO_4 and 200 ppm of oxygen. The first run (mockup-10) was made at 200°C for 400 hr; the second (mockup-11) was for 200 hr at 250°C; and the third (mockup-12) was for 200 hr at 200°C. New specimens were exposed in each run, but the same solution was used for the entire series. Solution samples were removed frequently and analyzed

so that the generalized corrosion rate based on nickel analyses could be followed. The solution used had been accidentally contaminated with a small amount of soluble nickel, but a number of runs made in the dynamic loops with aliquots of the same solution showed no abnormal results.

The results of the nickel analyses for the first two runs can be seen in Fig. 49. The nickel analyses obtained during the third run were erratic, but, in general, they showed a continued decrease in the nickel concentration of the solution. For example, at the start of the third run (mockup-12), the nickel content of the solution was 163 ppm; at the conclusion of the run, it was only 125 ppm. At present, this result defies explanation.

The corrosion rates of the pin-type specimens are given in Table 9, mockup runs 10 through 12. The results obtained from the coupon specimens can be seen in Fig. 50. It should be noted that at 200°C no marked velocity effect was apparent and that at all velocities the corrosion rate appeared to be constant and did not decrease with increased exposure time. The steel pins showed similar behavior. The specimens in run 12 did not reflect the anomaly that was found in the solution analyses.

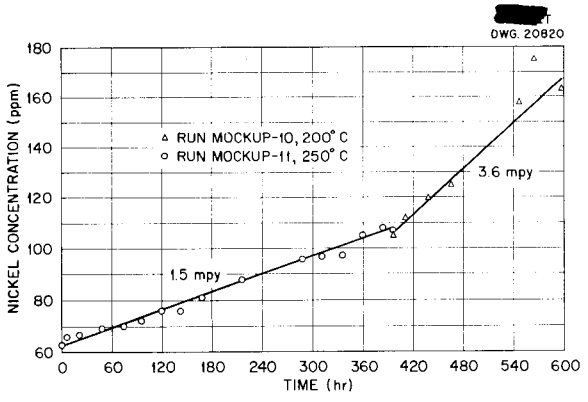

Fig. 49. Rate of Increase of Nickel in the Mockup Solution, 0.17 *M* UO_2SO_4.

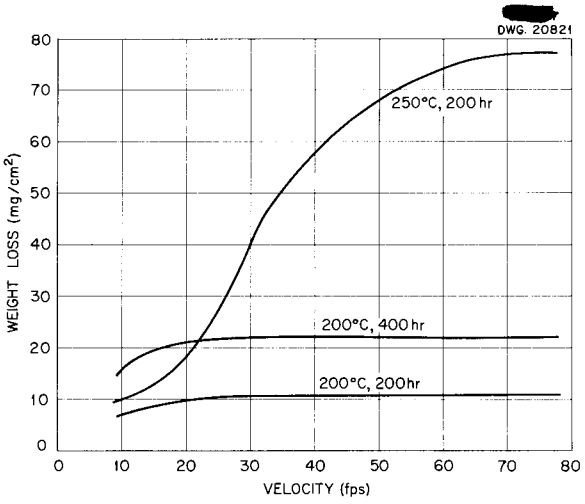

Fig. 50. Effect of Velocity on the Corrosion Damage of Type 347 Stainless Steel in 0.17 *M* UO_2SO_4 in the Mockup.

Uranyl Fluoride-Stainless Steel Systems. Two runs with uranyl fluoride solutions were completed during this quarter. In run J-22, the loop was filled with a uranyl fluoride solution which contained 13.6 g of uranium per liter. The pH of this solution was 3.8. After the solution was heated to 250°C, the pH decreased to 2.5 and the uranium concentration was only 11.7 g/liter. On the basis of the amount of uranium precipitated, sufficient hydrofluoric acid was pumped into the loop without stopping the run to dissolve the uranium which had presumably precipitated as hydrated uranium trioxide. The acid did not change the pH of the loop solution, but it did dissolve the precipitated uranium, as was evidenced by the increase in the uranium concentration to its original value. For the remainder of the run, the solution composition did not change, and, at the completion of the run, there was no evidence of any precipitated uranium trioxide. This run was particularly interesting in that it demonstrated that once a precipitate of uranium trioxide had formed, it could be dissolved by the addition of a small, calculated amount of acid.

The second run, J-23, was made with a solution of uranyl fluoride containing 40 g of uranium per liter. Solution analyses during the run did indicate a change in the solution concentration. However, at the conclusion of the run a very small amount of hydrated uranium trioxide was found in the loop, and thus there was an indication that a small amount of acid would be necessary to stabilize the system. The details of both runs, J-22 and J-23, as well as the corrosion rates of specimens included in the runs, are given in Table 9.

Loop J has been operated in excess of 4000 hr with uranyl fluoride solutions ranging in uranium concentration from 5 to 40 g of uranium per liter. No evidence of either general or localized severe attack was found upon inspection of the part of the pressurizer that was exposed to the gaseous phase. The rupture disk was removed and examined carefully, and the extent of corrosion on it was no greater than that normally found in a uranyl sulfate system. In general, the attack on the stainless steel specimens in the liquid phase was slightly less than that found when uranyl sulfate of the same concentration was used.

Titanium Loop Runs. The titanium loop, which was constructed of titanium and designated as loop G, has been used to make three runs. The pump contained parts made of Stellite and of stainless steel, but these parts were only in contact with low-temperature solution. Past experience has shown that the corrosion rates of these materials in low-temperature solution are extremely low.

The purpose of the first run in the titanium loop was to determine the stability of 0.02 *M* UO_2SO_4 (5 g of uranium per liter) at 250°C with a partial pressure of 200 psi of oxygen. After operation for one day, it was observed that the uranium concentration had decreased by about 20%, and during the next three days, the uranium concentration decreased to 0.7 g/liter and the run was terminated. With this large change in uranium concentration, the pH change was only 0.6 pH unit, that is, from 3.0 to 2.4. An examination of the interior of the loop showed that brown crystals had been deposited on all surfaces. Chemical and spectrographic analyses showed that the precipitate contained cobalt, uranium, and sulfate, with only a trace of titanium. X-ray analysis indicated a single compound with a well-defined pattern which did not match the pattern for any known uranium or cobalt compounds. The composition of the precipitate, based on chemical analysis, was: uranium, 62%; cobalt, 6.9%; sulfate, 12%; and titanium, 0.08%. The mole ratio of U:Co:SO_4 was approximately 2:1:1.

The source of the cobalt was traced to a bearing which was supposed to have been made of Stellite but was actually made of tantalum-tungsten carbides with a cobalt binder. Although Stellite contains a higher percentage of cobalt than do the carbide bearings, the alloyed cobalt in the Stellite was considerably more resistant to the uranyl sulfate solution than was the cobalt in the carbide bearing at the temperature in the pump can.

After the titanium loop was cleaned and the carbide bearing was replaced with a Stellite bearing, a second run was made with uranyl sulfate of the same concentration as that used in the first run, that is, 0.02 *M*. After 14 days of operation the run was stopped, and it was found that the uranium concentration had decreased by 15% and the pH had decreased from 3.0 to 2.2. An examination of the interior of the loop showed that there was a yellow film distributed over the entire loop surface. X-ray analyses of a portion of this precipitate revealed no

identifiable compound of either uranium or titanium. Chemical analysis showed the precipitate to contain 19% titanium, 66% uranium, and no sulfate. The atomic ratio of titanium to uranium was about 4:3. Ignition of the precipitate to 1000°C for 2 hr did not change its appearance, and, as a result of the heating, the weight loss amounted to only 5%.

After the second run, the loop was cleaned as well as possible and the next run was made with 0.02 *M* UO_2SO_4 and 0.005 *M* H_2SO_4 at 250°C. The duration of this run was also 14 days, and analyses of the solution indicated no change during the course of the run. However, at the end of the run, a very thin film of yellow precipitate was observed on the interior surface of the loop. The precipitate was in an amount too small to analyze, but it appeared to be identical to that formed during the previous run. Since the amount was so small, it is quite possible that the precipitate was that which had not been removed from the preceding run.

The titanium loop is not being operated at present because the titanium impeller is being used in the HRE pump. A new impeller will be fabricated after delivery of new titanium blanks, and the loop will again be placed in operation.

Loop Descaling Experiment. When uranyl sulfate or uranyl fluoride solutions are circulated in stainless steel systems at 250°C, a heavy, tightly adhering, black scale is formed on the steel surfaces. The true surface area of such a scale is very large, and thus the conditions are ideal for adsorption of small traces of contaminating ions on the surface. With continued exposure, the oxide film grows in thickness through deposition of corrosion products, and the contaminants become incorporated in the oxide film. Hence, to remove the contamination, it is necessary to remove the scale. Therefore the following descaling experiment was carried out.

Loop H, which had been used to circulate various solutions for a total of several thousand hours, was filled with a solution designed to remove the scale but not seriously attack the underlying steel of the loop. The solution, developed by C. D. Watson and R. J. MacNamee, had the following composition: 1.0 *M* HCl, 1.4 *M* H_2SO_4, and 0.2 *M* H_2O_2. The solution contained a mixture of alkyl pyridines as an inhibitor and was circulated in the loop at 85°C for 4 hours. Newly machined corrosion specimens were exposed in the loop, and the extent of corrosion on these specimens is shown in Table 9, run H-15. Based on the nickel analysis of the solution, the corrosion rate of the system as a whole was 1.8 in. per year.

At the conclusion of the run, it was found that the system was completely descaled; however, the scale had not dissolved to any great extent and remained as a loose deposit in the piping system. Because of its high density, the scale was difficult to flush from the system.

The interior of the loop was not examined during the run; so it is not known whether it might have been possible to allow a shorter time for descaling and thereby reduce the corrosion damage to the system. Future experiments are planned, in conjunction with C. D. Watson and R. J. MacNamee, in which a loop will first be contaminated with a solution containing fission products at the trace level and then decontaminated with a solution similar to the one first used.

Corrosion by Water at 250°C. Since uranium solutions as dilute as 0.02 *M* have become of interest and the possibility exists that even more dilute solutions may be considered, it was felt that it would be of value to determine the corrosion rate of several alloys in water by using the same

experimental techniques as those used with the uranium solutions. Since most of the dynamic test loops have been operated with 200 psi of oxygen (1000 to 2000 ppm) at 250°C, the first run was made with those conditions of temperature and pressure. A second run was made at the conclusion of the first, and in this run, the conditions were identical to those in the first, except that a hydrogen partial pressure of 200 psi was substituted for the oxygen. Runs M-1 and M-2 in Table 9 show the corrosion rates of the various alloys (pin-type) tested in these runs.

There was included in each run a coupon holder containing ten type 304 ELC stainless steel coupons past which the solution flowed at a rate of 10 to 80 fps. In both runs, the corrosion rates of the coupons at all velocities were the same and equal to those of the type 304 ELC stainless steel pins.

All the austenitic steels developed very thin, bluish-grey films irrespective of the amount of gas dissolved in the water. The titanium and zirconium pins had either blue or purple films, while the zirconium-tin and zirconium-titanium alloys developed black films and, in general, showed substantial weight gains. The alloys that showed striking differences in the extent of corrosion in the two runs were the Stellites, Inconel, Inconel X, and chromium plate. In each case, the corrosion resistance was much better in the run with hydrogen than in the run with oxygen. For example, the chromium plate was completely dissolved in the run with oxygen, while in the hydrogen run, the chromium plate was unchanged.

During the run with hydrogen, the solution did not change, that is, within the limits of detection by the analytical methods used. When the solution contained oxygen, the chromium concentration uniformly increased to 84 ppm; all the chromium was in the hexavalent state. An increase in the hydrogen ion concentration accompanied the increase in chromium. After operation for one week, the pH of the system decreased from its original value of 5.9 to 3.9. For the remainder of the run, the pH slowly decreased and was 3.3 at the end of the run. The nickel concentration remained low (<3 ppm) until the pH was about 3.4, whereupon the nickel content increased rapidly and reached a high of 28 ppm at the conclusion of the run. The iron concentration was consistently less than 1 ppm.

Discussion. Most of the results presented in Table 9 need no further explanation. In several cases, however, the significance of the data is not self-evident. In runs A-41 through A-49 and runs H-16 through H-20, pins were exposed to solutions flowing at the rate of 13 to 17 fps and at 77 fps. In all cases the pins exposed to the low-velocity streams developed heavy, black coatings and those exposed to the high-velocity streams developed only very thin films, which possibly formed during the cooling period after the run was stopped. Pins which did not develop heavy films corroded at a high, constant rate, while those which did develop heavy films had practically zero corrosion rates after the first 50 to 100 hours. The coupons, in general, behaved in a similar manner. The coupons exposed to low-velocity streams did not corrode appreciably after the first 100 hr, but those exposed to high-velocity streams corroded at a constant rate. With coupons, the relationship between corrosion rate and the presence of film was the same as that for the pins.

The corrosion rates of both pins and coupons exposed to high-velocity streams were dependent on the uranium concentration and not, apparently, on the room-temperature pH of the solution. Thus, the average corrosion rates for the pins exposed to high-velocity streams of uranyl sulfate solution containing 40, 25, and 15

(plus acid) g of uranium per liter were 240, 190, and 120 mpy, respectively; the room-temperature pH of each solution was 2.5, 2.8, and 1.7, respectively.

An inspection of pin and coupon data in Figs. 35 through 40 shows that in the same system the weight losses per unit area of pins and of coupons were comparable. For example, the pins exposed to uranyl sulfate solution containing 25 g of uranium per liter flowing at 15 fps lost an average of 6 mg/cm^2, and a coupon exposed to the same stream lost 4 mg/cm^2. The maximum velocity of the stream passing the trailing edge of the last coupon was 77 fps, and that of the stream passing the pins in the high-velocity region was the same. At the end of 200 hr, the weight loss per unit area was 87 mg for pins and 81 mg for coupons. In all cases, however, the pins in the high-velocity stream showed a slightly larger weight loss per unit area than the last coupon in the holder. This difference was probably due to different flow patterns in the two types of holders.

In the previous quarterly report,[7] it was stated that if one part of the system corroded extensively, corrosion products originating at that point were distributed throughout the system. Three examples of this phenomenon have recently been obtained. Loop F was a new loop at the beginning of run F-20. At the conclusion of the run, the nickel analysis of the solution indicated a generalized corrosion rate of 32 mpy. In run F-21, where the conditions were the same as those for run F-20, the generalized corrosion rate was 21 mpy. The specimens gave a reverse effect, that is, in run F-20 the pin corrosion rates were lower than those in run F-21. In runs H-16 and H-17, the same effect can be noted. Run H-15 was a scale-removal run, and, hence, at the beginning of run H-16, the loop was free of scale and comparable to a new loop. The corrosion rate in run H-16 was 8.7 mpy, and in run H-17 it was 4.7 mpy. The pins exposed to the low-velocity stream showed the opposite behavior. In all cases, the pins in the low-velocity stream of a new loop developed considerably heavier films in the first run than in subsequent runs. In high-velocity streams, little or no film formed, and the behavior referred to above was only slightly noticeable in the data for pins exposed to streams flowing at 77 fps. A new loop, loop D, appeared to give the same type of results as did loops H and F (see runs D-1 and D-2), but it is possible that the potassium pertechnetate added as an inhibitor in this loop and/or the copper present in the solutions may have been at least partly responsible for the low rates in run D-1. Thus in new loops, the system, as a whole, usually corrodes at a higher rate in the initial runs than in subsequent runs; the reverse conditions are usually found for the specimens.

A similar reduction in the extent of corrosion of specimens exposed to low- and intermediate-velocity streams was noted in runs in which a previously used uranyl sulfate solution rather than a new solution was circulated in a loop. These observations suggest, among other things, a relationship between film formation and the presence or rate of buildup of corrosion products in the solution. Further studies of this possible relationship are planned.

Not all the runs made in loop D can be clearly interpreted because of the presence of copper in all the solutions. After run D-4, it was discovered that the solution contained about 1.8 g of copper per liter. A check of the solutions used in runs D-1 and D-2 showed that these solutions contained about 3.5 g of copper per liter. The source of the copper was found to be the pump rotor. The stainless steel rotor can had a small hole in it, and the solution had dissolved copper from the rotor. The dissolution of the

copper caused the pH of the solution to rise, and, at the conclusion of run D-4, some uranium trioxide was actually found in the loop. Hence it has not been completely determined whether the pertechnetate ion was of value as an inhibitor. However, plans are now being made to re-examine the inhibitory action of pertechnetate ions on the corrosion of stainless steel in uranyl sulfate systems. In addition, it is planned to investigate molybdate, silica, and possibly other ions as inhibitors.

Experiments designed to evaluate the effect of gas bubbles in circulating uranyl sulfate solutions on the corrosion damage of stainless steel have proved unsuccessful. In run F-20, the specimens in the stream containing gas bubbles appeared to corrode at a lower rate than those which were exposed to the stream that was supposed to contain only dissolved oxygen. In run F-21, the reverse conditions appeared. Gas analyses taken from various locations in the loop showed that the gas separator built into the loop was inefficient and that all specimens were exposed to solutions containing various concentrations of gas bubbles. Since the loop appeared to be of questionable value in determining the effect of gas bubbles, it has been converted to a normal loop and will be used to test an in-pile loop assembly (cf., section above on "Pump Loop Operation and Maintenance").

The generalized corrosion rate of the mockup, based on nickel analyses, appeared to be normal for the first two runs during which a rate of 1.5 mpy was obtained at 200°C and a rate of 3.6 mpy was obtained at 250°C. The nickel analyses obtained from the solution during the third run (200°C) were unexpected and unexplained. Analyses made on aliquots of the solution which showed a continued decrease in the nickel content showed no change in uranium concentration and, hence, ruled out the possibility of solution dilution. Future experiments may clarify this anomalous result.

In each mockup run, the pin and coupon data were consistent, although both showed much higher rates than the rates for the system as a whole, based on nickel analyses. This large difference was probably related to the fact that the mockup had been run previously for several hundred hours at 250°C and had a heavy scale on most surfaces, whereas the pins were new in each run. In run 11 (250°C), the only mockup run for which comparable loop data exist, the specimen corrosion rate and even the rate based on the increase of nickel concentration were in good agreement with the rates obtained from loop data. At 200°C, the specimens showed a constant corrosion rate at all stream velocities and therefore that velocity had very little effect on the corrosion rate. This behavior was quite different from that observed at 250°C and clearly indicated a need for a study of corrosion rates at several temperatures if an understanding of the corrosion process is desired. Similarly, only a limited amount of information exists on the effect of oxygen concentration on the corrosion rate of stainless steel, and it is impossible to evaluate the effect the low oxygen concentration had on the observed results of the mockup operation.

The data obtained in 1.26 *M* UO_2SO_4 at various temperatures are of value only in a rough, qualitative fashion. Since the exposure times were constant throughout, no information was obtained on how the corrosion rates varied with time at the different temperatures. It is possible, for example, that at 275°C the corrosion rate for a second 100-hr period would have been much lower than that for the first. At the same time, it is possible that at lower temperatures the rate might not change so rapidly with time. Only

when rates as a function of time have been established at various temperatures and velocities will the data have quantitative significance. It was, however, interesting to note that the corrosion rate of pins exposed to low-velocity streams did not appear to increase when the operating temperature was increased from 250 to 275°C.

Only a limited amount of data has been collected for specimens exposed in 0.02 *M* UO_2SO_4 containing 0.005 *M* H_2SO_4 at temperatures in excess of 250°C. The data which exist, however, indicate that corrosion rates are about the same at 250, 275, and 300°C. In fact, in high-velocity streams, the corrosion rate may have been lower at temperatures above 250°C. At 300°C, solution analyses have shown low concentrations of nickel, which would appear to indicate a very low generalized rate of attack. However, the solubility of nickel in uranyl sulfate solutions at temperatures above 250°C has not been demonstrated, and it may be that nickel analyses have given erroneous results.

The films formed on specimens exposed at 300°C in 0.02 *M* UO_2SO_4 and 0.005 *M* H_2SO_4 were thin and had a metallic luster, whereas on the specimens exposed at 250°C, the films, although thin, were not so lustrous. Specimens exposed at 300°C have been submitted to T. Willmarth for examination. Tests are now in progress to determine the rate of attack of stainless steel, zirconium, and titanium at 300°C in dilute solutions. It is hoped that in the future it will be possible to increase the temperature to 325°C.

Titanium and zirconium have been exposed to a number of different solutions, and their corrosion resistance to uranyl sulfate in the various concentrations tested has been excellent. Even at 300°C in dilute uranyl sulfate solutions, titanium and zirconium have shown little or no measurable corrosion damage in streams flowing at velocities as high as 77 fps. Most of the tests to which these metals have been subjected have been of rather short duration, and final appraisal of the corrosion resistance of these two metals should be withheld until longer testing periods have been completed. Only crystal-bar zirconium and zirconium-tin alloys have been tested, but an allotment of Zircalloy-2 was recently received and some specimens of this alloy are now being tested.

SMALL-SCALE DYNAMIC CORROSION PROGRAM

R. A. Lorenz G. E. Moore

The small-scale dynamic corrosion program was inactive during most of this quarter because of higher priority problems.

Fabrication of the torus rotator I,[10] which will rotate 20 tori simultaneously, is 50% complete. Torus rotator II, an experimental model of different design than model I, has given a linear velocity of 20 fps in two runs of 15- and 50-hr duration with uranyl sulfate at 250°C and 1000-psi total pressure. This rotator is now being modified to improve the design so that it will be capable of rotating four tori simultaneously at 250°C and 1000-psi pressure at velocities of up to 45 fps.

IN-PILE LOOP DEVELOPMENT AND DESIGN

C. D. Zerby C. W. Keller
R. J. Kedl T. H. Mauney
W. L. Ross

Preliminary detail and layout designs have been completed for the in-pile loop to conform with the latest modification for the addition of copper sulfate as an internal, homogeneous catalyst for the recombination of hydrogen and oxygen. The details of the modification to the loop were reported in the previous

[10] W. L. DeRieux and J. R. McWherter, *HRP Quar. Prog. Rep. Mar. 31, 1953*, ORNL-1554, p. 65.

quarterly report.[11] From the new drawings, a loop was built which is essentially a mockup of the in-pile loop; it includes all the heaters, the coolers, the corrosion-sample holders, and the ORNL small pump, and it conforms to the general geometry expected for the in-pile loop. The measured volume of the loop, including the pump but excluding the pressurizer volume of 400 ml, is 1000 ml. Instrumentation for this "high-temperature loop" is of a much simpler design than that required for the in-pile loop, but it is quite satisfactory for the initial test work.

The high-temperature loop has operated for 23 hr with water at various temperatures and pressures, including the expected operating conditions of the in-pile loop. Twenty-two hours of operation, with the loop at 250°C and the pressurizer at 280°C, have already been achieved with no apparent difficulty; the flow rate under these conditions was measured to be 5.8 gpm, which gives a maximum velocity of 50.5 fps in the corrosion sample holders. Startup and shutdown procedures are being carefully analyzed to assure that gases are not evolved into the main circulating stream. Although some gas is being evolved into the main stream during startup, it is believed that this condition can be minimized. When the pressurizer temperature is raised sufficiently above the loop temperature to give a superpressure of steam, the gassing condition ceases.

The high-temperature loop will be used to determine modifications needed in design and layout and to establish certain operating procedures for the mockup of the in-pile loop.

The mockup of the in-pile loop will be fabricated as soon as drawings can be altered to conform with design modifications. This loop will be a complete duplicate of the in-pile loop in every possible detail, including instrumentation. Instruments are now on order for the mockup and for the in-pile loop; the maximum delivery date quoted is December 1, 1953.

Several corrosion-sample holders that are identical to those to be used in the in-pile loop have been prepared for testing in the dynamic corrosion test loops so that they can be compared with the standard sample holders. A "core" sample holder and an in-line sample holder are now in a loop operating at 250°C with a uranyl sulfate solution containing 40 g of uranium per liter plus 0.01 *M* $CuSO_4$, which is the solution expected to be used in the in-pile loop. The first samples will be removed after 200 hr of exposure.

IN-PILE LOOP PROGRAM

G. H. Jenks D. T. Jones
R. A. Rosenberg

Operating Methods and Equipment. The general plan for carrying out corrosion measurements with the in-pile loop is, briefly, the following:

A loop assembly, the suitable performance of which has been demonstrated, will be placed in position in the reactor. The assembly will be left undisturbed until the desired operating time has been accumulated or until a failure of the system forces a removal of the entire assembly. Operations such as sampling, and fuel and gas addition, which are designed to follow the course of the experiment and to control experimental conditions, will be carried out from the face of the shield. Draining and purging of the loop prior to removal will also be carried out while the loop is in its operating position; again, equipment at the face of the shield will be used. Provisions will be made during the installation for containing any radioactive solution or gases which

(11) G. H. Jenks *et al.*, *HRP Quar. Prog. Rep. Mar. 31, 1953*, ORNL-1554, p. 66.

might be liberated in a break in any part of the system.

At the termination of an experiment, the loop will be withdrawn and moved to facilities provided in one of the remote chemical cells in Building 4501. Here the loop assembly will be cut open and small sections which contain corrosion specimens will be removed. These small sections will be transferred to facilities in the Solid State Division Building where the specimens will be removed and examined.

The status of some of the methods and equipment required to implement this operational scheme is discussed in the following.

Operating Characteristics of Loop. The proposed operating characteristics of the in-pile loop were described previously, but, for convenience, they are briefly reviewed here. The temperature of the main stream will be 250 ± 2°C. The temperature of the pressurizer will be that which will result in a steam pressure of 930 psi, about 280°C. This temperature will be controlled to within ±1°C. The pressurizer will contain 70 psi of excess oxygen at the start of a measurement. The total volume of fuel in the system will be about 1150 ml; 850 ml of this volume will be in the main circulating stream, 200 ml will be in the pressurizer, and 90 ml will be in the cold rotor region of the pump. The gas volume in the pressurizer will be 200 ml. The area of the surface in contact with the main stream solution will be about 2000 cm^2. The area in contact with solution in the pressurizer will be 270 cm^2. The rate at which fuel will circulate in the main stream will be about 350 ml/sec. A side stream will circulate through the pressurizer at a rate of 3 ± 0.5 ml/sec. Copper sulfate, in solution, will be used to catalyze the recombination of hydrogen and oxygen. The copper concentration will be sufficient to maintain a steady-state pressure of 100 psi of stoichiometric gas dissolved in the main stream. Under these various operating conditions, the pressure of stoichiometric gas in the pressurizer will be about 12 psi.

Gas Additions. The first loops to be placed in the reactor will be constructed of type 347 stainless steel. As corrosion proceeds in the stainless steel system, oxygen will be consumed and the pressure of excess oxygen will decrease. The oxygen consumed will be replaced from time to time by adding oxygen gas to the pressurizer. In each gas addition, the pressure will be returned to the initial 70 psi.

The frequency with which gas additions will be made will depend upon (1) the minimum oxygen pressure which must be maintained to avoid accelerated corrosion and (2) the over-all loop corrosion rate. It has been estimated that the rate of reduction in excess oxygen pressure will be 2.8 psi/day for a corrosion rate of 1 mpy. It is assumed that the oxygen pressure may be allowed to drop to 25 psi, but no lower. Hence, for a corrosion rate of 1 mpy, the interval between oxygen additions may be two weeks. For corrosion rates greater than 1 mpy, the permissible interval will be proportionately less.

Another characteristic of corrosion in the systems under study is the consumption of hydrogen ions – a result of the solubility of nickel in the solution. This loss of hydrogen ions if allowed to proceed without replacement, would lead to precipitation of uranium and copper by hydrolysis. To prevent such precipitation, it is planned to add acid each time oxygen is added.

The amount of acid to be added can be determined from the oxygen consumed. Roughly, 1.5 atoms of oxygen react for each stainless steel atom which is oxidized. Two hydrogen ions are consumed for each nickel ion which

enters solution. The fraction of nickel in stainless steel is approximately 0.1. Consequently, the ratio of consumption of oxygen atoms to hydrogen ions is 7.5 to 1. It is assumed that oxygen gas disappears from the system only in the oxidation of steel. It is also assumed that all oxidized nickel stays in solution and that the hydrogen ion balance is not affected by other constituents of the steel.

It should be pointed out here that the indirect information obtained from oxygen consumption measurements will be checked by testing samples of fuel solution which will be withdrawn at infrequent intervals, probably during the regular weekly shutdown of the reactor. Methods for withdrawing samples are being developed.

Determinations of Oxygen Pressure in Loop. The oxygen pressure in the system will be determined from a knowledge of the total pressure, the steam pressure in the pressurizer, and the stoichiometric gas pressure in the pressurizer.

Total pressure in the system will be determined by means of a transducer gage which will be installed at the face of the shield and joined to the gas space in the pressurizer through a 40-mil-ID tube.

Steam pressure will be determined from temperature measurements in the pressurizer. It is planned to use thermocouples for measuring temperatures.

The pressure of stoichiometric gas in the pressurizer will normally be quite low, about 12 psi. However, this pressure will be determined by the activity of the copper catalyst which, under certain conditions, may change. In order to be certain of the stoichiometric gas pressure, it will be necessary to decrease the neutron flux at the core so that partial or complete recombination of hydrogen and oxygen may take place. The stoichiometric gas pressure can then be determined from the resulting decrease in pressure.

The neutron flux can be stopped completely by shutting down the reactor. Such stoppage will be necessary when a precise measure of the pressure is required. However, a rough measure will be suitable during a large fraction of the operating time. This could be obtained by operating the reactor at 50% of full power or through the use of an adjustable cadmium shutter. Plans are being made for the incorporation of a shutter in the in-pile system.

Method of Adding Oxygen and Acid. Acid addition will be made by adding sulfur dioxide gas. Studies by Sherwood (cf., chapter on "Aqueous Solution and Radiation Chemistry") have shown that rapid oxidation of small quantities of sulfur dioxide to sulfuric acid can be expected at the high temperatures prevailing in the loop and that no reactions are encountered which lead to precipitation. Oxygen will be added as oxygen gas. To permit the introduction of SO_2 under pressure, a mixture containing the two gases in the required ratio will be employed. As discussed above, hydrogen ions and oxygen atoms must be supplied in a ratio of 1 to 7.5. The ratio of sulfur dioxide to oxygen in the gas mixture should then be about 1 to 8. A mixture of this composition can support a pressure of 535 psi at 24°C before condensation of SO_2 occurs.

The following general method is to be used for adding the gas mixture. A supply tank will be charged with the mixture to a pressure of 500 psi at room temperature. The pressure in the loop will be reduced to 300 psi by lowering the temperature in the pressurizer to 215°C. Gas from the supply tank will then be allowed to expand into the pressurizer. The amount of gas added to the loop will be determined

from pressure and temperature measurements in the supply tank.

Equipment. The equipment required for making the gas addition is shown in the upper portion of Fig. 51. The equipment consists, essentially, of the tank labeled "metering volume," and the tubing and valve assembly connecting the tank with the pressurizer. The volume of the tank is about 200 ml, and the tank is accurately calibrated. The tank is equipped with a transducer gage and a thermocouple well. The valves are of the autoclave 30,000-psi series. The tubing between the pressurizer and the first valve has an internal diameter of 20 mils. The remaining tubing has an internal diameter of 50 mils. This equipment, as well as the additional equipment needed in preparing the gas mixture and in charging the metering tank, is being constructed and tested.

Provision for Filling Connecting Tubing with Water. The two tubes which connect the pressurizer with equipment at the pile face will be maintained full of water at all times during operation. This practice will be followed in an effort to prevent the formation of explosive mixtures in the tubing and to confine radioactive materials to the pressurizer.

No serious problem will be involved in filling the transducer gage line. This tube may be filled before startup when the system will be at atmospheric pressure. In normal operation, the tube will require no further attention during a measurement.

Addition of water to the other tube will present more of a problem. Gas will be added to the system through this tube, and, consequently, it must be refilled after each gas addition. The addition must be made under high pressure and must be accurately metered to avoid dilution of the fuel solution. The amount of water required per addition will be about 0.5 ml.

The method which has been advocated for carrying out these water additions makes use of the thermal expansion of water. A container, the volume of which is about 16 ml, will be attached through valves to the gas addition line. The container and connecting tubing will be completely filled with water. To make an addition, the valve to the gas addition line will be opened, and the water in the 16-ml volume will be expanded into the line by heating. A temperature increase of about 65°C will effect the required expansion of 0.5 ml.

The equipment needed for these operations has been designed and is being constructed.

Draining and Purging. When the loop is to be removed from its operating position in the reactor, it will be freed of a major portion of the fission-product activity produced during reactor operation. The following general methods and equipment will be used in carrying out the necessary draining and purging.

Solutions from the loop will be bled through a small connecting tube into one of several receptacles at the face of the reactor. The drain tube will be equipped with a water-cooled jacket, and hence solutions in the loop may be at high temperature at the time of drainage. Wash solutions will be added to the loop through a second tube.

A tank of 1.5-liters capacity will serve to receive and store the bulk of the fuel solution. Wash solutions which must be recovered will be collected in a larger wash tank. Other wash solutions will be disposed of through a hot drain. To aid in tracing the recovery of uranium and in following decontamination, the fuel and wash tanks will be equipped with facilities for measuring the volume of liquid in the tanks and for withdrawing liquid specimens.

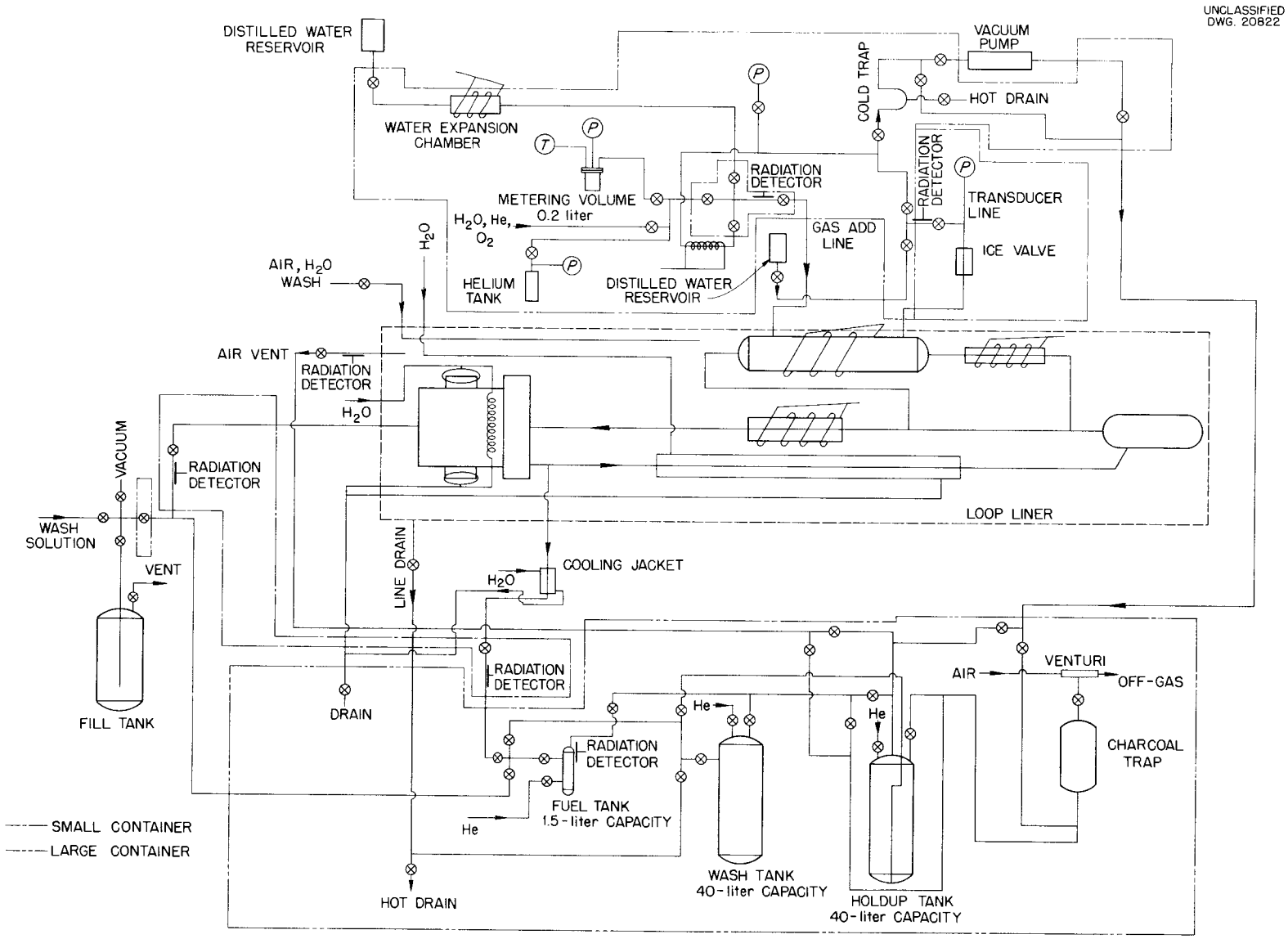

Fig. 51. Flow Sheet for In-Pile Loop.

A large fraction of the radioactive gases from the loop will be collected in a third tank, the gas holdup tank. The gases will remain in this tank until it is safe to release them to an off-gas system. Those gases which are not collected in the tank will be fed directly into the off-gas line.

The drain system, assembled with interconnecting lines, is shown schematically in the lower portion of Fig. 51. The wash and holdup tanks each have a capacity of 40 liters. In general, the connecting tubing is of 50-mil internal diameter. Autoclave 30,000-psi series valves are used throughout.

Mechanical designs of a preliminary nature have been made for the components of the drain system and for the assembly. Detailed designs are under way. No suitable hot drain is available in the LITR building at present, but one will probably be installed. An off-gas system is available which, when supplemented by the gas holdup tank, will be adequate for handling the radioactive gases which will be encountered.

Containment of Leaks and Breaks. An obvious requirement of the design of the in-pile system is that it provide for the containment of radioactive solutions or gases which may be released in a rupture. The following features are being incorporated in the design with this objective.

The experimental hole in the LITR in which the loop will be operated is lined with a close-fitting steel liner. The inner end of the liner is closed. The end at the reactor face opens into a small, boxlike enclosure which contains the critical valves, gages, and tubing. The designation "critical" is used for that equipment which seals the lines leading directly to the loop. A leak in the critical equipment could lead to the release of the entire contents of the loop. This equipment will normally be replaced after each complete in-pile operation.

A second, larger container at the reactor face encloses other equipment which is noncritical but which will handle radioactive materials. This container is connected with the smaller one through a conduit. Tubing from the loop passes into the large container through the small container and the conduit. The equipment in the large container is installed on a semipermanent basis. A leak is not likely to release a serious amount of activity, and, consequently, the operation of the equipment may not be impaired.

The loop proper will be sealed within a separate steel jacket which will fit within the hole liner. All leads from the loop to the face of the reactor will pass through pressure seals in the jacket. The loop and jacket will comprise an integral unit, and will be removed and replaced together. However, this is the only jacket which will be replaced after each normal operation; the other containers will remain in position and be re-used. Preliminary designs for the containing equipment have been completed.

Withdrawing Loop from Reactor. Preliminary designs of methods and equipment for withdrawing the loop from the reactor have been completed. This work has been carried out by a design group under the direction of H. G. Duggan of the Engineering Division. The same group is continuing with detailed designs.

Remote Chemical Cell. Preliminary designs are being made of the equipment which will be used in the remote chemical cell. A design group under the direction of A. M. Tripp of the Engineering Division is engaged in this work.

STATIC CORROSION STUDIES

J. L. English

Static corrosion studies during this quarter were confined to a relatively few number of investigations immediately concerned with the homogeneous reactor project. These investigations included (1) a cursory evaluation of the corrosion behavior of 22 stainless alloys in 0.17 *M* UO_2SO_4 at 250°C, (2) an examination of Malcomized and Stellite 21 coatings on type 304 stainless steel in oxygenated 0.02 *M* UO_2SO_4 at 250°C, and (3) an examination of various grades of ceramic materials in air-aerated 0.02 *M* UO_2SO_4 at 95°C.

In addition, routine acceptance-type corrosion tests were performed with type 347 stainless steel specimens taken from different alloy melts to be used in the fabrication of pipes and fittings for the 4000-gpm test loop. The acceptance tests consisted of the Huey Test (boiling 65% nitric acid) and the Streicher Test (electrolytic oxalic acid etch). Both tests are used to determine the degree of susceptibility, or lack thereof, of the austenitic stainless steels to intergranular corrosion attack in the condition tested. Thus far, the results from these tests have not warranted rejection of any of the welded and nonwelded type 347 stainless steel sections.

Evaluation of Stainless Alloys in 0.17 *M* UO_2SO_4. An evaluation was completed on the corrosion behavior of 22 types of stainless alloys exposed at 250°C in 0.17 *M* UO_2SO_4. The corrosion performance of specimens given a preliminary pretreatment in dilute nitric acid at 250°C and subsequently exposed in uranyl sulfate containing no excess dissolved oxygen was compared with that of nonpretreated specimens exposed in low and high oxygen-containing sulfate solutions at 250°C.

Test specimens were run in duplicate for a period of 1000 hr, unless stated otherwise, under the following three conditions:

1. pretreatment in 1 wt % nitric acid at 250°C for 24 hr followed by exposure at 250°C in 0.17 *M* UO_2SO_4 containing approximately 25 ppm of dissolved oxygen (no excess oxygen partial pressure),
2. exposure of nonpretreated specimens at 250°C in 0.17 *M* UO_2SO_4 containing approximately 125 ppm of dissolved oxygen (25-psia oxygen partial pressure),
3. exposure of nonpretreated specimens at 250°C in 0.17 *M* UO_2SO_4 containing approximately 2900 ppm of dissolved oxygen (500-psia oxygen partial pressure).

The tests were run in 225-ml-capacity stainless steel autoclaves with test solution volumes of 150 ml. Prior to use, the autoclaves were pickled for 20 min in 10% HNO_3–4% HF solution at 60°C. After thorough washing in distilled water, the autoclaves were pretreated initially for 24 hr in 1% HNO_3 at 250°C.

The corrosion specimens were tested in the as-received condition; surfaces were either machined or abraded on No. 80 and 120-grit emery papers, respectively. All specimens were vapor-degreased in trichloroethylene before testing.

Weekly examinations were made of the test specimens and the solutions. The specimens were weighed and examined microscopically; 10-ml solution volumes were removed for total uranium and dissolved nickel analyses. The original uranyl sulfate solutions were used throughout the tests, with the exception of weekly replacements for the 10-ml volumes removed for chemical analyses. In the tests with excess dissolved oxygen present, 125 and 2900 ppm, 30% H_2O_2 was added in predetermined quantities to the uranyl sulfate solutions at weekly intervals to produce the desired oxygen partial pressures by thermal decomposition at 250°C.

Upon completion of the tests, the specimens were freed of adhering corrosion films by cathodic treatment in inhibited 5% H_2SO_4 at 75°C. The time of the defilming operation was 3 min, and the cathodic current density was 20 amp/dm^2.

The defilmed weight losses and 1000-hr corrosion rates are given in Tables 12 and 13. The values shown for the nitric acid pretreated specimens include the corrosion damage suffered by the specimens during the nitric acid pretreatment at 250°C.

A few interesting trends were established by the corrosion data. The best over-all corrosion performance - under all conditions - was exhibited by Armco PH 17-4, a precipitation-hardened alloy of the following nominal chemical composition (in wt %): C, 0.05; Cr, 16.5; Ni, 4.25; Cu, 4.0; and Fe, balance. The alloy was tested in the annealed condition in the present investigation. The superiority of the alloy was markedly evident in the pretreated condition - no excess oxygen and untreated - in systems with

TABLE 12. DEFILMED WEIGHT LOSSES OF STAINLESS STEEL ALLOYS EXPOSED IN 0.17 *M* URANYL SULFATE AT 250°C FOR 1000 HOURS

STAINLESS STEEL ALLOY TYPE	WEIGHT LOSS (mg/cm^2)								
	HNO_3 Pretreatment			125 ppm of O_2			2900 ppm of O_2		
	1	2	Avg.	1	2	Avg.	1	2	Avg.
302	0.5	0.4	0.5	1.2	1.4	1.3	1.2	1.4	1.3
303	0.5	0.5	0.5	0.7	0.7	0.7	1.0	1.0	1.0
304	0.6	0.7	0.7	0.6	1.1	0.9	0.9	0.7	0.8
304L	0.8	0.8	0.8	0.5	0.6	0.6	1.1	1.2	1.2
309 SNb[a]	1.2	2.8	2.0[c]	4.5	3.6	4.1[c]	3.5	3.4	3.5[c]
310	0.9	1.0	1.0[c]	1.3	1.2	1.3	1.4	1.3	1.4
316	0.6	0.5	0.6	1.4	1.1	1.3	1.1	1.2	1.2
316L	0.4	0.6	0.5	0.8	1.3	1.1	1.3	0.9	1.1
316 Nb	2.1	2.3	2.2	1.9	2.1	2.0	1.5	1.5	1.5
317	Failed			1.4	3.8	2.6	1.0	0.8	0.9
321	0.6	0.9	0.8	1.0	0.8	0.9	1.0	0.8	0.9
329[b]	0.8	0.9	0.9	1.0	1.2	1.1	1.0	1.1	1.1
347	1.4	1.7	1.6	0.8	1.0	0.9	0.9	0.9	0.9
410	Failed			Failed			Failed		
414	0.3	0.3	0.3	Failed			Failed		
430	0.5	0.5	0.5	0.8	0.5	0.7[c]	11.9	15.4	13.7[c]
430F	0.4	0.4	0.4	Failed			Failed		
442	0.3	0.3	0.3	1.5	1.1	1.3	0.6	0.6	0.6
443	0.5	0.5	0.5	0.7	0.9	0.8	0.5	0.6	0.6
446	0.6	0.6	0.6[c]	1.3	1.6	1.5[c]	1.4	1.3	1.4[c]
Carp. 20	1.8	1.8	1.8[c]	1.6	1.6	1.6[c]	1.8	1.8	1.8[c]
PH 17-4	0.1	0.2	0.2	0.1	0.1	0.1	0.6	0.6	0.6

[a] 1175-hr test.

[b] 985-hr test.

[c] Pitting corrosion observed.

TABLE 13. CORROSION RATES ON STAINLESS STEEL ALLOYS EXPOSED IN 0.17 *M* URANYL SULFATE AT 250°C FOR 1000 HOURS

STAINLESS STEEL ALLOY TYPE	CORROSION RATE (mpy)								
	HNO_3 Pretreatment			125 ppm of O_2			2900 ppm of O_2		
	1	2	Avg.	1	2	Avg.	1	2	Avg.
302	0.2	0.2	0.2	0.5	0.6	0.6	0.5	0.6	0.6
303	0.2	0.2	0.2	0.3	0.3	0.3	0.5	0.5	0.5
304	0.3	0.3	0.3	0.2	0.5	0.4	0.4	0.3	0.4
304L	0.3	0.3	0.3	0.2	0.2	0.2	0.5	0.5	0.5
309 SNb[a]	0.4	1.0	0.7[c]	1.7	1.3	1.5[c]	1.3	1.3	1.3[c]
310	0.4	0.4	0.4	0.6	0.5	0.6	0.6	0.5	0.6
316	0.3	0.2	0.3	0.6	0.5	0.6	0.5	0.5	0.5
316L	0.2	0.2	0.2	0.4	0.6	0.5	0.6	0.4	0.5
316 Nb	0.9	1.0	1.0	0.8	0.9	0.9	0.6	0.7	0.7
317	Failed			0.6	1.6	1.1	0.4	0.4	0.4
321	0.3	0.4	0.4	0.4	0.3	0.4	0.4	0.3	0.4
329[b]	0.4	0.4	0.4	0.5	0.5	0.5	0.5	0.5	0.5
347	0.6	0.7	0.7	0.4	0.4	0.4	0.4	0.4	0.4
410	Failed			Failed			Failed		
414	0.1	0.1	0.1	Failed			Failed		
430	0.2	0.2	0.2	0.4	0.2	0.3[c]	5.3	6.9	6.1[c]
430F	0.2	0.2	0.2	Failed			Failed		
442	0.1	0.1	0.1	0.7	0.5	0.6	0.3	0.3	0.3
443	0.2	0.2	0.2	0.3	0.3	0.3	0.2	0.3	0.3
446	0.3	0.3	0.3[c]	0.6	0.7	0.7[c]	0.6	0.6	0.6[c]
Carp. 20	0.8	0.8	0.8[c]	0.7	0.7	0.7[c]	0.8	0.8	0.8[c]
PH 17-4	<0.1	<0.1	<0.1	<0.1	<0.1	<0.1	0.3	0.3	0.3

[a] 1175-hr test.

[b] 985-hr test.

[c] Pitting corrosion observed.

125 ppm of dissolved oxygen. The improvement was not so pronounced, however, in the high-oxygen-content system.

Other alloys exhibited somewhat peculiar behavior. Type 317 stainless steel failed in the nitric acid pretreated system but not in the low- and high-oxygen-content systems. Types 414 and 430F stainless steel alloys were satisfactory in the nitric acid pretreated systems but failed in the low- and high-oxygen-content systems. On the other extreme, type 410 stainless steel (nonhardened) failed in all three systems. The term "failure" denotes reduction of the uranyl ion in solution and severe corrosion damage to the test specimens.

Types 309 SNb, 310, 430, 446, and Carpenter 20 stainless steels exhibited definite tendencies toward pitting corrosion attack in one or more of the three environments tested. The pits were usually shallow and did not exceed a depth of 5 to 10 mils.

On approximately ten of the stainless alloys, the use of a preliminary

nitric acid pretreatment was beneficial in improving generalized corrosion behavior, as compared with data obtained on untreated specimens exposed in low- and high-oxygen-content uranyl sulfate solutions. The material exceptions to this behavior were types 304, 304L, 310, 316 Nb, 317, 321, 329, 347, 443, Carpenter 20, and PH 17-4.

One alloy, type 430 straight-chromium-grade stainless steel, showed a very marked oxygen dependence in its corrosion behavior. In solutions containing 125 ppm of dissolved oxygen, the average corrosion rate after 1000 hr was 0.3 mpy. With high dissolved oxygen contents, 2900 ppm, the corrosion rate increased to an average value of 6.1 mpy.

Corrosion Behavior of Malcomized and Stellite 21 Coatings on Type 304 Stainless Steel. The corrosion resistance of Malcomized and Stellite 21 coatings on type 304 stainless steel was examined in oxygenated 0.02 *M* UO_2SO_4 solutions at 250°C. Test specimens were prepared by the Chapman Valve Company. The Malcomizing process consisted of a two-step exposure in ammonia gas at temperatures ranging from 454 to 566°C (850 to 1050°F). Increased surface hardness of the stainless steel is attributed to the reaction of nitrogen from the ammonia gas with chromium in the metal to form chromium nitrides. The thickness of the Malcomized layer on the type 304 stainless steel specimen varied between 2 and 5 mils. The measured hardness at a depth of 1 mil was 1024 Vickers (69 Rockwell C); at a depth of 4 mils below the surface, the Vickers hardness number was 712 (61 Rockwell C).

The Stellite 21 hard-faced type 304 stainless steel specimen was prepared by inert-arc deposition of the facing alloy. Stellite 21 has the following nominal chemical composition (in wt %): C, 0.2 to 0.35; Cr, 25 to 30; Ni, 1.5 to 3.5; Mo, 4.5 to 6.5; Fe, 2 (max); and Co, balance. The hardness of the deposited layer was 60 Rockwell 30-N (42 Rockwell C).

The specimens and test solutions were contained in 225-ml-capacity stainless steel autoclaves. Specimens were run singly in separate autoclaves with solution volumes of 150 ml. Insulation of the test materials from the autoclaves was obtained by using Teflon tape.

The tests were operated at 250°C with an estimated dissolved oxygen content of 900 ppm (150-psia oxygen partial pressure). The oxygen partial pressure was produced by the thermal decomposition of 30% H_2O_2 added to the test solutions at room temperature.

Both tests were stopped for examination at the end of 100 hours. The Malcomized specimen exhibited signs of severe corrosion attack, both generalized and localized in nature. The defilmed weight loss was 22.1 mg/cm^2 for a 100-hr corrosion rate of 96 mpy. Total uranium in the sulfate solution underwent a reduction from the initial value of 5 g/l to a final value of 1.9 g/liter. Testing was not resumed at this point.

The Stellite 21 specimen appeared in excellent condition after 100 hr; the as-removed weight loss was 0.2 mg/cm^2, and the surfaces were free of localized corrosion attack. The specimen was returned to the test solution, and the test was continued for a total period of 916 hr; after that time the defilmed weight loss was found to be 1.0 mg/cm^2 (0.5 mpy). Prior to defilming, the surfaces of the specimen were coated uniformly with a very thin, adherent, lustrous, purple-brown film. No signs of pitting corrosion were observed. As-removed weight losses were linear with exposure time after the initial 200 hr of testing. The slope of the curve, 0.0005 mg/cm^2/hr, was equal to a constant corrosion rate of 0.2 mpy after the initial attack.

The results of this study demonstrated effectively the poor corrosion resistance of nitrided surfaces in dilute uranyl sulfate solutions at 250°C. On the other hand, Stellite 21 hard facing on type 304 stainless steel appeared promising for use in similar systems where wear resistance and resistance to galling and seizing are necessary design requisites.

Corrosion Behavior of Ceramic Materials in Uranyl Sulfate Solutions. Nineteen ceramic materials and one plastic sample were submitted by L. M. Doney of the Ceramic Laboratory for exploratory examination of corrosion behavior in air-aerated 0.02 *M* UO_2SO_4 solutions at 95°C. This medium and temperature were selected arbitrarily as an easy method for elimination from further testing of those materials which exhibited poor corrosion resistance. The ceramics which exhibited good corrosion performance will be subjected to the more drastic exposure conditions imposed by higher uranium concentrations and higher operating temperatures.

The test specimens were received in odd sizes and shapes; total surface areas ranged between 12 and 35 cm^2. The densities of the materials varied from 1.3 to 3.7 g/cm^3.

The corrosion tests were run for a period of 2484 hr (14.8 weeks), and the specimens were examined at two-week intervals. Corrosion evaluation was made on the basis of color changes of the specimens and of the test solutions and on weight changes of the specimens. Whenever feasible, specimens were dried to constant weight at each weighing period. The cumulative as-removed weight losses and corrosion rates are given in Table 14. Unless noted, the test solutions did not undergo any change in color during operation.

Total uranium analyses on the uranyl sulfate solutions at completion of the tests showed no reduction of uranyl ion concentrations. Seven of the ceramics and the Chemplas (a phenolic resin) showed sufficiently poor corrosion behavior to disqualify them from any further testing. The ceramics were: AB-2, AC-17, AC-21, AT-200, 150, 4320, and 7370.

TABLE 14. CORROSION OF CERAMIC MATERIALS AFTER 2484 hr IN AIR-AERATED 0.02 *M* URANYL SULFATE SOLUTIONS AT 95°C

TEST NO.	MATERIAL DESIGNATION	SUPPLIER	WEIGHT LOSS (mg/cm^2)	CORROSION RATE (mpy)	SPECIMEN CONDITION
2301-2	AB-2	Coors Porcelain Co.	3.8	1.6	Original white color
2300-1	AC-8	U. S. Stoneware Co.	0.4	0.2	Original white color
2307-1	AC-11	U. S. Stoneware Co.	0.4	0.2	Original white color
2310-1	AC-12	U. S. Stoneware Co.	0.4	0.2	Original white color
2309-1	AC-13	U. S. Stoneware Co.	0.4	0.2	Original white color
2309-2	AC-17	U. S. Stoneware Co.	7.9	3.2	Original white color
2308-1	AC-18	U. S. Stoneware Co.	0.6	0.2	Original white color
2311-1	AC-19	U. S. Stoneware Co.	0.5	0.2	White with pale yellow
2308-2	AC-21	U. S. Stoneware Co.	2.4	0.9	White with pale yellow
2310-2	AC-22	U. S. Stoneware Co.	1.7	0.6	White with pale yellow
2300-2	AC-80	U. S. Stoneware Co.	0.4	0.2	Original light gray color
2304-1	AT-200	Coors Porcelain Co.	6.0	2.3	Original white color
2304-1	Chemplas	General Ceramics Co.	6.8		Original color; swollen
2301-1	CI-7	Coors Porcelain Co.	0.5	0.3	Original white color
2307-2	H-150	U. S. Stoneware Co.	0.6	0.2	Original white color
2306-2	P-40	U. S. Stoneware Co.	0.4	0.2	Original white color
2306-1	150	U. S. Stoneware Co.	2.9	1.4	Yellow discolorations
2303-1	4320	Norton Co.	54.0	27.6	Heavy brown films; solution discolored
2303-2	7370	Norton Co.	38.1	14.3	Heavy red-brown film; solution discolored

METALLURGY

E. C. Miller, Section Chief

WELDING OF AUSTENITIC STAINLESS STEELS

W. J. Leonard

Welds in 1- and 1 1/4-in. types 347 and 304L stainless steel plates in several combinations were made by using the HRP procedural specification as a welding guide. Each weld involved initial heliarc root passes, and then three stainless steel lime-coated welding rods were used: types 347 and 308L and composition "H" (fully austenitic, columbium-stabilized). The welds were x rayed, examined metallographically, and sectioned for bend tests; all were satisfactory. Corrosion test pins containing the welds were cut from each of the nine welded plates and are now being given a variety of heat treatments to establish which condition will result in maximum corrosion resistance in loop tests.

Specimens of type 347 stainless steel welds made under high-restraint conditions were received from an outside source, and the weld cracks were investigated by x-ray and metallographic methods in an effort to study crater cracking and fissuring. No definite results were obtained with the limited number of samples received.

Type 347 stainless steel is being induction melted and cast into buttons of 1-in. diameter and cooled as slowly as possible to simulate a weld puddle. These specimens are being examined microscopically for structures or segregation of components that might cause cracking or lack of corrosion resistance.

EXAMINATION OF CORROSION OF WELDED AUSTENITIC STAINLESS STEEL PINS

W. O. Harms W. J. Leonard

An attempt has been made to evaluate the results of dynamic corrosion tests of 126 welded pin-type specimens which were tested under various conditions of uranyl sulfate solution concentration, flow rate, temperature, and time. The specimens were machined from 1/4-in. welded plates.

The program was designed as a survey to compare combinations of various austenitic type stainless steels heliarc welded with type 347 stainless steel and a few other combinations. The stainless steel combinations investigated were (by type number) 347-347, 304-304, 321-321, 304L-304L, and 304-347. Five special welds were also included: four of type 347 stainless steel welded with (1) type 307 stainless steel lime-coated rod, (2) unshielded type 347 stainless steel bare rod, (3) type 310 stainless steel lime-coated rod, and (4) type 347 stainless steel lime-coated rod, and a fifth of type 304L stainless steel heliarc welded with type 308L stainless steel rod. The test conditions included uranyl sulfate solutions ranging in concentration from 5 to 300 g of uranium per liter (with additions in some cases), flow rates from approximately 10 to 100 fps, periods of time from 90 to more than 1000 hr, and temperatures from 125 to 250°C.

Test Results and Observations. The test results and observations are grouped in Table 15 on the basis of comparable test conditions. Unqualified statements as to the general superiority of any one combination cannot be made because the relative corrosion resistance of a given combination varied with the test conditions, and some discrepancies in test data were unavoidable.

Nonwelded austenitic stainless steel pins in a given run were, for the most part, less severely attacked than welded pins. This difference was most pronounced in solutions containing

TABLE 15. TEST CONDITIONS AND VISUAL EXAMINATION OF WELDED PINS EXPOSED IN DYNAMIC CORROSION LOOPS

GROUP NO.	URANIUM CONCENTRATION IN UO_2SO_4 (g/l)	TEMPERATURE (°C)	TIME (hr)	FLOW RATE (fps ± 10%)	OXYGEN CONCENTRATION (ppm)	pH	ADDITIONS	DEFILMED WEIGHT LOSS (mg) Specimen Designations Represent AISI Stainless Steel Type Numbers for Base Metal-Weld Metal-Base Metal Combinations										AVERAGE WEIGHT LOSS (mg) FOR NONWELDED STAINLESS STEEL PINS IN SAME HOLDER	NATURE OF ATTACK (see notes)
								347-347-347	304-347-304	321-347-321	304L-347-304L	304-347-347	304L-308L-304L	347-307-347 (lime coated)	347-347-347 (unshielded)	347-347-347 (lime coated)	347-310-347 (lime coated)		
A	5	250	1038	11	1000 to 2000	2.1 to 2.2	200 psi O_2 0.005 *M* H_2SO_4	4.9 3.3	5.5 3.3	6.2 6.0	3.7							3.8	(*a*)
B	15	250	1065	12	1000 to 2000	2.9 to 2.2	200 psi O_2	1.9	2.7 1.2 1.8 1.3	2.9 2.1	1.3 2.0	1.8 1.3						2.5	(*b*)
C-1	15	250	2548	12	1000 to 2000	2.8 to 2.1	200 psi O_2				3.0 3.3	8.3 3.5						6.7	(*c*)
C-2	15	250	2548	16	1000 to 2000	2.8 to 2.1	200 psi O_2	4.8 7.7		6.9 8.1								4.5	(*c*)
D	15	250	992	11	1000 to 2000	1.8 to 2.0	200 psi O_2 0.016 *M* H_2SO_4	16.2 15.3	13.1 12.5	12.7 16.6	11.7 8.9		12.5 7.2					16.7	(*d*)
E-1	40	250	97	16	1000 to 2000	1.7 to 1.8	200 psi O_2	13.5 5.2		13.3 5.2								6.5	(*e*)
E-2	40	250	97	16		2.6	100 psi O_2 + 8 cm^3 O_2/min	27.2 29.3		25.6 25.7								22.4	(*e*)
E-3	40	250	94	17	1000 to 2000	2.6 to 2.7	200 psi O_2 50 ppm Cl as KCl	8.6 14.6		13.6 11.9								16.7	(*e*)
E-4	40	250	90	14	1000 to 2000	1.25 to 1.45	200 psi O_2 0.042 *M* H_2SO_4	66.8				70.9 78.6						58.5	(*e*)
F-1	40	250	97	77	1000 to 2000	1.7 to 1.8	200 psi O_2	92.7 88.7		100.8 109.2								82.5	(*f*)
F-2	40	250	97	77		2.6	100 psi O_2 + 8 cm^3 O_2/min	91.5		106.2 97.7								100.4	(*f*)
F-3	40	250	94	77	1000 to 2000	2.6 to 2.7	200 psi O_2 50 ppm Cl as KCl	97.3 89.4		97.8 90.5								82.2	(*f*)
G	40	250	559	20	1000 to 2000	1.35 to 1.5	200 psi O_2 0.042 *M* H_2SO_4	373.6										87.3	(*g*)
H	40	250	1036	15	1000 to 2000	1.3 to 1.75	200 psi O_2 0.042 *M* H_2SO_4	575.8 466.8	383.3 447.1	342.7 363.8	270.9 395.1							71.6	(*h*)
I	40	250	499	20	1000 to 2000	1.8 to 2.3	0.1 *M* $CuSO_4$ 0.005 *M* H_2SO_4 200 psi O_2				21.5 33.0		21.6 30.6	22.8 24.2	20.4 34.1	25.6 29.8	20.3 21.2	29.9	(*i*)

TABLE 15 (continued)

GROUP NO.	URANIUM CONCENTRATION IN UO_2SO_4 (g/l)	TEMPERATURE (°C)	TIME (hr)	FLOW RATE (fps + 10%)	OXYGEN CONCENTRATION (ppm)	pH	ADDITIONS	DEFILMED WEIGHT LOSS (mg) Specimen Designations Represent AISI Stainless Steel Type Numbers for Base Metal-Weld Metal-Base Metal Combinations										AVERAGE WEIGHT LOSS (mg) FOR NONWELDED STAINLESS STEEL PINS IN SAME HOLDER	NATURE OF ATTACK (see notes)
								347-347-347	304-347-304	321-347-321	304L-347-304L	304-347-347	304L-308L-304L	347-307-347 (lime coated)	347-347-347 (unshielded)	347-347-347 (lime coated)	347-310-347 (lime coated)		
J-1	300	125	928	18		1.5 to 1.7	180 psi O_2	4.9		6.4 6.8								3.9	(*j*)
J-2	300	125	928	16		1.5 to 1.7	180 psi O_2		5.3 4.8		5.4 5.2	4.7 5.1						5.1	(*j*)
K-1	300	150	997	16	200 to 600	1.5 to 1.7	200 psi O_2		22.0 9.4		18.6 15.1	24.5 27.6						23.0	(*k*)
K-2	300	150	997	20	200 to 600	1.5 to 1.7	200 psi O_2	18.3		41.9 44.0								17.0	(*k*)
L-1	300	175	308	21	300 to 500	1.5 to 1.7	200 psi O_2	30.7		46.8 60.3								24.4	(*l*)
L-2	300	175	308	16	300 to 500	1.5 to 1.7	200 psi O_2		22.7 35.9		22.8 33.5	32.9 23.0						33.2	(*l*)
M	300	250	117	12	2000 to 3000	1.5 to 1.6	250 psi O_2	71.3 108.3	175.5 187.5		93.8 132.3							42.6	(*m*)
N	300	250	117	5	8000 to 9000	1.5 to 1.6	250 psi O_2	26.3 42.3	36.7 27.3		28.4 20.4							24.3	(*n*)

(*a*) Attack was uniform on all specimens.

(*b*) Attack was uniform on all specimens.

(*c*) Attack was uniform on all specimens.

(*d*) Attack was uniform on all specimens. Weight losses were five to eight times greater than for group B pins. (Group B pins were tested in solutions containing 15 g of uranium per liter without excess sulfuric acid, but the duration of test was 73 hr longer.)

(*e*) Attack was uniform on all pins except those involving type 304 in solutions containing excess sulfuric acid, where the weld was much more severely attacked than the base metal. It was observed that the welds in these specimens were much more magnetic than the weld in the 347-347-347 pin in the same run, and thus there was indication that the former contained more ferrite.

(*f*) Attack was uniform on type 347 stainless steel specimens except for those in solutions with chloride additions, where the weld was selectively attacked. All type 321 stainless steel pins were more or less selectively attacked in the welds, this being especially evident on those pins which were exposed to solutions with chloride additions. This effect was much more pronounced than in corresponding type 347 stainless steel pins. The fivefold increase in flow rate as compared with that for group E specimens brought about a 10- to 20-fold increase in corrosion attack.

(*g*) This pin was severely attacked at the weld.

(*h*) All pins were severely corroded at welds. Note that the weight loss of type 347 stainless steel specimens was greater than that of other combinations. Attack was most severe on the upstream side of pins in all cases. The type 347 stainless steel pins corroded over almost the entire width of the exposed area, while attack on other pins was confined principally to the welds. In the latter cases attack apparently began at the weld-base metal interface and proceeded in both directions, slowly into the base metal and rapidly into the welds. The tenfold increase in time as compared with that for group E effected a 20-fold increase in weight loss of pins.

(*i*) Principal attack on type 304L stainless steel pins was in the welds, while on other combinations the attack was uniform.

(*j*) Attack was uniform on all specimens. The base metal in all pins retained a dark-blue protective film even after the defilming procedure. The film on the weld metal in all pins was yellow and apparently protective.

(*k*) The weight loss of pins involving type 321 stainless steel was almost twice that of the other welded pins, the major part of the attack having been on the base metal. It is significant that the type 321 stainless steel plate stock from the original weldment was magnetic and that a photomicrograph of this material revealed a large amount of ferrite in the austenitic matrix. The superior corrosion resistance of the type 347 stainless steel welds relative to type 321 stainless steel base metal was even more apparent at higher temperatures (see notes on groups L and M below). On other pins the welds were more severely attacked than the base metal.

(*l*) The pins involving type 321 stainless steel lost nearly twice as much weight as other welded pins, and, as observed for group K, the welds were in better condition than the base metal. In other pins, corrosion in the welds was more severe than in base metal.

(*m*) Under these conditions the pins involving type 304 stainless steel were most severely attacked. In all cases the greatest weight loss was in the weld metal.

(*n*) Attack was more or less uniform, with the weld metal more severely corroded in all cases.

300 g of uranium per liter at 250°C and in solutions containing 40 g of uranium per liter and 25 mole % excess sulfuric acid at 250°C. Under the latter conditions the difference increased rapidly with time, being greater by a factor of about seven after 1036 hr than at 90 hours.

All pins received had been electrolytically defilmed by the normal procedure in inhibited 5% H_2SO_4, and they were examined macroscopically without metallographic preparation. A number of specimens have been submitted for metallographic examination and will be reported at a later date. Preliminary microscopic examination, however, has indicated that, in general, the difference in the behavior of various combinations under the same or different test conditions is not attributable to abnormal effects within the structure of either the base metals or the welds.

All austenitic stainless steel pins were bent through 180 deg at the weld and only one failure was observed. This was due to a void which existed in the original weld, not to selective attack in the corrosion test.

SELECTIVE OXIDATION OF AUSTENITIC STAINLESS STEELS

W. O. Harms T. W. Fulton
E. C. Miller

It was found recently that pretreatment in moist hydrogen at 1000 to 1150°F enhanced considerably the corrosion resistance of 18-8 austenitic stainless steel in certain loop environments. Consideration of the experiments and of the literature indicated that selective oxidation by the limited moisture content had produced a very thin, tenacious film of highly protective oxide, which served as a barrier to diffusion and further oxidation of the specimens when exposed to the loop environments. Additional work is in progress to determine the optimum conditions of time, temperature, and moisture concentration to achieve protection against corrosion, as well as to determine whether the film has any value at higher solution velocities.

Initial Pretreatment and Results of Corrosion Tests. Four pin-type specimens of type 347 stainless steel machined from special heats of varying columbium-to-tantalum ratios were subjected to a sensitizing heat treatment (24 hr at 1000°F) in a hydrogen atmosphere. The original purpose of this treatment was to test the effectiveness of the stabilizing elements with regard to corrosion resistance in uranyl sulfate solutions in the dynamic loops. It was noted that the pins were covered with a thin, light-blue film as the result of the treatment.

On subsequent exposure to loop environments, these pins showed rather extraordinary corrosion resistance as compared with other type 18-8 stainless steel specimens.

In Table 16 the defilmed weight changes of these pretreated specimens (runs I-4 and H-14) are compared with the average weight loss of other type 18-8 stainless steel pins in the same run. Even after exposure for 499 hr, the electrolytically defilmed pins from run I-4 retained, to a small extent, a faint blue color. The defilmed pins from run H-14 showed evidence of corrosion attack, but they were in better condition than other wrought stainless steel pins from the same run.

These test results prompted an investigation of the pretreatment conditions. It was noted that unless dehydrating agents in the gas-purification train are regularly reactivated, stainless steel specimens heated in a hydrogen atmosphere in the approximate temperature range of 1500 to 1600°F and lower exhibit thin oxide films when removed from the furnace. Experience

TABLE 16. COMPARISON OF DYNAMIC CORROSION TESTS ON PRETREATED TYPE 347 STAINLESS STEEL SPECIMENS AND UNTREATED TYPE 18-8 STAINLESS STEEL SPECIMENS

RUN NO.	PIN NO.	URANIUM CONCENTRATION OF SOLUTION (g/l)	ADDITIONS	TIME (hr)	VELOCITY (fps)	WEIGHT CHANGE (mg)	AVERAGE WEIGHT CHANGE OF TYPE 18-8 STAINLESS STEEL PINS IN SAME RUN (mg)
I-4	2125 2127	40	200 psi O_2 0.1 *M* $CuSO_4$ 0.005 *M* H_2SO_4	499	14	-0.1 +1.2	-24.5 -24.5
H-14	2029 2031	40	200 psi O_2	113	13	-10.5 -10.7	-20.5 -20.5
L-15	2532	5	200 psi O_2 0.005 *M* H_2SO_4	684	22	-1.1	-3.6

had shown that the "critical dew point" of hydrogen gas, that is, the dew point above which a visible film will form, for the 1500 to 1600°F furnace temperature range is approximately -60°F, which corresponds to a moisture content of 0.0055 vol %. The dew point of the gas in the original pretreatments, however, was not known, but it can safely be assumed to have been that required for formation of the protective film observed.

In the meantime, a set of pins had been prepared for evaluation of metallurgical factors in corrosion. Among the factors being studied was the effect of sensitization of type 304 stainless steel on corrosion resistance. Two as-machined pins were heated to 1100°F in helium (moisture content unknown) for 24 hr, furnace cooled, and subjected to a solution containing 5 g of uranium per liter (see run L-15, Table 16). The results were again encouraging, not so much, perhaps, from the standpoint of weight loss as compared with other pins in the run as from the general appearance of the specimens after the run. The corroded and defilmed pins still exhibited a faint blue color.

EXAMINATION OF HRE CORROSION SPECIMENS

A. R. Olsen

During this period, a set of corrosion samples was removed from the corrosion elbow of the HRE. With the cooperation of the Solid State Division, these samples were removed from the holder, weighed, cathodically defilmed, and reweighed, remotely. Although the residual activity of this set of samples was only 20 r at contact by the time the Solid State Division facilities were available, they were handled on the basis of the initial 500+ r; so it appears that the higher activity levels can be handled, if necessary.

Most of the residual activity was removed with the scale during cathodic treatment. The corrosion results are given in the chapter on "Status of the HRE." The five titanium samples in this group will be tested in the notch bend apparatus when sufficient data from unexposed standards are available for comparison.

FRACTURE OF TITANIUM

A. R. Olsen

The apparatus necessary for conducting notched slow-bend tests was designed and built, and preliminary tests were scheduled to start late in July.

Equipment failure has caused a delayed in the program to determine the absorption of hydrogen from chemical (corrosion) reactions. Glassware necessary for the revised design has been received, and these tests should be started by August 1.

PROPERTIES OF TITANIUM

W. J. Fretague

Commercial Titanium. Impact tests have been performed on as-swaged and on as-swaged and cathodically treated commercial titanium. Details of specimen preparation were described previously.[1] The cathodic treatment given to four of the as-swaged and machined specimens consisted of a 168-hr treatment in approximately 1 *M* H_2SO_4 at a current density of 0.03 amp/in.^{2} and ambient temperature. The data obtained are plotted graphically in Fig. 52. Four commercial titanium specimens were vacuum annealed at 600°C following machining and prior to testing. The impact data obtained are presented graphically in Fig. 53. A more complete history of these specimens was given in ORNL-1554.[1]

Corrosion impact specimens of as-swaged and machined commerical titanium, of vacuum annealed (600°C for 1 hr and furnace cooled, following machining) titanium,[1] and of vacuum-annealed and cold-worked titanium[1] have been submitted to the Dynamic Corrosion Group for exposure to uranyl sulfate solution prior to impact testing.

Fatigue tests have been performed on hot-rolled and annealed titanium 75A sheet fatigue specimens. Details of thermal and mechanical treatments were presented in ORNL-1554.[1] Test histories of the various specimens prior to testing and the respective stress levels and cycles to failure are presented in Table 17.

Mention was made in a previous report[2] of an experiment being conducted to determine the effect of the oxide films that are present on the surface of commercial titanium on the rate of absorption of hydrogen by titanium. Metallographic examination of a specimen of 1/4-in.-thick titanium 75A plate heated at 250°C in a purified hydrogen atmosphere for approximately one month revealed considerably more titanium hydride phase in the microstructure than in a similar specimen of as-received plate. It is planned to determine the hydrogen content of the two specimens by vacuum fusion analysis, as a check.

A sample of commercial titanium (Ti-75A, heat X922) obtained from the Radiation Chemistry Group was analyzed for hydrogen by vacuum fusion. This was part of a thermocouple well assembled in a titanium bomb and irradiated in hole C-44 of the LITR. The bomb contained enriched (12.96%) uranium sulfate solution (292.5 mg of uranium per milligram of solution). The pressures of hydrogen and oxygen (present in a 2:1 ratio) varied from 1000 to 2500 psi total at the temperatures of the test (190 to 260°C). The total pressure at the end of the exposure is not known. The uranyl sulfate solution contained 0.019 *M* Cu^{++}. The titanium was etched for 2 to 4 min in a 3% HCl–3% HF solution prior to exposure in the uranyl sulfate solution. Two small samples (0.2663 and 1.4095 g) were cut from the irradiated thermocouple well in the Solid

[1] W. J. Fretague, *HRP Quar. Prog. Rep. Mar. 31, 1953*, ORNL-1554, p. 83-87.

[2] *Ibid*, p. 86.

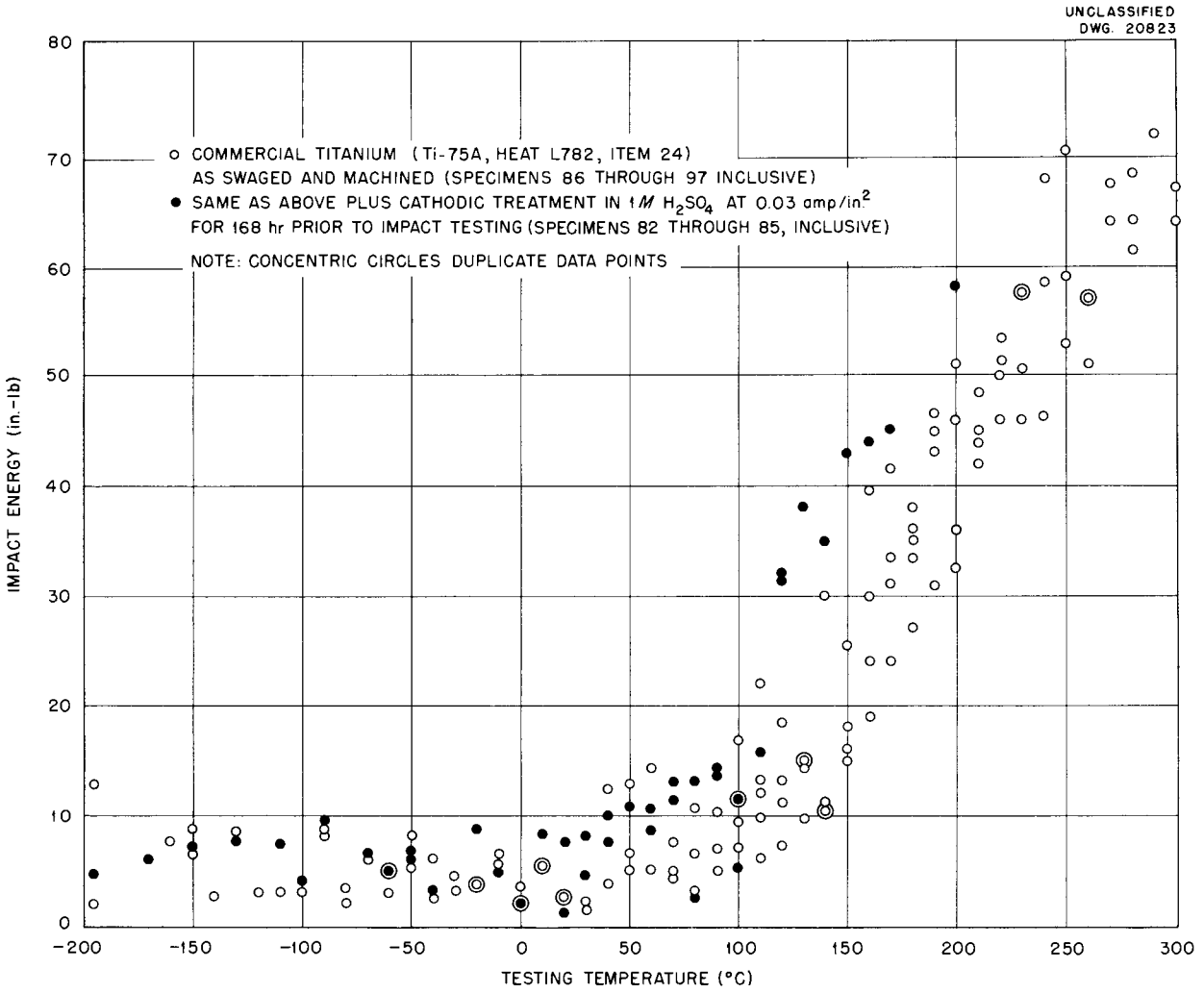

Fig. 52. Comparison of Impact vs. Temperature Behavior of Commercial Purity Titanium Before and After Cathodic Treatment.

State Division facilities. Vacuum-fusion analyses obtained from the Analytical Chemistry Division are given in Table 18. Metallographic samples of irradiated and as-received titanium (Ti-75A, heat X922) are being examined for evidences of a hydride phase.

Bureau of Mines Titanium. Impact tests have been performed at room temperature and at liquid nitrogen temperature on arc-melted, swaged, vacuum-annealed, and machined specimens of Bureau of Mines titanium (lot 1056, R-83A). Table 19 presents the data obtained. It appears that for the temperature range investigated there is no transition from ductile to brittle fracture in this higher purity titanium. Details of thermal and mechanical history of these specimens were presented in ORNL-1554.[2]

ZIRCONIUM-ALUMINUM SYSTEM

W. J. Fretague E. C. Miller

Three alloys of zirconium-aluminum were prepared by arc-melting grade I

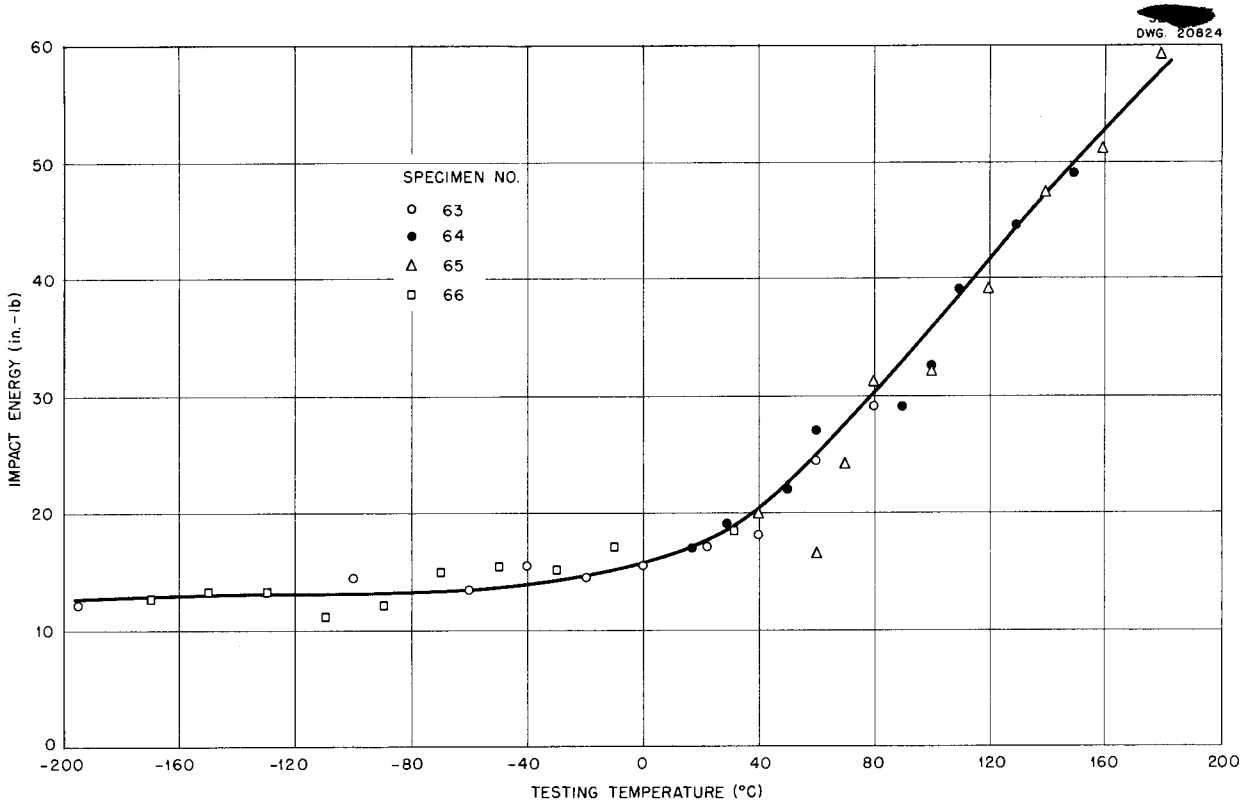

Fig. 53. Impact vs. Temperature Behavior of Vacuum-Annealed Commercial Purity Titanium.

crystal-bar zirconium with 99.99+ aluminum (R84A) to determine crystal structure and mechanical properties of zirconium-aluminum compound (22.82 wt % Al) reported to be formed in the solid state by the peritectoid reaction:[3]

$Zr_4Al_3 + Zr_2Al_3 = ZrAl$, at 1250 ± 50°C .

Table 20 gives the nominal compositions of the alloys prepared.

Available information[4] on the gamma phase (50 at. % Ti–50 at. % Al) in the titanium-aluminum system indicates an ordered face-centered-tetragonal crystal structure with an axial ratio (c/a) very close to unity. The frequent similarity of behavior of titanium and zirconium when alloyed with other metals prompted an investigationinto the crystal structure and mechanical properties of zirconium-aluminum alloys at or near the stoichiometric zirconium-aluminum composition.

All the alloys listed in Table 20 cracked on cooling from the molten condition. Attempts will be made to remelt these alloys under conditions designed to permit a slower cooling rate. If successful, the alloys will be cold-worked slightly, homogenized at 1250°C to permit the peritectoid reaction, and then sampled for metallographic and x-ray diffraction examination prior to further fabrication.

(3) *Phase Diagrams of Zirconium Base Binary Alloys; A Study of the Systems of Zirconium with Tin, Molybdenum, Copper, Wolfram, Chromium, Silicon, Aluminum, and Magnesium*, Armour Research Foundation, COO-89, p. 131-143 (Apr. 14, 1952).

(4) E. S. Bumps, H. D. Kessler, and M. Hansen, *Trans. Am. Inst. Mining Met. Engrs.* **194**, 609-614 (1952).

TABLE 17. FATIGUE PROPERTIES OF HOT-ROLLED AND ANNEALED TITANIUM-75A SHEET EXPOSED TO VARIOUS CORROSIVE ENVIRONMENTS PRIOR TO TESTING

SPECIMEN NO.	SPECIMEN HISTORY PRIOR TO TESTING	STRESS (psi)	NUMBER OF STRESS CYCLES BEFORE FAILURE
1	Hot rolled at 850°C from 1/4-in.-thick plate to 0.032-in.	40,500*	4.1×10^7
2	sheet; surface ground; vacuum annealed for 1 hr at 600°C	45,000*	1.66×10^5
3	and furnace cooled; machined into sheet fatigue specimens	50,000*	1.64×10^5
4		50,000*	8.0×10^4**
5	Same as for specimens 1 through 4 plus cathodic treatment	45,000	1.33×10^7
6	in 1 *M* H_2SO_4 for 168 hr at 0.03 amp/in.^{2}; both sides of specimen blank exposed to H_2SO_4 solution; machined into sheet fatigue specimens	45,870	2.23×10^5
7	Same as for specimens 5 and 6 except that only one side	42,240	2.64×10^5
8	of specimen blank was exposed to H_2SO_4 solution; machined into sheet fatigue specimens	43,890	1.36×10^5
9	Same as for specimens 1 through 4 plus static exposure to	44,200	1.63×10^5
10	uranyl sulfate solution containing 300 g of uranium per liter; initial gas pressure in bomb at room temperature was 100 psi O_2 and 200 psi H_2; after 72 hr at 250°C, total pressure was 120 psi; repressurized and run 128 hr at 250°C; final total pressure 50 psi; specimen blanks exposed on both sides to UO_2SO_4; machined into sheet fatigue specimens; reference test No. 2361	45,000	8.6×10^4
11	Same as for specimens 9 and 10 except that only one side	44,480	6.5×10^4
12	of specimen blank was exposed to UO_2SO_4 solution; machined into sheet fatigue specimens	44,550	7.9×10^4

*Data previously reported in Table 18 of *HRP Quar. Prog. Rep. Mar. 31, 1953*, ORNL-1554. Measurements of thicknesses of specimens revealed that variations in individual specimens (from 0.027 in. specified) required slight adjustments in the stress levels previously reported.

**This specimen was subjected to a preload prior to beginning of test.

TABLE 18. O_2, N_2, AND H_2 ANALYSIS OF COMMERCIAL TITANIUM (Ti-75A, Heat X922)

SAMPLE	HISTORY	WEIGHT (g)	ANALYSIS (wt %)		
			O_2	N_2	H_2
N1255	Irradiated in uranyl sulfate solution; reference test Ti-5, V-13	0.2663	0.11	0.004	0.027
N1258	As received	0.586	0.021	0.008	0.020

TABLE 19. IMPACT ENERGY VS. TESTING TEMPERATURE FOR ARC-MELTED, SWAGED, AND VACUUM-ANNEALED BUREAU OF MINES TITANIUM (Lot 1056, R-83A)

SPECIMEN NO.	NOTCH NO.	SCALE USED (in.-lb)	TEMPERATURE (°C)	IMPACT ENERGY (in.-lb)	REMARKS
B-1-1	1	0 to 200	33	96	Did not break
	2	0 to 200	-195.6	127	
B-1-2	1	0 to 200	32	94	Did not break
	2	0 to 200	-195.6	72	Did not break
	3	0 to 200	-195.6	120	Did not break
B-1-3	1	0 to 100	22	85	Did not break
	2	0 to 100	-195.6	98	Did not break
	3	0 to 200	32	95	Did not break
	4	0 to 200	-195.6	78	Did not break
B-2-4	1	0 to 200	26	127	Did not break completely
	2	0 to 200	-195.6	144	Did not break completely
B-3-4	1	0 to 200	26	113	Did not break completely
	2	0 to 200	-195.6	146	Did not break completely

TABLE 20. NOMINAL COMPOSITION OF ARC-MELTED ZIRCONIUM-ALUMINUM ALLOYS

MELT NO.	ALLOY NO.	ALUMINUM (wt %)
1	1ZA-22.82	22.82
2	1ZA-21.32	21.32
3	1ZA-24.32	24.32

ZIRCONIUM-INDIUM SYSTEM

W. J. Fretague J. O. Betterton

An experiment to determine the properties of a zirconium-indium alloy was outlined in ORNL-1554.[2] The final composition (after repeated arc melting) of the alloy was calculated to be 27.01 at. % indium (calculated from the weight loss in melting, which was assumed to be entirely a loss of indium). Metallographic examination of the as-melted alloy revealed a single-phase structure. An x-ray diffraction pattern taken on the as-melted metallographic sample with the Norelco x-ray spectrometer revealed a face-centered-cubic lattice and a lattice parameter of 4.445 Å. Since attempts to cold-swage the alloy were unsuccessful, it was remelted and placed in a high-purity iron capsule. The assembly was evacuated and welded, and then hot-swaged at 700°C. Upon removal of the high-purity iron capsule, it was observed that the alloy had crumbled into a number of small pieces and had the general appearance of hot-short material. It is possible that a low-melting high-indium constituent segregated at the grain boundaries of the alloy (not observed in the as-cast microstructure) to cause this behavior. Metallographic examination of samples of the hot-swaged alloy showed a structure not appreciably different from the single-phase structure observed in the as-cast sample.

A small sample of the as-cast alloy was cold-worked slightly and homogenized at 1100°C for five days. This homogenized sample still appeared to be composed of a single phase. The alloy was remelted and will be homogenized at 1100°C before attempts are made to fabricate it.

ZIRCONIUM STRUCTURAL ALLOYS

W. J. Fretague

Two melts (F879 and F909) of Zircaloy II were received from WAPD as 1/4-in. plate. The rolled plate was cut to lengths for impact specimens, several of which were transferred to the Dynamic Corrosion Group. Approximately 50 lb of 1/4-in.-dia Zircaloy II rod have been received from WAPD for similar test specimens.

EFFECT OF RADIATION ON IMPACT STRENGTH OF METALS

R. G. Berggren J. C. Wilson

The effect of radiation on the impact strength of metals became of immediate interest largely as a result of some measurements,[5] made at ANL, of the notched-bar impact strength of a few steels irradiated at Hanford. These measurements, made at room temperatures, showed a drastic reduction in impact strength for some of the steels. The importance of this effect is apparent when it is noted that structural components of nuclear reactors are subject to multiaxial stresses and are also exposed to reactor radiation. In particular, they are exposed to fast neutrons for long periods of time, with attendant, possibly large, changes in physical properties. The notched-bar impact behavior is probably the best single test available to assess the performance of a given material under such multiaxial stress conditions, before and after exposure to reactor radiation.

A program has been initiated to study the effect of radiation on the impact strength of various metals, and the study is, at present, in essentially a survey stage. Specimens of the various metals were machined into notched-bar impact specimens and heat treated, and part of each group was placed in one of several irradiation facilities. After irradiation, both the unirradiated control and the irradiated specimens were tested over a range of temperatures in a remotely operated impact testing machine.

The test specimens were subsize cylindrical Izod bars with a circumferential notch. They were 0.204 in. in diameter, and the circumferential V notch was 0.020 in. deep with an included angle of 45 deg and a root radius of 0.005 inch. The notches were at 1-in. intervals, and the over-all length of the specimen was from 6 to 12 inches. This geometry, selected to conserve reactor space and material, was originated at ANL (dwg. NR-K-1852A).

The impact testing machine, Fig. 54, is a Tinius Olsen plastics testing machine modified for remote operation, subsize specimens, and temperature control. The modifications include remote specimen positioning, vise operation, pendulum trip and return; facilities for cooling or heating the specimen in testing position in a temperature range of from 300 to -196°C; and temperature indication by means of thermocouples located on the vise near the specimen. The temperatures indicated by the vise-mounted thermocouples were compared with those indicated by a thermocouple in a dummy specimen, and the error was observed to be less than 8°C at the extreme temperatures and less than 1°C over most of the temperature range.

High-Purity Iron. The iron tested was purchased from the National Research Corporation and was of the vacuum-melted type. Analysis showed the following composition: N_2, 3.2×10^{-4}%; O_2, 2×10^{-2}%; C, 1.5×10^{-3}%. The stock was swaged to 1/4 in. in diameter, and impact specimens were

[5] W. F. Murphy, *Naval Reactor Materials Testing Division Program M-9, Group 2*, ANL-FF-100z (July 13, 1951); *Naval Reactor Materials Testing Division Program M-3 - Post Irradiation*, ANL-FF-100ac (Aug. 15, 1951); *Naval Reactor Materials Testing Division Program M-7, Group 9-B*, ANL-FF-100af (Aug. 17, 1951); G. J. Deily, *Modified Izod Impact Tests - NRD Materials Testing Division Program M-15*, ANL-FF-100an (Dec. 6, 1951).

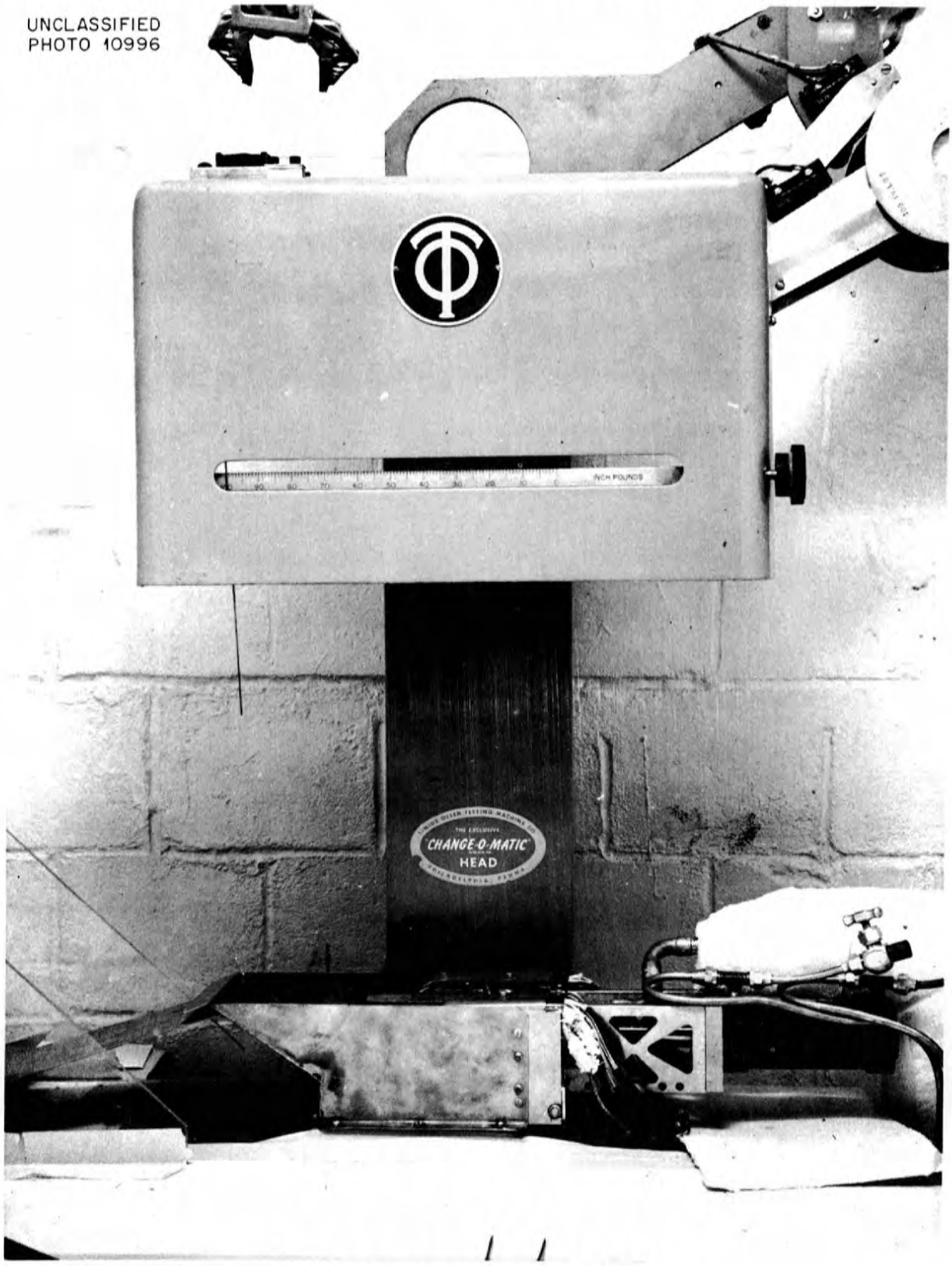

Fig. 54. Impact Testing Machine.

machined from this rod and vacuum-annealed 1/2 hr at 1570°C. Part of the stock was exposed in the HB-4 hole of the LITR to a dosage of from 0.5×10^{17} at one end of the specimens to 2.5×10^{17} nvt (fast) (greater than 0.5 Mev, measured by threshold detectors) at the other end.

The data showed considerable scatter that was attributable, in part, to large grains in some of the specimens. No difference was apparent in impact strength or transition temperature between the irradiated and the control specimens from the ten control and ten irradiated notches tested.

Carbon Steels. Three groups of carbon steel specimens were tested. The first carbon steel was an ASTM-A-70 steel irradiated at Hanford. These specimens, machined from small irradiated tensile bars, were 0.178 in. in diameter and the other dimensions were those described above. The tests were made in collaboration with ANL and are reported in more detail elsewhere.[6] The hardness of the steel increased from Rockwell A-30 for the control specimens to Rockwell A-42 for the irradiated specimens. The impact energy data, presented in Fig. 55, show a rise in transition temperature and a lowering of "ductile" impact

[6] D. O. Leeser, G. J. Deily, and K. F. Smith, "Effect of Irradiation on the Notched-Bar Impact Properties of Some Plain-Carbon Steels," *Radiation Damage Conference, March 23-24, 1953*, Oak Ridge National Laboratory (to be published).

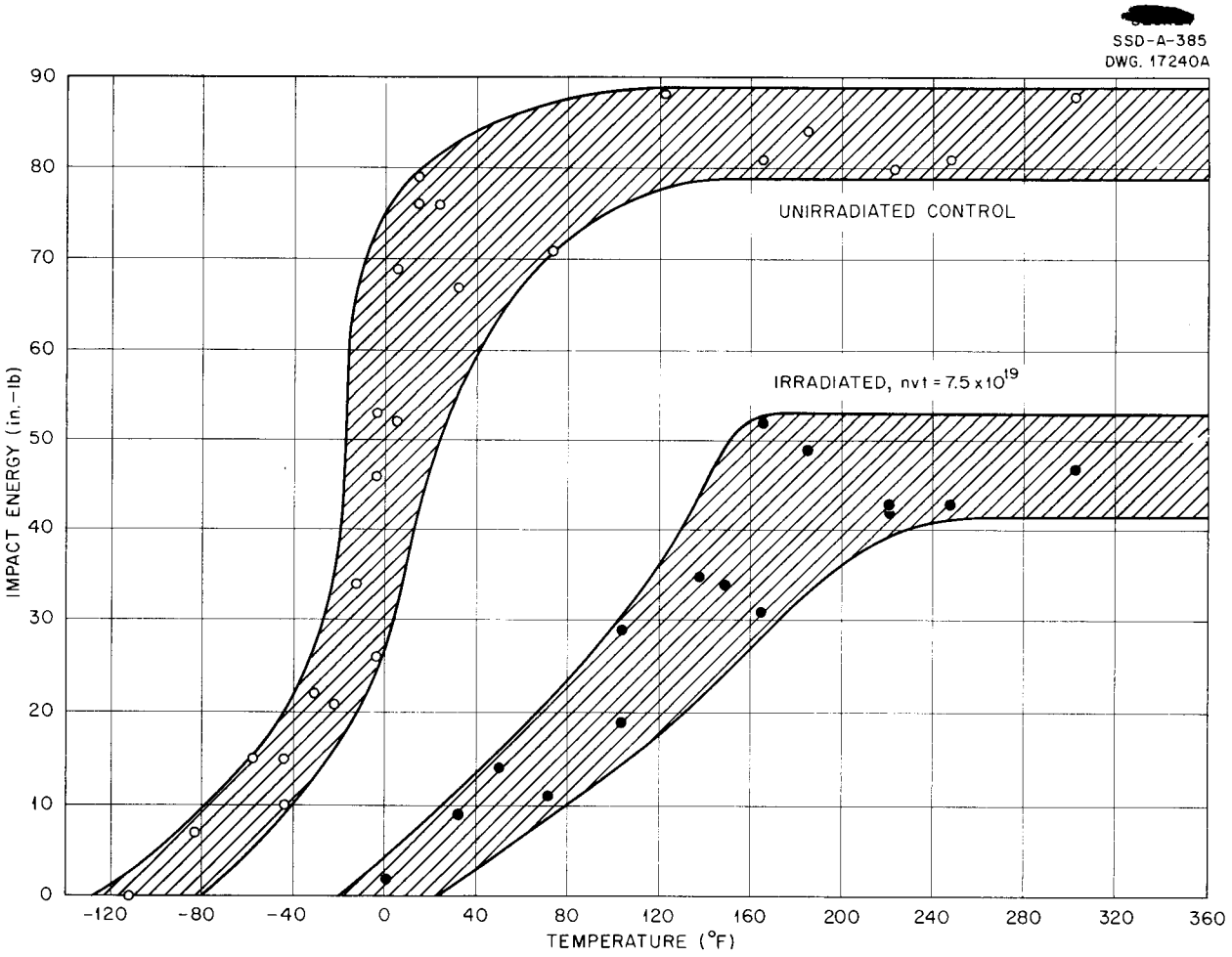

Fig. 55. Impact Energy of Irradiated ASTM A-70 Steel.

energy. The irradiation dosage was 7.5×10^{19} nvt (thermal).

Figure 56 shows results for a low-carbon steel (0.17% C, 0.20% S, 0.12% P, 0.70% Mn, grain size ASTM-8, Diamond Pyramid Hardness 136) annealed in helium and irradiated in a donut hole (1867) of the ORNL graphite reactor to a dosage of 8.3×10^{17} nvt (fast) and 3.0×10^{18} nvt (fast) (> 0.1 Mev). This steel was thought to be SAE 1040 and was irradiated before results of chemical analysis were available.

Figure 57 shows results for a steel of similar analysis (grain size ASTM-6, DPH 119 to 125) that was annealed 1/2 hr at 1630°F, in vacuum, and irradiated in a vertical beryllium stringer of the LITR to a calculated dosage of 2×10^{18} nvt (fast), as measured by cadmium ratio.

Stainless Steels. A type 304L stainless steel, annealed for 1 hr and air quenched and irradiated in the vertical beryllium stringer of the LITR to a dosage of 1.7×10^{19} nvt (fast), as measured by cadmium ratio, gave no fractures upon testing of either the control or the irradiated specimens at temperatures down to -196°C.

Type 304 stainless steel, annealed, and type 347 stainless steel, both in the annealed and as-received condition, irradiated in hole HB-4 of the LITR to a dosage of from 1.5×10^{17} to 7.5×10^{17} nvt (fast) (> 0.5 Mev),

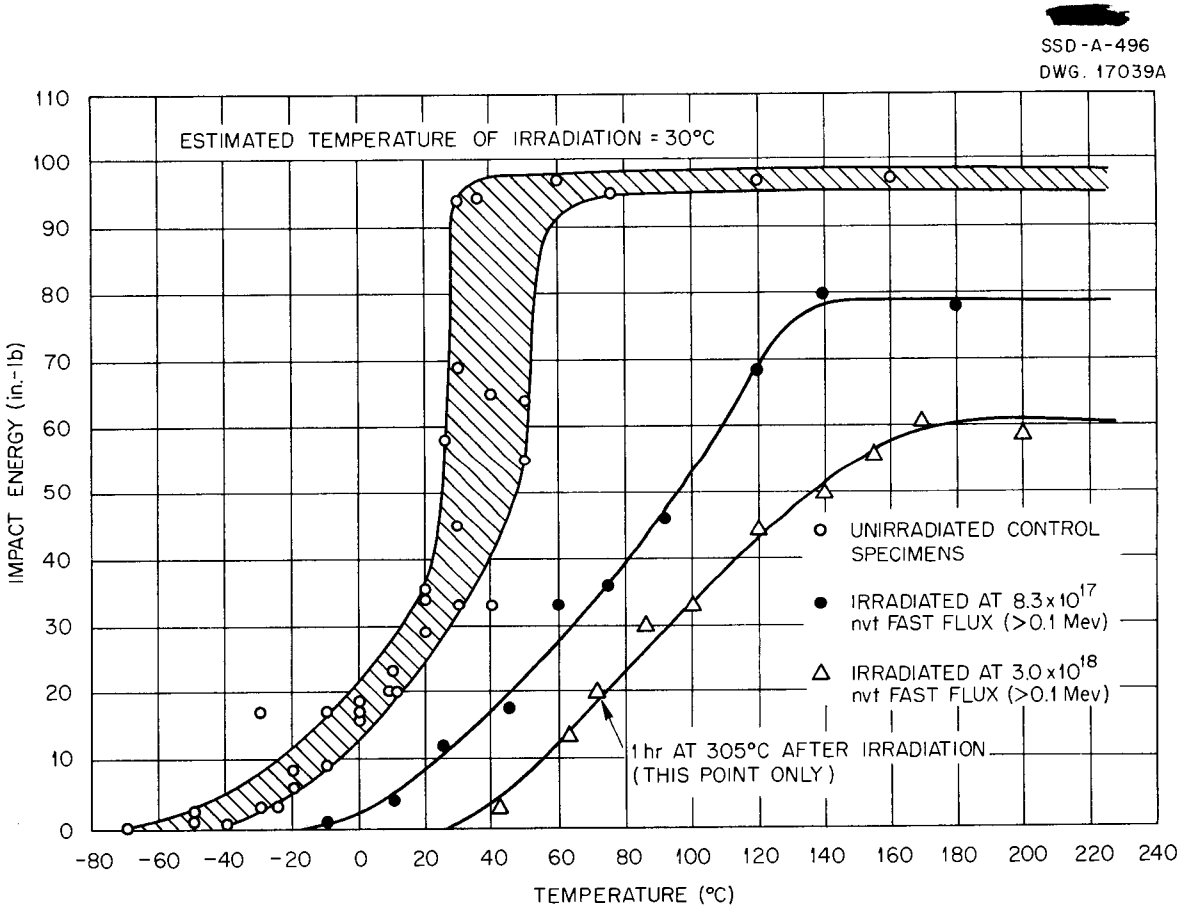

Fig. 56. Impact Energy of Low-Carbon Steel Annealed in Helium.

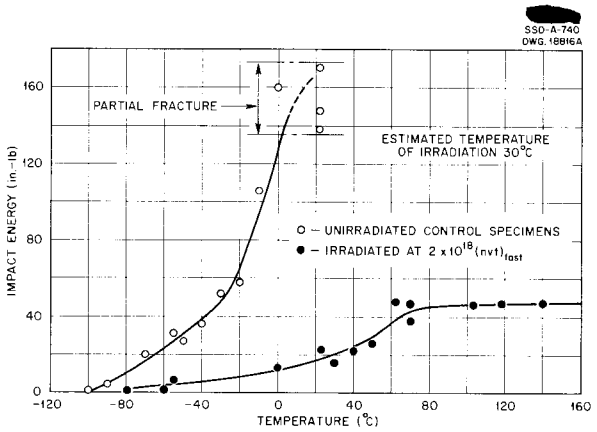

Fig. 57. Impact Energy of Low-Carbon Steel Annealed in Vacuum.

gave no fractures upon testing of either the control or the irradiated specimens at temperatures down to -196°C.

In the specimens of stainless steel tested, it is apparent that the geometry was such that insufficient triaxiality of stresses was induced in the notch to cause fracture and that the energy of the hammer was dissipated in bending the specimen. Nevertheless, the stainless steels tested did not experience a marked reduction in impact strength at these radiation dosages, insofar as this survey indicates.

Titanium. Both iodide and commercial purity titanium were tested. The iodide titanium was arc-melted, swaged, vacuum annealed at 500°C for 1 hr, and furnace cooled; specimens were then machined from this stock. Hydrogen analyses of the two batches tested were 0.014 and 0.008%. Part of each of these batches was irradiated in hole HB-4 of the LITR to a dosage of from 1.5×10^{17} to 7.5×10^{17} nvt (fast) (> 0.5 Mev). There was considerable scatter in the impact test data for the control specimens, but the impact values for the irradiated specimens were well within this scatter band. There was no observable radiation effect at this dosage.

Commercial purity titanium, purchased from the Titanium Metals Corporation and designated as Ti-75A, was prepared by swaging and vacuum annealing at 500°C for 1 hr and furnace cooling. Hydrogen analyses were 0.008 to 0.012%. The specimens were irradiated in the facility in which the iodide titanium was irradiated and were given the same dosage. Impact results for the irradiated specimens fell within the scatter band of the control specimens. The impact energies recorded for both irradiated and control specimens were considerably lower than those obtained for the iodide titanium specimens.

Discussion. The tests on the carbon steels were made without difficulty and the results are considered reliable.

There is some question as to the interpretation of the results of the tests on titanium in that the hydrogen concentrations were close to the hydrogen solubilities at the testing temperature, and titanium hydrides may have been precipitated or dissolved during the changes of temperature imposed by the testing procedure.

The geometry of the specimens was such that definitive tests on the stainless steels could not be made. It will be necessary to use other geometries to test these steels.

The tests of the high-purity iron should be considered as preliminary.

Conclusions. Definite and marked radiation effect on the notched-bar impact strength was observed in the carbon steels tested. No loss in impact strength was observed in the high-purity iron, austenitic stainless steels, or titanium at the dosages used in this survey.

AQUEOUS SOLUTION AND RADIATION CHEMISTRY

OXIDATION OF SULFUR DIOXIDE IN URANYL SULFATE SOLUTION

D. W. Sherwood C. H. Secoy

Present plans for intermittent addition of acid to the in-pile loop involve the addition of a mixture of a measured amount of sulfur dioxide and oxygen to react in the presence of the ions of the solution to form sulfuric acid. A series of laboratory experiments has been made to test the feasibility of this procedure with reference to the speed of oxidation and the possible reducing action of the sulfur dioxide with regard to the uranyl ion in solution. The data obtained indicate that there is no damage to the solution and that the desired oxidation occurs in less than 1 hr at 200°C.

The solution used contained 40 g of uranium per liter (as uranyl sulfate) and was made approximately 3.3×10^{-3} *M* in nickelous ion and 1.5×10^{-2} *M* in cupric ion to simulate the probable composition of the operating solution after exposure to loop metal. The nickel and copper were added as sulfates.

In each determination, approximately 0.9 ml of the solution was used; the operations were carried out in quartz tubing. The solution was first degassed, and then the desired quantity of sulfur dioxide was added by allowing a pressure of approximately 6.5 mm of the gas to flow into an evacuated volume that was about nine times the volume of the refrozen solution it contained. The solution was then brought to room temperature to absorb the gas, which was calculated to be 71 cm^3 STP per liter of solution – the desired amount for loop operation. After very slow refreezing of the sulfur dioxide-containing solution, nearly an atmosphere of oxygen (650 to 700 mm) was added and the quartz tube was sealed off. The remaining oxygen was about ten times the amount calculated as necessary for reaction with the sulfur dioxide; however, the oxygen pressure was less than the pressure of 70 psi indicated for the loop. (No appreciable hydrogen pressure is indicated for loop operation.) In one run, five times the calculated amount of sulfur dioxide was used, and in another case, ten times. Such additions were made by repeating the addition, by absorption, of the calculated amount the appropriate number of times. When ten times the calculated amount of sulfur dioxide was added, the last four additions resulted in formation of yellow precipitate that was probably uranyl sulfite or a uranyl double salt. This precipitate disappeared promptly upon heating.

The sealed tubes were heated in a small furnace (resistance-wire-wound aluminum block) for 1 hr at 200°C, cooled, and opened for analysis. The results of the analyses are given in Table 21. The small amounts of the samples made the analyses somewhat difficult; however, the following points may be noted:

1. In most cases a small increase in uranyl ion concentration was found. This may have been due to incomplete condensation of water vapor before the sample was evacuated. Each sample was pumped several times after it froze, and such water loss may have occurred. In *each* case the sulfate ion increase in concentration was greater than the uranyl ion concentration increase, except for samples 7-2 and 8-1, which were *not* heated; these two samples failed to show the greater gain for sulfate ion than for uranyl ion. However, the analyses for sulfate ion indicate, without exception, an increase. Inaccuracies of gas measurement and analytical difficulties apparently preclude quantitative

TABLE 21. THERMAL OXIDATION OF SULFUR DIOXIDE BY OXYGEN IN URANYL SULFATE SOLUTIONS

SAMPLE NO.	ESTIMATED SO_2 ADDED (moles/liter)	TEST CONDITIONS	ION CONCENTRATIONS (moles/liter)					ΔSO_4^{--} (moles/liter)	ΔpH
			Found			Corrected for H_2O Loss			
			UO_2^{++}	SO_4^{--}	SO_3^{--}	SO_4^{--}	SO_3^{--}		
3-24-1	0	Original solution	0.189	0.190					
3-24-2	0.003	Heated for 1 hr at 200°C	0.227	0.239		0.199		0.009	-0.41
6-1	0.003	Heated for 1 hr at 200°C	0.249	0.254		0.193		0.003	-0.29
7-1	0.003	Heated for 1 hr at 200°C	0.194	0.204		0.199		0.009	-0.42
7-2	0.003	Not heated	0.202	0.200	0.00225	0.187	0.00211	-0.003	-0.16
8-1	0.003	Not heated	0.194	0.192	0.00263	0.187	0.00256	-0.003	-0.26
11-1	0.016	Heated for 1 hr at 200°C	0.183	0.201	None*	0.208		0.018	-0.77
10-1	0.032	Heated for 1 hr at 200°C	0.192	0.244	None*	0.240		0.050	-1.12

*Less than lower limit of test (<0.00038 *M*).

correlation of the increases in ion concentration with the extremely small amount of sulfur dioxide added. However, sample 10-1, which was given about ten times the usual sulfur dioxide charge, shows a correspondingly large sulfate increase.

2. The analyses for sulfite show about the calculated amount for the samples that were not heated (samples 7-2 and 8-1), while samples which were heated showed no detectable sulfite, even though large amounts of sulfur dioxide were added.

3. The pH of each solution showed a decrease from that of the original solution, and the change was less for those solutions not heated to oxidize the sulfur dioxide.

Hence, it is concluded from these experiments that the proposed method for oxidation of sulfur dioxide in uranyl solution to offset the acidity decrease caused by corrosion is satisfactory with respect to the chemistry involved.

EXPLORATORY STUDIES ON AQUEOUS-SOLUTION THORIUM BLANKET SYSTEMS

P. A. Agron
J. S. Gill
E. V. Jones
M. H. Lietzke
W. L. Marshall
C. H. Secoy
R. W. Stoughton
W. C. Waggener

No known thorium compound other than thorium nitrate meets the requirements of adequate solubility, radiation stability, and low neutron capture losses for a simple water-solution breeder blanket. However, the possibility exists that the proper combination of complexing anions or cations might be produced in a system in which thorium is reasonably soluble. Therefore exploratory studies have been made with anion combinations of

phosphate, sulfate, and/or fluoride and other combinations such as thorium sulfate-lithium sulfate, thorium sulfate-magnesium sulfate, thorium selenate-lithium selenate, and thorium selenate-magnesium selenate.

It is generally known that thorium phosphate and thorium fluoride are quite insoluble and that the sulfate is only moderately soluble, with a negative temperature coefficient above about 40°C. It is also known that all three of these anions in dilute concentration form strong complex cations with Th^{4+} in aqueous solutions. It seemed possible that by the use of a proper mixture of two (or all three) of these anions an aqueous thorium system might be devised in which the thorium was reasonably soluble.

Concentrated H_3PO_4 apparently dissolves thorium phosphate to the extent of about one thorium group to each five phosphate groups at elevated temperatures, with apparent solubilities of up to 1100 g of thorium per liter of solution. On cooling to room temperature, such a solution or mixture appears stable, although the definite Tyndall effect observed in the cases investigated indicated large, molecular aggregates. The viscosity appears high at elevated temperatures and extremely high at room temperature – too high for stirring. Up to about 5 or 10 wt % of water can be added at the higher thorium concentrations, with some decrease in viscosity. Some concentrated hydrofluoric acid can be added to the concentrated H_3PO_4 mixture, but precipitation appears to occur before any significant improvement in properties becomes evident; dissolving ThF_4 in H_3PO_4 appears to give a similarly viscous mixture at a phosphate-to-thorium ratio of 5. Of course, the viscosity can be lowered by dissolving less thorium in H_3PO_4, but then the phosphate-to-thorium ratio is higher. Solutions in H_2PO_3F seem to act similarly to those in H_3PO_4, with no improvement in solubility or viscosity. Adding H_2SO_4 to H_3PO_4-$Th_3(PO_4)_4$ mixtures lowered the solubility under otherwise similar conditions and appeared to offer no advantages. Thorium oxide was found to dissolve in concentrated H_3PO_4 to the extent of about one thorium group to about five phosphate groups.

Although apparently stable phosphate solutions containing up to 1100 g of thorium per liter have been prepared, the high viscosity and extreme corrosiveness of these solutions leave considerable doubt as to their applicability.

Preliminary results obtained upon dissolving $Th(OH)_4$ in a HF-H_2SO_4 mixture containing 1 HF molecule and 1 1/2 H_2SO_4 molecules per molecule of $Th(OH)_4$ indicated that a solubility of about 200 g of thorium per liter was possible, although there was evidence of the presence of a colloid. Later work indicated a much lower solubility and a negative temperature coefficient. Immediate dissolution occurred, followed by slow precipitation. Changing the F^--to-SO_4^{--}-to-Th(IV) ratios while maintaining stoichiometric neutrality showed no improvement in solubility. The pH of all the supernatant solutions indicated that some hydrolysis occurred during the precipitation. A solution made up to contain 50 g of thorium (as the nitrate) per liter plus 1 mole of HF, 1 mole of HNO_3, and 1 1/2 moles of H_2SO_4 per mole of thorium showed some precipitation upon standing for a few days; no hydrolysis would be expected to occur in this solution.

It is concluded that media containing combinations of the anions, fluoride, sulfate, and phosphate, do not show much promise for thorium blanket systems. It is possible that some mixed fluoride-containing medium would be suitable, since these have

not been exhaustively studied in adequate equipment; however, the evidence obtained to date makes such a possibility appear unlikely.

A large number of exploratory tests with various combinations of thorium sulfate or thorium selenate with lithium and magnesium salts of the same anions have been made. It is concluded that the addition of lithium or magnesium salt increases the solubility of the thorium salt at 25°C, but not to a very great extent. The maximum thorium content obtained has been of the order of 100 to 150 g of thorium per liter.

In all cases, thorium selenate is more soluble than thorium sulfate but, again, by only a small amount that is insufficient to compensate for the higher cross section of selenium.

At temperatures above 100°C, the solubility of the thorium salt decreases rapidly. The formation of the precipitate is slow, and its dissolution at room temperature is extremely slow. There is a strong possibility that the apparent solution at 25°C is actually metastable and that, if given sufficient time, much of the thorium would precipitate.

From these observations, systems of this type appear unsatisfactory for a breeder blanket, and it seems unlikely that any aqueous-solution thorium blanket system can be found other than thorium nitrate.

HOMOGENEOUS REACTOR SOLUTIONS UNDER IRRADIATION

B. O. Heston
W. E. Hill
Q. V. Larson
C. H. Secoy
F. H. Sweeton
W. C. Yee

The experimental program to determine the stability of irradiated uranyl sulfate and uranyl fluoride solutions and the corrosion of the container by these solutions has continued. Since the previous report,[1] test H10 has been completed under conditions the same as those for test H7, and test H11, in which the fission density corresponds to approximately 2.3 kw/liter, has been started.

Corrosion. The corrosion results of test H10 are plotted in Fig. 58 and can be compared with those of test H7; these two tests were supposedly identical. It can be seen that the two curves obtained are of the same general type. The slopes of the curves are small at first but change to a much greater slope after a week or two. The two tests differed by about one week in the time elapsed before the changes in the slopes began.

The test now in process is giving a very small amount of corrosion, about 0.05 mil in 10 weeks, and the corrosion rate is constantly decreasing. The data obtained from this test during its first six and one-half weeks of operation are included in Fig. 58.

Improved experimental equipment and techniques for out-of-pile corrosion tests have been developed and are now in use to obtain data considerably better than those obtained previously. The data from the first test, which has been run about one week, are sufficiently sensitive to show the progress of corrosion over time intervals as short as 1 hour. Further discussion will be left until the test is completed.

Solution Decomposition. The analyses of the solutions removed from the bombs of tests H7, H8, and H9 have recently been completed and the results for tests H7 and H9 are shown in Table 22, along with those for tests H2 and H5. The data from test H8 are omitted because after this test was run it was found that the solution (5 g of uranium per liter) was unstable, even without radiation. In each of the first three tests shown in Table 22, most of the uranium was precipitated, but in test H9, it was found that, within the

(1) F. W. Sweeton and W. C. Yee, *HRP Quar. Prog. Rep. Mar. 31, 1953*, ORNL-1554, p. 87-89.

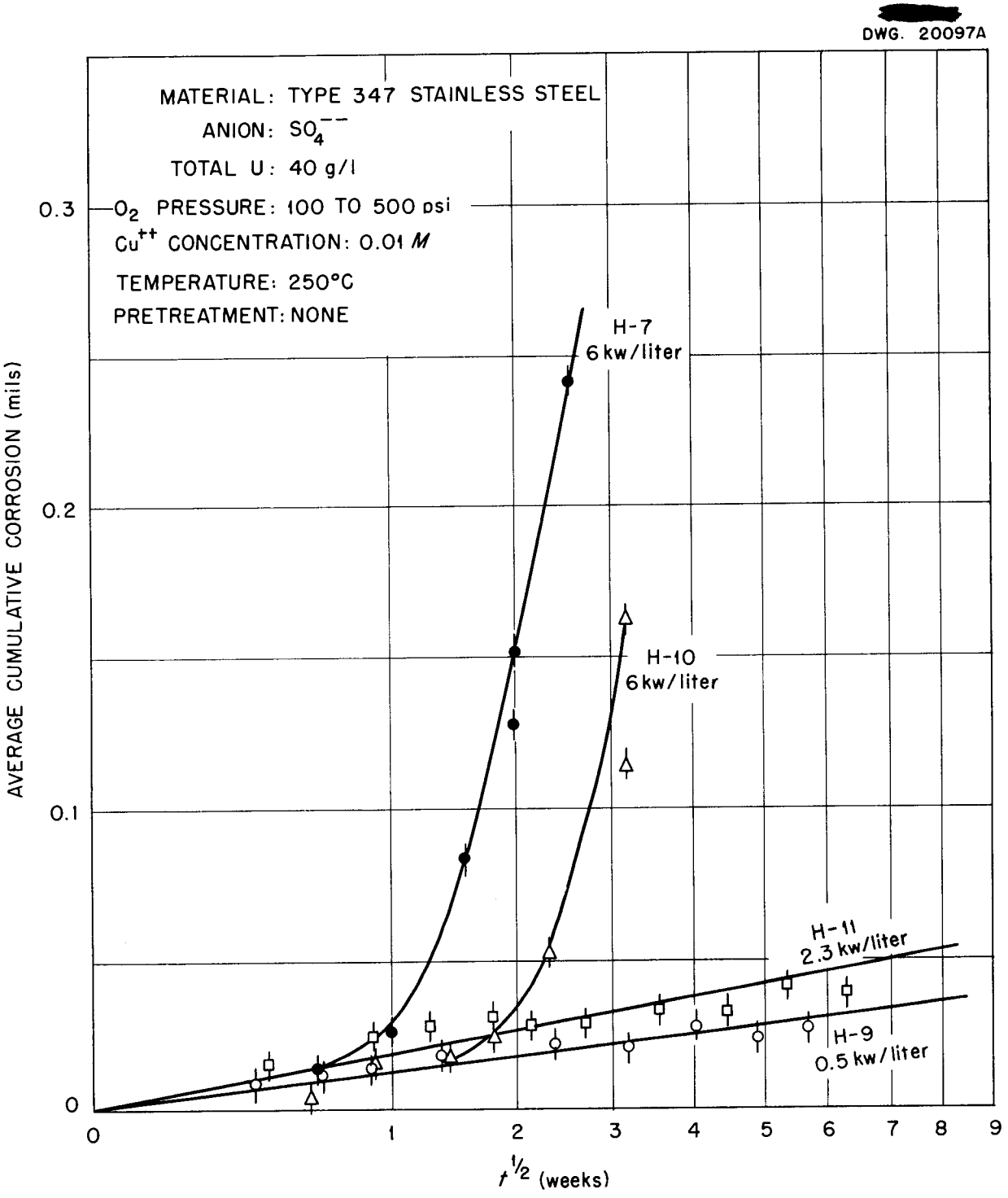

Fig. 58. Corrosion at Various Fission Densities.

TABLE 22. ANALYSES OF SOLUTIONS AFTER IRRADIATION IN TYPE 347 STAINLESS STEEL BOMBS AT 250°C

	TEST H2	TEST H5	TEST H7	TEST H9
TEST CONDITIONS				
Pretreatment	CrO_3	None	None	None
Initial concentration of uranium, g/liter	43.9	42.4	38.7	39.5
Power density, kw/liter	4.5 to 6	6	6	0.5
Oxygen partial pressure at start, psi at 250°C	900	920	120	100
Oxygen partial pressure at end, psi at 250°C	350	180	0	90
Anion	SO_4^{--}	F^-	SO_4^{--}	SO_4^{--}
Concentration of Cu^{++}, *M*	0.01	0.03	0.01	0.01
Length of test, weeks	14	9	2.6	7
ANALYTICAL RESULTS				
Uranium left in solution, %	31	15	38	97
Copper left in solution, %		23	166*	141*
Weight of stainless steel oxidized, mg	223	221	110	12.8
Surface wetted by solution, cm^2	16	16	22	22
Oxidized Fe in solution,** %		0.1	8.4	5.7
Oxidized Ni in solution,** %	54	11	86	272*
Oxidized Cr in solution,** %		0.0	0.2	9.6
SO_4^{--} (F) left in solution, %			29	96
SO_4^{--} converted to S^{--}, %			1.3	0.9
Estimated pH at start	2.7	3.4	2.7	2.7
Final pH	4.3	3.7	2.1	2.9

*No reason is known for these obviously high values.

**Based on assumption of oxidation in proportion to composition of stainless steel.

experimental error of the determination, all the uranium was in solution. It can be seen that only a small amount of the corrosion products was soluble. The analyses indicate that in one case an appreciable amount of sulfate ion was precipitated, but that in another there was essentially no sulfate ion. At present, it is not known whether the small amount of sulfide ion found in the solution is significant.

Of these four tests, test H9 is of the most interest. Apparently because of low flux, the corrosion rate was low throughout the whole period, and, within experimental error, no loss of uranium from solution was detected.

Future Plans. Test H11 is to be terminated soon to allow other important tests to be started. The first of these is expected to be an exploratory study of the corrosiveness of irradiated uranyl sulfate and uranyl fluoride solutions on titanium. The out-of-pile corrosion testing is being expanded to give better comparisons with in-pile data. One of the problems of immediate interest is the effect, if any, of oxygen partial pressure on corrosion in this particular type of experiment.

RELATED CHEMISTRY RESEARCH

EFFECTIVE CAPTURE CROSS SECTION FOR Pa^{233}

J. Halperin R. W. Stoughton

A value of 120 ± 15 barns for the neutron capture cross section of Pa^{233} for thermal reactor neutrons was reported in ORNL-1462.[1] The value depended on the relative amounts of U^{233} and U^{234} produced in the irradiation of thorium metal slugs and, hence, depended upon the neutron capture cross section for thorium. The determination of the value of 120 barns involved the use of the thermal value for thorium capture, 7 barns. More recently, a calculated correction was made for thorium resonance absorption by using Untermyer's value[2] for the resonance integral (12.5 barns for the particular slugs irradiated). With this correction and with the use of the effective cross section for thorium, the effective cross section for neutron capture by Pa^{233} in thermal reactors become 150 ± 15 barns.

EFFECTS OF HEAVY ISOTOPE BUILDUP IN THE CORE OF A U^{233} BREEDER REACTOR

J. Halperin R. W. Stoughton

The most recent cross section values have been used to calculate the buildup of U^{234}, U^{235}, and U^{236} in the core of a U^{233} breeder reactor and to determine the resulting effects on neutron economy and total uranium concentration. Five cases were considered:

1. starting with pure U^{233} in the core and adding pure U^{233};
2. starting with pure U^{233} in the core and adding U^{233} containing 5% U^{234};
3. starting with U^{233} containing 5% U^{234} in the core and adding the same material;
4. starting with U^{235} in the core and adding pure U^{233};
5. starting with U^{235} in the core and adding U^{233} containing 5% U^{234}.

Any U^{233} produced in the blanket may be expected to contain between 0 and 5% U^{234}, depending on the blanket-processing frequency.

In all cases, the maximum neutron losses (per net neutron reproduced in the core) were less than 1%. Also, in all cases, the losses go through a maximum at about a flux time of 3×10^{21}, through a negative minimum (that is, a net neutron gain) at about a flux time of 4×10^{22}, and approach a positive equilibrium at a flux time of above about 6×10^{23}. The integrated losses show a small net neutron gain between flux times of about 2×10^{22} and 5×10^{23}. For a reactor with a core flux of about 1.5×10^{15} and with a total fuel holdup (in core, heat exchanger, chemical processing equipment, etc.) of four or five times that in the core, a flux time of 10^{22} corresponds to about one year of operation; hence, for such a reactor, the integrated net effect is a small neutron gain from about the second to the fiftieth year of operation. The total uranium concentration will gradually increase by a factor of about 2.6 to 3.5, depending on the U^{234} content of the U^{233} blanket product; this equilibrium value will likewise be approached above a flux time of 6×10^{23}. The details of these calculations will appear in ORNL-1567.[3]

---

[1] J. Halperin, C. V. Ellison, D. E. Ferguson, and R. W. Stoughton, *Capture Cross-Section of Pa^{233} for Thermal Pile Neutrons*, ORNL-1462 (May 5, 1953).

[2] S. Untermyer, *Reactor Engineering and Services Division Quarterly Report Dec. 1, 1950 Through Feb. 28, 1951*, ANL-4596, p. 23-28.

[3] J. Halperin and R. W. Stoughton, *Effects of Heavy Isotope Buildup on U^{233} Breeders*, ORNL-1567 (to be published).

CHEMISTRY OF CORROSION

G. H. Cartledge R. P. Yaffe

The investigation of the electrochemical behavior of type 347 stainless steel in dilute sulfuric acid has been greatly extended during this quarter. The first phase of the study was designed as a survey of the effect on the electrode potential of small additions of various ions to the acid solution. In all, about 50 ions have been tested as additives, and many of them have been found to have no effect. Surprisingly, reproducible and consistent results have been obtained.

Since hard metals, such as iron and steel, do not usually give reliable potentials at room temperature, the present work has been done at 85°C. At this temperature the electrodes acquired sufficiently stable potentials in a matter of minutes, after the initial conditioning. The data have shown that when an added salt, such as zirconyl sulfate or potassium bromate, makes the electrode potential more noble, a plot of the electrode potential vs. the logarithm of the concentration of the added salt is linear. This has been found to be quite generally true when no obvious chemical disturbances are present. These curves correspond to Nernst-equation slopes, RT/nF, for electrode reactions, with $n = \frac{1}{2}$ or 1, approximately.

The study of corrosion inhibitors has continued; the elements technetium, rhenium, vanadium, molybdenum, tungsten, ruthenium, and osmium, in their highest valence states, have been tested. From the wide range of properties manifested by these ions, it should be possible to determine the specific properties responsible for inhibitory action. Besides technetium, the only element in the above group that showed good inhibitory behavior under the test conditions employed was tungsten. Both molybdates and tungstates were studied previously at 25°C and shown to be comparable to chromates at that temperature. In the present study at 100 and 25°C, alternately, no corrosion of SAE 1010 carbon steel has resulted in two months of exposure to 0.01 *f* sodium tungstate, but the molybdate solution failed quickly.

Further details of these studies may be found in the Chemistry Division report.[4]

---

[4] *Chem. Semiannual Prog. Rep. June 20, 1953*, ORNL-1587 (in press).

SLURRY CHEMISTRY

F. R. Bruce, Section Chief

THORIUM OXIDE SLURRIES

The purpose of the thorium slurry development program is to produce a nonabrasive, noncorrosive, readily dispersible thorium slurry containing 500 to 1000 g of thorium per liter that is chemically stable in water at 250°C. Since the projected use of the slurry is as a blanket for a breeder type of power reactor, the slurry must, in addition to the above requirements, be highly resistant to radiation damage and must contain a minimum of species other than thorium. The total opacity to thermal neutrons of the species other than thorium must be 10%, or less, that of the thorium.

The thorium compound which appears, at first glance, most likely to fulfill the above criteria is thorium oxide; however, the commercially available oxide prepared by the high-temperature calcination of thorium oxalate has proved, in slurry form, to be highly abrasive to stainless steel. Hence, the first phase of the program has been to investigate the various methods of preparing thorium oxide in an effort to produce a nonabrasive material and to develop an accelerated abrasion test in order to evaluate these studies. This phase of the program is well advanced in that an accelerated abrasion test has been developed and is now in use.

Initial results indicate that the thoria slurry produced by calcination of thorium oxalate at 500°C and hydrolysis for four days at 250°C is less abrasive than the Ames oxide that is sieved (325 mesh) but not hydrolyzed at 250°C. Thorium hydroxide hydrolyzed at 250°C in water has also proved to be nonabrasive.

Oxides prepared by calcination exhibit low settled volumes (1500 to 2000 g of thorium per liter) upon hydrolysis in water at 250°C. Slurries prepared by hydrolysis at 250°C of either the hydroxide or the carbonate, however, show low bulk densities or high settled volumes (300 to 500 g of thorium per liter).

Autoclaving thorium oxide at 250°C in water with uranium in the form of either UO_2CO_3, UO_2SO_4, or UO_2F_2 and at low uranium-to-thorium ratios resulted in the production of a refractory mixed oxide of the uranium in the thoria. The addition of NaF or LiF to a slurry of the mixed oxide and hydrolysis in water at 250°C under CO_2 pressure was efficacious in leaching the uranium from the mixed oxide.

PREPARATION AND PROPERTIES OF THORIUM OXIDE SLURRIES

W. W. Floyd
J. P. McBride
L. E. Morse
W. L. Pattison

Thorium oxide is a white, granular, slightly hygroscopic solid with a density of 10 g/cm^3, a melting point of 3050°C, and a boiling point of 4400°C.[1] The common method of preparation is ignition of the hydroxide or the salt of an oxyacid.

Although thoria is one of the most refractory substances known, its density and chemical inertness are known to depend on the condition of its formation.[2,3,4] It seems reasonable that the hardness of the oxide would show an analogous dependency. The studies reported below

(1) C. D. Hodgman, *Handbook of Chemistry and Physics*, 34th ed., Chemical Rubber Pub. Co., Cleveland, Ohio, 1952.

(2) V. Kohlschutter and A. Frey, *Z. Elektrochem.* **22**, 145 (1916); *Soc. Chem. Ind. (London)* **35**, 688 (1916).

(3) A. S. Newton, H. Lipkind, W. H. Keller, and J. E. Iliff, *Production and Separation of U^{233}*, Paper 8.3, p. 458, NNES-IV-17B.

(4) A. G. v. Heyden, British Patent Spec. 402,010 (Nov. 23, 1933).

give the information which has been obtained to date on the effect of the method of preparation on the properties of thorium oxide slurries.

Preparation of Thorium Oxide from Thorium Oxalate. An investigation has been initiated on the effect of temperature and duration of calcination on the purity, particle size, crystalline character, slurryability, and abrasiveness of the thoria produced by the ignition of pure thorium oxalate. The thorium oxalate for use in the study was prepared by precipitation from a hot (50 to 75°C) thorium nitrate solution by the addition of excess oxalic acid solution:

$$Th(NO_3)_4 + 2H_2C_2O_4 \xrightarrow[H_2O]{50\text{ to }75^\circ C} Th(C_2O_4)_2 \cdot 6H_2O + 4HNO_3 .$$

The resulting mixture was filtered while hot, washed repeatedly on heated filters, and air dried on the filters.

Effect of Calcination Temperature on Purity of Thoria. Separate portions of the dried thorium oxalate were ignited at 300, 500, 700, and 900°C until decarbonization to the oxide was essentially complete. The course of the decomposition reaction was followed by removing samples from time to time and igniting them at 900°C for 4 hours. Three hours of ignition at 900°C is sufficient to completely decompose thorium oxalate to the oxide. Hence, the per cent of loss in weight of the samples upon ultimate ignition at 900°C gave a measure of the decomposition. Table 23 gives the data obtained.

In the first preparation of the oxalate, 1 kg of thorium nitrate hydrate and 663 g of oxalic acid dihydrate yielded 934 g of thorium oxalate hydrate (assumed to be the hexahydrate). In another preparation, the same amounts of reactants gave 970 g of the thorium oxalate hydrate.

TABLE 23. WEIGHT LOSSES UPON ULTIMATE IGNITION AT 900°C OF RESIDUES FROM CALCINATION OF PRECIPITATED THORIUM OXALATE

CALCINATION TEMPERATURE (°C)	CALCINATION TIME	ULTIMATE IGNITION LOSS (%)
300	6 days	4.2
	7 days	4.4
	10 days	4.1
	11 days	4.2
	13 days	4.5
	17 days	4.7
	21 days	4.6
	38 days	2.5
500	65 hours	1.8
	72 hours	1.5
	89 hours	1.4
	96 hours	1.4
	120 hours	0.5
	1 hour	1.5
	2 hours	1.3
	3 hours	1.5
	4 hours	1.4
	5 hours	1.3
	6 hours	1.2

Heating 445 g of the thorium oxalate for 38 days at 300°C gave 220 g of thoria, which, upon ultimate ignition at 900°C, lost less than 3 wt %. After calcination at 500°C for 120 hr (5 days), 489 g of the oxalate yielded 243 g of thoria, which lost less than 1 wt % upon ultimate ignition. Calcination for 6 hr at 700°C of 510 g of thorium oxalate hydrate left as a residue 240 g of oxide, which lost less than 2% of its weight upon ultimate ignition. Ignition of 460 g of the oxalate for 3 hr at 900°C produced 218 g of thoria.

Although the data given in Table 23 primarily represent the results obtained after extended heating periods, the data also indicate that oxide residues of nearly constant weight were obtained relatively early at each

calcination temperature. Indeed, with calcination at 500°C, another preparation of thorium oxalate was found to yield better than 98% pure thoria upon heating for 6 hours.

Every effort was made to minimize the adsorption of water and carbon dioxide by the samples used for following the decomposition, but the observed weight losses upon ultimate ignition, as given in Table 23, may, in part, be due to adsorbed water and gas. It would appear, however, that the minimum temperature at which thorium oxalate hydrate may be conveniently decomposed to pure thorium dioxide is about 500°C. This conclusion is substantiated by Born,[5] who reports that the decomposition of thorium oxalate proceeds as follows:

$$Th(C_2O_4)_2 \cdot 6H_2O \xrightarrow{80 \text{ to } 100^\circ C} Th(C_2O_4)_2 \cdot 2H_2O \xrightarrow{300^\circ C} Th(C_2O_4)_2 \xrightarrow{400 \text{ to } 500^\circ C} ThO_2 .$$

In addition, the thermogravimetric analytical data of Duval and Dupuis on thorium oxalate indicate that the ThO_2 horizontal may not begin before 610°C.[6]

Particle-Size Analysis. Samples of the final products obtained by igniting the thorium oxalate hydrate at 500, 700, and 900°C were submitted to T. E. Willmarth. Photomicrographs were prepared from which particle-size analyses were made by I. H. Gary of Willmarth's group. A condensation of the size distribution data is given in Table 24.

The average particle size of the material ignited at 500°C was 4 microns, while that of the material ignited at 700 and 900°C was 5 microns. The material ignited at 900°C had a slightly higher proportion of the larger particles. The crystallites from all preparations were well-defined platelets that appeared to be unaggregated.

TABLE 24. SIZE DISTRIBUTION OF THORIA PRODUCED BY THORIUM OXALATE CALCINATION

PARTICLE SIZE (microns)	RATIO OF PARTICLE SIZE TO TOTAL NO. OF PARTICLES (%)		
	Ignited at 500°C	Ignited at 700°C	Ignited at 900°C
<2	36.2	27.6	29.6
2 to 10	52.3	55.5	51.5
10 to 16	10.9	14.5	14.8
>16	0.5	2.4	4.1

These observations and the similarities of the size distributions lend significance to and affect the interpretation of the x-ray diffraction data, which are discussed below.

X-ray Diffraction Studies. The x-ray diffraction data for the materials were obtained by R. D. Ellison of the Chemistry Division. All preparations gave the characteristic peaks of thorium dioxide. However, the broadness of the peaks was found to vary significantly and inversely with the temperature of calcination. It was estimated that, *if* the line broadening were due entirely to a particle-size effect, the temperature of calcination markedly affected the average particle size of the thoria from thorium oxalate and that the average particle size in the "low-burned" material should be approximately 0.05 to 0.1 micron. The well-defined character of the crystallites in the photomicrographs, the "large" average particle size, and the nearly same percentage of particles of less than 2 microns in all preparations tend to discount this explanation.

An alternative explanation of the line broadening, which has been suggested by Ellison, is that the oxide crystals produced by low-temperature calcination of oxalate are

(5) H. J. Born, *Z. physik. Chem.* **179A**, 256-262 (1937).

(6) C. Duval, *Inorganic Thermogravimetric Analysis*, p. 496-497, Elsevier Pub. Co., New York, 1953.

strained and that the amount of strain varies inversely with the temperature. A study is under way to resolve this problem and to correlate the observed data with the slurryability and abrasive properties of the thoria.

Slurry Properties. Studies of the slurry properties of the thoria produced by the calcination of thorium oxalate are in progress. The slurries formed by the calcined oxalate are, in general, readily dispersed, settle slowly, and are very fluid at a concentration of about 1000 g of thorium per liter. When the thoria prepared by ignition at 500°C was autoclaved at 250°C in water for as long as four days, neither its slurryability nor its settled volume (1500 to 2000 g of thorium per liter) appeared to change significantly. A similar preparation showed no change in its dry x-ray diffraction pattern after being autoclaved in water at 250°C for 18 hours.

Abrasive Properties. The investigation of the effect of the temperature of calcination on the abrasive properties of thoria produced by the decomposition of the oxalate is in progress and will be discussed in detail below. In one experiment, the material prepared by ignition at 500°C for 120 hr was autoclaved for four days in water at 250°C and its abrasiveness relative to Ames ThO_2, sieved (325 mesh) but not hydrolyzed at 250°C, was tested. It proved not only to be much less abrasive but to degrade rapidly in particle size so that at the end of the abrasion test the settled volume of the material was only 500 g/l, as compared with the original value of 1500 g/liter.

Preparation of Thorium Oxide from Thorium Hydroxide. A material of possible use in the production of a thorium oxide suitable for use in a slurry is thorium hydroxide. Freshly precipitated from nitrate solution, the hydroxide is a gelatinous, amorphous solid. On drying it forms a dihydrate that is hard, and on aging it becomes crystalline in character.[7] X-ray diffraction patterns obtained for samples of the hydroxide dried at 80°C for 24 hr exhibited the characteristic peaks of thorium dioxide.[8] No information has been obtained on the possible crystalline character of amorphous hydroxide subjected to an extended digestion in pure water. Indications are, however, that even under hydrolysis at 250°C in water for as long as 64 hr the hydroxide remains soft and nonabrasive and may be amorphous (cf., Table 26 below). If the product formed by the hydrolysis in water at 250°C of either the hydroxide or carbonate is dried, it becomes gritty, exhibits the characteristic ThO_2 x-ray diffraction pattern, and shows a three to four times decrease in settled volume (increase in bulk density), even after rehydrolysis in water at 250°C for 16 hours.

Since the hydroxide becomes crystalline on drying, a study of the effect of prolonged hydrolysis at 250°C on the crystalline character of the hydroxide would require that the x-ray data be obtained on undried samples of the solid. Such a study is planned.

Two methods of preparing the oxide from thorium hydroxide were investigated: calcination of the dry material and hydrolysis in water at 250°C.

Calcination of Thorium Hydroxide. Thorium hydroxide was precipitated from 0.5 *M* thorium nitrate at 75°C by adding excess 1:1 NH_4OH–H_2O, dropwise, with stirring. The resulting solid was recovered by filtration and dried. Heating a portion of the solid at 300°C (high enough to decompose the residual NH_4NO_3) for 24 hr did not give a residue of constant weight. Ignition at 900°C of a sample of this material resulted in a further weight loss of 3 to 7%. A portion heated at 500°C for 8 hr attained constant weight.

(7) W. J. Bohm and H. Niclassen, *Z. anorg. u. allgem. Chem.* **132**, 1,(1924).

(8) R. D. Ellison, Chemistry Division, personal communication.

An additional weight loss of only 0.7% was observed on ultimate ignition. All materials exhibited the characteristic diffraction pattern of ThO_2.[8]

Hydrolysis of Thorium Hydroxide in Water at 250°C. For the hydrolysis study, thorium hydroxide was precipitated cold (ice bath) from an approximately 0.5 *M* thorium nitrate solution by the addition of excess 1:1 NH_4OH–H_2O. The precipitate was filtered, thoroughly washed, and recovered as an aqueous slurry without drying of the solid. A portion of the hydroxide slurry was autoclaved for 64 hr at 250°C. The resulting slurry settled extremely slowly, dispersed readily, and showed a settled volume after long standing of 500 g of thorium per liter. An abrasion test of 2 1/2-hr duration showed this slurry to be completely nonabrasive, as compared with the Ames oxide (cf., Table 26 below).

Photomicrographs of the dried solids obtained from an aliquot of the hydrolyzed slurry indicated 80% of the slurry particles to be less than 3.3 microns in size. X-ray data indicated the dried material to be ThO_2.[8] The dried material was difficult to reslurry and gave a settled volume of 2200 g of thorium per liter.

Other Methods for Preparing Thorium Oxide. Scouting experiments were performed on a variety of methods for preparing thoria. Since none of these methods exhibited any particular advantages over the methods discussed above, they are reported with a minimum of detail.

Thorium oxycarbonate produced by aqueous phase reaction of ammonium carbonate and thorium nitrate was readily decomposed at 375°C in 3 1/2 hr to a better than 97% pure thoria. A similar preparation of oxycarbonate upon hydrolytic decomposition in water at 250°C yielded a slow settling, nonabrasive slurry (cf., Table 26 below) having a settled volume of 350 g of thorium per liter. The slurry showed a gray discoloration that was presumably the result of chemical attack on the walls of the autoclave by the carbonate.

Thorium peroxide precipitated from thorium nitrate solution proved to be nonquantitative, extremely bulky, and hard to handle, and it contained considerable nitrate.[9] Decomposition to relatively pure thoria was obtained at 300°C, and 92% of the particles in the product were less than 3.3 microns.

Thorium oxalate was completely decomposed at 250°C in water to yield a slow settling, fine-particle slurry, contaminated with about 4% iron from chemical attack on the oxide film of the autoclave.

AN ACCELERATED ABRASION TEST FOR THORIUM OXIDE SLURRIES

J. P. McBride W. L. Pattison

The initial pumping experiments with thorium oxide slurries have shown that the slurries made from Ames oxide prepared by the calcination of thorium oxalate at 650°C or higher temperatures are highly abrasive to stainless steel.[10] It was necessary, therefore, that the thorium slurry developmental program have the primary objective of producing a nonabrasive thorium oxide slurry. Since such a program would require not only the investigation of many different methods of slurry preparations but also of a large number of variables in each, the need for an accelerated abrasion test was imperative. Such a test has been developed and is now in use. The initial results have been very encouraging.

Description of the Abrasion Tester. The abrasion tester is of the jet-impingement type in which the slurry to be tested is thrown against a thin

[9] J. W. Hamaker and C. W. Koch, *Production and Separation of U^{233}*, Paper 7.2, p. 357, NNES-IV-17B.

[10] A. S. Kitzes, Reactor Experimental Engineering Division, personal communication.

test plate (1.5-mil steel shim stock) at high velocity and the time of penetration is noted. In the absence of penetration at a reasonable time, a qualitative examination of the surface of the test plate suffices to evaluate the relative abrasiveness of the slurry in question.

The essential part of the abrasion tester is a Lucite cup which holds 20 ml of the slurry being tested and through the side of which projects an atomizer type of nozzle with a pickup tube that extends down into the body of the slurry. Nitrogen at 40 psi is allowed to flow through the nozzle to lift the slurry through the pickup tube and project it against the test plate, which is inclined at a 45-deg angle to the slurry stream. The slurry, after striking the test plate, flows back into the body of the slurry, which is maintained in a dispersed condition by a magnetic stirrer. Hence, the 20 ml of slurry being tested is circulated up through the pickup tube, against the plate, and back into the body of the slurry many times during the test period. A spray trap, consisting of a 2 1/2-in. pipe, is attached to the top of the Lucite cup. Although the amount of slurry lost during the test is insignificant, some water is lost by evaporation and from the spray, and it is necessary during a test to add water continuously through the top of the spray trap at a constant rate to maintain a constant slurry concentration. The time of penetration of the test plate is noted by means of a sight glass placed behind the plate. A spotlight placed on the slurry side of the test plate aids in the determination of the time of penetration.

Development of the Abrasion Test. In an effort to develop a test which would give appreciable results in a short time, as well as to provide for differentiating between the abrasion properties of slurries, several different test plates were tried. Aluminum and brass foils, 1 to 2 mils thick, while giving penetration in a very short time, failed to differentiate between ThO_2 and $UO_3 \cdot H_2O$ as to time of penetration. Copper foils tended to yield and flow so that the penetration times were highly uncertain. Steel shim stock, 1.5 mils thick, proved ideal in that it gave reproducible results and differentiated between the abrasive properties of thorium oxide and uranium oxide slurries.

M. J. Feldman of the Solid State Division measured the hardness of the shim stock on a Tukon hardness tester. The results are given in Table 25, along with handbook values for type 347 stainless steel.

TABLE 25. HARDNESSES OF VARIOUS METALS

METAL	KNOOP HARDNESS NUMBER
Type 347 stainless steel, annealed	147 to 188*
Type 347 stainless steel, cold rolled	196 to 326*
1.0-mil steel shim stock	197
1.5-mil steel shim stock	213
1.5-mil steel shim stock, annealed	62.3

*_Metals Handbook_, 1948 ed., Americal Society for Metals, Cleveland, Ohio.

Abrasive Properties of Thorium Oxide Slurries. The philosophy behind the abrasion test described above is that relative abrasive properties of slurries pumped in the test loops will, in general, be reflected by the relative abrasiveness indicated in the abrasion tester. Hence, it is felt that a slurry preparation which proves to be less abrasive in the laboratory test, as compared with a slurry of known abrasive character (Ames oxide), will also be less abrasive in the test

loops. With this in mind, a series of abrasion tests have been initiated; the preliminary results are given in Table 26.

While the technique of performing the abrasion testing is not fully developed, as yet, the preliminary data of Table 26 are extremely encouraging. Thoria prepared by calcining thorium oxalate at 500°C for 120 hr and hydrolyzing at 250°C in water for four days has been shown to be markedly less abrasive than Ames ThO_2, sieved (325 mesh) but not hydrolyzed at 250°C. In addition, during the test, as mentioned in the first section of this chapter, the particles degraded markedly, and the settled volume of the material changed from 1500 to 500 g of thorium per liter. The results with the $Th(OH)_4$ which had been hydrolyzed for 64 hr at 250°C were likewise encouraging in that no visible abrasion was observed in a 2 1/2-hr test. The fluorinated oxides proved to be quite abrasive, and it may be that corrosion-erosion phenomena were being observed.

OTHER THORIUM SLURRY SYSTEMS

W. W. Floyd L. E. Morse
J. P. McBride W. L. Pattison

Thorium Fluoride. Hydrated thorium fluoride was precipitated from a thorium nitrate solution containing 200 g of the salt by the addition of 52 ml of concentrated hydrofluoric acid. The gelatinous precipitate was thoroughly washed and dried in a desiccated oven at 60°C. After drying for an additional four days at 105°C, the recovered solid weighed 91.4 grams.

A portion of this material lost 10.8% of its weight on heating for 4 hr at 500°C. An additional heating

TABLE 26. ABRASIVE PROPERTIES OF THORIUM OXIDE SLURRIES

SLURRY PREPARATION	SLURRY CONCENTRATION (g of Th per liter)	TEST PLATE	KNOOP HARDNESS NUMBER	DURATION OF TEST (min)	RESULTS
Ames ThO_2, sieved (325 mesh)	250 to 1000*	1.5-mil shim	213	22	Penetration
$UO_3 \cdot H_2O$ platelets	250 to 500*	1.5-mil shim	213	85	No effect
Ames ThO_2, sieved (325 mesh)	250	1.5-mil shim, annealed	62.3	32	Penetration
Ames ThO_2, sieved (325 mesh)	250	1.5-mil shim, annealed	62.3	41	Penetration
ThO_2 ignited at 500°C and hydrolyzed four days at 250°C	250	1.5-mil shim, annealed	62.3	61	No evidence of penetration, particles degrade
$Th(OH)_4$ hydrolyzed more than 64 hr at 250°C	250	1.5-mil shim, annealed	62.3	150	No effect
$ThOCO_3$ hydrolyzed more than 24 hr at 250°C	250	1.5-mil shim, annealed	62.3	26	No effect
ThO_2-ThF_4 (F/Th = 0.5) hydrolyzed four days at 250°C	350	1.5-mil shim, annealed	62.3	3	Penetration
ThO_2-ThF_4 (F/Th = 0.9) hydrolyzed at 250°C for 64 hr; 500 psi CO_2	217	1.5-mil shim, annealed	62.3	6	Penetration

*Constant volume not maintained; concentration estimated from the initial and final volumes of slurry.

time of 19 hr increased the weight loss to 19.9%. X-ray analysis revealed that some pyrohydrolysis had taken place, but there was no evidence of $ThOF_2$.[8] Hence, the original precipitated material was probably the tri- or tetrahydrate.

A second portion of the material upon overnight hydrolysis in water at 250°C yielded a slow settling, dark-gray slurry with a settled volume containing 550 g of thorium per liter. The gray contamination was probably the result of chemical attack on the autoclave by the hydrolysis products of thorium fluoride.

Fluorinated Thorium Oxide. Two preparations of fluorinated thorium oxide slurries were made by autoclaving at 250°C for three to four days mixtures of thorium oxide and thorium fluoride in mole ratios of fluoride to thorium of 0.5 and 0.9. The resulting white slurries settled slowly and showed no evidence of packing. The slurry containing the lower fluoride gave a settled volume of 1900 g of thorium per liter, while the higher fluoride material showed a much lower value of 800 g of thorium per liter. Both materials showed pronounced abrasive properties (Table 26).

Chemical analysis of the original materials showed the second fluoride preparation to have a sodium fluoride impurity equal to 20 mole % of the total fluoride, which may account for its enhanced reaction.

Photomicrographs of the hydrolyzed material with a fluoride-to-thorium mole ratio of 0.9 showed it to contain extremely small particles having an average size of 0.15 micron and a size range of 0.04 to 1.4 microns.

An interesting property of the fluorinated oxides is their ready solubility in 8 *N* HNO_3 at room temperature, even after hydrolysis at 250°C.

Thorium Pyrophosphate. Thorium pyrophosphate was prepared by adding a solution of sodium pyrophosphate ($Na_4P_2O_7$) to a 0.17 *M* solution of thorium nitrate. The mixture was digested at 75°C for 30 min and cooled, and the precipitate was recovered by filtration. Thorium pyrophosphate is soluble in 3.0 *M* HCl, which is the basis of its separation from the rare earths.

Heating an aqueous suspension of the material at 250°C for 16 hr gave a thick paste that was not soluble in 3 *M* HCl and that presumably resulted from the decomposition of the pyrophosphate in the presence of water at the elevated temperature.

Mixed Oxides. Several mixed oxides that contained thorium and other materials having low thermal-neutron capture cross sections were prepared by the precipitation of an oxalate mixture and subsequent ignition to the oxides.

Lead oxalate and bismuth oxalate were precipitated with thorium oxalate in equimolar proportions to the thorium and were converted to the oxides by ignition at 500°C. Samples of the mixed oxides were then autoclaved for 16 hr at 250°C in water. Both the PbO-ThO_2 and the Bi_2O_4-ThO_2 mixtures caked badly and were not suitable as slurries.

Freshly precipitated thorium oxalate was added to a supersaturated solution of magnesium oxalate, and the slurry was heated at 80°C with stirring for 1 hr in order to induce precipitation of the magnesium. After cooling, the resulting precipitate was recovered by filtration and ignited at 500°C for 6 hours. Hydrolysis in water at 250°C yielded a good slurry of lower bulk density (~1000 g of thorium per liter) than slurries made up from calcined thorium oxalate.

THORIUM-URANIUM SLURRY SYSTEMS

J. P. McBride W. L. Pattison

A thorium-uranium system in which the thorium was in an "unstable" slurry and the uranium was in solution would

offer economic advantages for use as a blanket or as a fuel. The thorium could be readily separated from the uranium, and the supernatant could be processed continuously for the U^{233} leached from the slurry solids. As a result, the bred fuel could be used sooner, and, consequently, the inventory costs for the initial charge of fissionable material in the core could be reduced. Investigation of the properties of thorium-uranium slurry systems is in progress.

Thorium-Uranium Oxides Prepared from the Carbonates. A slurry of thorium oxycarbonate and uranium oxide monohydrate (platelets) containing 3 mole % of uranium to thorium was hydrolyzed in water at 250°C for 18 hr under 500 psi of CO_2 pressure. The resulting orange-colored slurry settled slowly, dispersed readily, and had a low bulk density (400 to 500 g of thorium per liter). Reheating the slurry at 250°C overnight in the absence of CO_2 pressure did not affect its slurry properties.

The solid phase appeared to be an intimate mixture of thorium and uranium in that it was not decomposed by boiling for 15 min in concentrated nitric acid. Shaking some of the solid in 8 *M* nitric acid overnight gave a dissolution of less than 0.5% of the uranium. Ignition of the solid at 900°C gave a product that was a uniform light-gray to white in color and from which 10% of the uranium was leached by treating overnight with concentrated nitric acid at room temperature.

Thorium Slurries in Uranyl Sulfate and Uranyl Fluoride. An aqueous suspension containing 40 g of thorium per liter as thorium hydroxide and a solution of uranyl sulfate plus 0.25% excess sulfuric acid at a concentration of 1 g of uranium per liter was heated overnight at 250°C. The resulting slurry solid was orange in color and of increased bulk density (>2000 g of thorium per liter), which indicated that the uranium had been absorbed by the thoria.

A second experiment, similar to that above, except that a fluorinated thorium oxide was used, showed an analogous result of particle growth and absorption of the uranium by the solid. The final pH of the supernatant was 6.6. The fluorinated oxide used in this experiment had a mole ratio of fluoride to thorium of 0.4 and had been prepared by autoclaving overnight at 250°C a slurry of thorium carbonate (75 g of thorium per liter) in 0.25 *N* sodium fluoride. The bulk density was 300 to 400 g of thorium per liter.

In an analogous experiment with a fluorinated oxide that had a fluoride to thorium mole ratio of 1.6, a uranyl fluoride solution was used rather than a uranyl sulfate solution, and again there was absorption of the uranium by the thorium solid. In contrast to the above experiments, however, no particle growth occurred.

Thorium-Uranium Slurries Containing Sodium Fluoride. Table 27 gives the results of a series of experiments in which mixtures of $Th(CO_3)_2$ and UO_2CO_2 were reacted with various concentrations of sodium fluoride at 250°C under a partial pressure of 500 psi of CO_2. The slurries resulting from the reactions shown in Table 27 settled very slowly and exhibited high settled volumes (300 to 400 g of thorium per liter). In the absence of sodium fluoride, a mixed oxide of thorium and uranium would have resulted from these experiments. The presence of sodium fluoride hindered the formation of the mixed oxide so that in the 0.5 *M* sodium fluoride experiment only 2% of the original uranium was found in the slurry solids on cooling the autoclave. The addition of fluoride enhanced the solubility of the slurry solids in 8 *N* HNO_3 so that the solids from experiments T_7S_{12} and T_7S_{14} (Table 27) dissolved completely in the acid.

TABLE 27. EFFECT OF SODIUM FLUORIDE ON THORIUM-URANIUM OXIDE SLURRIES AUTOCLAVED AT 250°C FOR 16 hr UNDER A PARTIAL PRESSURE OF 500 psi OF CO_2

EXPERIMENT NUMBER	THORIUM CONCENTRATION (g/l)	URANIUM CONCENTRATION (g/l)	SODIUM FLUORIDE CONCENTRATION (moles/liter)	FINAL pH	CHEMICAL ANALYSES AT ROOM TEMPERATURE				SOLUBILITY OF SOLID IN 8 *M* HNO_3*		
					Supernatant		Solid				
					Uranium (ppm)	Thorium (ppm)	F-to-Th Ratio	CO_3-to-Th Ratio	Concentration Factor	Uranium (ppm)	Thorium (g/l)
T_7S_9	75	2.5	0	2.3	44		0		1.25	12	0.245
T_7S_{10}	110	3.0	0.05	8.6	1	2	0.13	0.11	1.6	76	8.65
T_7S_{12}	61	3.0	0.25	9.0	875	25	0.45	0.03	(1.1)	1900	82.0
T_7S_{13}	60	3.0	0.50	9.0	1030	5	1.63	0.03	1.1	59	37.5
T_7S_{14}	75		0.25	9.0		14	0.41	0.06	0		76.0

*Slurries were concentrated by removal of part of the supernatant and the addition of nitric acid to give a suspension in 8 *M* HNO_3, which was agitated overnight at room temperature.

A second solid phase containing uranium as a yellow-green crystalline substance, probably $Na_4UO_2(CO_3)_3$, was found in experiments T_7S_{12} and T_7S_{13} (Table 27), which indicated that the uranium solubility in these systems had been exceeded. The major portions of this substance clung to the interior walls of the autoclave. Failure to recover all this material from the bombs probably accounts for the low uranium material balance observed.

The high-fluoride slurries were contaminated with a rust-colored impurity, which was probably iron produced by chemical attack on the autoclave.

Two aliquots of the slurry from T_7S_{12} were treated as follows: slurry solids of one were thoroughly washed and resuspended in water; the second aliquot was untreated. Both were then heated at 250°C overnight in the absence of CO_2. The supernatants of the resulting slurries were water white, which indicated that in the absence of CO_2 pressure the soluble uranium complex had been destroyed and the uranium reabsorbed by the slurry solid. The final pH of the washed and resuspended material after autoclaving was 6.5; that of the unwashed slurry after autoclaving was 8.6.

Thorium-Uranium Oxide Slurries Containing Lithium Fluoride. Two experiments were performed in which lithium fluoride was added to portions of an aqueous slurry containing 84 g of thorium and 1.2 g of uranium per liter as the mixed oxide, and the resulting mixtures were autoclaved overnight at 250°C under 500 psi of CO_2. The mole ratios of fluoride to thorium were 1:1 and 2:1. The resulting slurries were of low bulk density (300 g of thorium per liter) and were ivory white in color rather than orange, which indicated that the uranium had been leached from the solid. The supernatants of both slurries had a green color and gave pH's of 7.9 in the 1:1 fluoride-to-thorium experiment and 7.4 in the 2:1 fluoride-to-thorium experiment. A small amount of a second solid phase of light-green crystals which clung to the interior walls of the autoclave was observed in each experiment. Analytical results were inconclusive in that low material balances were observed for the uranium and lithium fluoride, the result possibly of incomplete recovery of the second solid phase from the bombs. The data are presented in Table 28.

Although the results are obscure in that a second solid phase was formed and poor material balances were observed, it is interesting to note that, on cooling the slurries, essentially all the uranium was found to have been removed from the thorium solids

Heating portions of the resulting slurries at 250°C in the absence of CO_2 resulted in a decrease of the

TABLE 28. EFFECT OF LITHIUM FLUORIDE ON THORIUM-URANIUM OXIDE SLURRIES CONTAINING 84 g OF THORIUM AND 1.2 g OF URANIUM PER LITER

LiF ADDED (mg/ml)	ANALYSIS OF RESULTING SLURRY*									
	Solid (mg/ml)					Supernatant (mg/ml)				
	Th	U	Li	F^-	CO_3^{--}	Th	U	Li	F^-	CO_3^{--}
10.4	84.3	0.055	1.03	6.06	1.43	0.006	0.356	0.52	0.39	4.13
20.8	83.2	0.036	2.23	6.96	0.66	0.011	0.432	0.55	0.41	5.64

*Autoclaved at 250°C for 16 hr under a partial pressure of 500 psi of CO_2

soluble uranium content of from 50 to 75% and considerable crystal growth, with consequent deterioration of desirable slurry properties. This points up the importance of CO_2 pressure, as was indicated in the case of the sodium fluoride experiments described above.

THORIUM OXIDE PELLET IRRADIATIONS

J. P. McBride W. L. Pattison

A blanket system considered as an alternate to a thorium slurry blanket is one made up of thorium oxide pellets through which heavy water is circulated. The use of such a system would permit the attainment of a much higher concentration of thorium and make possible the use of stainless steel rather than zirconium as a core structural material. Disadvantages of the pellets are the engineering difficulties associated with their use and the lack of information on their stability to radiation. To date, one radiation damage experiment has been carried out on the oxide pellets.

Prior to the irradiation, the average densities of pellets of various sizes, given in Table 29, were determined by weighing in air and in water.

In the radiation experiment in question, one-half the pellets (two 1/2-in., fifteen 1/4-in., and fifty 1/8-in.) were canned in air in aluminum and irradiated in the LITR at room temperature for three weeks at a thermal-neutron flux of 5×10^{12} neutrons/cm^2·sec. The estimated gamma flux was such as to give an energy absorption of about 0.4 watt/gram.

TABLE 29. AVERAGE DENSITIES OF PELLETS

PELLETS		AVERAGE DENSITY (g/cm^3)
No.	Diam. (in.)	
2	1/2	8.74
2	1/2	8.71
15	1/4	8.80
15	1/4	8.80
50	1/8	8.76
50	1/8	8.92

Examination of the pellets after they had been cooled for one week revealed that the two 1/2-in. pellets had remained intact, while three of the 1/4-in. and three of the 1/8-in. pellets had shattered. All pellets were gray-black in color. The interior of the aluminum can was unaffected, which indicated that no undue heating or chemical attack had occurred.

The fact that the 1/2-in. pellets were intact leads to the supposition that the breaking of the smaller pellets was not due to thermal stress and might indicate that some of the pellets were initially inferior.

Further tests on the chemical and physical properties of the irradiated pellets and a second irradiation experiment are in progress.

PHYSICAL STUDIES OF SLURRIES

A. S. Kitzes W. Q. Hullings
R. B. Gallaher P. R. Crowley
C. A. Gifford

THORIUM OXIDE STUDIES

Preparation. In ORNL-1554, it was reported that thorium oxide prepared by calcining the oxalate at 300°C was less abrasive to stainless steel than the corresponding material calcined at 800°C.[1] Calcining at the lower temperatures to decrease the hardness of thorium oxide also produced a more chemically reactive oxide, that is, it was readily soluble in hot nitric acid, whereas the high-temperature oxides are difficult to dissolve in the same reagent. The low-temperature materials, however, contained residual thorium oxalate which may have accounted for the increased chemical reactivity. Calcining at 325°C for at least 48 hr completely decomposed the thorium oxalate. The decomposed material appears to be as abrasive as the material calcined at 800°C; however, abrasion tests have not been completed.

To determine whether a low-temperature oxide would undergo changes in properties upon standing, freshly prepared material was autoclaved at 250°C for one week. At the end of this time, it was found that the oxide was no longer readily soluble in hot nitric acid. From this test, it can be concluded that thorium oxide, regardless of method of preparation, will convert to the chemically inert form, which is apparently the most stable crystal formation.

Abrasion Tests. Three materials that stand up well under abrasion by thorium oxide slurries have been found. They are commercial, hard-chrome-plate on stainless steel, Stellite, and oxidized zirconium. The abrasion resistance of these materials was determined with the abrasion tester described in ORNL-1121,[2] in which the abrasive action of the Ames oxide of thorium was qualitatively determined by pumping slurry for 24 hr through an 0.008-in. gap between the rim of a rotating wheel and a polished test plate parallel to the axle of the wheel. The zirconium was oxidized by heating a strip of metal at 700°C for 1 hr in an atmosphere of oxygen; a dense, shiny film was produced.

The Ames oxide of thorium, which is a high-temperature calcination material with particles that are 44 microns or less in diameter, is less abrasive than larger particle-size material. A slurry of this material when tested in the abrasive tester against stainless steel was found to be slightly abrasive. Very light scratches were observed after 24 hr of testing. Studies are planned of the effects of temperature and length of calcination of thorium oxalate on crystal structure, reactivity, surface area, particle size, density, and hardness of the resulting thorium oxide and the effect on these properties of autoclaving the same samples. It is felt that from these studies the optimum thorium oxide and method of preparation may be found.

Thermal Conductivity. In a previous report,[3] measurements on the thermal conductivity of thorium oxide slurried in gelatin solutions at room temperature were reported. The gelatin solutions were found to decompose at

(1) R. N. Lyon *et al.*, *HRP Quar. Prog. Rep. Mar. 31, 1953*, ORNL-1554, p. 120.

(2) A. S. Kitzes *et al.*, *HRP Quar. Prog. Rep. Aug. 15, 1951*, ORNL-1121, p. 156-160.

(3) A. S. Kitzes *et al.*, *HRP Quar. Prog. Rep. Jan. 1, 1953*, ORNL-1478, p. 109-110.

temperatures higher than room temperature and thus the method was unsuitable for determining the thermal conductivity of thorium oxide slurries at the proposed operating temperatures of a thorium oxide blanket.

An equation developed by Maxwell,[4] which relates the electrical conductivity of a mixture of spherical particles dispersed in a continuous phase to (1) the electrical conductivities of the particles and of the continuous phase and (2) the volume fraction of the particles, has recently been reapplied to thermal conductivity calculations by Orr[5] and found to be satisfactory. Maxwell's equation is

$$K_e = \frac{K_c[2K_c + K_d - 2V(K_c - K_d)]}{2K_c + K_d + V(K_c - K_d)} ,$$

where

$K_e \equiv$ equivalent thermal conductivity of mixture,

$K_c \equiv$ thermal conductivity of continuous phase,

$K_d \equiv$ thermal conductivity of discontinuous phase,

$V \equiv$ volume fraction of discontinuous phase.

On the basis of this equation, thermal conductivities of aqueous thorium oxide slurries have been calculated over the temperature range from 25 to 250°C and for concentrations of up to 2000 g of thorium per liter. The results of these calculations, together with the experimental results reported previously, are shown in Table 30.

The values used in the calculations for the thermal conductivity of water were taken from Bingham and Jackson.[6] The values for the thermal conductivity of thorium oxide obtained from data taken at MIT,[7] Battelle,[8] and Rutgers (work under direction of R. B. Sosman by E. Ruh with specimen prepared at ORNL, private communication), as shown in Table 31, were corrected by using Maxwell's equation to account for the test specimens containing void spaces. The corrected values of

[4] J. C. Maxwell, *A Treatise on Electricity and Magnetism*, vol. 1, 3d ed., p. 440, Oxford Univ. Press, London, 1892.

[5] C. Orr, Jr., *The Transference of Heat Between a Pipe Wall and a Liquid-Solid Suspension Flowing Turbulently Inside the Pipe*, NP-4310 (Dec. 1952).

[6] E. C. Bingham and R. F. Jackson, *Bull. Bur. Standards* **14**, 59-86 (1919).

[7] F. H. Norton and W. D. Kingery, *The Measurement of Thermal Conductivity of Refractory Materials*, NYO-601 (Jan. 1, 1952).

[8] K. L. Johnson, O. L. Linebrink, and H. R. Nelson, *Thermal Conductivity of Hot-Pressed Thorium Oxide*, M-3475 (Nov. 25, 1946).

TABLE 30. CALCULATED AND EXPERIMENTAL THERMAL CONDUCTIVITY VALUES FOR THORIUM OXIDE SLURRIES

SLURRY CONCENTRATION (g of Th per liter)	THERMAL CONDUCTIVITY (cal/cm·sec·°C)						
	AT 25°C	At 50°C	At 100°C	At 150°C	At 200°C	At 250°C	At 25°C*
0	0.00145	0.00154	0.00163	0.00163	0.00158	0.00149	0.00145
250	0.00157	0.00166	0.00175	0.00175	0.00170	0.00160	
500	0.00169	0.00179	0.00188	0.00188	0.00182	0.00171	0.00165
750	0.00182	0.00192	0.00203	0.00201	0.00195	0.00183	
1000	0.00195	0.00207	0.00217	0.00216	0.00208	0.00196	0.00186
1250	0.00210	0.00222	0.00233	0.00230	0.00222	0.00209	
1500	0.00225	0.00238	0.00249	0.00246	0.00237	0.00222	0.00209
1750	0.00242	0.00255	0.00266	0.00262	0.00253	0.00237	
2000	0.00260	0.00273	0.00284	0.00281	0.00269	0.00253	

*Experimental values.

TABLE 31. THERMAL CONDUCTIVITY OF THORIUM OXIDE

TEMPERATURE (°C)	THERMAL CONDUCTIVITY (kcal/cm·sec·°C)
Rutgers Data, ρ = 9.45	
30	0.0340
40	0.0335
50	0.0325
60	0.0315
80	0.0295
100	0.0285
Battelle Data, ρ = 9.0	
100	0.0295
150	0.0224
200	0.0182
300	0.0133
400	0.0111
MIT Data, ρ = 8.16	
300	0.0140
400	0.0116
500	0.0100
600	0.0088
800	0.0071
1000	0.0058

thermal conductivity are plotted in Fig. 59; the values used in making the calculations for Table 30 were taken from the smoothed curve of Fig. 59.

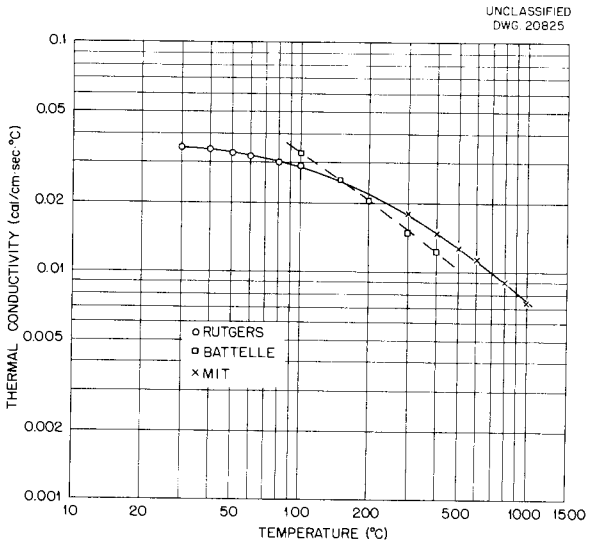

Fig. 59. Thermal Conductivity of Thorium Oxide, Corrected Values.

THORIUM HYDROXIDE PEPTIZED WITH THORIUM NITRATE OR URANYL NITRATE

Colloidal thorium hydroxide peptized with either thorium nitrate or uranyl nitrate to form a homogeneous suspension at room temperature is not stable when autoclaved for 24 hr at 250°C. The precipitated solids were found to be thorium oxide and, where uranyl nitrate was used, an unidentified uranium compound.

Additions of $NiSO_4$, $CuSO_4$, and NaH_2PO_4 did not improve the stability of the sols at the elevated temperatures. During one autoclaving at 250°C, a thorium hydroxide sol peptized with uranyl nitrate decomposed so rapidly that a 2000-psi pressure gage was ruptured.

THORIUM-URANIUM COMPOUNDS

Another possible breeder reactor is a one-core reactor in which the fuel contains thorium and uranium (thorium-to-uranium ratio of about 80:1) as a slurry. To prevent large increases in the reactivity of the reactor system, it is preferable that the thorium and uranium be homogeneously associated with each other at all times. Thorium-uranium compounds have been prepared in various proportions by the controlled precipitation of thorium oxide with urea at 100°C from a solution of thorium and uranyl nitrates. Precipitation is complete when the pH reaches 5.2. The separated solids are then calcined at 325°C to remove the excess nitrates and urea.

The resulting calcined solids, reddish orange to light orange in color, depending upon the uranium content, are stable when autoclaved

at 250°C for 48 hours. Slurries of these compounds are mildly abrasive when tested against stainless steel in the abrasion tester. From x-ray diffraction patterns, thorium oxide has been identified in the compound, but the composition of the uranium compound is still unknown. The compounds are probably solid solutions of uranium oxide in thorium oxide.

THORIUM OXIDE CIRCULATING LOOP

During this quarter, the loop for circulating thorium oxide slurries at a temperature of 150°C was put into operation. The loop described in ORNL-1121[2] was modified by substituting a fluid-bearing canned-rotor pump for the conventional centrifugal pump. A cross section of the pump is shown in Fig. 60 to illustrate the modified stator cans designed for eliminating stagnant areas and streamlining the flow through the cans. Accumulation of solids in the stagnant areas of the original cans presented some difficulty in previous tests. The cans and the other internal surfaces, except the pump volute and the impeller, were chrome plated to increase the abrasion resistance of these parts to the erosive action of thorium oxide.

After 144 hr of operation at 150°C with a slurry containing 70 to 340 g of thorium (as the oxide) per liter, the pump failed. Examination of the disassembled pump showed that the lower stator cans, 0.020 in. thick, had been perforated, apparently because of the abrasive action of the oxide; and the solid rotors, constructed of laminated iron with aluminum shorting rings, had been badly corroded. The solid corrosion products from the rotor could also have contributed to the perforation of the can walls. No evidence of abrasion was observed upon visual inspection of the upper can. The chrome plate was still intact, although the upper rotor was beginning to be pitted. A new can is now being fabricated, and both rotors will be canned in 400 series stainless steel to prevent corrosion. Thorium oxide slurries will again be loaded in the loop.

For the 144-hr run at 150°C, a slurry containing 70 g of thorium (as the oxide) per liter was circulated for the first 24 hr; the concentration was then increased to 160 g of thorium per liter by adding dry oxide, and circulation was continued for 24 hours. The loop was again shut down and the concentration was increased to 340 g of thorium per liter by the addition of oxide. A total of 96 hr of operation had been accumulated with the high-concentration slurry when the pump failed.

Ames thorium oxide with particles that were 44 microns or less in diameter was used to prepare the slurry. During the entire run, the pH of the slurry dropped from 6.4 to 5.5, the iron content of the solids increased from 0.15 to 0.55 mg per gram of slurry, and the chromium content increased eightfold, that is, from 0.006 to 0.05 mg per gram of slurry. The nickel content showed the smallest increase - from 0.015 to 0.025 mg per gram of slurry.

URANIUM STUDIES

Uranium Slurry Loops. Two loops have been in operation during this quarter with uranium slurries. In one loop, T, the pressurizer is not an integral part of the loop. It is isolated and connected to the circulating stream only by means of an S-shaped stainless steel tube to minimize formation of a vortex and the accumulation of solids. In all other respects, loop T is similar to loop S, which was described previously.

Several shakedown runs have been made in loop T at 250°C with $UO_3 \cdot H_2O$ (alpha-form) slurries. The results of

UNCLASSIFIED
DWG. 20826

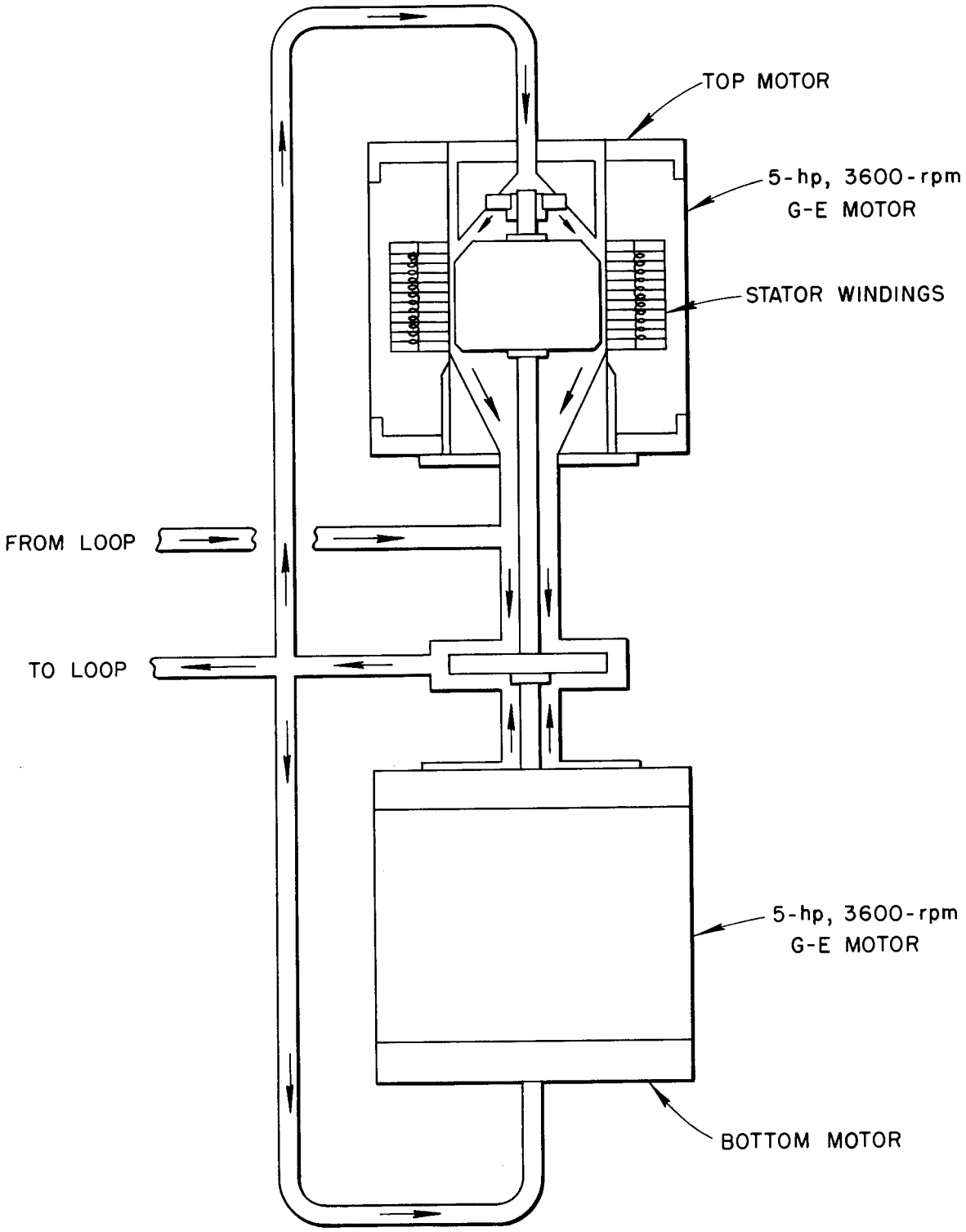

Fig. 60. Pump Showing Placement of Conical Inserts in Cans to Direct Flow Through Pump and Motors.

these shakedown tests can be summarized as follows:

1. Solids were lost from the circulating portion of the loop through the pressurizer connection during the time the loop was being heated from room temperature to 250°C. The density of the water changed by approximately 20% during the heating period. In expanding, it entrained solids, and thereby the concentration of solids in circulation was reduced.

2. Isolation of the pressurizer from the circulating loop did not prevent the formation of a vortex at the loop pressurizer connection. Solids were still centrifuged out of the circulating stream at this point, and thereby the concentration of solids in circulation was still further reduced.

3. No plating out of solids on the pipe walls of the circulating system was observed.

To minimize vortex formation at the pressurizer connection and to prevent accumulation of solids, the loop was redesigned as shown in Fig. 61. The pressurizer connection was inserted into the circulating stream, parallel to the direction of flow. A trap to prevent the solids from reaching the pressurizer and to act as a gas separator was inserted between the loop and the pressurizer. Flow from the bottom of the trap still enters the circulating stream at the downstream side of the orifice flow restrictor.

This new system is now being tested. A slurry containing 200 g of uranium (as the oxide) per liter is being circulated at 250°C. To date, no data are available to show whether the slurry concentration is being maintained in the new system.

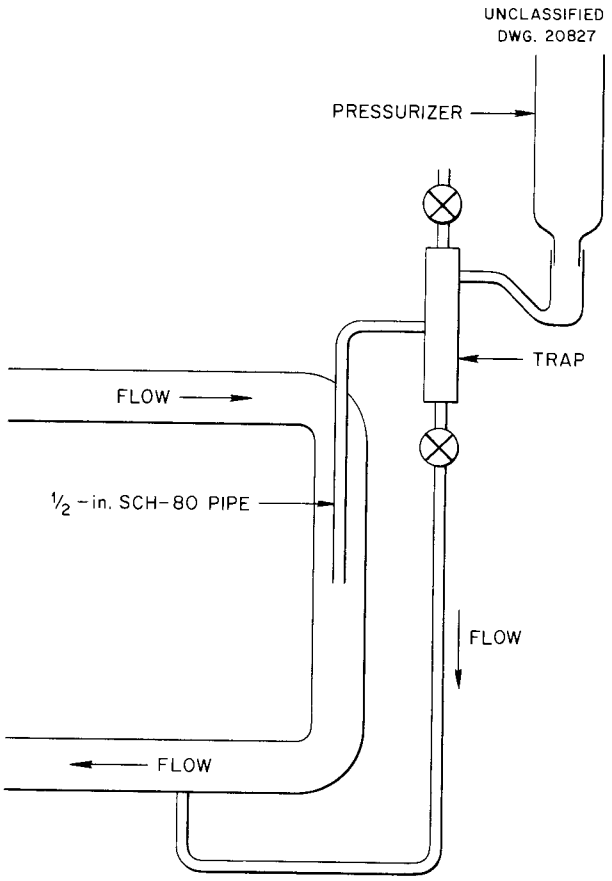

Fig. 61. Revised Loop T Pressurizer Connection.

Uranium Oxide Slurries with Various Additives. Previous results of static bomb tests in which various additives such as Fe^{+++} and Ni^{++} have been added to calcined UO_3 prior to hydration indicate that Ni^{++} favors the production of the alpha form of the oxide, whereas the beta form is enhanced by the presence of Fe^{+++}.

A uranium oxide slurry containing Ni^{++} [as $Ni(NO_3)_2$] was circulated in loop S for 117 hr at 250°C to determine whether the Ni^{++} would prevent the conversion of the alpha to the beta form of the oxide. Contrary to expectation, the nickel nitrate did not prevent the conversion of alpha to beta oxide. There was some plating out of the slurry on the pipe walls, and the corrosion attack appeared to be greater than usual.

Other additions, such as uranyl sulfate and NaH_2PO_4, will be made to uranium slurries to determine the

influence of these additives on the stabilization of a particular form of oxide and on the plating-out problem.

Alternative Uranium Slurry Systems. Although $UO_3 \cdot H_2O$ is a desirable slurry component for a homogeneous reactor fuel in terms of neutron economy, noncorrosiveness, and nonabrasiveness, a number of difficulties have been encountered in the use of this material during the past year. Foremost among these difficulties is the tendency of β-$UO_3 \cdot H_2O$ (the stable form at temperatures above 200°C) to form cakes on pipe and pressurizer walls during circulation at 250°C. The mechanism of this phenomenon is not yet understood, and all efforts to overcome the difficulty have, to date, been unsuccessful.

It has been demonstrated that α-$UO_3 \cdot H_2O$ can be successfully circulated at 150°C. Also, a run of short duration at 250°C with a barium sulfate slurry gave no indication of caking out. Therefore, since it can be concluded that not all slurries will plate out, efforts have been made to find and test other uranium compounds which will behave satisfactorily as a slurry fuel component. During this quarter, a number of uranium slurries have been circulated in loop S.

UO_2CO_3 Slurries. In ORNL-1554,[1] it was reported that a UO_2CO_3 slurry was circulated in loop S at 250°C under a blanket of 600 to 800 psi of CO_2 pressure. After 24 hr of operation, the UO_2CO_3 decomposed into UO_3, which accumulated in the pressurizer. To improve the thermal stability of the carbonate, sodium carbonate was added to the slurry.

For one run, the UO_2CO_3 slurry was prepared in the presence of 0.02 *M* Na_2CO_3 by circulating UO_3 platelets (β form) at 150°C under a pressure of 600 to 800 psi of CO_2.

For a second run, the UO_2CO_3 slurry was prepared with 0.005 *M* Na_2CO_3 at 150°C. In both runs, after equilibrium had been reached, the temperature of the loop was raised to 250°C. Within 48 hr after equilibrium was established at 250°C, solids began accumulating in the pressurizer, and results of the chemical analyses of samples drawn periodically indicated decomposition of the carbonate to UO_3. It can be concluded from these runs that UO_2CO_3 slurries are not suitable as reactor fuels because of their thermal instability at 250°C.

Uranyl Phosphate, $(UO_2)_3(PO_4)_2 \cdot H_2O$. To determine whether the accumulation of solids in the pressurizer and the plating out of solids on pipe walls, usually experienced with the circulation of oxide slurries at 250°C, are problems associated only with the circulation of oxide slurries or are problems typical of uranium slurries in general, a slurry containing 100 g of uranium (as the phosphate) per liter was circulated in loop S at 250°C for 140 hours. The phosphate prepared according to the procedure described by Ryon and Kuhn[9] is very insoluble in water at 250°C and is thermally stable at elevated temperatures.

During the course of the run, the concentration varied somewhat. The concentration remained at 100 g of uranium per liter for the first 74 hr of operation and then dropped to an average concentration of 61 g/l and remained constant to within ±10% for the remainder of the run. The decrease in concentration from 100 to 61 g/l was probably due to accumulation of solids in the various stagnant areas of the loop, such as the pump can and bearing and the abrasion-sample holder.

The pH of the slurry varied from 3.4 to 3.9, and there was no evidence of erosion or corrosion. There was no increase in the iron, nickel, or chromium contents of the solids, and

[9] A. D. Ryon and D. W. Kuhn, *Solubility of Uranyl Ammonium Phosphate in Nitric Acid and Ammonium Nitrate Solutions as a Function of Temperature*, Y-315 (Jan. 10, 1948).

the soluble uranium content of the supernatant averaged about 12 ppm.

Inspection of the pump casing, the impeller, and the pipe walls showed no evidence of erosion, although the light oxide film on these parts had been removed. The pump impeller was found to have lost 5 g in weight, as compared with its weight when originally installed.

A run is now in progress in which uranyl phosphate is again being circulated at 250°C. No data are available, as yet.

Magnesium Diuranate, MgU_2O_7. Another alternative slurry fuel being studied is hydrated magnesium diuranate. One run has been made in which a slurry containing 100 g of uranium per liter was circulated at 250°C for over 200 hr in loop S. During this period, the solid gradually accumulated in a bulky precipitate on the pressurizer walls.

Preliminary chemical analyses indicate no increase in the iron, nickel, and chromium contents of the slurry; the pH of the slurry is 10.0. The magnesium diuranate was prepared by the thermal decomposition of magnesium diuranyl acetate at 700°C.[10]

U_3O_8. Early work at ORNL indicated that U_3O_8 is not a stable material under reactor conditions because of its tendency to be easily oxidized to UO_3 by oxygen. However, if U_3O_8 is mixed with 4% PbO, oxidation to UO_3 may be eliminated.[11] A study of this possibility was carried out by autoclaving mixtures of U_3O_8 containing 0, 2, 4, and 6% PbO under approximately 100 psi of oxygen pressure. The results of these tests indicate that oxidation of U_3O_8 is not eliminated by the addition of PbO and that further effort to stabilize U_3O_8 against oxidation should not be expended.

Solubility of Carbon Dioxide in Water. In connection with the testing of uranyl carbonate, it was desired to know the solubility of carbon dioxide in water as a function of temperature and pressure. This information was obtained by pressurizing loop S with various amounts of carbon dioxide and withdrawing liquid samples from the system after equilibrium had been reached at various temperatures. The results of this study are shown in Fig. 62, where the equilibrium concentration of carbon dioxide in water is plotted against water temperature for various partial pressures of carbon dioxide in the pressurizer.

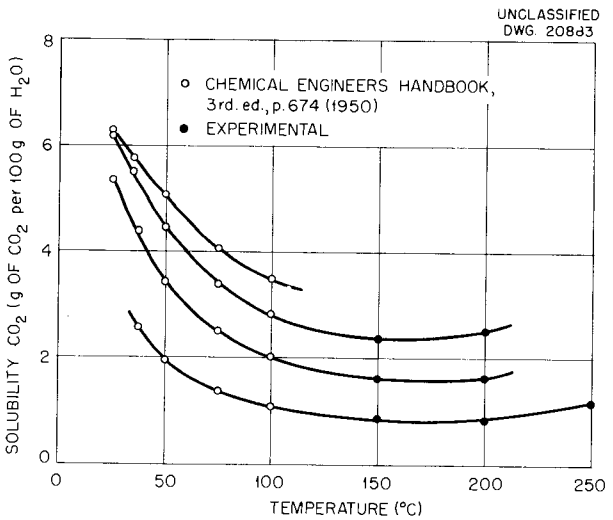

Fig. 62. Solubility of CO_2 in Water as a Function of Temperature and Partial Pressure of CO_2.

(10) H. R. Hoekstra and J. J. Katz, *Alkaline Earth Polyuranates*, AECD-2647 (July 12, 1949).

(11) H. C. Urey *et al.*, *The Heavy Water - Slurry Pile*, A-743 (June 30, 1943).

CHEMICAL PROCESSING

F. R. Bruce, Section Chief
D. E. Ferguson — W. E. Tomlin
R. G. Mansfield — G. I. Cathers
O. K. Tallent — J. P. Sanders

CHEMICAL PROCESSING OF A U^{233} BREEDER REACTOR

A schematic flow sheet for the proposed processing of a two-region, approximately 400-megawatt, U^{233} breeder reactor is given in Fig. 63. The rates of processing indicated are based on an economic optimization of the processing and represent the average for the four two-region reactors studied.

Fuel solution containing about 2000 g of U^{233} per day is passed through a calcium fluoride bed to remove the rare-earth fission products and other insoluble impurities. This step, alone, removes a calculated 90% of the reactor poisons contained in the fuel solution. In addition, fuel solution containing about 200 g of U^{233} per day is sent to the blanket processing plant for complete decontamination. This processing will maintain the level of poisons in the fuel solution at 3%.

The blanket processing consists of removing about 80 kg of thorium containing 375 g of U^{233} and Pa^{233} from the blanket per day and isolating uranium and thorium by the Thorex process.

For a one-region U^{233} breeder reactor, only the Thorex plant is necessary, and the rate of processing may be set to maintain the poisons in the reactor at the optium level.

ADSORPTION OF RARE EARTHS FROM DILUTE URANYL SULFATE SOLUTION

Additional batch tests indicate that calcium fluoride is an efficient material for removing rare earths from a dilute uranyl sulfate solution. The mechanism of this removal appears to be metathesis of the calcium fluoride, which yields rare-earth fluorides and calcium sulfate. Since the solubility of calcium sulfate is greater at lower temperatures, an adsorption process

DWG. 20828

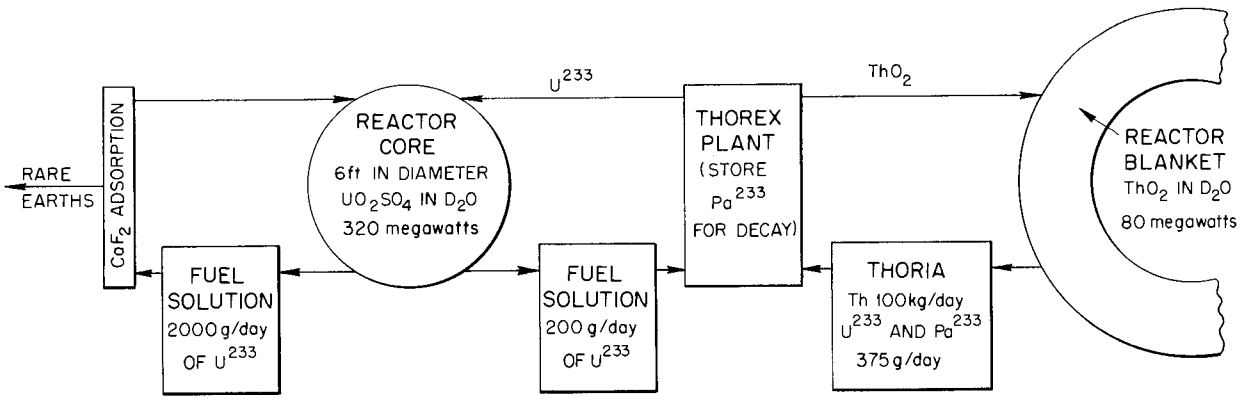

Fig. 63. Schematic Chemical Processing Flow Sheet for Two-Region Breeder Reactor.

must be operated at an elevated temperature to avoid precipitation of calcium sulfate inside the reactor.

A material suitable for packing a calcium fluoride column has been prepared both by fusion of reagent-grade calcium fluoride under an inert atmosphere and by a cold hydrostatic-pressing procedure. The advisability of using natural fluorite mineral is doubtful because of the impurities; attempts to grow crystals of CaF_2 in aqueous solutions were not successful.

Solubility of Calcium Sulfate in Uranyl Sulfate. Determinations of the solubility of calcium sulfate in a solution containing 5 mg of uranium (as UO_2SO_4) per milliliter that was 0.002 *M* in H_2SO_4 show that the solubility is an inverse function of the temperature. The solubility values are given in Table 32. To determine the solubilities, 5 ml of solution containing 5 mg of uranium (as UO_2SO_4) per milliliter that was 0.002 *M* in H_2SO_4 was heated and agitated with 0.1 g of $CaSO_4 \cdot 2\ H_2O$ at a given temperature for 24 hr and then filtered at the same temperature. The filter bomb used was patterned after the design furnished by W. L. Marshall and V. S. Gill of the Chemistry Division.

TABLE 32. SOLUBILITY OF $CaSO_4$ IN 0.02 *M* UO_2SO_4

TEMPERATURE (°C)	SOLUBILITY OF $CaSO_4$ (mg/ml)
250	0.13
215	0.20
150	0.92
75	1.53

Thorium Fluoride as an Adsorbent. Under batch conditions at 75°C, thorium fluoride has been found to adequately remove rare earths from a simulated core solution. In this experiment, 50 ml of a solution containing 5 mg of uranium (as UO_2SO_4) per milliliter and 0.60 mg of a rare-earth sulfate mixture and Y^{91} tracer per milliliter that was 0.002 *M* in H_2SO_4 was agitated for 4 hr at 75°C with 2.5 g of ThF_4. A sample was filtered at 75°C. The results showed that 96% of the rare earths was removed.

The mechanism of the removal of the rare earths by ThF_4 is also a metathesis reaction in which the thorium is replaced by the rare earths.

Continuous Adsorption Tests at 250°C. Equipment for contacting fuel solution with inorganic adsorbents at elevated temperatures has been constructed and tested. At 250°C, fluorite mineral (suggested by the Vitro Corp.) removed 99% of the rare earths from a 0.02 *M* UO_2SO_4 solution; however, about 20% of the uranium precipitated in the equipment. In similar tests with no adsorbent in the equipment, large fractions of the uranium again precipitated. Since this precipitation appears to be due to hydrolysis and reduction of uranium, the equipment is being modified to make provisions for oxygen addition to prevent reduction, and 30 mole % excess sulfate as sulfuric acid will be added to prevent hydrolysis in future tests.

Preparation of a Material Suitable for Column Packing. One method of adapting calcium or thorium fluoride to continuous decontamination of reactor fuel would be its use in a column. This would require a granular fluoride with particles of about -30 +70 mesh. These particles would have to have a reactive surface that was porous or irregular, so that the reactivity of the granular material would be comparable to that of a finely divided salt.

Attempts to produce large crystals of thorium fluoride by slow diffusion of thorium nitrate and hydrofluoric acid into a large volume of water

produced the usual gelatinous precipitate. Similar results were obtained with calcium. Digestion of finely divided reagent-grade calcium fluoride with 1 *M* HNO_3 for 60 hr in a rocking autoclave at 250°C also failed to produce a material suitable for column packing.

Samples of fused calcium and thorium fluorides have been tested and found to be inactive at room temperature. That the chemical inertness of the fused salts might be due to an oxide film on the surface of the grains suggested carrying out the fusion in an inert atmosphere. Two batches of reagent-grade CaF_2 were heated in a high-temperature furnace in the Metallurgy Division Laboratory. One batch, heated under helium to 1385°C, sintered to a hard mass, but did not completely fuse. The second batch was heated to 1385°C in a stream of hydrogen and fused. There was no apparent difference in the two batches after cooling. They were ground and sieved to -35 +70 mesh and tested for rare-earth removal at room temperature. Only about 15% of the rare earths were removed from a 0.02 *M* UO_2SO_4 solution by this material in a 16-hr batch contact. However, since fluorite mineral is an efficient adsorbent only at elevated temperatures, a room temperature test does not give conclusive results.

To determine the rare-earth removal of the fused CaF_2 at a higher temperature, batch adsorption tests were carried out in a rocking autoclave at 250°C. In addition to the fused materials, a sample of hydrostatically pressed (60 tons/in.^{2} pressure) reagent-grade fluoride was tested. More than 99% of the rare-earth-tracer activity was removed in every case. The results of the experiments are given in detail in Table 33.

Some precipitation of UO_3 occurred during heating in the autoclave because of hydrolysis of the uranyl sulfate; therefore, sufficient sulfuric acid was added to the simulated fuel solution to bring the acidity to 0.06 *N* for a second series of autoclave tests. The contact time for this series was 1 hour. In addition to hydrostatically pressed CaF_2, the materials tested consisted of three batches of reagent-grade calcium fluoride which had been mechanically pressed at 50 tons/in.^{2} in a hydraulic-ram press. One batch was ground and sieved as it came from the press; the other two were heated to 600°C for 45 min after pressing. This annealing resulted in a very hard

TABLE 33. RESULTS OF BATCH ADSORPTION TESTS OF CaF_2

Materials of test: 0.5 g of CaF_2 (-35 +70 mesh) mixed with 10 ml of solution containing 0.02 *M* UO_2SO_4, radio-yttrium as tracer, and 0.6 g of stable rare-earth sulfates per liter

ADSORBENT	TEMPERATURE OF TEST (°C)	DURATION OF TEST (hr)	RARE EARTHS REMOVED (%)
Reagent-grade CaF_2 sintered under helium at 1375°C	Room	1	50
Reagent-grade CaF_2 fused under hydrogen at 1385°C	Room	16	15
Reagent-grade CaF_2 sintered under helium at 1375°C	250	2	100
Reagent-grade CaF_2 fused under hydrogen at 1385°C	250	2	100
Reagent-grade CaF_2 hydrostatically pressed	250	2	100

material. One batch of annealed fluoride was tested without further treatment; the other was boiled with 2 *M* H_2SO_4 for 1/2 hr, washed with distilled water, and dried before testing. This acid treatment was used in an attempt to make the surface more reactive.

All the types of calcium fluoride investigated, with the exception of the unannealed, mechanically pressed fluoride, showed good mechanical strength, and, since the bulk of the grains retained their original size, they would be good column material. The unannealed, mechanically pressed CaF_2 was not cohesive and crumbled easily into a powder. Only the solution contacted with acid-washed, annealed CaF_2 showed any uranium loss. The reason for this is not apparent.

The results of the tests are recorded in Table 34. The removal of rare earths was complete for all the materials tested.

COST OF PROCESSING

The removal of fission and corrosion products from the fuel solution of a two-region breeder reactor may be accomplished by a combination of calcium fluoride adsorption, which removes an estimated 90% of the poisons, and complete decontamination of the fuel in the blanket-processing plant to remove the remaining impurities. A preliminary cost estimate indicated the cost of calcium fluoride adsorption to be about 40 cents per gram of U^{233}. Optimizing the relative amounts processed by the two processes results in a total feed decontamination cost of 70 cents per gram of U^{233}.

The capital cost of a 1-ton per day Thorex plant for processing the blanket of a two-region U^{233} breeder reactor was estimated to be $7,500,000.00. The unit cost of processing in this plant, including amortization, is $10.00 per kilogram of thorium. If the U^{233} content of the blanket is 5 g per kilogram of thorium and if the optimum amount of fuel solution is added to this plant, the total cost of the Thorex processing is $2.00 per gram of U^{233}, including inventory charges.

TABLE 34. RESULTS OF BATCH ADSORPTION TESTS OF CaF_2

Materials and conditions of test: 500 mg of CaF_2 (−35 +70 mesh) sealed in a pyrex tube with 10 ml of solution containing 5.0 g of uranium (as UO_2SO_4) per liter, radio-yttrium as tracer, 0.06 *N* H_2SO_4, and 0.6 g of stable rare-earth sulfates per liter; tube heated at 250°C for 1 hr in rocking autoclave

ADSORBENT	URANIUM CONCENTRATION (mg/ml)	RARE EARTHS REMOVED (%)
Reagent-grade CaF_2 mechanically pressed at 50 tons/in.^{2}, no subsequent heating	5.10	100
Reagent-grade CaF_2 mechanically pressed at 50 tons/in.^{2} and subsequently annealed 45 min at 600°C	5.10	100
Reagent-grade CaF_2 hydrostatically pressed at 60 tons/in.^{2}	5.10	100
Reagent-grade CaF_2 mechanically pressed (50 tons/in.^{2}), annealed at 600°C for 45 min, and washed with hot 2 *M* H_2SO_4	4.70	100

Based on calculations made for four two-region reactors with 3% fission-product poisons in the core, the total cost of chemical processing of the core and the blanket will be about 1.3 mills per kilowatt-hour of electricity produced. If the poisons are allowed to remain at 5%, the cost will be less than 1.0 mill per kilowatt-hour; a similar analysis for a one-region reactor indicated that the chemical processing cost for 3% poisons will be about 1.0 mill per kilowatt-hour, and, for 5% poisons, about 0.7 mill per kilowatt-hour.

Cost of Chemical Processing of Blanket. The present design for a two-region U^{233} breeder reactor employs either a 2-ft-thick blanket of thorium oxide slurry in D_2O with approximately 1000 g of thorium per liter or a 1-ft-thick thorium oxide pellet blanket cooled by D_2O, which would be equivalent to 4200 g of thorium per liter. Calculations have been made for four such reactors that each develop 3.2×10^5 kw of heat power in the 6-ft-dia core tank of 1/2-in.-thick zirconium (cf., chapter on "Intermediate-Scale Homogeneous Reactor Design" for details of calculations). The core solution was assumed to be uranyl sulfate in D_2O, to contain 3 vol % gas bubbles, and to have a fission-product-poison cross section of 3% of the U^{233} cross section. Equilibrium amounts of protactinium and the higher isotopes of uranium were assumed to be present. A summary of the results of these calculations is given in Table 35.

For the reactors described in Table 35, approximately 100 kg of thorium, or less, must be processed each day per reactor. Present power demands indicate that, at most, ten such reactors would be constructed in the vicinity of a chemical processing plant. Therefore, Thorex plants for processing in the neighborhood of 1000 kg of thorium per day are of interest.

Cost estimates of such plants have been made by extrapolating the results of a detailed cost estimate, made by A. R. Irvine of the Engineering Department, for a plant of 3000 kg/day capacity. The estimate was prepared for a plant for processing thorium which contained 1 g of U^{233} per kilogram of thorium and which had been cooled for 30 days. The plant was designed to include several units which

TABLE 35. CHARACTERISTICS OF A TWO-REGION U^{233} BREEDER REACTOR

	REACTOR			
	I	II	III	IV
Type of blanket	Slurry	Slurry	Pellet	Pellet
Ratio of atoms of U^{233} to Th	0.003	0.005	0.003	0.005
Blanket volume, liters	10,700	13,500	4,400	4,400
Blanket processing rate, liters/day	97.2	75.5	26.5	17.5
Thorium processed, kg/day	97.2	75.5	111.8	73.8
Heat power in the blanket, kw	6.1×10^4	10.6×10^4	5.0×10^4	9.0×10^4
Total power from the reactor, kw	3.81×10^5	4.26×10^5	3.7×10^5	4.1×10^5
Average flux in core	2.24×10^{15}	2.29×10^{15}	2.06×10^{15}	2.09×10^{15}
Average flux in blanket	6.1×10^{13}	5.1×10^{13}	2.90×10^{13}	2.82×10^{13}
Critical concentration, g of U^{233} per liter	1.326	1.293	1.469	1.439

could be eliminated in a homogeneous reactor processing plant. However, the addition of such units for D_2O recovery would probably be equivalent to these costs.

In extrapolating to the smaller capacity plant, the ratio of the plant capacities to the 0.6 power was used to factor the capital cost. Chemical, laboratory, process services, and waste disposal costs were assumed to be proportional to plant capacities. Labor, supervision, and maintenance costs were assumed to be constant over this range of plant capacity. Overhead was assumed to be equal to the sum of labor and maintenance. The capital cost was amortized at 16% per year. The results of these calculations are given in Fig. 64 as the capital, operating, and total cost as a function of plant capacity.[1]

It should be noted that the unit operating cost in a 1000-kg/day plant is \$10.00 per kilogram of thorium. If it is assumed that the U^{233} content of the thorium is 5 g per kilogram of thorium, the unit cost of operation is \$2.00 per gram of U^{233}.

Cost of Chemical Processing of Core. In the core of a two-region U^{233} breeder reactor, the nongaseous fission-product poisons may be divided into two categories, namely, (1) those

[1] D. E. Ferguson and J. P. Sanders, *Economics of Chemical Processing for a Uranium-233 Breeder*, ORNL CF-53-6-173 (June 18, 1953).

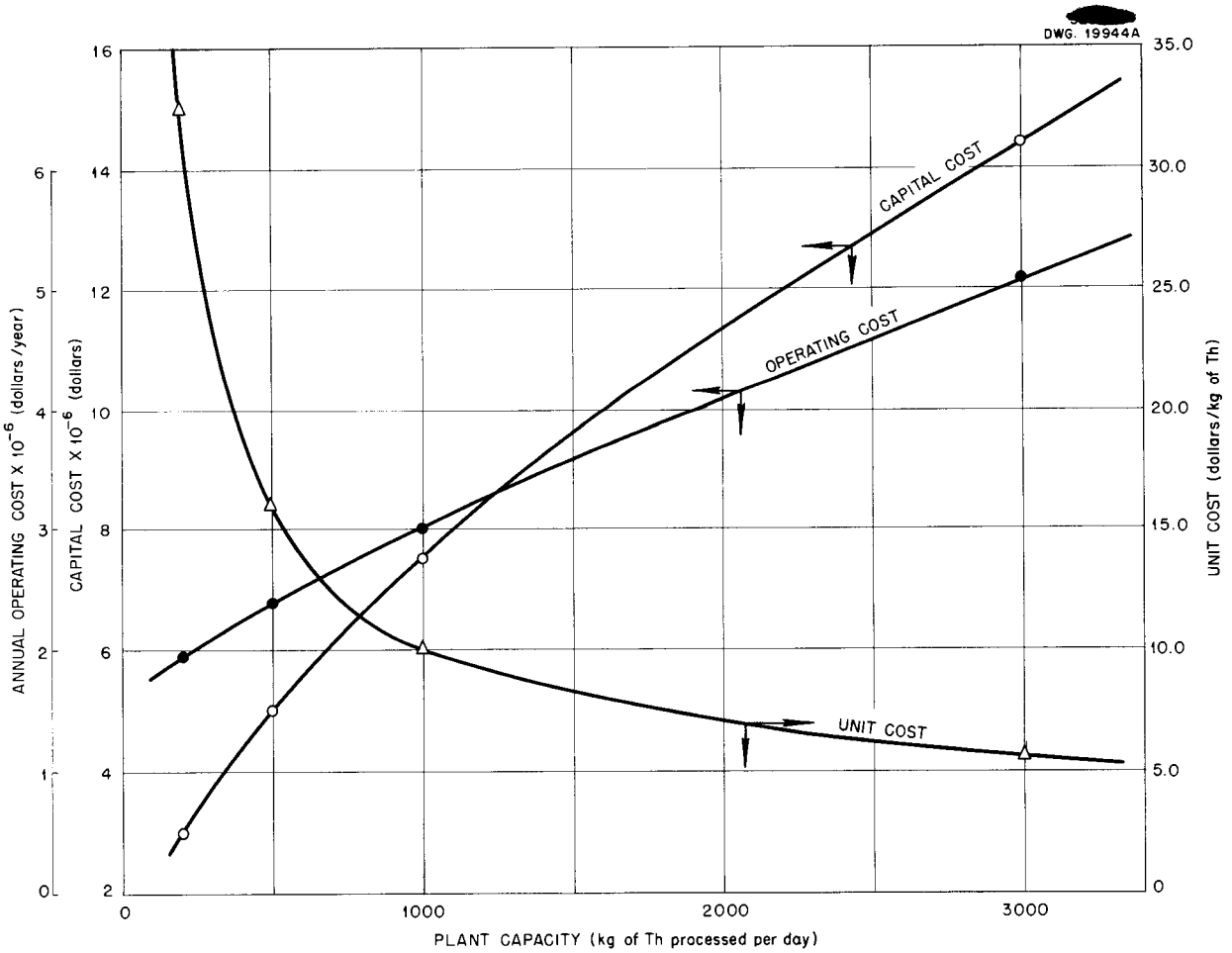

Fig. 64. Cost of Chemical Processing as a Function of Thorex Plant Capacity.

having, on the average, a 40,000-barn cross section and (2) those having, on the average, a 40-barn cross section. It is assumed that upon absorption of a neutron, the poison atom of group (1) is converted to a group (2) atom. Therefore these high-cross-section poisons are removed rapidly by burnup, and their concentration is essentially independent of the chemical processing rate

The lower-cross-section poisons are assumed to produce another atom of the same group upon absorption of a neutron and therefore are removable only by chemical processing. The present developments indicate that about 90% of this group may be removed by adsorption in a bed of calcium fluoride at a relatively low cost. The remaining portion may be removed by a Thorex process.

In order to determine the cost of processing by calcium fluoride adsorption, a very preliminary flow sheet has been drawn and a cost estimate made.[1] The calculations indicate that the total capital cost will be approximately $576,000.00, and that yearly operating costs (including amortization) will be around $232,000.00. If the processing rate is 2000 g of U^{233} per day for 300 days per year, the cost per gram of processed U^{233} is approximately $0.40.

The core solution, after D_2O recovery and appropriate cooling, may be added to the Thorex plant to be processed with the blanket material. For a reactor operating with a core power of 320 megawatts, approximately 200 g of U^{233} from the core must be processed each day. This would add approximately 2000 g per day to the 1000-kg Thorex plant. If the operating cost is divided by the total U^{233} processed, the unit cost would be approximately $1.50 per gram of U^{233} processed. However, inventory charges on this additional storage of core solution will bring the cost to approximately $2.00 per gram.

The knowledge of the relative cost of processing by these two methods and also the yield of fission products which can be removed by calcium fluoride relative to the yield of those which cannot be removed makes it possible to optimize the two processing rates so that the minimum cost per gram for total decontamination is achieved.[1]

If it is assumed that the cost of processing by calcium fluoride adsorption is $0.40 per gram of U^{233} and that of Thorex processing is $2.00 per gram of U^{233}, the cost of total decontamination for the optimum processing rates is $0.70 per gram of U^{233}. In this computation it is assumed that 90% of the fission-product poisons are removable by calcium fluoride processing.

Total Cost of Chemical Processing. The rate of chemical processing of the core solution is almost inversely proportional to the poison fraction (ratio of absorptions in poison to absorptions in U^{233}) in the core. Also, the total cost of chemical processing per unit of electrical energy generated depends on the amount of poison allowed to build up in the reactor.

For the four reactors described in Table 35, the cost of both core and blanket processing in mills per kilowatt-hour of electricity is given in Table 36. For these calculations, a 20% efficiency in converting heat to electricity was assumed. If the poison fraction in the core is 0.05, the total cost of chemical processing will be approximately 0.9 mill per kilowatt-hour.

Chemical Processing in a One-Region U^{233} Breeder Reactor. Table 37 gives the results of calculations for one-region U^{233} breeder reactors with breeding gains similar to those of the two-region reactors described in Table 35. The fission-product-poison fraction was assumed to be 3%. The unit chemical processing cost was

TABLE 36. COST OF CORE AND BLANKET PROCESSING

	REACTOR			
	I	II	III	IV
Electrical energy produced, kw-hr/day	1.83×10^6	2.05×10^6	1.78×10^6	1.97×10^6
Cost of blanket processing, $/day	970	760	1120	740
Cost of CaF_2 processing, $/day	810	800	820	820
Cost of Thorex processing, $/day	810	800	820	820
Total cost of chemical processing, $/day	2590	2360	2760	2380
Total cost of chemical processing, mills/kw-hr	1.4	1.2	1.5	1.2

TABLE 37. COST OF PROCESSING ONE-REGION U^{233} BREEDER REACTOR

	REACTOR			
	I	II	III	IV
Diameter of reactor, ft	15	20	20	20
Concentration of Th, g/l	400	200	400	400
Concentration of U, g/l	7.25	2.83	4.65	6.86
Processing rate, liters/day	985	5113	3098	2091
Th process, kg/day	394	1023	929	836
U^{233} processed, kg/day	7.1	14.4	14.4	14.3
Heat power, kw	10^6	2×10^6	2×10^6	2×10^6
Electrical energy, kw-hr/day	4.8×10^6	9.6×10^6	9.6×10^6	9.6×10^6
Chemical processing cost, mills/day	3.9×10^6	10.23×10^6	9.29×10^6	8.36×10^6
Chemical processing cost, mills/kw-hr	0.8	1.1	1.0	0.9

assumed to be $10.00 per kilogram of thorium, and the electrical efficiency was assumed to be 20%.

If the fission-product poisons were allowed to build up to 5%, the chemical processing cost would be reduced to 0.5 to 0.8 mill per kilowatt-hour. Although the chemical processing costs appear to be lower in the one-region reactor than in the two-region reactor, increased charges on a larger inventory in the reactor will add to the cost of power.

SUMMARY OF CHEMICAL PROCESSING DEVELOPMENT BY THE VITRO CORPORATION OF AMERICA

Various minerals and inorganic compounds for use as adsorbents for

removal of fission products from aqueous reactor fuel have been examined in exploratory tests at the Vitro Corporation, West Orange Laboratory; the results are given in more detail in their progress report.[2] Both batch and fixed-bed adsorption column runs have been used in room-temperature tests, together with batch tests under pressure at 250°C to simulate reactor processing conditions. Continuous adsorption tests at 250°C in a high-temperature and high-pressure adsorption column are planned upon completion of suitable equipment. The solutions tested were either 1.0 or 0.02 *M* in UO_2SO_4 and were usually spiked with 0.4 μc of fission-product activity (Purex waste) per milliliter.

Of the minerals tested, fluorite (CaF_2) has shown the most promise. Removal of 70 to 80% of the Purex waste activity was usually observed at 250°C, and close to 100% removal was obtained when Ce^{144} tracer was diluted with 0.6 g of $Ce_2(SO_4)_3$ per liter to duplicate the expected rare-earth fission-product concentration for a four- to five-day processing cycle.

Apatite, variscite, and monazite sands (phosphate minerals) gave good decontamination, but they also removed a very considerable amount of uranium. Fluorite generally removed less uranium (approximately 4 to 25%). The removal of uranium is now being studied further because it would lead to additional processing cost. Activity removal data may also be affected by this precipitation of uranium. Galena (PbS) was an effective adsorbent, but it removed 67% of the uranium in a 0.02 *M* solution. Ilmenite sand (iron-titanium oxide) was relatively poor for decontamination at both 25 and 250°C.

More effective decontamination was observed at 250°C than at room temperature in nearly all tests on fairly good adsorbent materials. This is not surprising because of the probable metathesis reaction, particularly in the case of fluorite. All the rare-earth fluorides and calcium sulfate are insoluble. Fluorite, or CaF_2, thus leads to minimum contamination of the reactor solution by the adsorbent itself. Further data on such ionic contamination are being secured, particularly in work with known inorganic adsorbent compositions. The high-temperature adsorption column now being constructed will permit study of inorganic compounds at conditions close to those expected in continuous processing of reactor fuel.

(2) *February Progress Report for Homogeneous Reactor Processing*, KLX-1610; *March Progress Report for Homogeneous Reactor Processing*, KLX-1613; *April Progress Report for Homogeneous Reactor Processing*, KLX-1614.

[redacted]